

eman ta zabal zazu



Universidad
del País Vasco

Euskal Herriko
Unibertsitatea

*A Computational Glance at
Organometallic Cyclizations and
Coupling Reactions*

Doctoral Thesis

presented by

Béla Fiser

to

The Department of Organic Chemistry I

The University of the Basque Country

UPV/EHU

Donostia, Gipuzkoa

July 2016

© 2016 - *BÉLA FISER*
ALL RIGHTS RESERVED.

A Computational Glance at Organometallic Cyclizations and Coupling Reactions

ABSTRACT

Organometallic chemistry is one of the main research topics in chemical science. Nowadays, organometallic reactions are the subject of intensive theoretical investigations. However, in many cases, only joint experimental and theoretical efforts could reveal the answers what we are looking for.

The fruits of such experimental and theoretical co-operations will be presented here. In this work, we are going to deal with homogeneous organometallic catalysis using computational chemical tools. Particularly, DFT study of palladium and gold-catalyzed reactions and special carbometalations will be described.

Chapter 1 gives an introductory overview of organometallic chemistry and catalysis in general using a historical perspective. It covers the 9 thousand years history of catalysis from 7000 BC (the earliest concrete evidence of man-made fermentation/biocatalysis) through several milestones (Libavius, Berzelius etc.) up to the present days of organometallic chemistry.

Chapter 2 is a short methodological summary and intended to shed some light on the theoretical foundations of the applied quantum chemical tools, but it is neither complete, nor deep, just enough to scratch the surface and give insight into the complexity of the theory.

The results of our calculations presented in three separate chapters, (**Chapter 3, 4 and 5**) in each of which the calculations discussed along with the

corresponding experimental findings of our collaborators and/or other scientists.

Chapter 3 describe specific issues of palladium-catalyzed reactions. In this part of the work, palladium(II)-catalyzed dynamic kinetic asymmetric C–P coupling for the asymmetric synthesis of QUINAP and other atropos P,N-ligands is discussed and the reaction investigated at the Mo6/6-31+G(d,p)/SDD//B3LYP/6-31G(d)/LANL2DZ level of theory. The computational results along with experimental evidences collected by our collaborators allowed to propose a mechanism based on the formation of cationic oxidative addition intermediates which under the reaction conditions, undergo a fast interconversion (Figure 0.0.1). Coordination of the isoquinoline N atom to Pd is essential to facilitate this process.

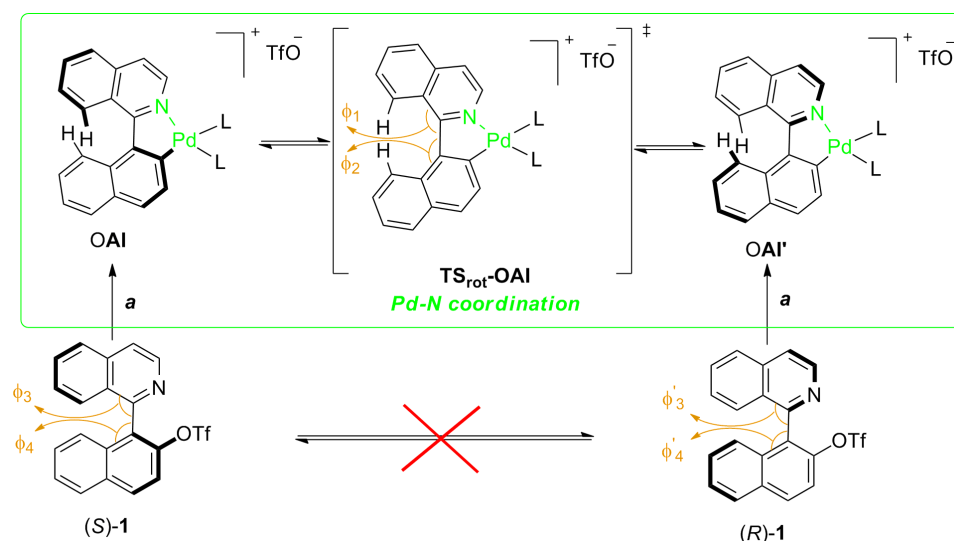


Figure 0.0.1: Proposed Mechanism for the Epimerization of Diastereomeric Oxidative Addition Intermediates (OAI and OAI').

The calculations also show that the energy requirements for a dynamic kinetic process are met, since the fast equilibrating palladacyclic intermediates evolve through

diastereomeric transmetalation steps of very large energy difference. The easiness of the final reductive elimination ensures the irreversibility of the process.

Chapter 4 can be divided into two parts in which gold(I)-catalyzed reactions are studied.

In the first section, the tandem gold(I)-catalyzed rearrangement/Nazarov reaction of propargylic ester derivatives studied in deeply computationally and the calculations revealed the details of the reaction mechanism (Figure 0.0.2) which allowed us to evaluate energetically the influence of the substrate structures on the reaction rate and on the regio- and stereoselectivity.

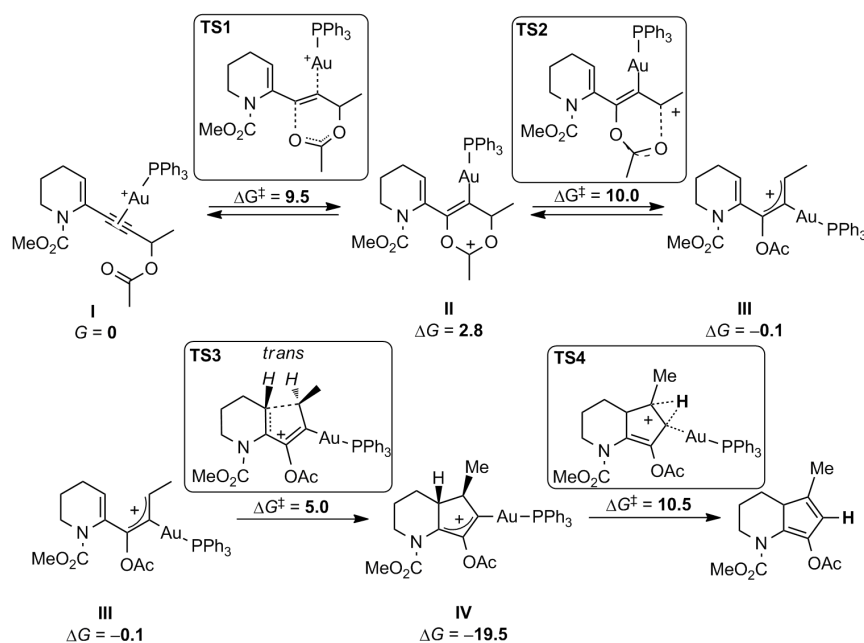


Figure 0.0.2: Reaction Mechanism. Top: Acetate Rearrangement in the Initial Steps of the Mechanism. Bottom: Cyclization Step from the pre-Nazarov cyclization complex **III** and Protodeauration. Gibbs Free Energy Changes (ΔG) and Barrier Heights (ΔG^\ddagger) are Given in kcal/mol.

In the second section, gold(I)-catalyzed cycloisomerizations calculated (Figure 0.0.3). The calculations showed that with both types of substrates, the oxyauration step has a low barrier or almost no barrier at all when it involves the internal position of a terminal triple bond, resulting in a *5-exo-dig* process. In contrast, the *6-endo-dig* mechanism is always favoured with substituted alkynes. The preference being purely geometrical and irrespective of the type of substitution, thus providing either β -enaminones or their reduced equivalents, β -amino ketones, in a robust, reliable, and convenient way.

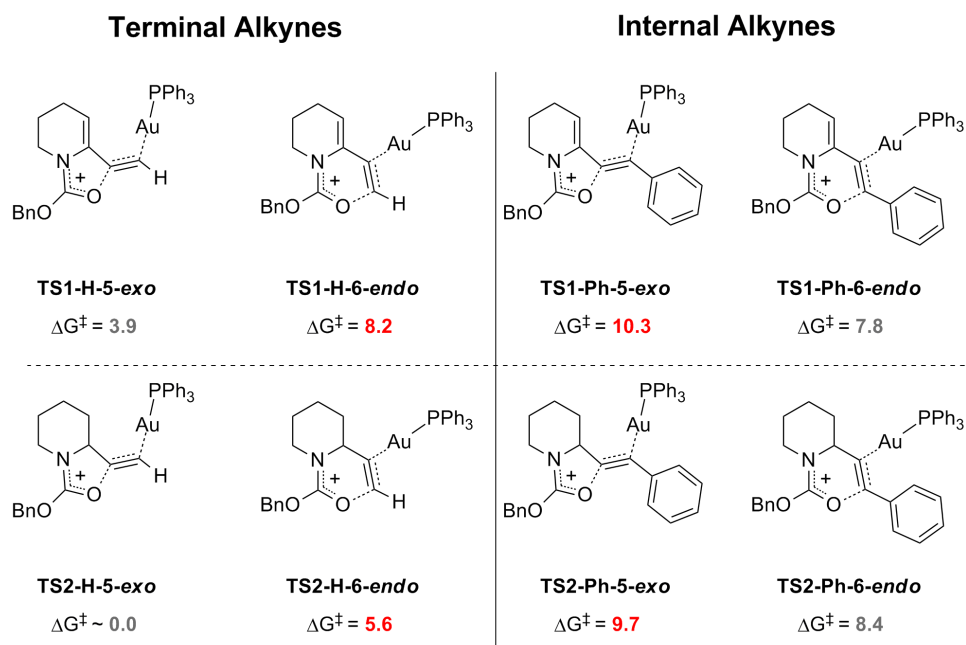


Figure 0.0.3: Transition State Structures and the Corresponding Barrier Heights for Terminal Alkynes and Internal.

Chapter 5 is a systematical study of intramolecular metal catalyzed cyclizations.

Group 10 alkyl metalations are studied systematically by means of DFT calculations and based on the results the extension of the Baldwin's rules for metal catalyzed ring closure reactions is proposed (Figure 0.0.4).

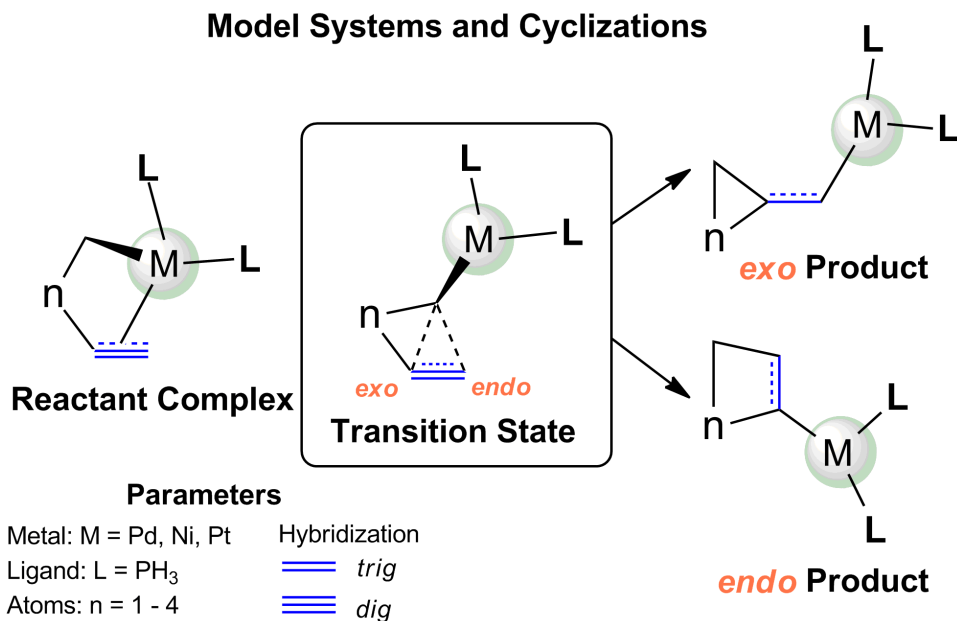


Figure 0.0.4: Studied Group 10 Alkyl Metalations.

An intuitive summary of the qualitative results created and the results could serve as a guide to explore not yet described cyclization processes based on the accessible computed activation energies and the qualitative comparison of the preferences.

Our manuscripts published in connection with the topics discussed in the thesis can be found in the **Appendix**.

A Computational Glance at Organometallic Cyclizations and Coupling Reactions

ABSTRACT

La química organometálica es uno de los campos más activos de investigación en ciencias químicas. Hoy en día, las reacciones organometálicas son sujeto de numerosas investigaciones teóricas. Sin embargo, en muchos casos, sólo los esfuerzos conjuntos teóricos y experimentales son capaces de encontrar las respuestas que buscamos. En este trabajo se presentan los frutos de tales colaboraciones experimentales/teóricas. Hemos empleado herramientas computacionales para estudiar reacciones catalizadas en condiciones homogéneas, y más concretamente describimos a continuación estudios DFT de reacciones de ciclación catalizadas por Paladio y Oro, así como algunos tipos de carbometalación.

Capítulo 1. Se da un repaso introductorio de la catálisis organometálica y catálisis en general usando una perspectiva histórica. Cubre los 9000 años de historia de la catálisis desde el 7000 a. C. (la más antigua evidencia de fermentación / biocatálisis hecha por el hombre) a través de diversos hitos (Libavius, Berzelius, etc) hasta la química organometálica de nuestros días.

Capítulo 2. Es una breve descripción metodológica que intenta dar luz sobre las formulaciones teóricas que se aplican en las herramientas químicas cuánticas, sin la intención de ser completa ni profusa, sino solamente arañando la superficie de esta parte tan compleja de la teoría.

Los resultados de nuestros cálculos se presentan en tres capítulos separados

(capítulos 3, 4 y 5), en cada uno de los cuales se entremezclan con los resultados experimentales de nuestros colaboradores y otros grupos de investigación.

Capítulo 3. Describe algunas características especiales de la química del paladio. En esta parte de la Tesis, se han estudiado reacciones de síntesis asimétrica de QUINAP, mediante un acoplamiento C-P dinámico cinético asimétrico catalizado por complejos de paladio (II). Además de QUINAP, se han estudiado otros atropo-ligandos P, N por métodos DFT al nivel de cálculo Mo6/6-31+G(d,p)/SDD//B3LYP/6-31G(d)/LANL2DZ.

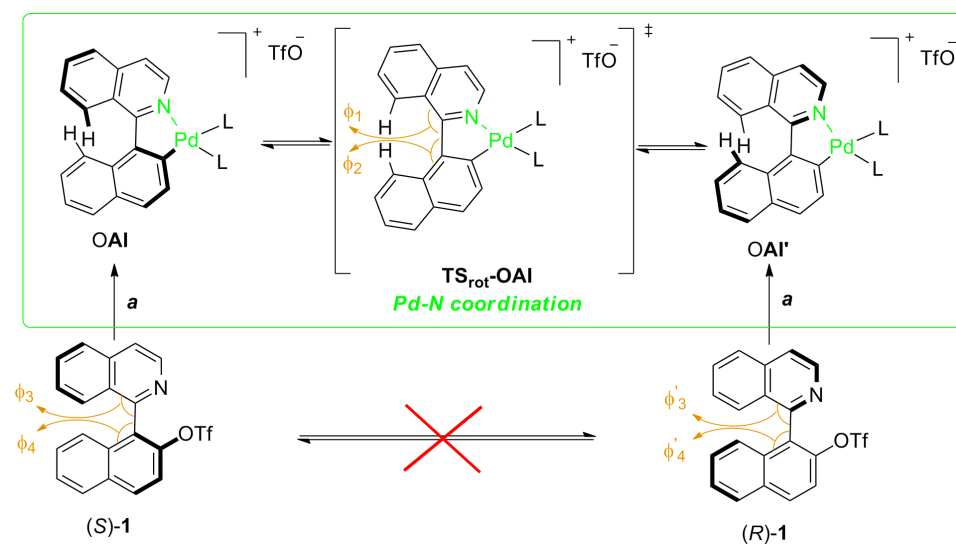


Figure 0.0.1: Mecanismo Propuesto para la Epimerización de los Intermedios Diastereoméricos de Adición Oxidante).

Los resultados computacionales junto a las evidencias experimentales recopiladas por nuestros colaboradores nos permiten proponer un mecanismo de reacción basado en la formación de intermedios catiónicos de adición oxidante, que en las condiciones de reacción sufren una interconversión rápida entre diferentes isómeros (Figura 0.0.1). La coordinación del nitrógeno de la isoquinolina al átomo de Pd es esencial para facilitar el proceso.

Los cálculos también muestran que se cumplen los requisitos energéticos para una resolución cinética dinámica, ya que los intermedios de reacción equilibran rápidamente y evolucionan por estados de transición de transmetalación de barreras de activación muy diferentes.

Capítulo 4. Se divide en dos partes en las que se estudian dos reacciones catalizadas por Au(I) diferentes. En la primera sección, se ha estudiado computacionalmente al detalle la reacción tándem de transposición / ciclación Nazarov catalizadas por Au(I) de ésteres propargílicos, y nuestros cálculos revelan el mecanismo detallado en la Figura 0.0.2, permitiéndonos evaluar energéticamente la influencia de las estructuras de los substratos en la velocidad de reacción y en la regio- y estereoselectividad.

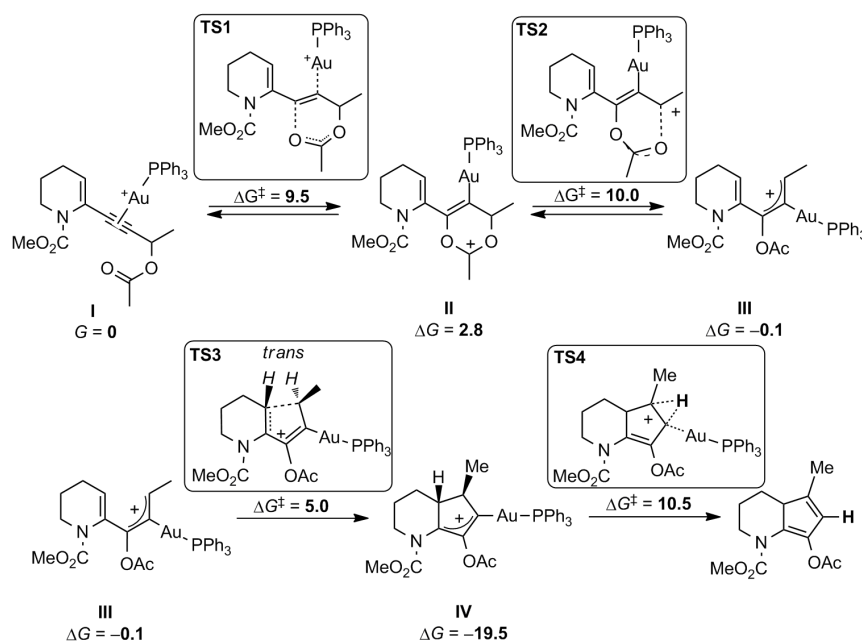


Figure 0.0.2: Mecanismo de Reacción. Arriba: Transposición de Acetato en los Inicios de la Reacción. Abajo: Paso de Ciclación desde el Complejo pre-Nazarov III y Protodesaturación. Los Cambios en la Energía Libre de Gibbs (ΔG) y Barreras de Activación (ΔG^\ddagger) se dan en kcal/mol.

En la segunda sección, se han calculado reacciones de cicloisomerización catalizadas por Au(I) (Figura 0.0.3). Los cálculos muestran que para ambos tipos de sustratos mostrados, el paso de oxaauración ocurre con una barrera de activación muy baja o inexistente cuando ocurre en la posición interna del triple enlace, resultando en un proceso 5-exo-dig. La preferencia es puramente geométrica e independiente del tipo de sustitución, dando lugar tanto las β -enaminonas como sus equivalentes reducidos, β -amino cetonas, de un modo robusto, apropiado y fiable.

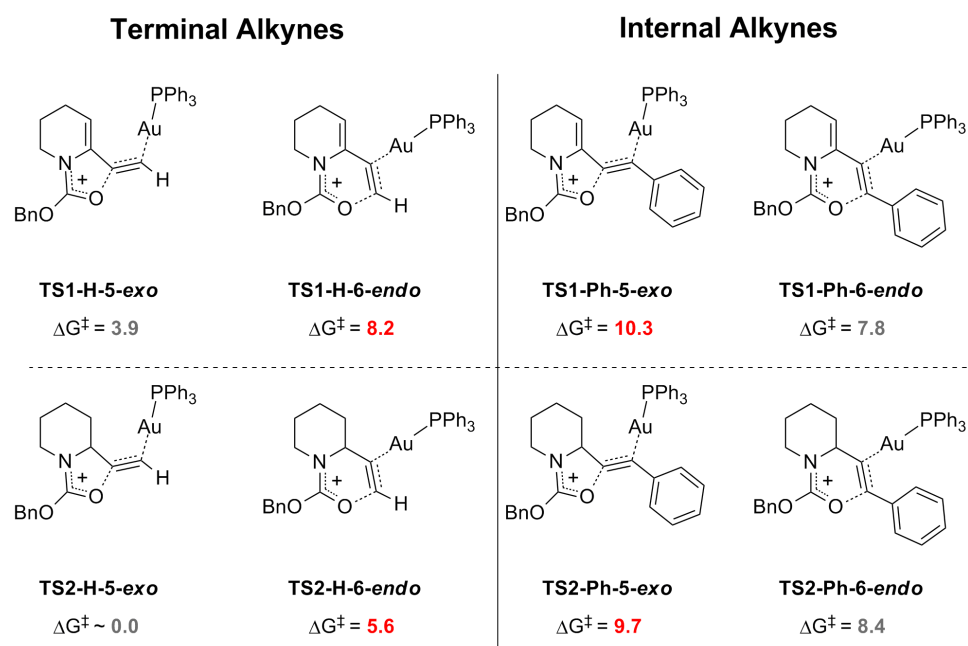


Figure 0.0.3: Estructuras de los Estados de Transición y sus Correspondientes Barreras de Activación para los Alquinos Terminales e Internos.

Capítulo 5. Es un estudio sistemático de reacciones de ciclación catalizadas por metales de transición. Se han estudiado sistemáticamente las ciclaciones con los metales del grupo 10 por métodos computacionales, y basándonos en los resultados, se propone una extensión de las reglas clásicas de Baldwin para ciclaciones a la catálisis metálica (Figura 0.0.4)

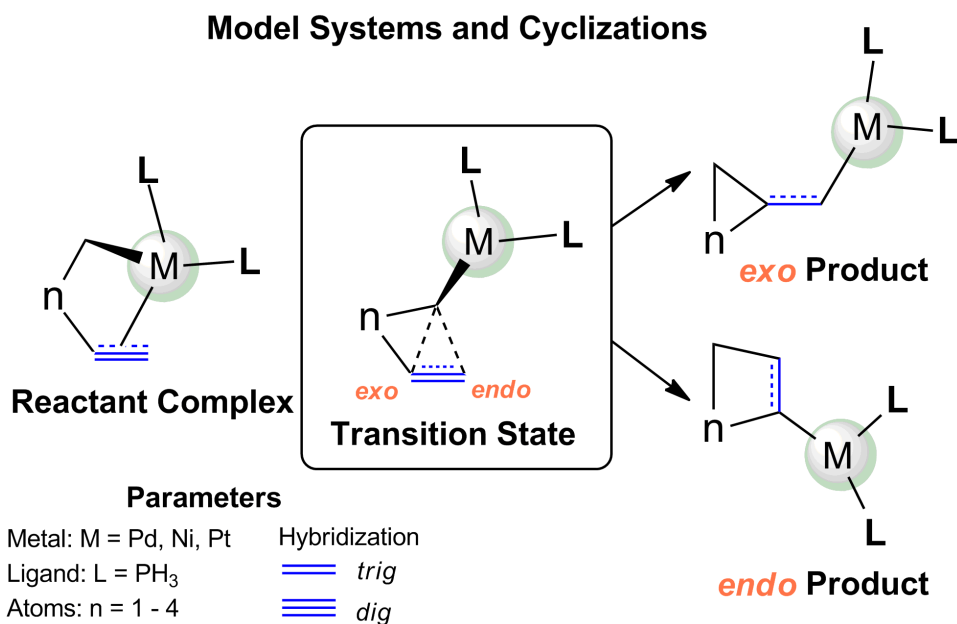


Figure 0.0.4: Metalaciones del Grupo 10 Estudiadas.

Los resultados cualitativos han dado lugar a un resumen intuitivo de los resultados que podría servir como guía para explorar nuevos procesos catalíticos de carbometalación.

Los manuscritos publicados como resultado de estos capítulos se adjuntan en el **Apéndice I**.

Contents

1	INTRODUCTION	1
1.1	Historical Aspects of Catalysis	1
1.2	Catalysis in General	5
1.2.1	Reaction Energetics and Types of Catalysis	5
1.3	Organometallic Catalysis	8
1.3.1	A Little More History	8
1.3.2	General Remarks	11
2	METHODS	12
2.1	The Ancient Greeks Already Knew...	12
2.2	Who's Who and What's What in Quantum Mechanics	16
2.2.1	A Quantum of History - History of Quantum	16
2.2.2	The Postulates of Quantum Mechanics	21
2.3	The Beauty of Approximations	23
2.3.1	Non-Relativistic Quantum Mechanics	24
2.3.2	Born-Oppenheimer Approximation	24
2.3.3	One-Electron Approximation and Hartree-Fock Method	28
2.4	Density Functional Theory	33
2.4.1	The origin	33
2.4.2	The Proof - Hohenberg-Kohn Theorems	34
2.4.3	Kohn-Sham Formalism	36
2.4.4	The Focal Point - Exchange Correlation	37

2.4.5	Jacob's Ladder or The Zoo of DFT?	38
2.5	Basis Sets and Basis Functions	41
2.5.1	Atomic Orbitals	41
2.5.2	Pseudopotentials	43
2.6	Model Chemistries	44
2.7	Solvent Models	44
2.8	General Remarks	47
3	PALLADIUM(II)-CATALYZED DYNAMIC KINETIC ASYMMETRIC TRANS-	
	FORMATION	48
3.1	Introduction	48
3.1.1	Chirality – History, Biology and Chemistry meet	48
3.1.2	How to Copy Nature?	50
3.1.3	Nature's Privilege – Privileged Ligands	53
3.1.4	Atropos P,N-ligands – Advantages and Disadvantages	54
3.2	Mechanisms and Experimental Background	58
3.3	Computational Methods	63
3.4	Results and Discussion	64
3.5	Conclusion	76
4	GOLD(I)-CATALYZED CYCLIZATIONS	77
4.1	General Introduction	77
4.2	Gold(I)-Catalyzed Nazarov Reaction	80
4.2.1	Introduction	80
4.2.2	Computational Methods	89
4.2.3	Results and Discussion	90
4.3	Gold(I)-Catalyzed Cycloisomerizations	101
4.3.1	Introduction	101
4.3.2	Computational Methods	106
4.3.3	Results and Discussion	108
4.4	Conclusions	115

4.4.1	Gold(I)-Catalyzed Nazarov Reaction	115
4.4.2	Gold(I)-Catalyzed Cycloisomerizations	115
5	BALDWIN TYPE RULES FOR METAL CATALYZED CYCLIZATIONS	116
5.1	Introduction	116
5.2	Computational Methods	122
5.3	Results and Discussion	123
5.3.1	General Considerations	123
5.3.2	Pure Anionic Cyclizations and Carbolithiations	124
5.3.3	Palladium Promoted Cyclizations	131
5.3.4	Nickel Promoted Cyclizations	137
5.3.5	Platinum Promoted Cyclizations	141
5.3.6	Scope of the Predictions	143
5.4	Conclusion	146
6	REFERENCES	147
7	APPENDIX	171

Listing of figures

o.o.1	Proposed Mechanism.	viii
o.o.2	Reaction Mechanism	ix
o.o.3	Transition States and Barrier Heights.	x
o.o.4	Model Systems.	xi
o.o.1	Mecanismo Propuesto.	xiii
o.o.2	Mecanismo de Reacción.	xv
o.o.3	Estructuras de los Estados de Transición.	xvi
o.o.4	Metalaciones del Grupo 10 Estudiadas	xvii
1.2.1	General Scheme of a Catalytic Cycle	5
1.2.2	Schematic Reaction Energy Profile Diagram	6
2.1.1	Theories and Their Application.	15
2.3.1	Potential Energy Curve	27
2.4.1	First Hohenberg-Kohn Theorem	35
2.4.2	Jacob's Ladder of Density Functional Approximations	39
2.5.1	Slater-type and Gaussian-type Orbitals	42
2.7.1	Implicit and Explicit Solvation Models	45
3.1.1	L- and D-Amino Acids.	49
3.1.2	Atropoisomers of BINAP.	52
3.1.3	P,N-Ligand Families.	55
3.1.4	General Steps of QUINAP Synthesis	56

3.1.5	DYKAT Techniques for the Synthesis of Heterobiaryls.	57
3.2.1	Proposed Mechanisms for the Epimerization.	59
3.2.2	Test Experiments with Triflate 2 and Nonaflate 4.	60
3.2.3	Ligand Screening, Condition Optimization and Scope	62
3.4.1	General Mechanism of the DYKAT for APN Ligand Formation	65
3.4.2	Activation Energies for the Axial Rotations	67
3.4.3	Stable Palladacyclic Intermediates	69
3.4.4	Transmetalation Process	70
3.4.5	Stable Transition States	72
3.4.6	Curtin-Hammet Conditions	73
3.4.7	Reductive Elimination	74
3.4.8	The Proposal of Virgil and Stolz et al.	75
4.1.1	Anion Exchange and C-C Bond Activation	79
4.2.1	Lewis Acid Catalyzed Nazarov Cyclization	81
4.2.2	Metal-Catalyzed 1,3-Acyloxy Migration of Propargylic Esters	83
4.2.3	Cyclopenta-fused N-heterocyclic Rings	84
4.2.4	Synthesis of the Substrates and the Possible Products of the Gold(I)- Catalyzed Nazarov Reaction	86
4.2.5	Competing Pathways	88
4.2.6	Model Substrates	90
4.2.7	Reaction Mechanism	91
4.2.8	Relative Gibbs Free Energies	94
4.2.9	Hydrolysis of Diene-Acetates	95
4.2.10	Predicted Formation of Intermediate XI	97
4.2.11	Torquoselectivity of the Ring Closure	99
4.3.1	Acetic Acid and Formamide and their Vinylogous Derivatives	101
4.3.2	Synthetic Exocyclic Vinylogous Amide Intermediates and Natu- ral Alkaloids	102
4.3.3	Gold(I)-Catalyzed Process to Produce Exocyclic Vinylogous Amides	104
4.3.4	Test Reactions to Study the 6-endo/5-exo Selectivity	105

4.3.5	Selected Model Substrates for Calculations	107
4.3.6	Structures of 1a-comp and 1b-comp	109
4.3.7	Transition States and Barrier Heights for Terminal Alkynes	110
4.3.8	Transition States and Barrier Heights for internal Alkynes	112
4.3.9	Energetic Comparison of the 5- <i>exo</i> and 6- <i>endo-dig</i> Pathways	113
5.1.1	Baldwin's Terminology of Cyclizations	117
5.1.2	Baldwin's Rules for Ring Closure	119
5.1.3	Favored Trajectories for Ring Closures	120
5.3.1	General Scheme of the Studied Model Systems	123
5.3.2	Selected Transition States I.	125
5.3.3	<i>dig</i> -Cyclization Processes	127
5.3.4	<i>dig</i> -Cyclization Processes	128
5.3.5	Summary of the Rules for <i>dig</i> and <i>trig</i> Cyclization Processes	130
5.3.6	Selected Transition States II.	132
5.3.7	Pd-Catalyzed 3- <i>exo-trig</i> Cyclization.	133
5.3.8	Literature Examples of Pd-Catalyzed Cyclizations I.	134
5.3.9	Literature Examples of Pd-Catalyzed Cyclizations II.	135
5.3.10	Selected Transition States III.	138
5.3.11	Literature Examples of Ni-Catalyzed Cyclizations	140
5.3.12	Selected Transition States IV.	142
5.3.13	Scope of the Predictions	144

SZERETTEIMNEK.

*It does not, therefore, depend on human
desire or effort, but on God's mercy.*

Romans 9:16

Acknowledgments/Eskerrak

FIRST AND FOREMOST, I would like to thank The Almighty, who took care of us and wrote more carefully this chapter of our life than I was ever thought about it.

Nire ikuskatzaile, Enrique Gómez Bengoa eskertu nahi dut. Eskerrik asko zure konfiantzagatik eta laguntza.

I am grateful to the entire Department of Organic Chemistry I at the University of the Basque Country (UPV-EHU), all the faculty members, staff and fellow doctoral colleagues.

Szeretnék köszönetet mondani, Drága Szüleimnek, Keresztszüleimnek, unokatestvéreimnek és családom minden tagjának, hogy támogattak a továbbtanulásban, s mindent megtettek azért, hogy soha semmiben se szenvedjek hiányt.

Szerető feleségemnek köszönöm házasságunk minden napját. Köszönöm, hogy mellettem álltál és feladtad az álmaidat azért, hogy követhesd az enyémekeket.

Köszönöm a barátaim támogatását, az egyetemi szobatársaim (Gy, Csab és Kohut) ösztönzését, s a helyiértelmiségnek a személyesen és a listán folytatott beszélgetéseket.

Köszönöm az imákat Áron, s köszönöm családot szeretetét, Édesanyád törődését, s mindazt amivel elhalmoztatok az egyetemi évek alatt. Isten áldjon titeket!

Köszönöm Janinak, hogy segíthettem erdőt ültetni!

Külön szeretném megköszönni András, Jani, Masi és Gyula, Gabi és Bandi, Edit és Laci törődését, s fáradozásait, amikor vendégül láttak minket hazalátogatá-

saink alkalmával. Köszönünk szépen mindent!

Korábbi szegedi munkatársaim (Anita, Edit, Eszter, Gabi, Heni, Kati néni, Klári, Lilla, Natalie, DJ, Franco, János, Methos, Mike, Szilárd) és mentoraim (Balázs, Milán, Robi, Béla és Imre bácsi) a Kémiai Informatika Tanszékről szintén nagyban hozzájárultak ahhoz, hogy ez a dolgozat elkészüljön. Sokat tanultam tőletek! Köszönöm!

The financial support of my studies from the FP7 Marie Curie Actions of the European Commission via the ECHONET ITN (“Expanding capability in Heterocyclic Organic Synthesis”, MCITN-2012-316379) is gratefully acknowledged.



I would like to thank every fellows (Alejandra, Caroline, Guilhem, Ivan, Júlia, Jokin, Malcolm, Martina, Silvia, Sylvestre and Tim), PIs (Prof. Enrique Gómez Bengoa, Prof. Joe Harrity, Prof. Stefan Bräse, Prof. Ernesto Occhiato, Prof. Floris Rutjes, Prof. Josep Bonjoch, Dr. Stephen Lindell, Dr. Pieter Nieuwland and Dr. Matt Tozer) and project managers (Ala and Marie) of the ECHONET.

It was a great pleasure to meet and work with you. Thanks for everything!

Special thanks goes to my secondment hosts (Ernesto and Dina in Firenze, Joe in Sheffield and Paul at the PeakDale) and colleagues (Martina, Júlia, Ben, Steve, Sylvestre and Olivier).

I must also acknowledge all of our collaborators within and outwith the ECHONET. Special thanks to Prof. Lassaletta and Prof. Fernández and their groups (Chapter 3), Prof. Occhiato and his group (Chapter 4) and Prof. Cuerva (Chapter 5) for the fruitful collaborations based on which this thesis was born.

I would like to thank Fomento de San Sebastián and the Talent House Team to provide accommodation for us in Donostia during my studies.



The technical and human support (Eskerrik asko Txema!) provided by IZO-SGI SGIker of UPV/EHU and European funding (ERDF and ESF) is acknowledged.

For allocation of a part of the computational resources used for this work the Department of Chemical Informatics (University of Szeged, Hungary) is gratefully acknowledged. László Müller and Máté Labádi for the administration of this computing systems is also acknowledged.

I am so grateful to all the people that have helped me along my way to achieve this point in my life. It's been an incredible journey and I hope this is not the end, but the beginning.

They are students. They have to suffer.

Anonymous

1

Introduction

1.1 HISTORICAL ASPECTS OF CATALYSIS

THE USAGE OF FERMENTATION (biocatalysis) to produce alcohol from sugar and to make bread rise is several thousands years old and can be linked with the birth of agriculture and food production [1, 2]. The earliest concrete evidence of this process used by mankind is a mixed fermented beverage of rice, honey, and hawthorn fruit found in pottery jars in a Neolithic village of Jianhu (China) and dated back to 7000 BC [3]. However, it was not clear what is responsible for the procedure until the XIX. century when Louis Pasteur determined that fermentation is caused by yeast [4–6].

In the early XIX. century, Johann Wolfgang Döbereiner invented a gas lighter (Döbereinersche Feuerzeug) which was used to light candles. It was quickly com-

mercialized and become extremely popular and by 1828 about 20 000 were in use in Europe [7]. Its modus operandi is based on two steps: 1) hydrogen gas production and 2) ignition. Hydrogen is produced by the reaction of zinc with sulfuric acid, while the ignition of H₂ is initiated by platinum sponge to flame lights [7, 8].

Let's step back three centuries to the mid XVI., when ether was first synthesized by Valerius Cordus (1514-1544) a german botanist and apothecary, from alcohol using sulfuric acid [9, 10]. This method is still used nowadays to prepare ether, but its relation with fermentation and Döbereiner's lighter is more important from our viewpoint. It may seem that there is no connection between these discoveries, but both, the fermentation, the production of ether using sulfuric acid and the ignition of hydrogen using platinum in the lighter are catalytic processes.

Although, the concept of catalysis, in the sense as used today, remained hidden until the XIX. century, the term was used by Andreas Libavius in 1597. His remarkable work, *Alchemia*, is the first systematic textbook of chemistry [11] and it contain the first historical note of catalysis as a chemical phenomenon.

”De magisteriis substantiae, ubi primum det metallorum transfor-
matione, magisterium substantiae fit vel genesi vel *catalysi*.”

— *Andreas Libavius: Alchemia* [1, 11]

However, Libavius used the phrase 'catalysis' to describe the decomposition of base metals into silver and gold rather than to define the catalytic phenomena which appears to be common in the above mentioned processes.

The birth of catalysis, the term used today, dated to the early XIX. century. In 1835, Jöns Jacob Berzelius discovered a common phenomena by systematically re-evaluating the observations of several scientist on different reactions (ether production from alcohols, gas combustion induced by platinum, enhanced conversion of starch to sugar by acids etc.) and shed light on its generality and proposed to call it catalysis [1, 10, 12, 13].

”It is then shown that several simple and compound bodies, solu-
ble and insoluble, have the property of exercising on other bodies

and action very different from chemical affinity. The body effecting the changes does not take part in the reaction and remains unaltered through the reaction. This unknown body acts by means of an internal force, whose nature is unknown to us. This new force, up till now unknown, is common to organic and inorganic nature. I do not believe that this force is independent of the electrochemical affinities of matter; I believe on the contrary, that it is a new manifestation of the same, but, since we cannot see their connection and independence, it will be more convenient to designate the force by a new name. **I will therefore call it the “Catalytic Force” and I will call “Catalysis” the decomposition of bodies by this force, in the same way that we call by “Analysis” the decomposition of bodies by chemical affinity.**

— *Jöns Jacob Berzelius* [1, 12, 13]

In Berzelius’s view, the catalyst can be seen as something that induced the reaction (“Catalytic Force”) by adding to the reacting “bodies” (substances), but it is not produced or consumed during the process [2]. He does not explained the nature of catalysis, but used the term as a description of a group of unexplainable (by using “Chemical Affinity”) reaction phenomena [14].

A few decades later, Wilhelm Ostwald’s research has contributed significantly to the understanding of catalysis. In recognition of his work on catalysis, chemical equilibria and reaction velocities, in 1909, he was awarded the Nobel Prize in Chemistry [15].

Ostwald formulated the “kinetic definition of catalysis”, by stating that “the nature of catalysis is to be sought not in the *inducement* of a reaction, but in its *acceleration*” [14].

”Catalysis is the acceleration of a slow-running chemical reaction via the presence of a foreign substance”.

— *Wilhelm Ostwald* [16]

The current definition recommended by IUPAC is not very different from his statement:

”Catalyst: A substance that increases the rate of a reaction without modifying the overall standard Gibbs energy change in the reaction; the process is called catalysis.”

— IUPAC *”Gold Book”* [17]

As one can see when comparing Berzelius’s [12] and Ostwald’s view [16] and the IUPAC recommendation [17], our picture about catalysis is refined over the years, but the basic concept has stood the test of time.

1.2 CATALYSIS IN GENERAL

1.2.1 REACTION ENERGETICS AND TYPES OF CATALYSIS

There is one thing which is common in all type of catalysts: as soon as they have successfully finished the first reaction, they are ready to start another one. This process can be repeated many times during the lifetime of the catalyst and it is called as "catalytic cycle" (Figure 1.2.1).

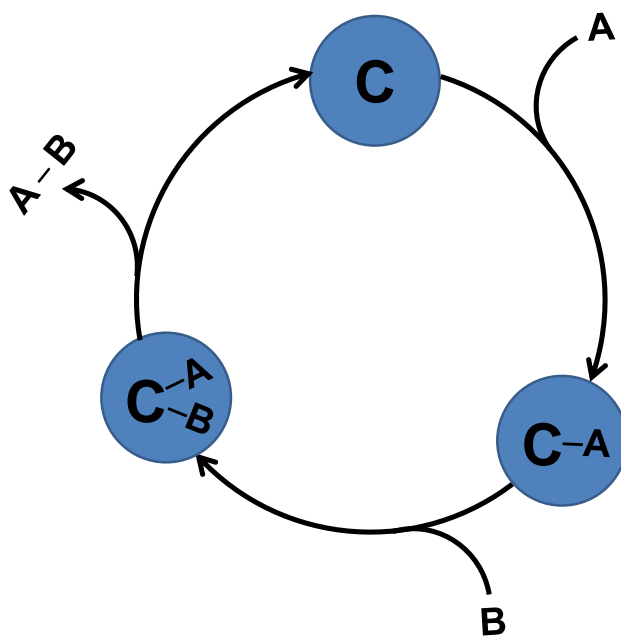


Figure 1.2.1: General Scheme of a Catalytic Cycle: $A + B \xrightarrow{C} A-B$, (addition reaction). A, B - Reactants, C - Catalyst, A-B - Product.

In the simplest case, a reaction contains three different species: reactant (R), transition state (TS) and product (P) (Figure 1.2.2). The energy difference between the TS and the R is the corresponding activation energy (E_a), which is needed to overcome for the completion of the reaction. By the usage of a catalyst, the reaction profile could change dramatically, E_a decreased, the energetic barrier is lower compared to the one of the uncatalyzed reaction and new species (intermediates) could appear in the reaction system. However, the relative thermodynamic stability (ΔE) of R and P remain the same in the catalyzed and uncatalyzed $R \rightarrow P$ process as well (Figure 1.2.2).

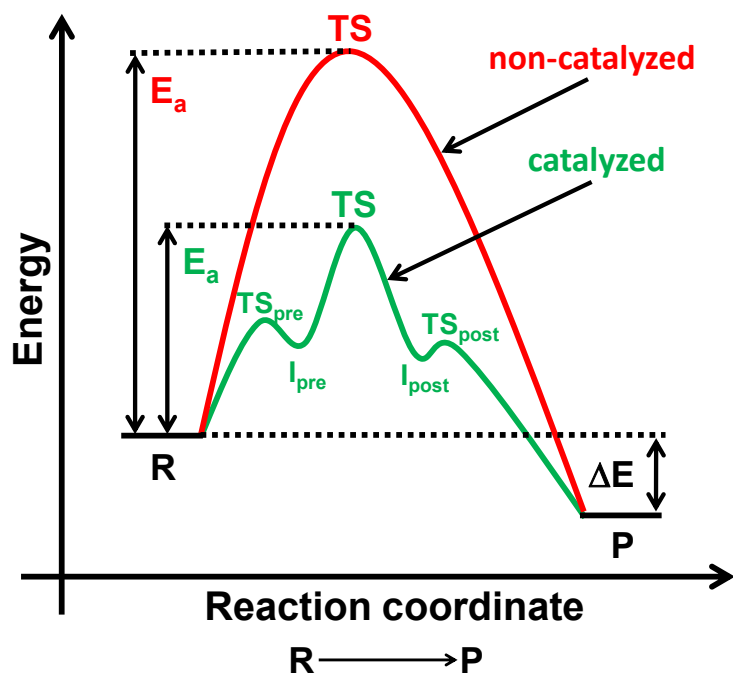


Figure 1.2.2: Schematic Reaction Energy Profile Diagram of Catalyzed (green) and Non-catalyzed (red) Reactions (E_a - Activation Energy, ΔE - Reaction Energy Difference). Starting Material or Reactant (R) Convert to Product (P) via the Intermediates (I_{pre} and I_{post}) and Transition States (TS_{pre} , TS and TS_{post}).

In general, a catalytic process could be homogeneous when reactants and catalysts are in the same phase or heterogeneous when the phase of the catalyst is different from that of the reactants.

In addition to these, there is another type of catalysis, biocatalysis. It covers catalytic processes occurring in living organisms using enzymes to facilitate chemical transformations of compounds [14].

From a structural point of view, homogeneous catalysts (Wilkinson's [18], Crabtree's [19] etc.) have well-defined structures and most of them operate in liquid phase, while the heterogeneous (or contact) ones (Pd/C [20], Raney-nickel [21, 22] etc.) are insoluble, metal-containing materials (solid phase) with the capability of adsorbing molecules of gases or liquids onto their surfaces [14].

The *ab ovo* separation of the reaction medium from the phase of the catalyst is a major advantage of heterogeneous processes over the homogeneous ones, because the isolation and re-utilization of the catalysts is cheaper and more simple. Furthermore, in terms of thermal stability, the heterogeneous catalysts also perform far better [2]. However, homogeneous catalysts are more selective and active, considering that each catalyst molecule works as a separate catalytic unit [23]. Moreover, theoretical investigation of homogeneous catalysis is more straightforward, than its heterogeneous counterpart, because the molecular structure of reactants and catalysts are known and therefore relatively easy to model the reaction mechanism using computational methods.

There are a quite good number of homogeneous catalysts including organic molecules, acids (Brønsted and Lewis) and metal containing complexes (e.g. organometallic compounds). Amongst these, metal containing complexes constitute one of the biggest and most important group of catalysts.

1.3 ORGANOMETALLIC CATALYSIS

1.3.1 A LITTLE MORE HISTORY

Organometallic chemistry, like a bridge, is lying somewhere between inorganic and organic chemistry and include properties of both fields.

Organometallic compounds can be formed by the unification of an organic fragment and a metal center into a single entity. Earlier, the presence of at least one metal-carbon (M-C) or metal-hydrogen (M-H) bond served as a distinctive sign, but thanks to the recent rapid development of the field, it is outgrown the initial frameworks and by now several species lacking the distinctive bonds also included into the organometallic category [24].

In 1757, Louis Claude Cadet de Gassicourt prepared the first organoarsenic compounds (although he did not know about that) during his attempts to make invisible inks [25]. He experimented with the reaction of various acids on arsenic-containing cobalt ores (CoAs_2 and CoAsS_2) and succeeded to synthesize a red liquid which was later called as "Cadet's fuming liquid". At this time, the early studies on the properties liquid were only qualitative and it took several decades to overcome the difficulties which arise from its horrible stench and inflammability.

In the late 1820s and early 1830s Jean Baptiste Dumas, worked with this material and tried to prepare a phosphorus analogue of Cadet's liquid, but he was unsuccessful. Although, he was able to partially analyze its chemical composition [25]. A little bit later, between 1837-1843, Robert Wilhelm Bunsen turned to his attention towards the investigation of Cadet's fuming liquid and successfully determined the chemical composition of the compounds within the liquid [25]. It turned out that it contain dicacodyl ($\text{As}_2(\text{CH}_3)_4$) and dicacodyl oxide ($[(\text{CH}_3)_2\text{As}]_2\text{O}$). Today, these are referred as the first organometallic species, but actually, they are not organometallic in the sense, that they contain metalloid (arsenic) instead of metal [25]. Despite the nit-picking over the definitions, undeniably this was the first step in the development of organometallic chemistry [26].

Around this time, in 1830, William Christopher Zeise at the University of Cop-

penhagen synthesized the first platinum/olefin complex, potassium trichloro(ethene)platinate(II) (Zeise's salt) [27]. He determined the formula of the compound, but his findings were harshly attacked by Justus von Liebig, arguing that it must contain oxygen as well. This controversy lasted until Zeise's formula verified independently by the decomposition of the salt [28] and achieving the same compound and its homologues with propylene and amylene by a new synthesis using ethylene and chlorplatinic acid [29].

However, not only the formula, but the structure caused not a little puzzled among chemist, because they were not able to explain it and the solution arrived only in the XX. century with the development of X-ray crystallography. But in the mean time, in the second half of the XIX. century several other milestones were reached in the combination of metals with organic compounds.

Some of these milestones can be associated with Edward Frankland, who synthesized the first organozinc compounds including zinc methyl, zinc ethyl (in Bunsen's laboratory) and zinc amyl (with Liebig) [30]. He prepared many more organometallic compounds using different metals such as cadmium, magnesium, tin, antimony, lead, mercury and others [31, 32]. Furthermore, he coined the term organometallic, which used to refer to this area of chemistry:

“I have applied the name organometallic to a family of compounds resulting from this investigation, the members of which contain a positive organic radical united directly with a metal.”

— *Sir Edward Frankland* [30]

The next milestone of organometallic chemistry is the synthesis of nickel carbonyl which was first done by Ludwig Mond and his co-workers in 1890 using metallic nickel and carbon monoxide [33]. Shortly thereafter, their findings was successfully used in metallurgy to purify nickel from its ores [34].

Last but not least, at the very end of the XIX. century, François Auguste Victor Grignard introduced new organomagnesium compounds and described their usage in the synthesis of alcohols and hydrocarbons [35]. These compounds are the so-called Grignard reagents and they are still successfully and widely applied

to form carbon–carbon bonds. It also show the importance of these reagents, that little more than 10 years after their discovery in 1912, Grignard was awarded the Nobel Prize in Chemistry [15]. He shared the prize with another french chemist, Paul Sabatier, who was awarded "for his method of hydrogenating organic compounds in the presence of finely disintegrated metals whereby the progress of organic chemistry has been greatly advanced in recent years" [15].

Another landmark of organometallic chemistry is the development of the first effective medicinal treatment for syphilis, Salvarsan (arsphenamine or compound 606) based on organoarsenic compounds. Salvarsan was synthesized by Alfred Berthelm in 1907, in Paul Ehrlich's laboratory. Its activity against syphilis was proved by Sahachirō Hata in 1909, in the same place [26] and marketed in Europe from 1910.

The advancement of organometallic chemistry has become increasingly faster throughout the XX. century. Numerous discoveries were achieved during the century, including the preparation of ferrocene [36] and the interpretation of its structure [37]. Furthermore, the development of different metal containing catalysts such as Gilman reagent [38], Ziegler–Natta catalyst [39], Wilkinson's [18] and Crabtree's catalyst [19] and the first application of homogeneous metal catalysis in industrial asymmetric synthesis [40] are also the results of the XX. century. In addition to these, several catalytic processes were developed in this time applying organometallic compounds such as Stille reaction (organostannanes) [41], Negishi coupling, Heck and Suzuki reaction (organopalladium) [42]. Finally, at the turn of the millennium, homogeneous gold catalysis emerged and become one of the most intensely studied area in synthesis [14].

The quarter-millennium long history of organometallic chemistry definitely sealed its fate as one of the main research topics in chemical science. Perhaps, the research arsenal changed a bit and new tools (e.g. computational chemistry) have been taken besides the original experimental studies, but the development still did not stop. Nowadays, organometallic reactions are the subject of intensive theoretical investigations and in many cases, the experiments and the theoretical calculations are not able to clarify the open issues without establishing co-operations.

1.3.2 GENERAL REMARKS

The fruits of such experimental - theoretical co-operations will be presented here. In this work, we are going to deal with homogeneous organometallic catalysis using computational chemical tools, particularly palladium and gold-catalyzed reactions were investigated. The computed results will be presented in three separate chapters (Chapter 3, 4 and 5) in each of which the calculations will be compared to parallel experimental investigations performed by our collaborators and/or other scientists.

*A twofold tale I shall tell: at one time it grew to be one alone out of many, at another again it grew apart to be many out of one. Double is the birth of mortal things and double their failing; for one is brought to birth and destroyed by the coming together of all things, the other is nurtured and flies apart as they grow apart again. And these things never cease their continual exchange, **now through Love all coming together into one, now again each carried apart by the hatred of Strife.***

Empedocles (ca. 495–435 BC), Peri Phuseôs

2

Methods

2.1 THE ANCIENT GREEKS ALREADY KNEW...

25 CENTURIES AGO a greek philosopher, Empedocles had a dream. He would like to understand the world around him using pure thinking (logic) and observations (experiments). Therefore, he has created the cosmogenic theory of the four Classical Elements: earth, water, air and fire. The theory also include two forces called *Love* and *Strife* which are responsible for the interaction and transformation of the elements [43].

By applying human reason and accepting the idea that everything is composed of the above mentioned four elements which are moved by the two opposing forces allowed him to explain some of his material experience. But it was neither quantitative nor complete.

The power of human reason was put to the proof during the centuries. Scientists gave birth to several theories which emerge and then fall, because they have not stood the test of time. Through this continuous process we get closer and closer to the realization of Empedocles' dream.

The XVI. century was a turning point when scientific revolution was started and Modern Science got underway. In 1543 just before his death, Nicolaus Copernicus published his work about the heliocentric description of the universe [44]. It was a shocking paradigm shift [45] from the Ptolemaic geocentric cosmology, which had been accepted since ancient times.

The XVII. century was "an Age of all others the most inquisitive" [46] and is just as important and exciting as the previous. In 1620, Francis Bacon published the *Novum Organum Scientiarum* (New Instrument of Science), in which he declared the necessity of replacing Aristotelian deduction by Inductive Science [47]. According to Bacon's view, the experiments are the most important tools in scientific advancement. The way of knowing is "not so much by instruments as by experiments" [47] which will lead the "restoration of learning and knowledge" [48]. His followers founded The Royal Society in 1662 based on the inspiration gained from Bacon's work [49]. Since then, it is continuously active and by now, it is one of the major scientific societies.

Perhaps the most influential scientist of all time, Isaac Newton (1642-1726) was born in this period which was a perfect time for a genius. He was gifted in multiple disciplines such as history, alchemy and mathematics, but his main achievements are related to mathematics and physics.

Nature and nature's laws lay hid in night;
God said "Let Newton be" and all was light.

— *Alexander Pope*

His book the *Philosophiae Naturalis Principia Mathematica* (Principia) was first published in 1687 [50] which was a great step towards Empedocles' dream, understanding and describing the world around us. The Principia has reformed our knowledge and laid the foundation of classical or Newtonian mechanics by

introducing Newton's laws of motion and the law of universal gravitation. It describes the motion and dynamics of "slow-moving", "smaller" or "bigger", but "heavy" macroscopic objects (apples, planets etc.).

The scientific and technological development does not stopped here. Thermodynamics and electrodynamics were born and grew up along with the classical mechanics to be complete and consistent theories of science. In the end of the XIX. century it seemed that the most important problems of physics were solved.

There are more things in heaven and earth, Horatio,
Than are dreamt of in your philosophy.

— *Hamlet, Scene V*

Only a few minor points needed further clarification, for example, the Frank-Hertz experiment, black-body radiation and the existence of line spectra. These and other seemingly small issues were led to the birth of a completely new theory, quantum mechanics [51] in the beginning of the XX. century. It is a tool to describe the properties of matter and light on the atomic and subatomic scale.

At this time, Albert Einstein developed two theories, the special- and general relativity to understand the exotic behaviour of high speed (speed of light) and/or "very heavy" objects.

Thus, Empedocles' vision been achieved and the world around us can be described using different theories or their combinations depending on the characteristics ("light" or "heavy" and "slow" or "fast") of the studied objects (Figure 2.1.1) [52].

In terms of theory and characteristics, the focal points of this work will be quantum mechanics and "light" objects (electrons and nuclei). However, our results and predictions are related to heavier species (molecules) and their interactions (reactions).

By now, we are living in an era when quantitative predictions could be done about specific materials using the so called *ab initio* approach [53]. In the context of *ab initio* the applied model is more simple than the one used by Empedocles. It consist of only two type of elements (electrons and nuclei) and one force

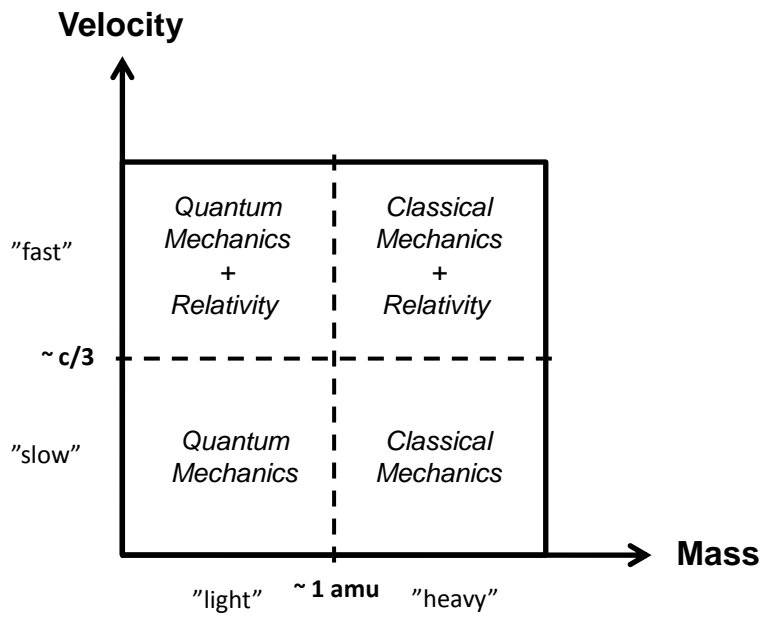


Figure 2.1.1: Theories and Their Applicability Area in Terms of Characteristics of the Studied Objects (c - Speed of Light, amu - Atomic Mass Unit) [52].

(Coulomb), although the dual nature (attraction and repulsion) of the latter is undeniable. Applying the laws of quantum mechanics on this simple system most of our physical reality at the molecular level is describable. Although, it is just an approximation, but a rather good one with which even Empedocles would be satisfied.

2.2 WHO'S WHO AND WHAT'S WHAT IN QUANTUM MECHANICS

2.2.1 A QUANTUM OF HISTORY - HISTORY OF QUANTUM

The word 'quantum' is the neutral form of the latin 'quantus', which means 'how great/ how large'. It was widespread long before the birth of quantum mechanics and not only at the fairgrounds of the Roman Empire. Long after the fall of the Roman Empire, it was used by apothecaries and physicians through the centuries in their recipes and prescriptions as a part of usually abbreviated phrases such as q.s. ('quantum satis' or 'quantum sufficit' - 'satisfactory' or 'sufficient amount'), q.p. ('quantum placet' - 'much as you like') and q.v. ('quantum vis' or 'quantum valeat' - 'as much is proper') [54]. The phrase 'quantum satis' is still used nowadays in food additive legislation [55].

In the XIX. century, the word was transferred from medical sciences to physics through the mediation of some polymath who worked as medical doctors and performed physics experiments as well. Most notably Julius Robert von Mayer and Hermann von Helmholtz, both of whom were physicians and physicists, can be suspected for the transfer. They referred to 'quantum' in the context of heat, when among others, laid the foundations of thermodynamics [56]. Moreover, Helmholtz coined the phrase 'electrical elementary quanta' or 'elementary quantum of electricity' (a.k.a. electron) as Philipp von Lenard remembered in his Nobel Lecture [57] and this term was used by Lenard and by Max Planck as well [58, 59]. Furthermore, another similar term, 'quanta of matter' was also used by Planck referring to the mass of the hydrogen atom [58, 59].

Besides the popularization of the word 'quanta' and 'quantum', Planck has a

much greater merit, the discovery of the quantization concept to explain the black-body radiation which was inexplicable by the classical approach [58, 60].

We consider (...) – this is the most essential point of the whole calculation – E to be composed of a very definite number of equal parts and use thereto the constant of nature $h = 6.55 \times 10^{-27}$ erg · sec. This constant multiplied by the common frequency ν of the resonators gives us the energy element ϵ in erg, and dividing E by ϵ we get the number P of energy elements which must be divided over the N resonators.

— *Max Planck* [61]

The basic assumption of the quantization concept is that the energy can only be transferred (absorbed or released) in "energy elements" (ϵ) which are proportional to the frequency (ν):

$$\epsilon = h\nu$$

where h is the Planck constant. However, the concept was too revolutionary to receive immediate widespread approval from the scientific community. In 1905, after five year of delay, most of the doubters were convinced about the validity of the idea by Albert Einstein's similar explanation of the photoelectric effect.

... it seems to me that the observations on "black-body radiation", photoluminescence, the production of cathode rays by ultraviolet light and other phenomena involving the emission or conversion of light can be better understood on the assumption that the **energy of light** is distributed **discontinuously** in space. (...) Each initial energy quantum of frequency ν_1 is absorbed and is – at least when the distribution density of the initial energy quanta is sufficiently low – by itself responsible for the creation of a **light quantum** of frequency ν_2 (...).

— *Albert Einstein* [62]

In his work, Einstein introduced 'light quantum' / 'Lichtquant' (a.k.a. photon) and defined it as the energy unit of electromagnetic radiation which is "localised in space move without being divided and which can be absorbed or emitted only as a whole" [62]. He also stated in the same place that the "wave theory of light which operates with continuous functions in space has been excellently justified for the representation of purely optical phenomena and it is unlikely ever to be replaced by another theory" [62]. This joint appearance of quantization and wave theory is the first indication of wave-particle duality.

In 1913, Niels Bohr combined Planck's quantization theory of radiation [61] with Rutherford's atom model [63] and proposed the Rutherford-Bohr model of the atom [64].

In the present first part of the paper the mechanism of the binding of electrons by a positive nucleus is discussed in relation to Planck's theory. It will be shown that it is possible from the point of view taken to account in a simple way for the law of the line spectrum of hydrogen.

— *Niels Bohr* [64]

According to Bohr, the atom consist of a small positively charged nucleus and around that, electrons are travel in circular orbits and they are held together by electrostatic forces and the total charge of the atom is zero. The orbits of the electron's are located at certain distances from the nucleus and assigned with definite energy levels. The energy gain and loss of electrons is associated with their transition between orbits (difference between the energy levels), but the stationary travel of the electrons in a given orbit does not lead to energy change [64, 65].

Based on his model, Bohr was able to explain the line spectra of hydrogen [64, 65], which was another great success – after the explanation of black-body radiation and photoelectric effect – of the early quantum theory. The model was extended for heavier atoms as well and it was successfully used to interpret previously inscrutable atomic properties [66].

A few years later, in 1924, Louis de Broglie coined the theory of wave-particle duality of matter [67]. His work relied on Planck's idea of quantization and Einstein's results on light ('light quantum' / 'photons') and relativity. He expressed the wave-particle duality of light, which not explicitly, but already appeared in Einstein's early work on photoelectric effect [62] and extended the idea of coexisting waves and particles to electrons and all other particles as well.

In 1924, the phrase 'quantum mechanics' was first used by Max Born in physical literature [68].

We became more and more convinced that a radical change of the foundations of physics was necessary, and thus a new kind of mechanics, for which we used the term **quantum mechanics**.

— *Max Born* [69]

The phrase itself was invented in the early 1920s, by a group of physicists including Max Born, Werner Heisenberg, Wolfgang Pauli and Pascual Jordan to indicate the groundbreaking results of the emerging new theory [69].

Although, by using Planck's quantization, several unsolved physical problems were successfully explained, but the theory behind them was phenomenological and was not traced back to fundamental concepts (first principles) and therefore, the period between 1900-1925 is called the age of old quantum theory.

In 1925 a new era begin when matrix mechanics were developed by Heisenberg, Born and Jordan [70-72].

About the same time wave mechanics was established with the introduction of the special wave function (Ψ) and the renowned non-relativistic equation by Erwin Schrödinger [73-76].

Erwin with his psi can do
Calculations quite a few.
But one thing has not been seen:
Just what does psi really mean?

— *Felix Bloch's memories* [77]

He relied on de Broglie's findings and used Hamilton's analogy between optics and mechanics to build his theory. As Felix Bloch – who was a student in Zürich at the ETH where Schrödinger worked at that time – recalled 50 years later, Schrödinger started to study de Broglie's work, because of the inspiration of Debye [77].

Once at the end of a colloquium I heard Debye saying something like: "Schrödinger, you are not working right now on very important problems anyway. Why don't you tell us some time about that thesis of de Broglie, which seems to have attracted some attention." (...) "My colleague Debye suggested that one should have a wave equation; well, I have found one!"

— *Felix Bloch's memories* [77]

Shortly thereafter Schrödinger revealed that wave and matrix mechanics are predicted the same experimental results, therefore they are equivalent theories [78].

In the same year, based on Schrödinger's work Born proposed the probabilistic interpretation of quantum mechanics [79].

Schrödinger's quantum mechanics therefore gives quite a definite answer to the question of the effect of the collision; but there is no question of any casual description. One gets no answer to the question, "what is the state after collision" but only to question, "how probably is a specified outcome of the collision" (...). I myself am inclined to give up determinism in the world of atoms. But that is a philosophical question for which physical arguments alone are not decisive.

— *Max Born* [80]

This was criticised by several prominent scientist such as Planck, Einstein, de Broglie and Schrödinger [77] and it is still an open question in theoretical physics mainly because of its philosophical aspects.

In 1927, Heisenberg discovered the uncertainty principle of quantum mechanics which states that the position of a particle and its momentum can not be known at the same time with arbitrarily high precision: the more precise the measurement of the momentum, the less precisely the position is known [81]. The principle prevails for other complementary physical properties as well (e.g. energy and time).

In the same year, quantum chemistry was born when Walter Heitler and Fritz London applied quantum mechanics in their studies on the bonding of the hydrogen molecule [82]. Their work opened a new scientific field and influenced several scientists among them Linus Pauling.

During the same period, Paul Dirac combined the theory of special relativity and quantum mechanics and deduced the relativistic wave equation (a.k.a. Dirac equation) in 1928. He discovered electron spin and predicted the existence of a particle which has a charge opposite to the electron [83].

In the early 1930s, as a culmination of the initial period, Dirac and John von Neumann formulated the mathematical basis of quantum mechanics using the theory of linear operators on Hilbert spaces [84, 85]. Quantum mechanics scarcely begun and already became one of the one most influential physical theory of the XX. century.

2.2.2 THE POSTULATES OF QUANTUM MECHANICS

As a results of Dirac's and Neumann's work, the axiomatic framework of quantum mechanics was created and six basic postulates were determined [51, 86].

Postulate I: The state of a quantum mechanical microsystem is completely described by a function, called the state or wave function, $\Psi(\boldsymbol{\tau}, t)$.

The wave function, $\Psi(\boldsymbol{\tau}, t)$ depends on time (t) and on the coordinates ($\boldsymbol{\tau}$) of the particle(s) in the studied system and contains all the information about the system that can be determined by measurements. According to the probabilistic

The following sections of the chapter were written mainly based on [51, 86, 87].

interpretation of the wave function, $\Psi^*(\boldsymbol{\tau}, t)\Psi(\boldsymbol{\tau}, t)d\boldsymbol{\tau}$ is the probability that the studied particle is in the volume element $d\boldsymbol{\tau}$ located at $\boldsymbol{\tau}$ at time t . Consequently, the wave function must satisfy certain mathematical conditions: it must be single-valued, continuous, and finite. Furthermore, in the case of a single particle, the probability of finding it somewhere in space is 1, so the wave function must satisfy the following normalization condition as well:

$$\int_{-\infty}^{\infty} \Psi^*(\boldsymbol{\tau}, t)\Psi(\boldsymbol{\tau}, t)d\boldsymbol{\tau} = 1 \quad (2.1)$$

Postulate II: Every observable known from classical mechanics are represented by linear, *Hermitian* operators in quantum mechanics.

Let's consider a physical observable A and the corresponding operator \hat{A} . The value of A is a real number, as it must be for all physical observables. For this reason, the expectation value of \hat{A} ($\langle A \rangle$) must be also real which means $\langle A \rangle = \langle A^* \rangle$. The operators which meets this criteria are called *Hermitian* operators.

Postulate III: The measured value of any physical observable of a system equal to one of the eigenvalues of the corresponding operator.

According to this postulate, if \hat{A} is the operator and a are eigenvalues, the following eigenvalue equation should be satisfied:

$$\hat{A}\Psi = a\Psi \quad (2.2)$$

Postulate IV: The expectation value of any physical observable ($\langle A \rangle$) is given by the following equation:

$$\langle A \rangle = \int_{-\infty}^{\infty} \Psi^*\hat{A}\Psi d\boldsymbol{\tau} \quad (2.3)$$

where \hat{A} is the corresponding operator and Ψ is the normalized wave function.

Postulate V: The state of a microsystem in time is given by the time-dependent Schrödinger equation:

$$i\hbar\frac{\partial\Psi(\boldsymbol{\tau}, t)}{\partial t} = \hat{H}\Psi(\boldsymbol{\tau}, t) \quad (2.4)$$

where $\hbar = h/2\pi$, h is the Planck constant (quantum of action) and \hat{H} - Hamiltonian (total energy operator).

The time-dependent Schrödinger equation was discovered by Erwin Schrödinger who studied the classical wave equation and the de Broglie relations (*vide supra*). It cannot be obtained using elementary methods, therefore it is considered as a postulate of quantum mechanics.

However, Schrödinger discovered first the time-independent version of the equation and then postulated the more general time-dependent form [86]. The time-independent Schrödinger equation applies if the state of the system is not changing in time. In this case,

$$\hat{H}\Psi(\boldsymbol{\tau}) = E\Psi(\boldsymbol{\tau}) \quad (2.5)$$

where E is the total energy of the system, while \hat{H} is the corresponding operator, the Hamiltonian.

Postulate VI: The total wave function of a microsystem must be antisymmetric for the exchange of all coordinates of identical particles with half-integer spin (fermion) and symmetric for the exchange of all coordinates of identical particles with integer spin (bozon).

This is the last postulate, the so-called antisymmetry principle from which the Pauli exclusion principle can be directly deduced.

2.3 THE BEAUTY OF APPROXIMATIONS

SCIENCE ITSELF IS BUILT ON MODELS AND APPROXIMATIONS with the goal to describe reality as accurately as possible. Approximations help us to save resources

and overcome the limitations of our theories and tools (e.g. computational power). From quantum mechanics to quantum chemistry the way is going through three main approximations.

2.3.1 NON-RELATIVISTIC QUANTUM MECHANICS

As it was noted before, Dirac deduced the relativistic wave equation, which has all the properties missing from the time-dependent Schrödinger equation. It is Lorentz invariant (space and time can be exchanged) and the spin is an intrinsic property of Dirac's theory [83, 84]. However, despite all the genuine features, the relativistic wave equation must be solved numerically, which is computationally very demanding and only feasible for small molecular systems. Therefore, usually the relativistic effects are not considered directly through the Dirac equation, but as an approximation, additional terms included into the Schrödinger equation to deal with them [51].

2.3.2 BORN-OPPENHEIMER APPROXIMATION

In 1927, Max Born and Robert Oppenheimer proposed a new description for the molecular spectra based on an approximate quantum mechanical treatment of electrons and nuclei in the molecules and this is known as Born-Oppenheimer (BO) approximation [88].

”The terms of molecular spectra are usually made up of parts of various orders of magnitude; the largest contribution comes from the electronic motion about the nuclei, then follows the contribution of the nuclear vibration, and finally that from the nuclear rotation. The basis for the possibility of such a classification obviously rests in the comparative magnitudes of nuclear and electronic masses.”

— *Born and Oppenheimer* [89]

Basically, the main idea behind the BO approximation is nothing else, but the separation of the motions of electrons and nuclei.

First of all, let's consider the non-relativistic time-independent Schrödinger equation and the corresponding Hamiltonian (\hat{H}), which is the sum of the kinetic and potential energy operators:

$$\hat{H}(\boldsymbol{\tau}) = \hat{T}(\boldsymbol{\tau}) + \hat{V}(\boldsymbol{\tau}) \quad (2.6)$$

$\boldsymbol{\tau}$ include the coordinates of nuclei (\mathbf{R}) and electrons (\mathbf{r}).

The Hamiltonian can be further broken down to the sum of the kinetic energy operators of electrons ($\hat{T}_e(\mathbf{r})$) and nuclei ($\hat{T}_N(\mathbf{R})$) and the potential energy operators of electron-electron ($\hat{V}_{ee}(\mathbf{r})$), nuclei-nuclei ($\hat{V}_{NN}(\mathbf{R})$) and electron-nuclei ($\hat{V}_{eN}(\mathbf{R}, \mathbf{r})$) interactions:

$$\hat{H}(\boldsymbol{\tau}) = \hat{T}_e(\mathbf{r}) + \hat{T}_N(\mathbf{R}) + \hat{V}_{ee}(\mathbf{r}) + \hat{V}_{NN}(\mathbf{R}) + \hat{V}_{eN}(\mathbf{R}, \mathbf{r}) \quad (2.7)$$

In the first step of the BO approximation, the nuclei are fixed somewhere in the space and therefore, the kinetic energy of nuclei is neglected ("clamped nuclei" approximation). It can be done, because of the big difference between the mass of an electron and a nucleus and therefore, there is a huge difference between their motility as well in favor of the electron. However, the electron-nuclei interactions should be taken into account, because the electrons are still "feel" the potential of the fixed nuclei. Furthermore, the nuclei-nuclei interactions are constant when the nuclei are in a given position of space.

The Hamiltonian can be written as

$$\hat{H}(\boldsymbol{\tau}) = \hat{H}_e(\boldsymbol{\tau}) + \hat{T}_N(\mathbf{R}) \quad (2.8)$$

This and other assumptions will lead us to the electronic or "clamped nuclei" Schrödinger equation

$$\hat{H}_e \Psi_e(\boldsymbol{\tau}) = E_e(\mathbf{R}) \Psi_e(\boldsymbol{\tau}) \quad (2.9)$$

where E_e is the electronic energy at a given position of nuclei. This equation is solved in the first step of the BO approximation.

Thereafter the nuclear Schrödinger equation is described as follows

$$(\hat{T}_N + E_e)\Psi_N(\mathbf{R}) = E\Psi_N(\mathbf{R}) \quad (2.10)$$

where E_e corresponds to the potential energy of nuclei, while E is the total energy of the system. Thus, the $E_e(\mathbf{R})$ function could be called as the *potential energy (hyper)surface* (PES) of the molecule. The appearance of PES is a consequence of the BO approximation and it comes from the separation of electronic and nuclear motion. If there is no BO approximation, a molecule can be described as an entity which exist in different energy states, but potential energy surfaces can not be assigned.

Every point of the PES is a solution of the electronic Schrödinger equation (important to note that it is not equivalent with the total Schrödinger equation, 2.5) and corresponds to a given configuration (geometry) of the nuclei of the molecule. For a molecule with N atoms, $3N$ total coordinates can be considered (x, y, z for each atom). But there is no need to taken into account translations and rotations (altogether 6 coordinates for non-linear systems), because the potential energy remains the same if a molecule is rotated and/or translated in a field free space. Therefore, $E_e(\mathbf{R})$ depends on $3N-6$ coordinates. Consequently, the $3N-6$ internal coordinates satisfactory to describe the molecular structure.

The PES relatively easily computable and provide enormous help to understand important chemical concepts, such as stability, transition states etc. (Figure 2.3.1).

As in the case of other functions, the *stationary points* (minima, maxima and inflection points) of the PES could be located by calculating the first partial derivative of $E_e(\mathbf{R})$ with respect to all variables and if it is zero in each case, a *stationary point* is found.

$$\sum_{i=1}^{3N-6} \frac{\partial E_e(\mathbf{R})}{\partial R_i} = 0 \quad (2.11)$$

These points can be distinguished by calculating the second derivatives ($\frac{\partial^2 E_e(\mathbf{R})}{\partial^2 R_i}$) and analyzing their signs. If the second derivatives are positive or zero the ana-

lyzed point is a minima. These points on the *surface* are represents stable (reactants, products etc.) or quasi-stable (intermediates) species and they are located at the bottom of the "valleys" on the PES (Figure 2.3.1, A and B). By moving from these points in any direction (slightly changing the geometry) the energy is going to be higher. If the second derivatives are positive in each case except one, a first order saddle point is located on the surface (Figure 2.3.1, TS). The points with such properties are transition states along the corresponding reaction coordinate. These points are minima in each directions except one, from which they are maxima (Figure 2.3.1, TS).

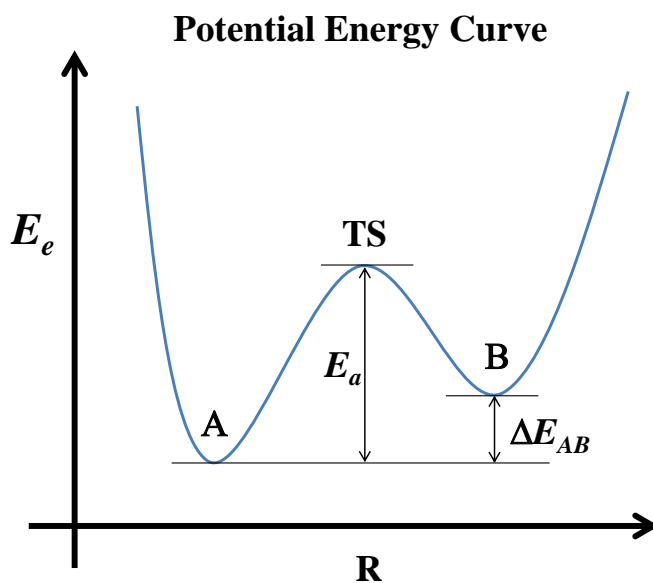


Figure 2.3.1: Potential Energy Curve - 2D Cut of a Potential Energy Surface. E_e - electronic energy (potential energy); E_a - activation energy; ΔE_{AB} - relative energy; TS - transition state (first order saddle point); A, B - stable conformations (minima); R - coordinates.

Finally, in the second step of the Born-Oppenheimer approximations the nuclear Schrödinger equation (eq. 2.10) will be solved in order to get the total energy

of the system along with the vibration and rotations of the nuclei.

To sum up the Born-Oppenheimer approximation: the significant difference in the relative masses of an electron and a nucleus enable us to divide the time independent Schrödinger equation into two independent equations, the electronic (2.9) and nuclear Schrödinger equation (2.10).

2.3.3 ONE-ELECTRON APPROXIMATION AND HARTREE-FOCK METHOD

The previously introduced approximations led us to the electronic Schrödinger equation (eq. 2.9), which can be rewritten into the following form:

$$\hat{H}_e \Psi_e(\boldsymbol{\tau}) = (\hat{T}_e(\mathbf{r}) + \hat{V}_{ee}(\mathbf{r}) + \hat{V}_{NN}(\mathbf{R}) + \hat{V}_{eN}(\mathbf{R}, \mathbf{r})) \Psi_e(\boldsymbol{\tau}) = E_e(\mathbf{R}) \Psi_e(\boldsymbol{\tau}) \quad (2.12)$$

It is impossible to find the exact solution of this equation for a fully interacting many-electron system. Therefore, approximate solutions were developed. One of the most suitable method to handle the many-electron problem is the one-electron approximation, when each electron is considered separately [51, 86, 87]. In order to achieve this, the electronic wave function ($\Psi_e(\mathbf{r})$) must be separated into the product of one-electron wave functions ($\psi_i(\mathbf{i})$) which is known as Hartree Product [51, 86]

$$\Psi_e(\mathbf{r}) = \Psi_e(\mathbf{1}, \mathbf{2}, \dots, \mathbf{n}) \rightarrow \psi_1(\mathbf{1})\psi_2(\mathbf{2})\dots\psi_n(\mathbf{n}) \quad (2.13)$$

in which the one-electron wave functions, e.g. $\psi_1(\mathbf{1})$, only depends on the coordinates of the respective electron.

The total wave function and within that the electronic part must satisfy the anti-symmetry principle (see above **Postulate VI**). Therefore, the wave function must changes sign if the coordinates of two electrons exchanged [51, 86].

$$\Psi_e(\mathbf{r}) = \Psi_e(\mathbf{1}, \mathbf{2}, \dots, \mathbf{n}) \rightarrow -\Psi_e(\mathbf{2}, \mathbf{1}, \dots, \mathbf{n}) = -\Psi_e(\mathbf{r}) \quad (2.14)$$

This criteria must be fulfilled with the one-electron product wave function as

well. However, a simple product wave function is not antisymmetric, as one can see for a two electron system ($\Psi_e(\mathbf{1},\mathbf{2})$).

$$\Psi_e(\mathbf{1},\mathbf{2}) = \psi_1(\mathbf{1})\psi_2(\mathbf{2}) \rightarrow \psi_1(\mathbf{2})\psi_2(\mathbf{1}) \neq -\Psi_e(\mathbf{2},\mathbf{1}) \quad (2.15)$$

For this reason, a linear combination used which satisfy the criteria. For two electrons such a linear combination could be the following

$$N[\psi_1(\mathbf{1})\psi_2(\mathbf{2}) - \psi_1(\mathbf{2})\psi_2(\mathbf{1})] \quad (2.16)$$

where N is a normalization constant (for 2 electrons it is $1/\sqrt{2}$). This satisfies the antisymmetry requirement and it has another very good feature, it can be rewritten as a determinant

$$N[\psi_1(\mathbf{1})\psi_2(\mathbf{2}) - \psi_1(\mathbf{2})\psi_2(\mathbf{1})] = N \begin{vmatrix} \psi_1(\mathbf{1}) & \psi_1(\mathbf{2}) \\ \psi_2(\mathbf{1}) & \psi_2(\mathbf{2}) \end{vmatrix} \quad (2.17)$$

which is very helpful when a system with many electrons must to be handled [51, 86]. Furthermore, this prevent two electrons to be at exactly the same position (at the same orbital at the same time), because

$$N \begin{vmatrix} \psi_1(\mathbf{1}) & \psi_1(\mathbf{1}) \\ \psi_2(\mathbf{1}) & \psi_2(\mathbf{1}) \end{vmatrix} = 0 \quad (2.18)$$

and thus, it satisfies the Pauli exclusion principle which is a consequence of the antisymmetry principle (*vide supra*). The generalization to n electrons

$$\Psi_e(\mathbf{1}, \mathbf{2}, \dots, \mathbf{n}) = \frac{1}{\sqrt{n!}} \begin{vmatrix} \psi_1(\mathbf{1}) & \psi_1(\mathbf{2}) & \dots & \psi_1(\mathbf{n}) \\ \psi_2(\mathbf{1}) & \psi_2(\mathbf{2}) & \dots & \psi_2(\mathbf{n}) \\ \vdots & \vdots & \ddots & \vdots \\ \psi_n(\mathbf{1}) & \psi_n(\mathbf{2}) & \dots & \psi_n(\mathbf{n}) \end{vmatrix} \quad (2.19)$$

If the one-electron wave functions ($\psi_i(i)$, orbital functions, depends only on the coordinates of the particles) are replaced by the corresponding spin-orbital functions ($\varphi_i(i) = \psi_i(i)\eta(i)$, depends on coordinates and spin, as well, where $\eta(i)$ can

be $\alpha(i)$ or $\beta(i)$) and the electrons are paired to have the same orbital wave functions, but differ in their spin, the resulting new determinant is the so-called Slater determinant [90].

$$\Phi_e(\mathbf{1}, \mathbf{2}, \dots, \mathbf{n}) = \frac{1}{\sqrt{n!}} \begin{vmatrix} \varphi_1(\mathbf{1})\alpha(\mathbf{1}) & \varphi_1(\mathbf{2})\alpha(\mathbf{2}) & \dots & \varphi_1(\mathbf{n})\alpha(\mathbf{n}) \\ \varphi_1(\mathbf{1})\beta(\mathbf{1}) & \varphi_1(\mathbf{2})\beta(\mathbf{2}) & \dots & \varphi_1(\mathbf{n})\beta(\mathbf{n}) \\ \vdots & \vdots & \ddots & \vdots \\ \varphi_{n/2}(\mathbf{1})\beta(\mathbf{1}) & \varphi_{n/2}(\mathbf{2})\beta(\mathbf{2}) & \dots & \varphi_{n/2}(\mathbf{n})\beta(\mathbf{n}) \end{vmatrix} \quad (2.20)$$

As a consequence of this formulation, each electron is associated with every orbital and therefore, they are indistinguishable, which is consistent with the general quantum mechanical considerations.

As the separation of the wave function is finished, the Hamiltonian (\hat{H}_e) must be also separated into one-electron operators. As it was shown above, the electronic Hamiltonian consist of four terms and among them three groups can be identified depending on the number of electrons involved in them:

- 1) zero-electron: $\hat{V}_{NN}(\mathbf{R})$
- 2) one-electron: $\hat{V}_{eN}(\mathbf{R})$ and $\hat{T}_e(\mathbf{r})$
- 3) two-electron: $\hat{V}_{ee}(\mathbf{r})$.

The zero-electron term is a constant, because it include only the nuclei-nuclei interactions (*vide supra*), while the one-electron part is obviously not problematic for the one-electron separation. The only term which causing problems is the one which describe the electron-electron interactions ($\hat{V}_{ee}(\mathbf{r})$) and as such term, it include information about two electrons at the same time. This can be overcome by the usage of a hypothetical mean field potential (effective potential, $\hat{V}_{e1}^{eff}(\mathbf{i})$) with which the effects of all the electrons in the system will be approximated.

$$\hat{V}_{ee}(\mathbf{r}) \rightarrow \sum_{i=1}^n \hat{V}_{e1}^{eff}(\mathbf{i}) \quad (2.21)$$

All electron in the system will be described as if they are moving individually in

this effective potential. Thus, the electronic Hamiltonian can be approximated as

$$\hat{H}_e \approx \sum_{i=1}^n [\hat{h}_{e1}(\mathbf{i}) + \hat{V}_{e1}^{eff}(\mathbf{i})] + \hat{V}_{NN}(\mathbf{R}) = \sum_{i=1}^n \hat{F}(\mathbf{i}) \quad (2.22)$$

where $\hat{h}_{e1}(\mathbf{i})$ is the one-electron part of the electronic Hamiltonian, $\hat{V}_{NN}(\mathbf{R})$ represents the nuclear-nuclear interaction potential (*vide supra*), while $\hat{V}_{e1}^{eff}(\mathbf{i})$ is the effective one-electron potential and $\hat{F}(i)$ is the Fock operator [51].

This is the so-called *independent particle model*, which computationally behaves as a one-electron model notwithstanding that all electron states must be known to calculate the effective potential. The goodness of the model highly depends on how accurately approximated the real two electron potential by the effective one-electron potential (2.21).

Based on the results of the one-electron approximation (Slater determinant wave function and one-electron Hamiltonian), the approximate solution of the electronic Schrödinger equation can be given by the Hartree-Fock method [87]. This is dealing with the Hartree-Fock equations

$$\hat{F}(\mathbf{i})\varphi_i = \varepsilon_i\varphi_i \quad (2.23)$$

where φ_i (orbitals) are one-electron spin-orbital functions (to construct the Slater determinant, *vide supra*) and ε_i are orbital energies.

The Hartree-Fock method minimize the energy to get the "best" approximation (Slater determinant wave function) of the wave function by determining an appropriate spin-orbital set [87].

To solve the Hartree-Fock equations, the Fock operator which include the effective one-electron potential ($\hat{V}_{e1}^{eff}(\mathbf{i})$) must be known. Therefore, $\hat{V}_{e1}^{eff}(\mathbf{i})$ needs to be selected, but the selection must be done carefully to get the best approximation of the electron-electron interactions (*vide supra*). The best selection of the effective potential can be described by two terms, the Coulomb and the exchange term,

which can be associated with the corresponding operators, \hat{J}_{ij} and \hat{P}_{ij} , respectively.

$$\hat{V}_{e1}^{eff}(\mathbf{i}) = \sum_j (\hat{J}_{ij} - \hat{P}_{ij}) \quad (2.24)$$

The Coulomb term describe the electrostatic interaction between an electron in an orbital ($\varphi_j(j)$) and the average charge distribution of the other electrons, while the exchange term arise from antisymmetry of the wave function and it includes a piece of flavor of correlation between electrons.

Thus, the Fock operator contain four terms:

$$\sum_{i=1}^n \hat{F}(\mathbf{i}) = \sum_{i=1}^n [\hat{h}_{e1}(\mathbf{i}) + \sum_j (\hat{J}_{ij} - \hat{P}_{ij})] + \hat{V}_{NN}(\mathbf{R}) \quad (2.25)$$

Among these, both the Coulomb and the exchange operator include in their expression one-electron spin-orbital wave functions ($\varphi_j(j)$), therefore the Fock operator also depend on the orbitals, what we are trying to determine with its help.

Thus, to find the above mentioned appropriate (energy minimum) spin-orbital set (\rightarrow "best" Slater determinant wave function), an initial orbital set ($\varphi_i^o(i)$) is necessary with which an initial Fock operator (\hat{F}_o) can be defined. Then, the Hartree-Fock equations can be solved using this initial guess. The solution provide a new set of orbitals ($\varphi_i^1(i)$) from which a new Fock operator (\hat{F}_1) can be constructed. This process can be repeated as long as need to reach convergence and by the iterative refinement of the initial guess a minimum of the electronic energy achived. Therefore, the Hartree-Fock method is also called *self-consistent-field* (SCF) procedure.

Up to this point, three main approximations used to simplify the initial relativistic quantum mechanical problem and to get a model where the Hartree-Fock method come into operation. The approximations advantageous, but they are also the origin of limitations of the method and therefore the calculated Hartree-Fock electronic energy (E_{HF}) differ from the exact electronic energy of the system (E_e). To overcome the limitations, several possible ways exist such as post-Hartree-Fock approach and semi empirical quantum chemistry.

In the post-Hartree-Fock approach to increase the accuracy of the calculations the correlation energy (E_{corr}) can be computed which is almost completely ignored by the Hartree-Fock method (no electron correlation, except the exchange term (*vide supra*), or even relativistic effects can be included. The semiempirical quantum chemical methods highly rely on parametrization of their formulas to reproduce the experimental values as close as possible.

However, no matter what kind of method employed, the main goal of (*applied*) *quantum chemistry* is to achieve a quantum mechanical description which can be used to study real chemical problems.

2.4 DENSITY FUNCTIONAL THEORY

2.4.1 THE ORIGIN

Density functional theory (DFT) is one of the most widely used computational tool in modern applied quantum chemistry. The basic concept of DFT appeared in the early days of quantum mechanics [91]. In 1927, shortly after the invention of the Schrödinger equation [73], Llewellyn Thomas and Enrico Fermi developed a model (Thomas-Fermi model) to approximately describe the electron density (ρ) and the ground state energy ($E(n)$) for systems which have large number of electrons (n) [92, 93]. They have proposed the idea to define the energy of a system as a function of the total electron density ($E(\rho)$).

More than 20 years passed until the same basic idea was applied again by John Slater in 1951, to develop the Hartree-Fock-Slater method [94], which was initially proposed as an approximation of the Hartree-Fock theory, but later recognised as an important milestone of density functional theory [95].

Notwithstanding the correlation between the energy and the electron density revealed by these methods, but the real proof of this idea arrived only in 1964, when Pierre Hohenberg and Walter Kohn published their paper about Inhomogeneous Electron Gas [96].

2.4.2 THE PROOF - HOHENBERG-KOHN THEOREMS

Hohenberg and Kohn proposed and proved two theorems [96] to demonstrate that the electron density of a non-degenerate electronic system unambiguously define the ground-state energy and the corresponding electronic properties [95].

The *electron density* ($\rho(\mathbf{r})$) is a function which describe the probabilistic distribution of electrons in space [51].

$$\int_{-\infty}^{\infty} \rho(\mathbf{r}) d\mathbf{r} = n \quad (2.26)$$

where n is the number of electrons in the system. If there is an external potential ($V_{ext}(\mathbf{r})$) which affect the electrons in the system, the electron density also affected and therefore, it depends on the external potential.

Considering the electronic Hamiltonian of a molecule (*vide supra*, 2.19), the potential which describe the electron-nuclei interactions ($\hat{V}_{eN}(\mathbf{R}, \mathbf{r})$) is an external potential from the viewpoint of the electrons. The others, the kinetic energy operator ($\hat{T}_e(\mathbf{r})$) and the electron-electron potential operator ($\hat{V}_{ee}(\mathbf{r})$) represents internal, electron dependent actions, while the nuclei-nuclei ($\hat{V}_{NN}(\mathbf{R})$) part is constant and no need to deal with it (*vide supra*). Thus, the electron density of the molecule depends on the $\hat{V}_{eN}(\mathbf{R}, \mathbf{r})$ potential ($V_{ext}(\mathbf{r})$). Therefore, if the external potential is known the electron density can be unambiguously determined.

Hohenberg and Kohn realised the reverse statement which is known as their *first theorem* and proved its validity [96] (Figure 2.4.1).

Theorem I: The external potential ($V_{ext}(\mathbf{r})$) affecting the electrons in the system, and the total energy (E), is a unique functional of $\rho(\mathbf{r})$.

Consequently, if the electron density of a system is known the external potential and the total energy can be determined unequivocally.

Then, in the *second theorem* the ground state electron density is connected with the total energy.

Hohenberg-Kohn Theorem I.

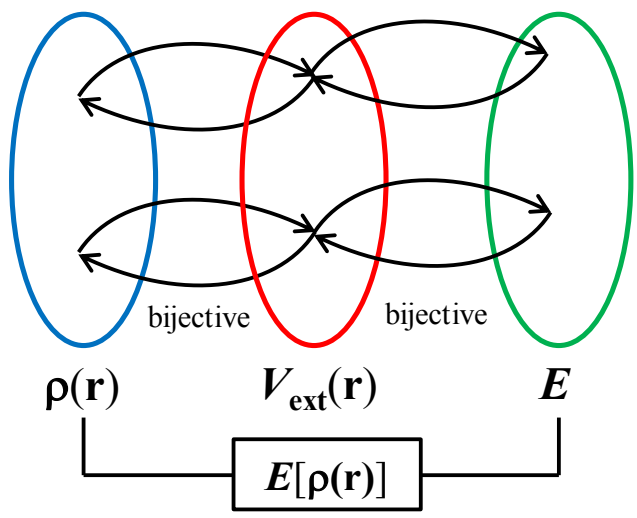


Figure 2.4.1: Schematic Representation of the first Hohenberg-Kohn Theorem.

Theorem II: It is proved that there exists a universal functional of the density, $F[\rho(\mathbf{r})]$, independent of $V_{ext}(\mathbf{r})$, such that the expression

$$E = \int V_{ext}(\mathbf{r})\rho(\mathbf{r})d\mathbf{r} + F[\rho(\mathbf{r})] \quad (2.27)$$

has as its minimum value the correct ground-state energy associated with $V_{ext}(\mathbf{r})$ [96]. Here $F[\rho(\mathbf{r})]$ includes the kinetic and the electron-electron interaction terms.

These theorems laid down and cemented the theoretical basis of DFT and expedite the development of the area.

2.4.3 KOHN-SHAM FORMALISM

The foundations of the current formalism of DFT is developed just a year after the publication of the Hohenberg-Kohn theorems. Kohn, in collaboration with Lu Jeu Sham, coined a way to solve the Hohenberg-Kohn theorems (Kohn-Sham formalism) for real systems (interacting electrons) [97]. For their approximation, they have used a special virtual non-interacting system and assumed that its overall ground-state $\rho(\mathbf{r})$ is equal to the density of the real interacting system.

The ground-state electron density ($\rho(\mathbf{r})$) was defined at a location \mathbf{r} by the following expression

$$\rho(\mathbf{r}) = \sum_{i=1}^n |\varphi_i^{KS}(\mathbf{r})|^2 \quad (2.28)$$

where $\varphi_i(\mathbf{r})^{KS}$ Kohn-Sham orbitals which can be calculated by solving the Kohn-Sham equations (2.29).

$$\hat{h}^{KS}(\mathbf{i})\varphi_i^{KS} = \varepsilon_i^{KS}\varphi_i^{KS} \quad (2.29)$$

where $\hat{h}^{KS}(\mathbf{i})$ represents the Kohn-Sham Hamiltonian, ε_i^{KS} is the Kohn-Sham orbital energy.

Thus, by using the above mentioned virtual system with non-interacting electrons, the kinetic energy term ($\hat{T}_e[\rho(\mathbf{r})]$) and the electron-electron interaction energy ($\hat{V}_{ee}[\rho(\mathbf{r})]$) of the real system can be written as the sum of the kinetic energy of the virtual system ($\hat{T}_e^{virt}[\rho(\mathbf{r})]$), the classical electron-electron repulsion in the virtual system ($\hat{V}_{ee}^{virt}[\rho(\mathbf{r})]$) and a correction term ($E^{XC}[\rho(\mathbf{r})]$), called exchange correlation energy to plug-in the electron-electron interactions into the formalism. Therefore, the Kohn-Sham Hamiltonian can be written as

$$\hat{h}_i^{KS} = \hat{T}_e^{virt}[\rho(\mathbf{r})] + \hat{V}_{ee}^{virt}[\rho(\mathbf{r})] + \hat{V}_{ext}[\rho(\mathbf{r})] + \hat{V}^{XC}[\rho(\mathbf{r})] \quad (2.30)$$

After all of these considerations, everything is known in equation 2.30, except one term, the exchange correlation term ($\hat{V}^{XC}[\rho(\mathbf{r})]$), but to solve the Kohn-Sham equations, it also needs to be determined.

2.4.4 THE FOCAL POINT - EXCHANGE CORRELATION

Thus, we reached the focal point of the Kohn-Sham formalism, how to deal with the exchange correlation term and the corresponding energy functional ($E^{XC}[\rho(\mathbf{r})]$). $\hat{V}^{XC}[\rho(\mathbf{r})]$ is the functional derivative of $E^{XC}[\rho(\mathbf{r})]$, so if the energy is determined easy to identify the corresponding potential as well. The solution of the Kohn-Sham equations iterative and resemble the features of the Hartre-Fock method. However, to start the calculations as mentioned before, \hat{V}^{XC} needs to be computed and included into the Kohn-Sham Hamiltonian. For this reason, the form of the electron density dependence of E_{XC} must be identified.

Usually, the exchange correlation energy functional is divided into two separate terms, an exchange ($E^X[\rho(\mathbf{r})]$) and a correlation term ($E^C[\rho(\mathbf{r})]$), even though this separation is not generally accepted by the scientific community [95]. The E_X represents the interactions between electrons of the same spin, while E_C is associated with the electron-electron interactions in case they have opposite spin.

$$E^{XC}[\rho(\mathbf{r})] = E^X[\rho(\mathbf{r})] + E^C[\rho(\mathbf{r})] \quad (2.31)$$

were $E^X[\rho(\mathbf{r})]$ exchange functional, $E^C[\rho(\mathbf{r})]$ correlation functional.

The DFT approximations can be separated into distinct groups based on the way of the electron density dependence of their exchange and correlation functionals. The functionals can depend on the local electron density (ρ) or they could be built in a way to depend on ρ itself and its gradient $\Delta\rho$ as well.

2.4.5 JACOB'S LADDER OR THE ZOO OF DFT?

Over the past 50 years which has elapsed from the introduction of the Kohn-Sham formalism, a huge number of different density functional approximations were developed. Especially from the 1990s the application and development of density functional theory is flourishing and the range of possibilities in the field drastically enlarged [95]. Not only the number of approximations increased, but the level of sophistication is also lifted up which led John Perdew to resemble the progress of DFT research to Jacob's Ladder [98] (Figure 2.4.2).

”Jacob left Beer-Sheba and went toward Haran. He came to a certain place and stayed there for the night, because the sun had set. Taking one of the stones of the place, he put it under his head and lay down in that place. And he dreamed that there was a ladder set up on the earth, the top of it reaching to heaven; and the angels of God were ascending and descending on it.”

— *Genesis 28:10-12* [99]

As one can see in the ”ladder” (Figure 2.4.2), there are five types of DFT approximations: 1) Local (Spin) Density Approximation (LDA/LSDA), 2) Generalized Gradient Approximation (GGA), 3) Meta Generalized Gradient Approximation, 4) Hybrid Methods (Hyrid GGA and Hybrid Meta GGA) and 5) Fully Non-Local approximation.

In an ideal case, a functional could deal with every applications regardless of whether the problem is physical or chemical. Unfortunately, there is no general functional and the discovery is unlikely even in the distant future. Therefore, the

Jacob's Ladder of DFT

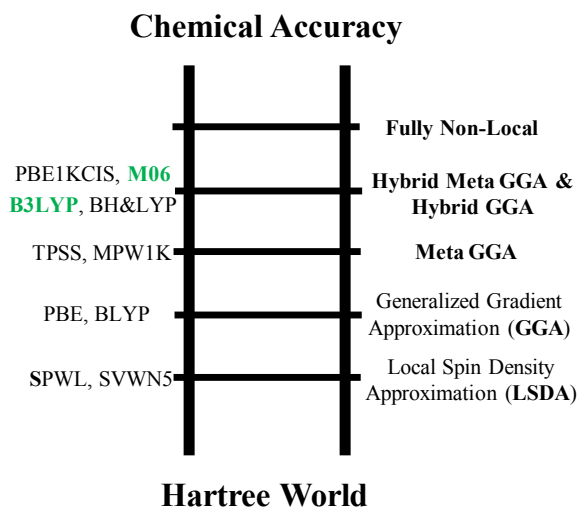


Figure 2.4.2: Jacob's Ladder of Density Functional Approximations [95, 98].

main goal of DFT method development is to create area specific functionals which could handle a certain set of problems for which they are designed. This is the reason why nowadays a plethora of different functionals available, each of which works well for certain problems, but fails for others [100]. The available functionals are not equally popular within the scientific community.

Some of the most common functionals are also indicated on the "Ladder" (Figure 2.4.2) and among these B₃LYP (Becke, 3 parameter, Lee-Yang-Parr) [101–103] and Mo6 [100] needs special attention.

It can be say without exaggeration that B₃LYP is the most successful functional of all time (if the successfulness is measured by the number of publications) [95]. It was used in numerous studies and due to its wide range of applicability (even if it is not perform well in some cases [95]), it has become a point of reference in applied density functional theory.

Mo6 is a member of a group called Minnesota Functionals (Myz) developed by Prof. Donald Truhlar and his co-workers. It has three sister functionals (Mo6-L

[104], Mo6-2X [100] and Mo6-HF [100]) and they are forming the Mo6 family of hybrid meta GGAs [100]. The Minnesota Functionals are relatively newly developed (the oldest is published in 2005 [105]) and they gained popularity thanks to their good performance on various system. Furthermore, their novelty and the continuous development of these group of functionals very appealing for the computational chemistry community. The Mo6 is parametrized for the study of non-covalent interactions, main-group thermochemistry and kinetics, inorganometallic and organometallic thermochemistry [100]. Nowadays, this is the most popular and probably the best choice for computational organometallic studies. This is the reason why it was also selected in some of our own computational investigations which will be presented later in the following chapters.

2.5 BASIS SETS AND BASIS FUNCTIONS

2.5.1 ATOMIC ORBITALS

In general, every problem is solved in a space (e.g. 3D linear vector space) which is defined by a collection of vectors (e.g. $\hat{i}, \hat{j}, \hat{k}$) called basis set. From a quantum chemical point of view, a basis set is a bunch of one-particle functions which used to build atomic and/or molecular orbitals ($\hat{\psi}_i$) by linear combinations. Let's consider χ_μ as an appropriate selection of functions (basis set) and their linear combinations to express $\hat{\psi}_i$ orbital functions,

$$\hat{\psi}_i = \sum_{\mu=1}^m c_{i\mu} \chi_\mu \quad (2.32)$$

where $c_{i\mu}$ scalar. The number of functions (m) and their "quality" (proper shape, ease of computation) highly affect the goodness of the orbital descriptions and therefore the calculations [51]. Theoretically any function can be selected, but the "quality" criteria limit the scope of suitable functions. Usually, the selected basis functions are atomic orbitals (AO) centered on atoms, but exists other applicable options (e.g. plane wave basis sets for periodic systems).

The atomic orbitals are convenient and the corresponding molecular orbitals (MO) can be built based on their linear combinations (LCAO). There are two main atomic orbital function families the *Slater-type orbitals* (STO) [106] and the *Gaussian-type orbitals* (GTO) [107] (Figure 2.5.1).

The Slater functions (S_{AO}) are originated from the analytical solutions of the Schrödinger equation of the hydrogen atom [106]. The general formula of the STOs can be given as

$$S_{AO} = N e^{-\zeta r} \quad (2.33)$$

where N is a normalization constant, ζ represents varied parameters which controls the width of the orbital and r is the radial (distance) parameter. This type of

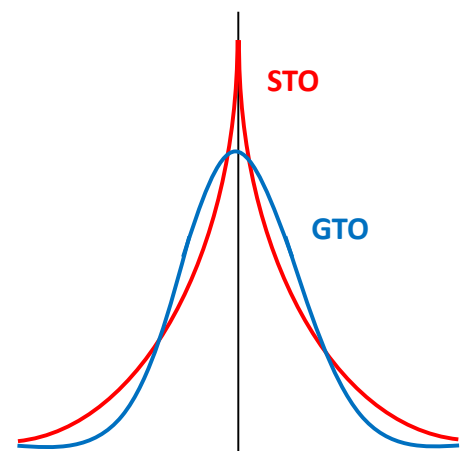


Figure 2.5.1: Schematic Comparison of Slater-type (STO) and Gaussian-type Orbitals (GTO).

functions have a rather good shape (H-atom-like and correct short/long range behaviour, Figure 2.5.1), but computationally demanding to deal with them. Therefore, a modification was proposed to change their formula to a *Gaussian-like* form [107]

$$G_{AO} = Ne^{-\zeta r^2} \quad (2.34)$$

which is very easy to compute (the product of two Gaussians is also a Gaussian) and therefore, more suitable for practical purposes [51]. The shape and the behaviour of these functions are different from the Slater functions (Figure 2.5.1), but the computational benefits significantly compensate the disadvantageous properties. Furthermore, STOs (and therefore their advantageous properties) can be approximated by the linear combination of several GTOs:

$$S_{AO} \approx \sum_{\mu} d_{\mu} G_{AO}^{\mu} = CGTO_{AO} \quad (2.35)$$

where d_{μ} optimized coefficients, while G_{AO}^{μ} Gaussian functions. The Gaussians

used in the approximation of STOs are called primitive functions, while the final basis is the *contracted* Gaussian-type orbital (CGTO) basis.

Several different basis set types used and they can be differentiated based on the number of functions associated with each atomic orbital. In the simplest case (minimal basis set), only one basis function (STO, GTO or CGTO) assigned to each AO. In case of two, three or more associated basis functions the basis set is called double-, triple-zeta or N-zeta. A special type of basis set is the split-valence basis in which the number of basis functions are differ for the core and the valence atomic orbitals. For example, in the case of 6-31G which is Pople's split-valence double-zeta basis set, the core orbital is a CGTO made of 6 primitive Gaussians, while the valence orbitals are described by two basis functions (double-zeta) each of them CGTOs (made from three primitive Gaussians and one primitive Gaussian). Furthermore, *polarization* (* - in Pople's notation) and *diffuse* (+ - in Pople's notation) functions are often used to increase the reliability of the basis sets (e.g. weak interactions, anionic systems) [51].

2.5.2 PSEUDOPOTENTIALS

Chemical transformations of molecules highly depend on the valence electrons. The core electrons are not involved in these processes, but affect the corresponding orbitals. The computational effort can be reduced significantly by focusing only on the valence electrons and approximate the effect of the core electrons. The core electrons are approximated with *pseudopotentials* or *effective core potentials* (ECPs). If these functions are originated from relativistic calculations the ECPs could include relativistic effects, which can be important in molecules with heavy elements and not necessarily need to apply relativistic theory to the rest of the system. There are two are very popular ECP types in the current computational chemistry literature, the Stuttgart-Dresden (SDD) energy-consistent effective core potentials [108, 109] and the Los-Alamos National Laboratory (LANL) shape-consistent effective core potentials (e.g. LANL2DZ - valence electrons are handled with double-zeta quality) [110–112]. These functions are inevitable to

reliably handle metal containing species by means of computational chemistry calculations (e.g. computational organometallic chemistry).

2.6 MODEL CHEMISTRIES

In modern quantum chemical research the level of theory defined by two separated, but still connected approximations: the selected calculation procedure (method) and the applied basis set. The combination of these two approximations are also called *theoretical model chemistry* [51]. The methods (Hartree-Fock, post-Hartree-Fock, Density Functional Theory etc.) are different in the way of their approximate solution of the Schrödinger equation. The accuracy, computational cost and resource requirements (e.g. memory) can significantly vary between the different methods. The level of theory applied for a calculation usually written as method/basis-set (e.g. HF/3-21G, B₃LYP/6-31G*). This notation clearly defines the applied approximations used during the quantum chemical calculations.

Further refinement of the calculations can be done by means of single point (SP) energy calculations. In this case, a geometry optimization performed in a "lower" level of theory, than the resulted optimized configuration of nuclei used to calculate the energy of the system at a "higher" level of theory. To specify the entire level of calculations the method-SP/basis-set-SP//method-geom/basis-set-geom notation used, where method-geom/basis-set-geom is the level of the geometry optimization.

2.7 SOLVENT MODELS

To model a chemical reaction in a realistic manner, the corresponding environmental factors (temperature, solvent effects etc.) must be also taken into account. Especially, the selection of an appropriate description of solvent effects (interaction between solvent and solute) is important, because most of the applied chemical synthetic protocols involve solvents [113].

Schematic Comparison of Solvent Models

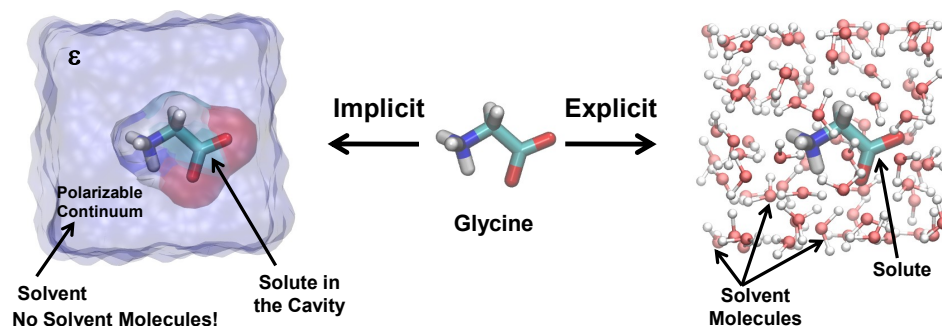


Figure 2.7.1: Schematic Comparison of Implicit and Explicit Solvation Models.

Solvent effects can be handled explicitly, implicitly or in a mixed/combined mode. In the case of the explicit treatment, solvent molecules are introduced into the calculated system and computed at the same (QM approach) or different level of theory (QM/MM approach) as the compounds of interest (Figure 2.7.1). In contrast implicit models represents the solvent as a polarizable continuous medium which has a dielectric constant (ϵ) and does not include individual (“explicit”) solvent molecules (Figure 2.7.1). In the combined mode, there are solvent molecules around the solute in the system, but the bulk phase is treated implicitly, as a polarizable continuum.

The main advantage of an implicit model is the significantly cheaper computational cost compare to an explicit model. However, specific solute-solvent interactions can’t computed (e.g. hydrogen bonds), thus in such cases where these interactions are important a combined approach (explicit introduction of a few solvent molecules) is recommended.

The electrostatics based solute-solvent interactions are considered in the implicit models. The solute is immersed into the continuum and a cavity is generated (Figure 2.7.1). Inside this cavity the charge distribution of the solute polarizes the continuum, which is back-polarizes the solute charge distribution. This is a self-

consistent process, which can be solved with an iterative procedure [114].

The properties of the cavity (shape and size) can be defined in various ways, but in any case it should exclude the solvent and keep as much as possible from the solute charge distribution within its boundaries [114].

In many cases, one of the main goal of the calculations is to determine the solvation free energy (ΔG_{sol}).

$$\Delta G_{sol} = \Delta G_{el} + G_{rep} + G_{dis} + G_{cav} + \Delta G_{tm} + P\Delta V \quad (2.36)$$

To get this quantity, the free energy of the solvated system is measured and compared to the sum of the free energies of the separated solute-solvent systems, the pure unperturbed liquid and the solute molecule(s) in gas phase.

In the expression G_{cav} is the cavity formation term (energy needs to form a suitable cavity within the liquid), ΔG_{el} electrostatic term, G_{rep} repulsion (it takes into account the presence of the cavity), G_{dis} dispersion term, G_{tm} free energy contribution (corresponds to the thermal motion of nuclei) and $P\Delta V$ cratic term (zero at standard states).

Several implicit models developed, within which six different groups of methods can be differentiated: (1) the apparent surface charge (ASC) methods, (2) the multipole expansion (MPE) methods, (3) the image charge (IMC) methods, (4) the generalized Born approximation (GBA), (5) the finite element methods (FEM), and (6) the finite difference methods (FDM) [114]. Among these, the ASC methods cover a large set of commonly applied implicit solvation models such as the Polarizable Continuum Model (PCM) [115], Conductor-like Screening Model (COSMO) [116] and the Integral Equation Formalism (IEF) [117–119].

These models form an integral part of today's quantum chemical research and their usage is unavoidable for the proper computational handling of organic reactions especially if they take place in a polar environment or charged species are involved.

2.8 GENERAL REMARKS

In the following chapters the above discussed theories will be used to study organometallic systems. This is a short methodological summary intended to throw some light on the theoretical foundations of the applied methods. However, it is neither complete, nor deep, just enough to scratch the surface and give insight into the complexity of the theory.

There's this farmer, and he has these chickens, but they won't lay any eggs. So, he calls a physicist to help. The physicist then does some calculations, and he says, um, I have a solution, but it only works with spherical chickens in a vacuum.

Leonard, The Big Bang Theory

3

Palladium(II)-Catalyzed Dynamic Kinetic Asymmetric Transformation

3.1 INTRODUCTION

3.1.1 CHIRALITY – HISTORY, BIOLOGY AND CHEMISTRY MEET

MOLECULAR CHIRALITY was discovered in 1848 by Louis Pasteur, a French chemist and microbiologist (vaccination, pasteurization etc.), when he separated two sodium ammonium tartrate isomers [120–122]. Despite the pioneering work of Pasteur, it

This chapter is based on the following manuscript: P. Ramírez-López, A. Ros, B. Estepa, R. Fernández, B. Fiser, E. Gómez-Bengo, J. M. Lassaletta, *ACS Catalysis*, vol. 6, pp. 3955–3964, 2016.

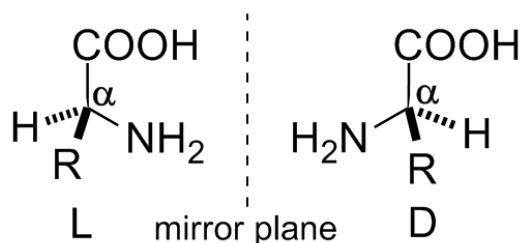


Figure 3.1.1: General Structures of the L- and D-Amino Acids.

took almost a century for the scientific community to understand the importance of chirality.

Chirality plays a central role in biology and thereby in chemistry as well, highly affecting pharmaceutical, agricultural and other chemical industries. As hands and feet are in mirror-image pairs, many molecules can exist in "left-" and "right-handed" forms. The proteinogenic amino acids (except glycine) have two chiral forms – L and D – (Figure 3.1.1), but only the L is indispensable for the synthesis of the enzymes which are molecular level "catalytic machines" in the living organisms. Therefore, the "biochemical industry" within the cells is based on exclusively "left-handed" species and this is the reason why in numerous cases a given compound biologically active, whereas its mirror-image counterpart is inactive or it has distinctly different activity [123].

Due to the handedness of cell components, the situation is the same in the case of drugs and their activity may depend on the used enantiomer. Many drugs on the market consist of chiral molecules [124] and since they must interact with their specific targets (appropriate type of receptor proteins), it is rare to have relevance of both enantiomers. Thus, one stereoisomer has the desired therapeutic influence, while the other may be inactive or, in certain cases, it might be harmful and produce undesired or toxic effects [125].

Furthermore, the production efficiency of any chemical process is highly depend on the additional costs such as the synthesis, separation and disposal of the unwanted compounds. Therefore, the selective synthesis of different chiral forms

of a compound is a crucial issue in industrial and academic chemical research.

Besides the usual point chirality (e.g. α -carbons in amino acids, Figure 3.1.1), there are two other chirality types axial and planar, in which, the rotation around a single bond or a dihedral is hindered, respectively.

Axial chirality was first discovered by Kenner and Christie in 1922 when they synthesized a tetrasubstituted biphenyl derivative [126]. Later, in 1927, Kuhn introduced the term *atropoisomerism* (*atropos* means 'not turn') to describe this phenomenon [127]. Until nowadays, several compounds were synthesized with such structural features, most of them are biphenyls, but there are a large group of binaphthyl derivatives, as well. These compounds are intensively used in catalytic applications as ligands.

3.1.2 HOW TO COPY NATURE?

The importance of chiral separation was recognized by the Nobel Committee in 2001 when they decided to give the Nobel Prize in Chemistry to Dr. William S. Knowles and Prof. Ryori Noyori "for their work on chirally catalysed hydrogenation reactions" and Prof. K. Barry Sharpless "for his work on chirally catalysed oxidation reactions" [123].

Knowles is one of the founding fathers of asymmetric synthesis. Although, "it had been almost axiomatic among chemists that only nature's enzymes could ever do" [40] really efficient selective synthesis, this is not deterred but rather inspired his work.

"In the early 1960's (...) we made a paper evaluation of a monosodium glutamate process. The racemic mixture was easy to obtain, but by the time we had resolved, the projected costs doubled (...). It looked as though if one wanted to beat "the bug" it would be necessary to have a catalyst which, when an asymmetric center was formed, would direct the reaction to give a predominance of the desired isomer. For this purpose the 100% efficiency of enzymes would not be needed to have something of real value."

— William S. Knowles, Nobel Lecture

Knowles and his co-workers developed a process using chiral phosphine ligands for catalytic asymmetric hydrogenation, but their first attempts gave only 15% enzymatic efficiency [128]. Thereafter, they kept working on the refinement of the mechanism by the modification of the ligands [40]. The real breakthrough happened when methylcyclohexyl-o-anisylphosphine (CAMP) was used as ligand and by this the efficiency jumped up to 88%. This was the first time to achieve enzyme-like selectivity with a man-made catalyst [40, 129].

The first industrial application of catalytic asymmetric synthesis was the commercial production of L-3,4-dihydroxyphenylalanine (L-DOPA) in 1974 at Monsanto which is also linked to Knowles and his co-workers. The idea is the same, but the selectivity was further improved for the industrial process up to 95% using ethane-1,2-diylbis[(2-methoxyphenyl)phenylphosphane] (DiPAMP - chelating diphosphine with two chiral phosphorus atoms) containing cationic rhodium complex as a catalyst [130, 131]. The success of L-DOPA has significantly expedite the growth of research in this area and bring into fashion the development and application of other catalytic asymmetric reactions in the subsequent years.

Another early example of molecular asymmetric catalysis was the enantioselective cyclopropanation of olefins using structurally well-defined chiral transition metal complexes and discovered by Noyori, Nozaki and their co-workers, however the stereoselectivity of the reaction was very low ($\sim 10\%$) [132–134].

There are many more important moments in chemical discovery in which Prof. Noyori was significantly involved, but one is prominent among them: the discovery of 2,2'-bis(diphenylphosphino)-1,1'-binaphthyl (BINAP). In 1980, Noyori together with Takaya and their co-workers successfully prepared BINAP, an axially chiral bis(triarylphosphine) [135]. The axial chirality of BINAP arises from the fact that the rotation is restricted about the single bond between its naphthyl groups, because of the occurring steric hindrance and therefore the *S* and *R* forms are atropoisomers (*vide supra*, Figure 3.1.2).

They have used it efficiently as chiral ligand of Rh(I) and Ru(II) in asymmetric hydrogenation which was a significant step forward in stereoselective synthe-

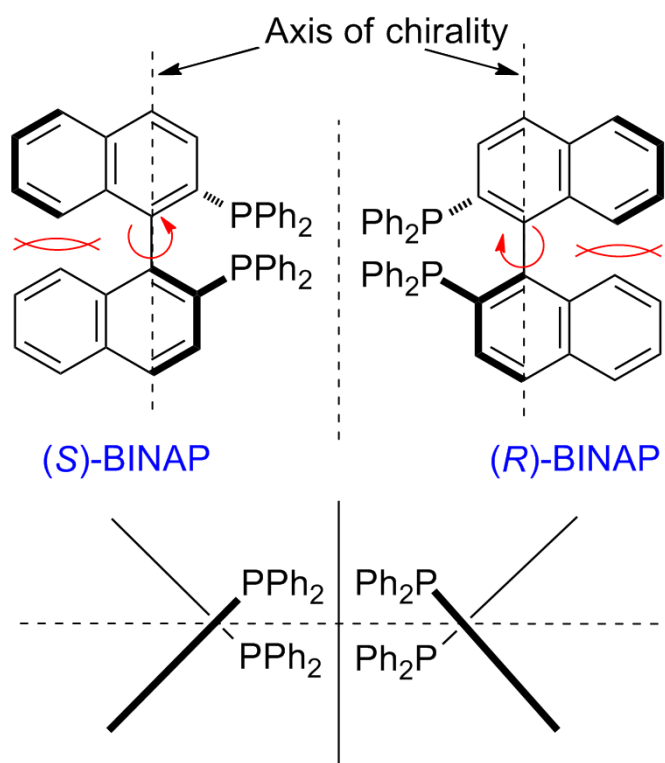


Figure 3.1.2: Structures of BINAP Atropoisomers.

sis [134]. Rh(I)-BINAP and Ru(II)-BINAP complexes have various kinds of applications in asymmetric catalysis such as enantioselective hydrogenation of α -(acylamino)acrylic acids or esters and α,β - and β,γ -unsaturated carboxylic acids, asymmetric synthesis of amino acids and enantioselective isomerization of allylic amines to enamines [123, 134, 136–139].

The scope of BINAP goes far beyond which was expected and the wide range of applicability makes it really interesting.

3.1.3 NATURE'S PRIVILEGE – PRIVILEGED LIGANDS

"Artificial" (man-made) and "natural" (enzymatic) asymmetric catalysts are essentially based on the same concept [140], but the former can be more general (wide range of substrates, but one type of reaction) than the latter, which is a rather surprising, though very useful difference [40].

"When we started this work we expected these man-made systems to have a highly specific match between substrate and ligand just like enzymes. Generally in our hands and in the hands of those that followed us a good candidate has been useful for quite a range of applications. This feature has substantially enhanced their value in synthesis."

— William S. Knowles, Nobel Lecture

The key is generality: the wider the scope, the more important your work is. There are even more surprising cases when the "artificial" catalysts are cover not only a wide range of substrates within one reaction, but it could be applicable in different reactions on a good number of substrates. These are the so-called privileged structures or privileged catalysts/ligands which can handle mechanistically unrelated reactions [141]. These include the aforementioned axially chiral BINAP and its "sister" BINOL (1,1'-bi-2-naphthol) which are among others covering the Diels-Alder, Mukaiyama aldol and Heck reaction [141].

3.1.4 ATROPOS P,N-LIGANDS – ADVANTAGES AND DISADVANTAGES

In 1993, as a result of the further development of BINAP, a new axially chiral ligand 1-(2-diphenylphosphino-1-naphthyl)isoquinoline (QUINAP) (Figure 3.1.3) was synthesized with two different heteroatoms (P and N) [142]. It was the first atropos P,N-ligand (APN) and it has excellent ligand properties [143]. However, its synthesis was quite challenging with two innate disadvantages: its resolution requires stoichiometric Pd(II) complexes and the ligand diversity is limited, because the phosphine introduced prior the resolution [144]. These problems have motivated the development of alternative APN ligands, on one side, and studies directed to improve the efficiency and economy of the synthetic methods, on the other. Since its initial synthesis, a series of other axially chiral P,N-ligands were developed and thus far five main families are available including QUINAP itself (Figure 3.1.3) [142, 145–148].

These ligands have also been successfully applied in asymmetric catalysis, matching or improving in some cases the results collected with QUINAP in previously developed or new catalytic reactions [144]. However, the methods required for their synthesis are still far from practical: in the best cases the synthesis requires resolution of diastereomers by chromatography or crystallization (PINAP) [147], while most of them (QUINAZOLINAP [145], PyPHOS [146], and StackPHOS [148]) have to be prepared by crystallization of stoichiometric amounts of Pd(II) complexes.

In the case of QUINAP, basically the synthesis can be divided into three main stages: the coupling of the two aryl fragments, the introduction of the phosphine and the resolution (Figure 3.1.4) [144]. Several alternative synthetic routes have been reported to overcome the difficulties of the different stages.

Baker, Sargent and co-workers have used sulfoxide intermediates, but their method struggled with significant loss of purity [149]. In 2007, Knochel and co-workers have used the same sulfoxide intermediates, but avoided the problem of low enantiomeric purity [150]. This method took advantage of the easy chromato-

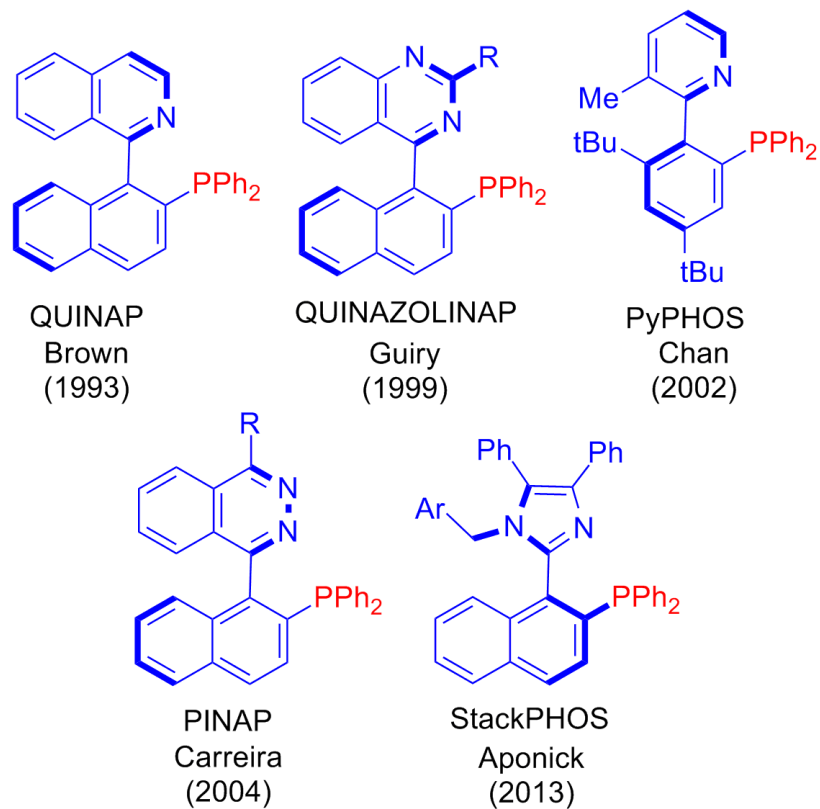


Figure 3.1.3: Atropos P,N-Ligand (APN) Families [144].

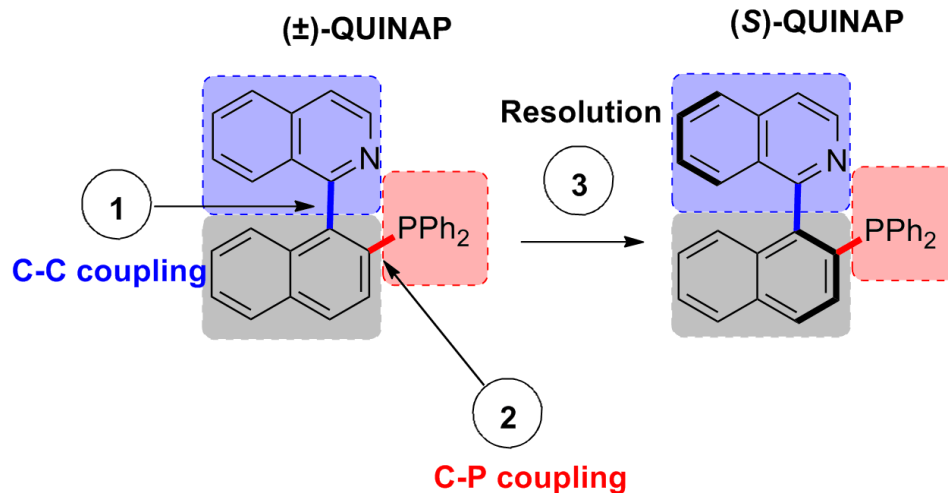


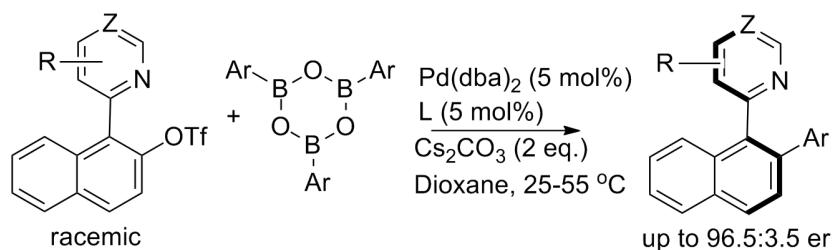
Figure 3.1.4: General Steps of QUINAP Synthesis: 1) C-C Coupling, 2) C-P coupling and 3) Resolution.

graphic separation of diastereomeric sulfoxide intermediates, and their easy transformation into enantiopure QUINAP after sulfoxide–lithium exchange, quenching with Ph₂P-Cl and sulfur, and reduction with Raney-Ni. Thereafter, Clayden and co-workers shortened the separation by exploiting the biased thermal equilibration of the diastereomeric sulfoxides ((*R*)(*R*)_{ax} favored over (*R*)(*S*)_{ax}) and succeeded in the development of a "dynamic thermodynamic resolution" leading to one pure hand of QUINAP [151]. It is the first asymmetric synthesis of QUINAP, but still requires the introduction of an enantiopure sulfinyl group as a sacrificial auxiliary.

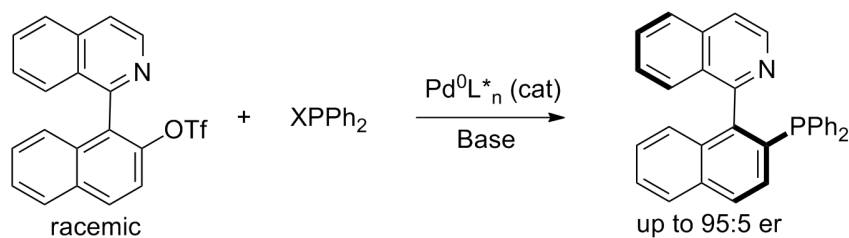
Therefore, there is still demand of a general methodology for the asymmetric synthesis of axially chiral heterobiaryls. Key findings related to this issue were published in 2013 by Fernández, Lassaletta and co-workers [152]. Their work is based on the dynamic asymmetric Suzuki-Miyaura coupling (Dynamic Kinetic Asymmetric Transformation - DYKAT) between racemic, configurationally stable heterobiaryl triflates and arylboroxines (Figure 3.1.5, eq. 1).

This strategy was applied in a parallel work for C-P bond forming reactions by

(1) Dynamic kinetic asymmetric Suzuki-Miyaura coupling by Lassaletta *et al.* [152]



(2) Dynamic kinetic asymmetric C-P bond formation by Lassaletta *et al.* [153] and by Stolz and Virgil *et al.* [154]



(3) Most recent work by Fernández, Lassaletta and co-workers

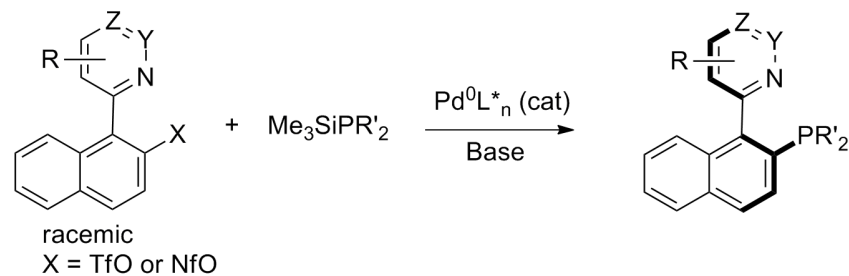


Figure 3.1.5: Dynamic Kinetic Asymmetric Transformation Techniques for the Asymmetric Synthesis of Heterobiaryls.

the same group (Figure 3.1.5, eq. 2) [153].

Simultaneously, Stoltz, Virgil and co-workers also reported the enantioselective synthesis of QUINAP according to a similar procedure (Figure 3.1.5, eq. 2) [154].

In both cases, a single example of axially chiral heterobiaryls was synthesized (QUINAP itself), but different mechanisms were proposed for the DYKAT (*vide infra*). In this work, the plausibility of the proposed mechanisms will be studied by means of DFT calculations. Furthermore, the results of the calculations will be used to shed light on the most recent experimental findings on the general synthesis of different APN ligands (isoquinoline, 3-methylpyridine, quinazoline and phtalazine derivatives) in an enantiomerically enriched fashion, envisaged by our collaborators Prof. Fernández, Prof. Lassaletta and their groups (Figure 3.1.5, eq. 3).

3.2 MECHANISMS AND EXPERIMENTAL BACKGROUND

As mentioned above, two different mechanisms (Figure 3.2.1, path **a** and **b**) were postulated to explain the dynamic resolution of the observed dynamic asymmetric cross-coupling in the reactions which were used for QUINAP synthesis.

On one side, Fernández, Lassaletta and co-workers assumed that the nitrogen atom of the isoquinoline coordinates to the Pd, leading to diastereomeric, cyclic **OAI** and **OAI'** intermediates, displacing the poorly coordinating triflate anion [152, 153] (Figure 3.2.1, path **a**).

The geometry of these **OA** intermediates suggests that the equilibration proceeds via a transition state **TS_{rot}-OAI** in which the angles φ_1 , φ_2 are just slightly wider than the corresponding angles φ_3 , φ_4 or φ'_3 , φ'_4 in (*S*)-**1** and (*R*)-**1**, respectively. Thereby the steric hindrance is reduced and the otherwise crashing hydrogen atoms can reach coplanarity with the stereogenic axis allowing the interconversion between the intermediates (Figure 3.2.1, path **a**).

On the other hand, Virgil, Stoltz *et al.* suggested that unsaturated T-shaped **OAI_b** and **OAI'_b** intermediates equilibrate via a square planar transition state **TS_{ot}**-

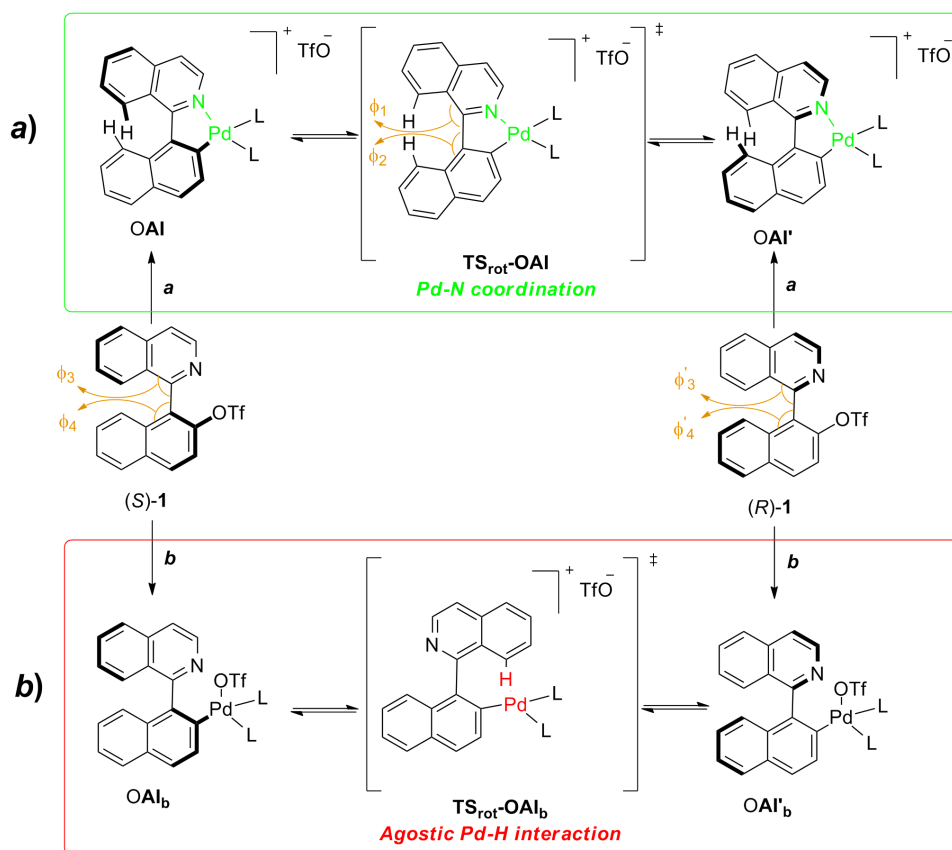


Figure 3.2.1: Proposed Mechanisms for the Epimerization of Diastereomeric Oxidative Addition Intermediates: **a** - Fernández, Lassaletta et al. [152, 153]; **b** - Stoltz, Virgil et al. [154].

OAI_b, stabilized by an agostic Pd–H interaction [154] (Figure 3.2.1, path **b**). In this proposal, the nitrogen atom on the heteroaryl moiety does not play any role and the dynamic resolution step of the DYKAT process should work with a structure which lack that nitrogen.

This assumption was tested experimentally by Prof. Fernández and Prof. Lasaletta and their groups, however C–P coupling product was not observed only **3** a hydrolysis product formed from the reaction when the substrate (**2**) contains naphthalene instead of the isoquinoline unit. Similarly, the C–P coupling also does not work with NOBIN-derived nonaflate substrate **4** and only **5** a hydrolysis product formed, indicating that the formation of a *five-membered* cationic palladacycle is essential to reactivity (Figure 3.2.2).

The results indicates that the presence of a coordinating isoquinolyl/pyridyl nitrogen is not only necessary to favor the formation of the cationic and configurationally labile palladacycle, but also to facilitate the chelate-assisted oxidative addition of the racemic triflate/nonaflate to the Pd⁰ center.

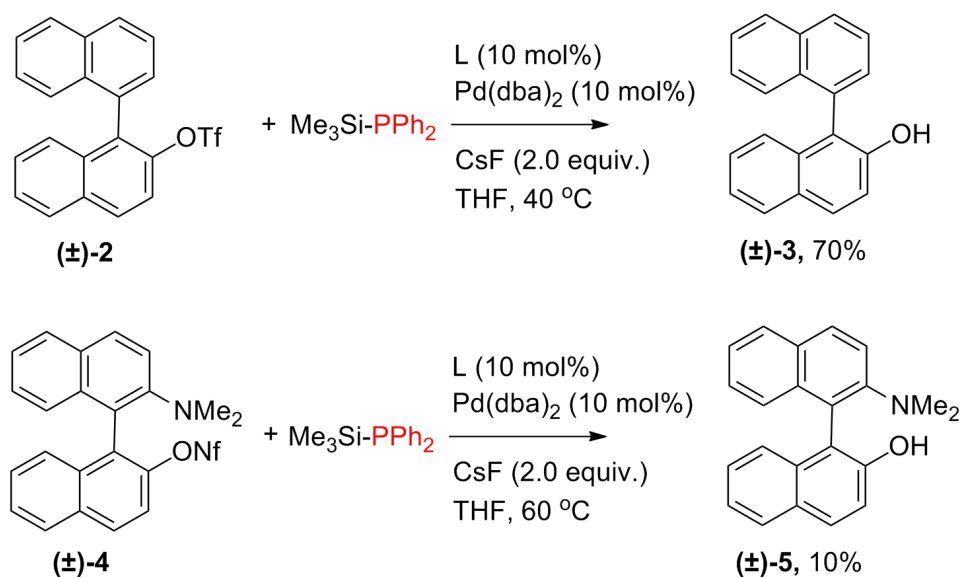


Figure 3.2.2: Test Experiments with Triflate **2** and Nonaflate **4**.

Hoping to extend the DYKAT methodology to the synthesis of other APN lig-

ands, the reaction conditions were optimized by our collaborators for QUINAP (Figure 3.2.3).

As a first step, thorough ligand screening were done using a set of 18 different chiral ligands and two Josiphos-type ligands with planar chirality were selected, (**L1** and **L2**) both containing a second metal center (Fe) (Figure 3.2.3, Ligand Screening). Thereafter, the reaction conditions were optimized using the selected ligands and the effect of the phosphorus reagent and the Pd precatalyst were explored. The best phosphide transfer system and the best palladium precatalyst were identified as $\text{Me}_3\text{SiPPh}_2$ / CsF and $\text{Pd}(\text{dba})_2$ giving a conversion of >95% and a selectivity 95.5:4.5 and 92:8 in the case of **L1** and **L2**, respectively (Figure 3.2.3, Condition Optimization).

Finally, knowing the best conditions for the (*S*)-QUINAP synthesis, they have successfully extended the scope of the methodology to related systems and they were obtained a series of different heterobiaryl phosphines (eg. 3-methylpyridine, quinazoline and phtalazine derivatives) in excellent yields (71 - 94%) and good enantiomeric excess (73:27 - 99.5:0.5 er) (Figure 3.2.3, Scope).

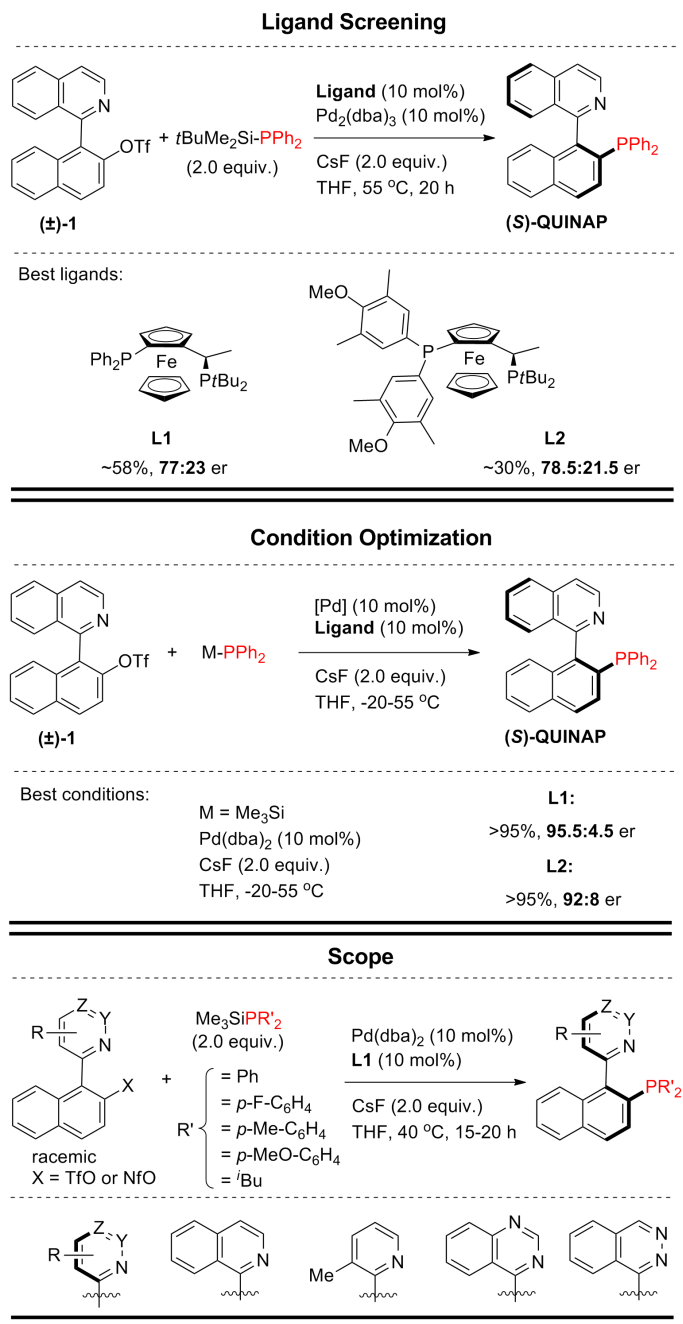


Figure 3.2.3: Ligand Screening and Reaction Condition Optimization for the Synthesis of QUINAP. Extended Scope of the Dynamic Kinetic C-P Cross Coupling Reactions.

3.3 COMPUTATIONAL METHODS

The structures were calculated by using the B₃LYP hybrid density functional [101–103] as implemented in Gaussian 09 [155]. Optimizations were carried out by using the standard 6-31G(d,p) basis set for C, H, O, N, S, F and P. For Pd and Fe, the LANL2DZ basis set [110–112] was used, which includes the relativistic effective core potential (ECP) of Hay and Wadt and employs a split-valence (double-zeta) basis set. Single point calculations were also performed using the Mo6 functional [100] combined with the 6-31+G(d,p) and SDD [108, 109] basis set and the polarizable continuum model (PCM) using the integral equation formalism [117–119] to take into account solvent effects on the previously optimized structures. Reported energy values correspond to Gibbs Free (G) energies. The critical stationary points were characterized by frequency calculations in order to verify that they have the right number of imaginary frequencies, and the intrinsic reaction coordinates (IRC) [156] were followed to verify the energy profiles connecting the key transition structures to the correct associated local minima.

3.4 RESULTS AND DISCUSSION

During the calculations, the selected optimal experimental conditions were mimicked as much as possible. The sum of all the species in the reaction system would produce transition structures too large and complex to be computed by the current computational methods, if desirable accuracy has to be achieved. In order to maintain the model system as close as possible to the experimental, a few simplifications were done.

(S)-QUINAP synthesis was selected as a case study and simplifications were made for the calculations. Thus, the model system contains triflate **1** (substrate) and Pd⁰-**L1** chiral catalyst, which has shown a good performance in the reaction (Figure 3.2.3), and symmetrical triphenyl phosphine (PPh₃) as a model for the incoming nucleophilic phosphide (Me₃SiPPh₂ in the case of QUINAP) during the transmetalation (vide infra). In this way, we were able to maintain the computational model as similar to the experimental one as possible, without compromising the accuracy of the method of choice.

We anticipated that the hypothesis of our colleagues is correct and the mechanism to transform the initial racemic triflate **1** into the final enantioenriched QUINAP product or in general to prepare other APN ligands (such as other isoquinoline, 3-methylpyridine, quinazoline and phtalazine derivatives, Figure 3.1.3) (Figure 3.1.5, eq. 3) in an enantiomerically enriched fashion, includes the three classical coupling steps (1. oxidative addition of palladium, 2. transmetalation (kinetic resolution) and 3. reductive elimination) and an additional in-between (between 1. and 2.) epimerization (dynamic resolution) step (Figure 3.4.1).

Our model is based on two central ideas; (i) the starting triflates **E** and **E'** are configurationally stable, whereas the oxidative addition to Pd(o) leads to the formation of configurationally labile Pd(II) intermediates (**OAI**), which are prone to epimerization, and (ii) the present DYKAT transformation is taking place under typical Curtin-Hammett conditions, meaning that the epimerization rate of the interconverting Pd(II) complexes (**OAI** and **OAI'**) is faster than their further evo-

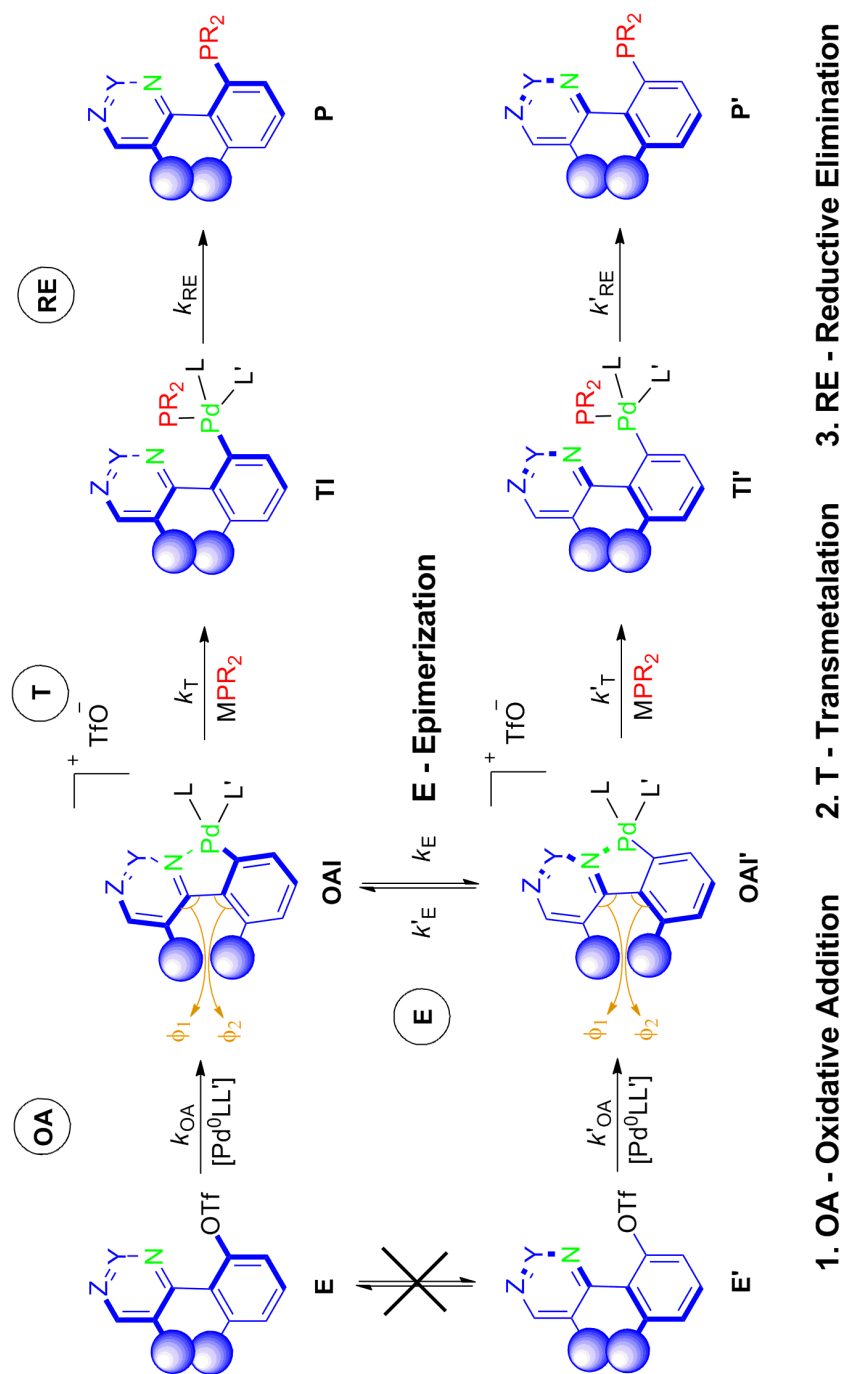


Figure 3.4.1: Main Steps of the General Mechanism for Pd-Catalyzed APN Ligand Formation [152, 153] and (Figure 3.1.5, eq. 3).

lution to **TI** and **TI'** through transmetallation (Figure 3.4.1). Thus, the transmetalation step is the stereodetermining one, and the two diastereomeric transmetalations must occur at sufficiently different rates as to induce enough selectivity in the formation of the final **R** and **S** products (**P'** and **P**, respectively). Another important issue is that the reductive elimination process must be fast again, making the transmetalation step irreversible (Figure 3.4.1).

We found computational evidence supporting our working hypothesis based on the following results. The studied enantiomeric compounds can interconvert through a *syn* or an *anti* process (Figure 3.4.2, top). The interconversion of the two enantiomeric triflates (**R**)-**1** and (**S**)-**1** is predicted to be an extremely slow process in the absence of palladium, since its activation energy is as high as 29.3 and 34.9 kcal/mol in the case of the *anti* and *syn* process, respectively (**TS**_{rot-1-*anti*} and -*syn*, Figure 3.4.2, top). Although, the rotation is easier through the *anti* process by 5.6 kcal/mol compare to the *syn*, but it still too high ($\Delta G^\ddagger_{anti} = 29.3$ kcal/mol) to be feasible at room temperature.

There is a clear difficulty in the substrate to adopt the necessary conformation for the rotation. In the absence of palladium, the angle formed by the planes of the two aromatic rings θ_0 is ca. 90°, but it must approach to 0° or 180° during the transition state **TS**_{rot-1-*syn*} or -*anti*, with the accompanying energetic cost. In the case of the *syn* approach, the repulsion between the N and O atoms increases substantially as they are forced to approach from the initial 3.4 Å in (**R**)-**1** (or (**S**)-**1**) to a much shorter distance of 2.4 Å during the transition state (**TS**_{rot-1-*syn*}).

Meanwhile, after the oxidative addition of Pd(o) to the C-OTf bond, the chelation complex (**R**)-**int1-PMe**₃ (it is equivalent to **OAI** (Figure 3.4.1), but without the triflate, so it is cationic) presents drastic geometrical changes in the right direction to facilitate the rotation/epimerization process, like the reduction of the θ_1 angle to 45° (Figure 3.4.2, bottom). Furthermore, the N-Pd distance, which is a favorable bonding interaction, is similar (ca. 2.1 Å) in (**R**)- or (**S**)-**int1-PMe**₃, as it is during the corresponding transition state (**TS**_{rot-**int1**}).

Due to this geometrical change, the energy barrier is dramatically reduced to

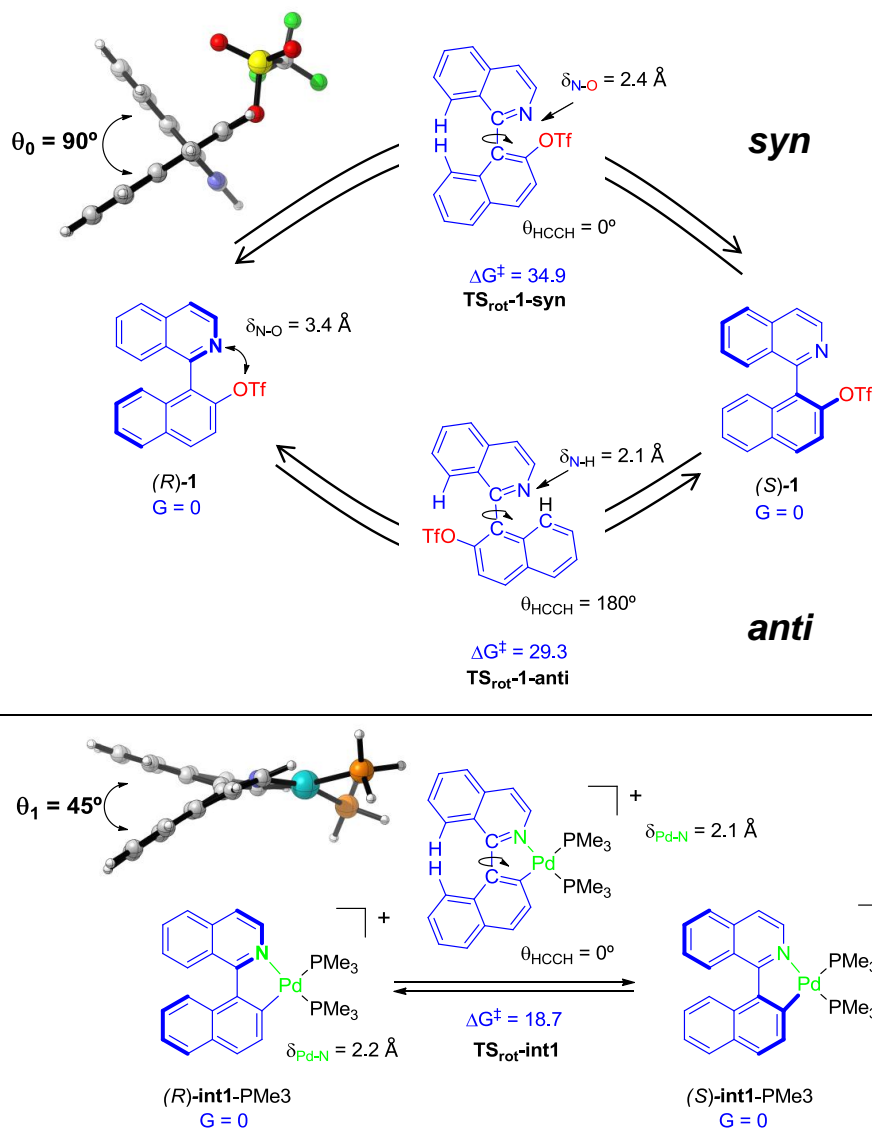


Figure 3.4.2: Activation Energies for the Axial Rotation of Initial Triflates and Palladacyclic Intermediates. Computed at the B3LYP/6-31G(d,p)/LANL2DZ Level of Theory.

18.7 kcal/mol, explaining the fast interconversion of both enantiomeric complexes in the experimental conditions. These results confirm the hypothesis, that the palladacyclic intermediates can easily racemize whereas the initial triflates can not.

The use of an achiral phosphine (PMe_3) as a first approximation implies that **(R)-int1-PMe₃** and **(S)-int1-PMe₃** are isoenergetic (Figure 3.4.2). By introducing the experimentally used chiral ligand **L1** the corresponding **R** and **S** complexes can still interconvert, but they are going to be diastereomeric and therefore, distinguishable in terms of energy. Thus, a total of eight diastereomeric species were located (Figure 3.4.3). Four of these species are the result of the fact that the palladium center is not forming a perfect square planar structure. The two cycles around the palladium atom are not coplanar, and form a pseudo-tetrahedral geometry with two different configurations. Also, the relative disposition of the two phosphorous atoms in the asymmetric di-phosphine (**L1**) with respect to the C and N atoms of the aromatic rings leads to the formation of the other four diastereoisomers.

The lowest energy intermediate pair is **(R)-int1-L1** and **(S)-int1-L1**, in which the equilibrium is clearly shifted towards the *pro-R* complex which is lower in energy than its *pro-S* counterpart by 3.9 kcal/mol. The difference between them is even higher ($\Delta G = +4.3$ kcal/mol) by increasing the level of theory to Mo6/6-31+G(d,p)(iefpcm,THF)//B3LYP/6-31G(d,p).

The rest of the intermediates are remarkably higher in energy than **(R)-int1-L1** (between 5.3 to 13.4 kcal/mol).

It is important to note that the overall lowest in energy intermediate (**R-int1-L1**) corresponds to the minor experimental enantiomer **R**. However, this is irrelevant in the present Curtin-Hammett conditions, since all possible isomers of **OAI** are involved in a fast equilibrium (Figure 3.4.1), and the final outcome of the reaction is determined by the relative activation energy of the different transmetalation transition states. At this point, attention must be drawn to the fact that the transmetalation step is not a classical transmetalation, since it actually consists of an isoquinoline/ $\text{Me}_3\text{SiPPh}_2$ ligand exchange, with subsequent abstraction of the silyl

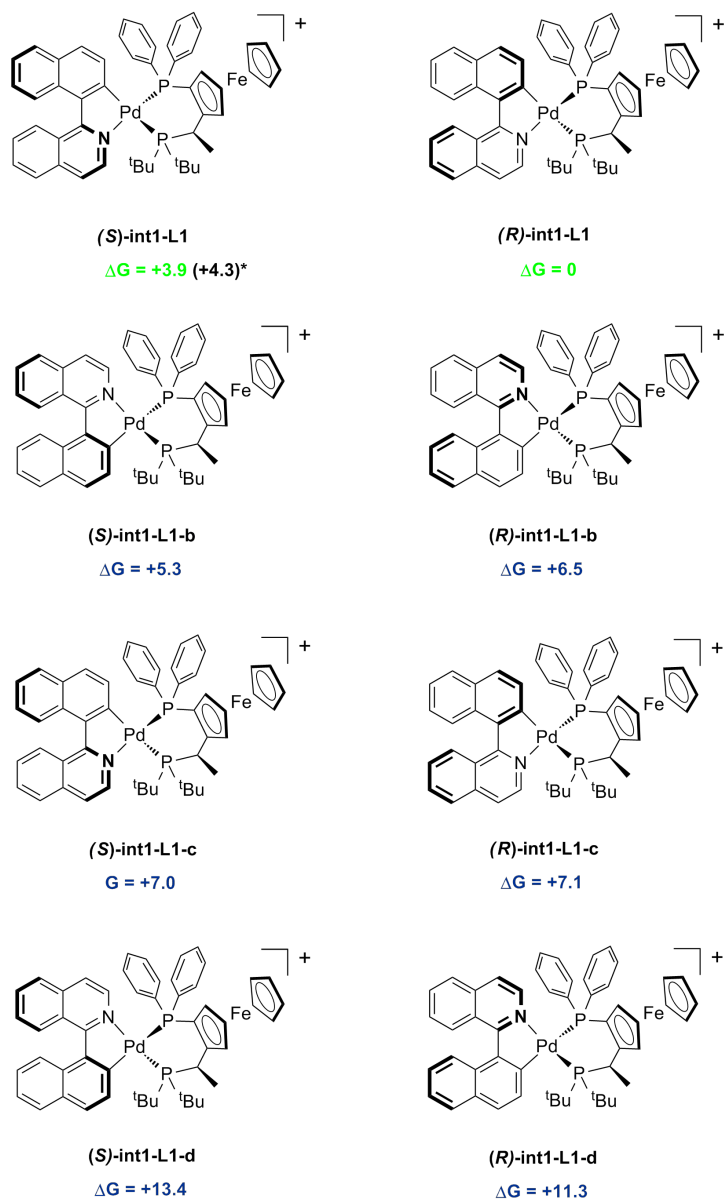


Figure 3.4.3: Stable Palladacyclic Intermediate Pairs and Their Relative Energies Compare to the Lowest Energy Structure. The Calculations were done at the B3LYP/6-31G(d,p)/LANL2DZ Level of Theory (* - Single Point Calculations at the M06/6-31+G(d,p)(iefpcm,THF)//B3LYP/6-31G(d,p) Level of Theory).

moiety by the CsF salt (Figure 3.4.4).

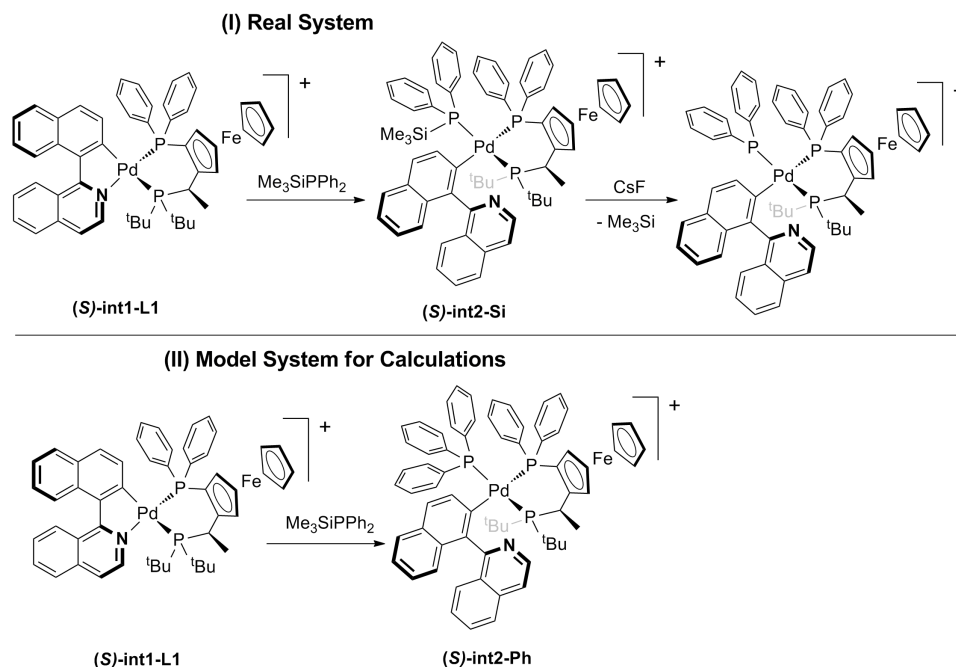


Figure 3.4.4: (I) The Transmetalation Process and (II) the Structural Model Used in the Calculations.

The calculations of the real system (I) is difficult, but a slightly altered model was envisioned (II), based on the replacement of the actual Me₃SiPPh₂ ligand by PPh₃ (**int2-Si** vs **int2-Ph**). This alternative has the great advantage that triphenylphosphine is conformationally much simpler than Me₃SiPPh₂, while maintaining a similar steric hindrance (Figure 3.4.4).

Initially we get appropriate transition structures of complexes containing two PH₃ ligands instead of diphosphine **L1**. These structures showed Ph₃P – Pd distances ranging from 3.1 Å to 3.5 Å. We also scanned the energy of the incoming triphenylphosphine at different distances in TS-like structures, i.e. **S-int1-L1**, **R-int1-L1** (Figure 3.4.3), and others, showing that the maximum energy was obtained at an average distance of 3.35 Å. We thus took this value as the standard P-Pd distance during the transition state, and computed all possible trajectories

of PPh₃. Noteworthy, the N-Pd distance was computed to be greater than 3.4 Å, indicating a complete decoordination of the nitrogen prior to coordination of the phosphorous. In all cases, the imaginary frequencies of the transition structures are low, ranging from ca. -14 to -35 cm⁻¹, but they undoubtedly correspond to the forming P-Pd bond vibration.

Thus, all possible transition structures for the approach of the nucleophilic phosphine were computed, maintaining in all cases similar distances for the coordination of the phosphine to palladium and decoordination of the isoquinoline-nitrogen from the metal. As mentioned before, there are eight main isomers for the **int1** type complexes, and for each of them we found at least two different transition state structures, depending on the departing trajectory followed by the isoquinoline. Consider for example the two lowest in energy structures for the **S** enantiomer (**S**)-**TS2-a** and (**S**)-**TS2-b** (Figure 3.4.5), the isoquinoline ligand leaves the palladium sphere towards the lower or upper face, respectively.

All of the possible alternatives were computed, resulting in a large range of activation energies (ca. 10 kcal/mol), but only the most stable ones are shown in Figure 3.4.5. To our delight, the most favored approach is (**S**)-**TS2-a** which is in agreement with the formation of the experimental *major S* enantiomer, and the difference compare to the lowest *pro-R* structure (**R**)-**TS2-a**, is 3.5 kcal/mol, large enough to explain a high selectivity in the process. Furthermore, the second most favored structure also corresponds to the **S** enantiomer, (**S**)-**TS2-b** ($\Delta\Delta G^\ddagger = +1.9$ kcal/mol).

Taking the results of Figure 3.4.3 and Figure 3.4.5 together, we are facing the typical situation where the minor, less stable isomer (**S**)-**int1-L1** reacts faster than the major unreactive one (**R**)-**int1-L1** and the stereoselectivity of the major isomer resulted from this Curtin-Hammett conditions are in agreement with the experimental results (Figure 3.4.6).

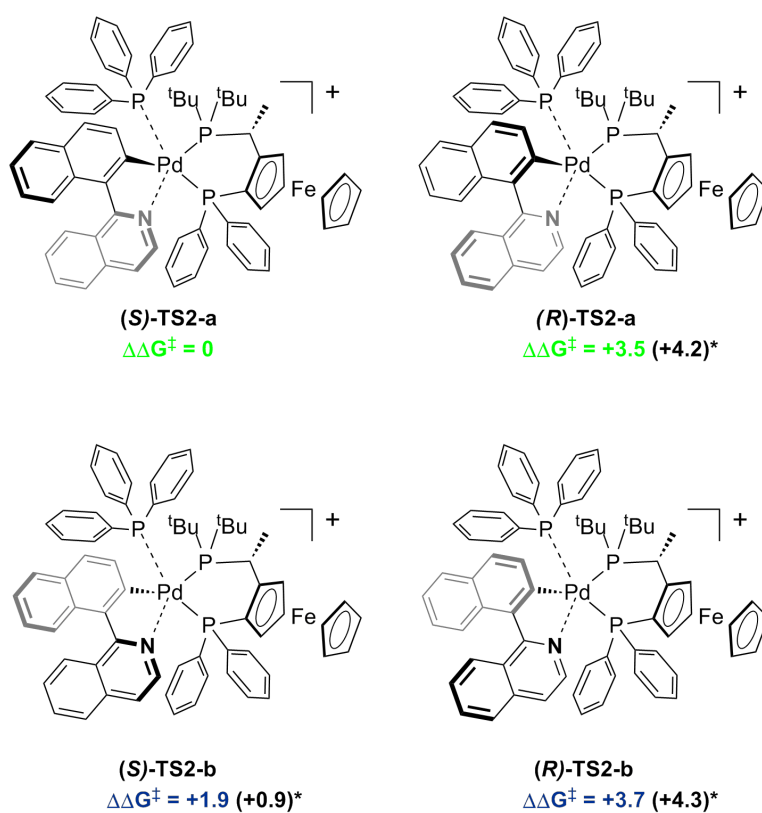


Figure 3.4.5: Most Stable Transition States for the Approach of the Nucleophilic Phosphine (PPh_3) to the Pd Center. Computed at the B3LYP/6-31G(d,p)/LANL2DZ Level of Theory (* - Single Point Results are also Shown Calculated at the M06/6-31+G(d,p)(iefpcm,THF)//B3LYP/6-31G(d,p) Level of Theory).

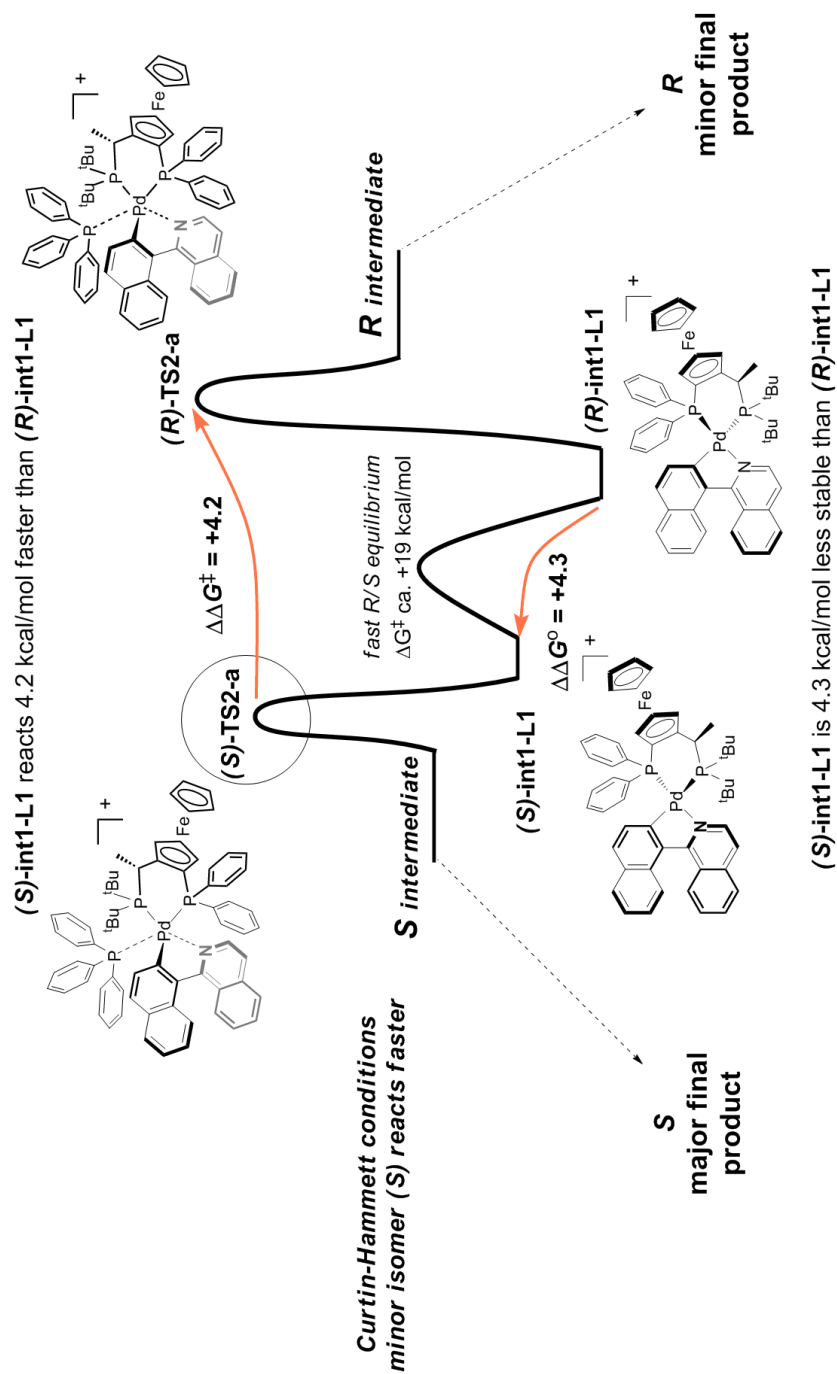


Figure 3.4.6: Curtin-Hammett Conditions in the Studied System.

The final step, the reductive elimination when the C-P bond is forming was also computed (Figure 3.4.7), affording interesting results. In the calculations one PMe_2 and two PMe_3 were used as phosphine source (for the C-P bond formation) and ligands (coordinated to the Pd), respectively.

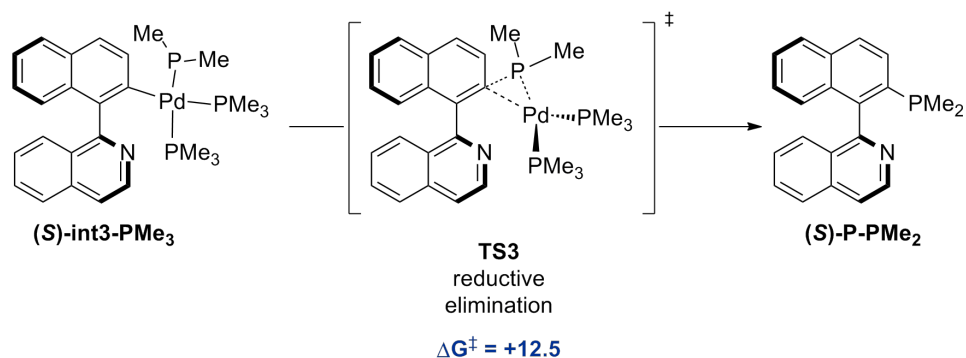


Figure 3.4.7: Computed Model Structures Involved in the Final, Reductive Elimination Step: Intermediate, Transition State (along with the Corresponding Activation Energy, ΔG^\ddagger) and Final Product. Calculations were Performed at the B3LYP/6-31G(d,p)/LANL2DZ Level of Theory.

First, the activation barrier for **TS₃** is very low ($\Delta G^\ddagger = 12.5$ kcal/mol) comparing to the energy demand of the other steps in this study, making the whole process after transmetalation irreversible. Secondly, the rotation barrier for the **int₃**-type intermediates and for the final QUINAP-type products raises to 34.7 and 32.5 kcal/mol respectively. Racemization processes at the final stages of the reaction are, thus, unfeasible, confirming that the formation of palladacycles by chelation with the nitrogen of the isoquinoline (like in (*R*)- or (*S*)-**int₁-PMe₃**, Figure 3.4.2, bottom) is a mandatory condition to allow the epimerization of the substrates.

Finally, we also checked the possible involvement of the palladium center in a Pd-H agostic bond (**int₄**, Figure 3.4.8), which has been proposed by Virgil and Stolz et al. [154] (Figure 3.2.1, path **b**) to explain the epimerization of the oxidative addition intermediates without the intervention of the nitrogen atom. To

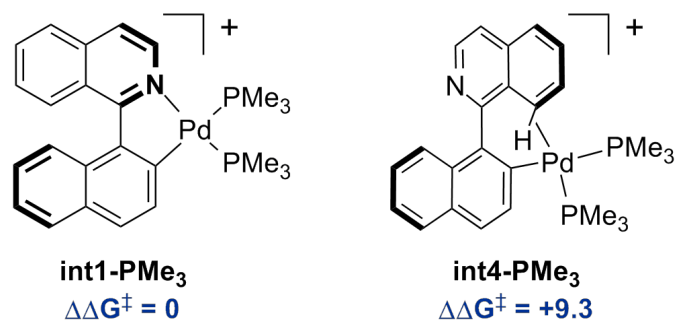


Figure 3.4.8: Plausibility of the Intermediate (**int4**) Proposed by Virgil and Stolz et al. Calculations were Performed at the B3LYP/6-31G(d,p)/LANL2DZ Level of Theory.

simplify the structures, two PMe₃ were used as ligands around the palladium.

The calculations show that Pd-H agostic bond containing model complex **int4-PMe₃** is remarkably less stable ($\Delta G = +9.3$ kcal/mol) than the corresponding simple **int1**-type palladacycle. This large energy difference is enough to completely discard the participation of **int4** in the mechanism.

3.5 CONCLUSION

In summary, the dynamic kinetic asymmetric C–P coupling between heterobiaryl triflates or nonaflates and trimethylsilylphosphines appears as an efficient, general methodology for the asymmetric synthesis of QUINAP, PyPHOS, QUINAZOLINAP, and PINAP analogues.

The computational results along with the collected experimental evidences allow to propose a detailed mechanism based on the formation of cationic oxidative addition intermediates which under the reaction conditions, undergo a fast interconversion.

The general mechanism to transform the initial racemic substrate into the final enantioenriched QUINAP product (or to prepare other APN ligands, such as other isoquinoline, 3-methylpyridine, quinazoline and phtalazine derivatives) in an enantiomerically enriched fashion, includes the three classical coupling steps: 1. oxidative addition of palladium, 2. transmetalation (kinetic resolution) and 3. reductive elimination. Furthermore, there is an additional in-between (between 1. and 2.) epimerization (dynamic resolution) step.

The proposal of Virgil and Stolz *et al.* to explain the epimerization of the oxidative addition intermediates without the intervention of the nitrogen atom of the isoquinoline but via the involvement of the palladium center in a Pd-H agostic bond was also examined.

The calculations and the experiments together revealed that the Pd-N coordination is essential to facilitate the epimerization.

The calculations also show that the energy requirements for a dynamic kinetic process are met, since the fast equilibrating palladacyclic intermediates evolve through diastereomeric transmetalation steps of very large energy difference. In the reaction, Curtin-Hammett conditions were identified in which the minor, less stable intermediate (**S**) reacts faster than the major one (**R**). Thus, the configuration of the major final product concur with the minor intermediate (**S**). Then, the easiness of the final reductive elimination ensures the irreversibility of the overall process.

Dimidium facti, qui coepit, habet; sapere aude, incipe.
(He who has begun is half done; **dare to know**, dare to begin!)

Quintus Horatius Flaccus, Epistularum Liber Primus

4

Gold(I)-Catalyzed Cyclizations

4.1 GENERAL INTRODUCTION

MANKIND USE GOLD SINCE ANTIQUITY and it is associated with wealth and prosperity and has long been plays an important role in different fields of life including trading, jewelry production, religious ceremonies and architecture [157].

Despite its widespread occurrence, it had to wait a long time to get a real role

This chapter is based on the following manuscripts:

- 1) D. Scarpi, S. Begliomini, C. Prandi, A. Oppedisano, A. Deagostino, E. Gómez-Bengoa, B. Fiser and E. G. Occhiato, *European Journal of Organic Chemistry*, vol. 2015, no. 15, pp. 3251–3265, 2015.
- 2) M. Petrović, D. Scarpi, B. Fiser, E. Gómez-Bengoa and E. G. Occhiato, *European Journal of Organic Chemistry*, vol. 2015, no. 18, pp. 3943–3956, 2015.

in chemistry as well. Probably, this is due to the assumptions that gold is too expensive and not reactive [158]. However, both statements can be disproved easily. The prices of gold catalysts are similar or even lower compared with other common metal catalysts (e.g. platinum, rhodium), while the reactivity of gold complexes is undeniable [158].

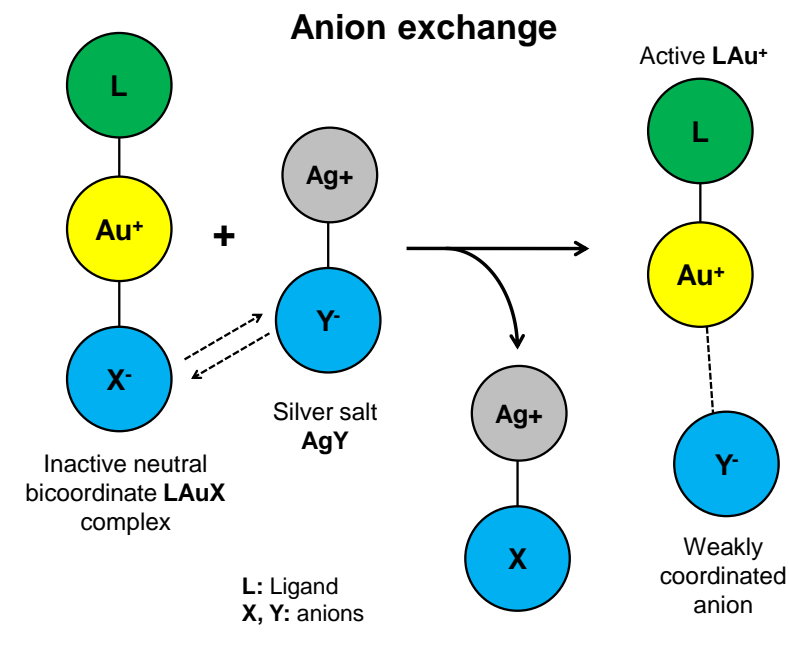
Huge changes started in the Millennium with the discovery of the efficient catalytic activity of AuCl₃ in the synthesis of furan [159, 160] and by now, we are in the "golden age" of gold-catalysis. Since 2000, the homogeneous gold catalysis is one of the most intensely studied topics of chemical synthesis [161–163]. In 2004, Prof. Hashmi wrote the first comprehensive review in this topic [164] and since his pioneering work, the vigorous research led to numerous applications in cyclizations and cycloisomerizations [163, 165], total [158, 166, 167] and asymmetric synthesis [162].

The success story of gold in catalysis is based on its peculiar properties (fine-tunability, functional group tolerance, large availability, π -affinity etc.) which makes it extraordinary within transition metals [160]. The remarkable fine-tunability of gold catalysts, LAuX_n (L: organic ligand, X: anion, n = 1 or 3) relies on the relative easy but careful change of their catalytic components (ligand, anion and oxidation state) and due to this, a wide range of reactions can be catalyzed by gold species under extremely mild conditions [160].

Although the triumphal march of homogeneous gold catalysis started with gold(III) halides [159], the cationic gold(I) complexes are more versatile despite their limited coordination motifs.

In contrary to other group 11 elements (Cu(I) and Ag(I) complexes) in which case tri- and tetraordinated complexes are common, for Au(I) the most favored coordination number is two in a linear arrangement [168, 169]. From a practical point of view this means that to prepare the active Au(I) catalysts from neutral bicoordinate complex LAuX (X = Cl, Br) one of the coordinated species needs to be removed. It is usually done by *in situ* anion exchange between LAuX (X = Cl⁻, Br⁻) and a silver salt (AgY) during which the highly coordinating anion X is eliminated as AgX, and the weakly coordinating anion Y as a counterion start to

act in the solution (Figure 4.1.1) [170].



C-C bond activation

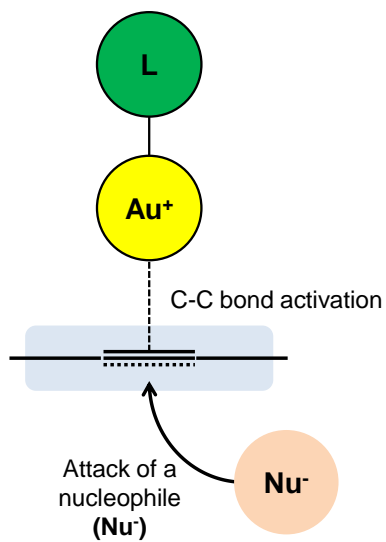


Figure 4.1.1: Anion Exchange and C-C Bond Activation in Gold(I) Catalysis.

The most fundamental within the numerous applications of gold(I) catalysis, is the activation of a carbon–carbon double or triple bond (Figure 4.1.1) [158, 165]. By the activation, the bond is ready to accept the attack of a nucleophile, which can not occur or only very slowly without the presence of the gold catalyst. This type of reaction could work with other metals as well (e.g. Ag, Hg, Pt), but LAu^+Y^- complexes are the most effective and they can be adapted to a wide variety of nucleophiles [163].

This coordination is common in gold(I)-catalyzed cyclizations and cycloisomerizations as well. In the following, case studies of these reaction types will be presented and studied by computational chemical tools.

4.2 GOLD(I)-CATALYZED NAZAROV REACTION

4.2.1 INTRODUCTION

THE NAZAROV CYCLIZATION REACTION is a 4π electrocyclization leading to 2-cyclopentenones [171, 172] (Figure 4.2.1).

The widespread presence of the 2-cyclopentenone moiety in natural products has always been a stimulus for synthetic organic chemists to find new methods for efficiently building this structure, with a varying degree of substitution and control of the stereochemistry [173]. Among the many approaches to 2-cyclopentenone, the Nazarov reaction ranks as one of the most important.

It was first reported by a Russian chemist Ivan Nikolaevich Nazarov and his co-workers in the early 1940s [174]. They have studied the hydration of dienyne using mercuric ion and acids which resulted in the formation of allyl vinyl ketones and in doing so they discovered a side reaction in which 2-cyclopentenones were formed [175]. Later, this side reaction proved to be their major result. It was named after Nazarov and it is earned popularity among the many various approaches to produce cyclopentenones.

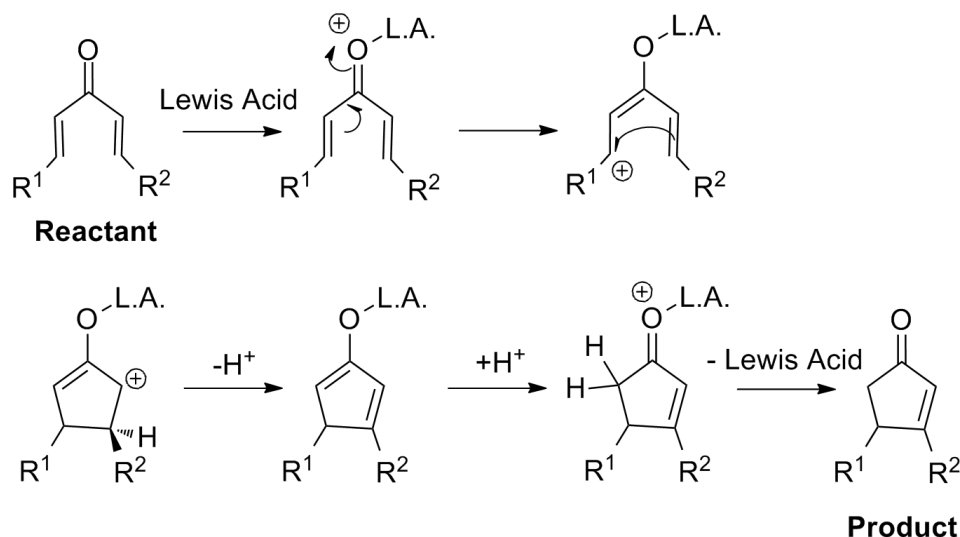


Figure 4.2.1: Mechanism of the Classical Nazarov Cyclization Activated by Lewis Acid.

In the beginning, Nazarov and his co-workers assumed that the allyl vinyl ketones are going through a direct acid-catalyzed ring closure to give the 2-cyclopentenones. In 1952, approximately ten years after its discovery, the correct reaction mechanism was revealed by Braude and Coles [176]. They suggested carbocation intermediates participating in the reaction and that the final product is produced via α,α' -divinyl ketones. These findings with further mechanistic studies, resulted the current definition of the classical Nazarov reaction: "Acid-catalysed cyclization of a divinylketone to give a cyclopentenone" [177] (Figure 4.2.1).

According to a more comprehensive definition, the Nazarov reaction is a cyclization process in which 2-cyclopentenones via divinyl ketones or their functional equivalents are produced under specific conditions, starting from a diverse set of precursors [175]. Two different variants of the reaction, classical and modern, can be distinguished depending on the precursors, reagents and substrates applied. The structural diversity of precursors ensure the versatility of the reaction.

The requisite 4π electron containing pentadienyl cation can be generated not only from classical dienones but also from a steadily increasing variety of uncon-

ventional substrates or processes [178] and thereby the reaction can be adapted to a wide variety of different conditions [175].

Suitably assembled propargylic esters with internal alkynes are particularly useful as substrates for the Nazarov reaction. The transition metal-catalyzed migration of the carboxylic group leads to competent pentadienyl cations through 1,3-acyloxy migration (Figure 4.2.2) which is generally favored over the 1,2-acyloxy migration of propargylic esters with internal alkynes [161].

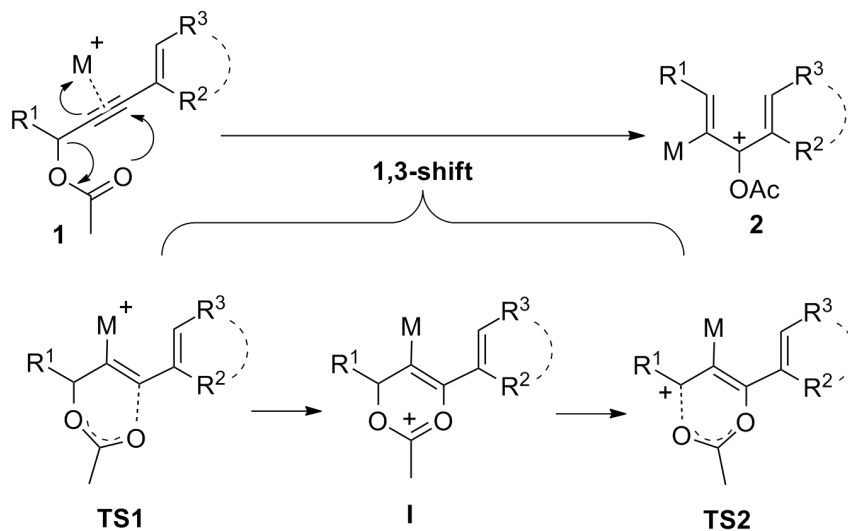
In particular, there are many examples of gold-catalyzed transformations [179, 180], especially in the last ten years Au- and the related π -acidic transition metal catalysis is flourishing [161].

A viable gold(I)-catalyzed example of the Nazarov process, in which 5-acyloxy-1,3-enynes **1** (Figure 4.2.2) undergo a [3,3]-rearrangement to pentadienyl cations **2** (precursor) which, after Nazarov reaction and eventual protodeauration, provide acetyloxy-substituted cyclopentadiene products **4**. Finally, hydrolysis of the latter leads to the target cyclopentenones **5** [181]. This strategy successfully provides cyclopenta-fused carbocycles **6** when the enyne double bond is embedded in a five-, six- and seven-membered ring (Figure 4.2.2) [181, 182].

Our collaborators, Prof. Occhiato and his group have long been working on the synthesis of cyclopenta-fused heterocycles by the Nazarov reaction [183–185], as well as in gold-catalysis [186] with significant results. These previous experiences prompted them to investigate if the same approach could still furnish annulated systems when embodying the double bond into N-heterocycles as one can see in **7** (Figure 4.2.3). In fact, this would serve as a new synthetic approach to produce diverse structural moieties (e.g. annulated pyrrolines and azepines) which are present in many natural compounds (Figure 4.2.3) [187–190], some of which (e.g. cephalotaxine) have already been synthesized via Nazarov reaction variants [191].

They have demonstrated that the tandem gold(I)-catalyzed propargylic rearrangement/Nazarov reaction of propargylic esters **7** (Figure 4.2.3) is a useful strat-

Metal-Catalyzed 1,3-Acyloxy Migration of Propargylic Esters



Gold(I)-Catalyzed [3,3]-Rearrangement and the Sequential Nazarov Reaction

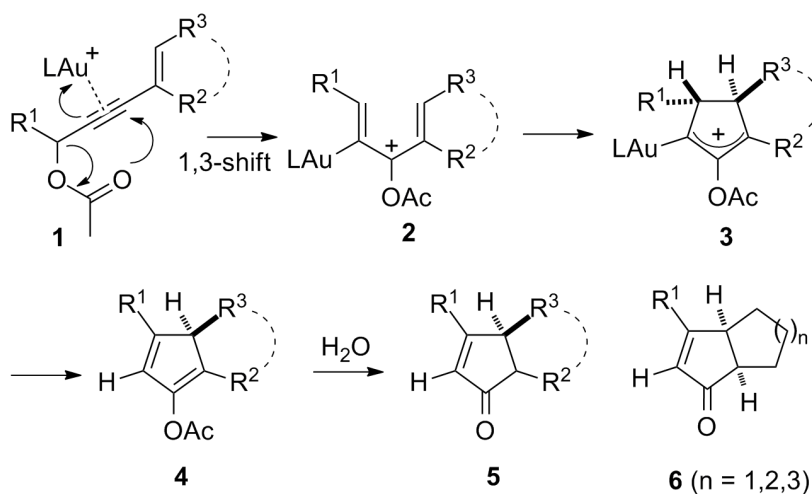
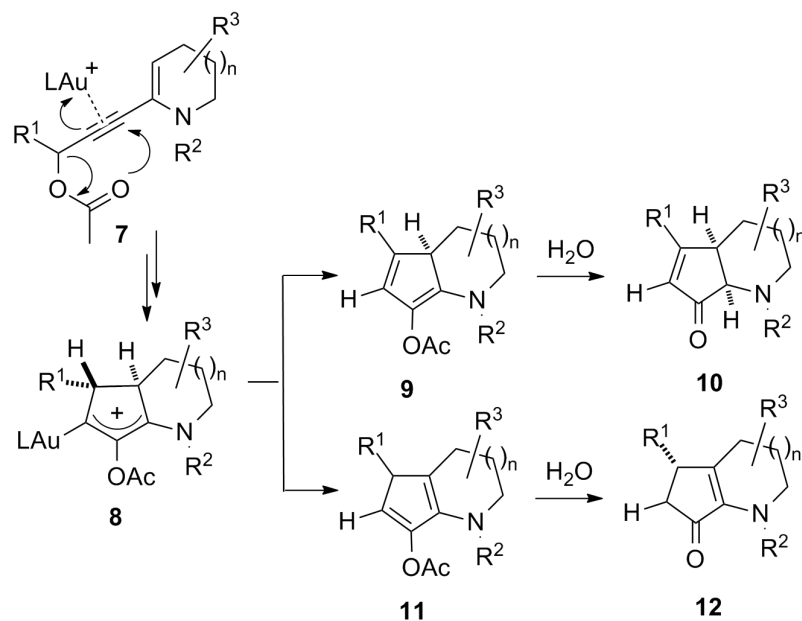


Figure 4.2.2: Top: General Metal-Catalyzed Process of 1,3-Acyloxy Migration of Propargylic Esters. Bottom: Sequential Gold(I)-Catalyzed [3,3]-Rearrangement/Nazarov Reaction of 5-acyloxy-1,3-enynes (**1**).

Cyclopenta-fused N-heterocyclic Ring Formation



Natural Compounds Containing Cyclopenta-fused N-heterocyclic Ring

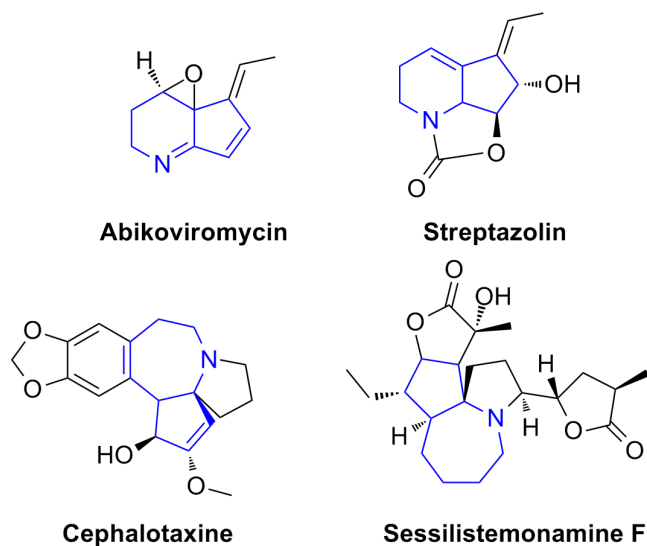


Figure 4.2.3: Top: Cyclopenta-fused *N*-heterocyclic Ring Formation by Sequential Gold(I)-Catalyzed [3,3]-Rearrangement/Nazarov Reaction. Bottom: Natural Compounds Containing a Cyclopenta-fused *N*-heterocyclic Ring.

egy for the synthesis of annulated *N*-heterocycles but, also, that the picture for this process is much more complex than that previously reported for non-heterocyclic systems, with a whole series of elements [*N*-protecting group, heterocycle ring size, gold(I) counterion, etc.] all influencing reaction rate and selectivity (regio- and stereoselectivity) in one way or another.

In particular, the importance to use proper protecting group on the nitrogen deserves special attention, as its involvement in gold-catalyzed rearrangement of closely related *N*-Boc enynes has been shown previously [186]. Thus, it poses a concern about a potential competition between the protecting group (e.g. carbonyl oxygen of *N*-Boc) and the carboxylic group of the propargylic ester in the nucleophilic attack to the activated triple bond. The possible reactivity of the protecting group towards the activated triple bond is a disadvantage here, but it could be an advantage elsewhere and it will be addressed separately in the second half of the chapter in a case study on *5-exo/6-endo-dig* selectivity.

Returning to the current topic, the sequential gold(I)-catalyzed [3,3]-rearrangement/Nazarov cyclization was studied by Prof. Occhiato and his co-workers using four different set of substrates each of which bearing different common *N*-protecting groups such as Boc, Cbz, CO₂Me and tosyl (Ts) (Figure 4.2.4). To avoid the above mentioned potential competition between the protecting group (*N*-alkoxycarbonyl group) and the acetyloxy group, they decided to optimize the reaction conditions with compound **16a** (Figure 4.2.4), which is bearing a *N*-Tosyl protecting group.

They found the best conditions (3 mol-% Ph₃PAuCl/AgSbF₆, in DCM at room temperature) for **16a** after screening a series of silver and copper salts (AgOTf, AgSbF₆, Cu(OTf)₂ etc.) and a good number of different solvents (toluene, DCM etc.). The major product was cyclopentenone **20a** accompanied with lower amounts of acetate **17a** and only traces (<5 %) of **18a** in almost every case, except when they used AgOTf as the source of the non-coordinating anion. In that case, the major product was **17a** while the minor was **20a** (Figure 4.2.4). Thus, the acetate **17a** was always obtained in mixture with corresponding cyclopentenone **20a** which has the

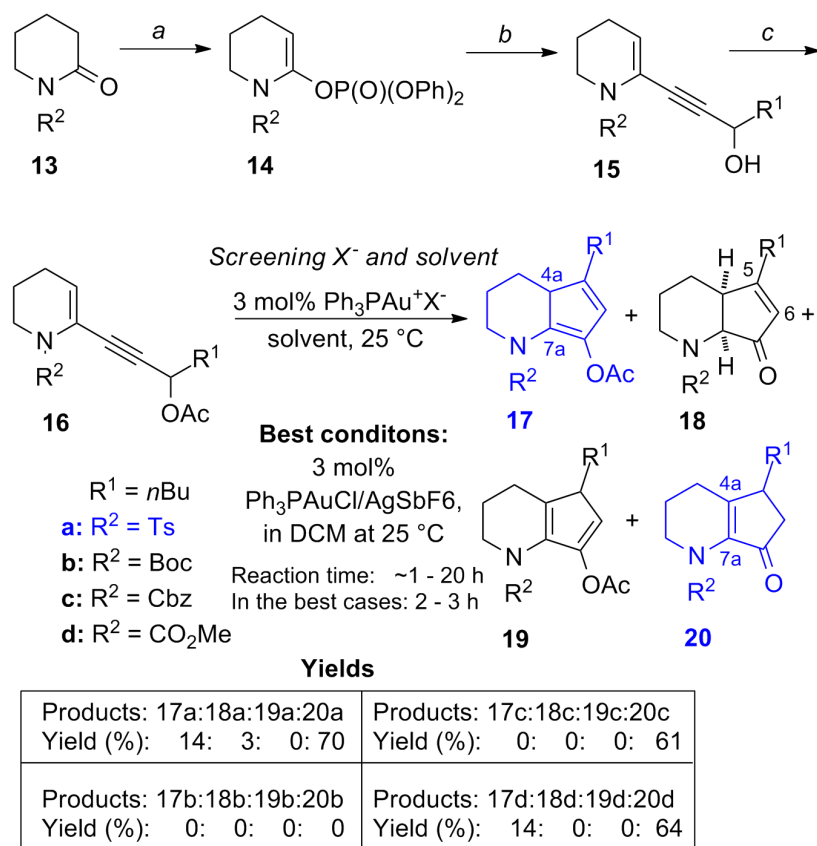


Figure 4.2.4: Synthesis of the Substrates (**16**) and the Possible Products of the Gold(I)-Catalyzed Nazarov Reaction (**17**, **18**, **19** and **20**). The Corresponding Yields are also Given at the Best Conditions. *a*, *b* and *c* are the Steps of the Substrate Synthesis. For Further Details See [192] or the Appendix.

more substituted double bond in **4a–7a** position and possibly deriving from the hydrolysis in situ of its acetate precursor **19a** (Figure 4.2.4).

Thereafter, they applied the optimized conditions in the case of the other substrate types as well (**16b**, **16c** and **16d**). The reactivity of substrates **16b–d** was much lower than **16a**, which is in agreement with the anticipated possible interaction of the carbamate carbonyl group with the activated triple bond before the acetate rearrangement. The reaction did not work with the *N*-Boc derivative **16b** and produced only degradation products plus a minor amount of the oxyuration product. In the case of Cbz (**16c**) the reaction resulted **20c** as a sole product, while the product ratio remained similar to **16a** (major **20**, minor **17**) when CO₂Me was the *N*-protecting group (Figure 4.2.4).

The fact that our collaborators could in most cases isolate acetates (**17a** and **17d**) and never their isomers (**19a** and **19d**) from the crude reaction mixtures of the gold-catalyzed reactions, suggests that acetates **17**, after their formation in the protodeauration step involving oxyallyl cation **8** (Figure 4.2.5), only slowly hydrolyze under the conditions of the gold-catalyzed reaction. The regioselectivity of the reaction seems to be determined with these substrates just before this stage. Instead, isomers **19** are quickly converted into the corresponding cyclopentenones **20** and for this reason they were never isolated.

Since cyclopentenone **20** is the major or only product in the reactions carried out in DCM when using AgSbF₆ as the anion source it could be assumed that, under these conditions, between the two competing processes the formation of acetate **19** from oxyallyl cation **8** is faster than formation of its isomer **17** and that then a fast hydrolysis of **19** under the reaction conditions occurs.

For the sake of the deeper understanding of our collaborators approach to synthesize annulated *N*-heterocycles by gold(I)-catalyzed Nazarov reaction, a detailed computational study was performed. The energetics and structural features of the reactants, intermediates, transition states and products involved in this process were computed and analyzed taken into account of the corresponding experimental findings.

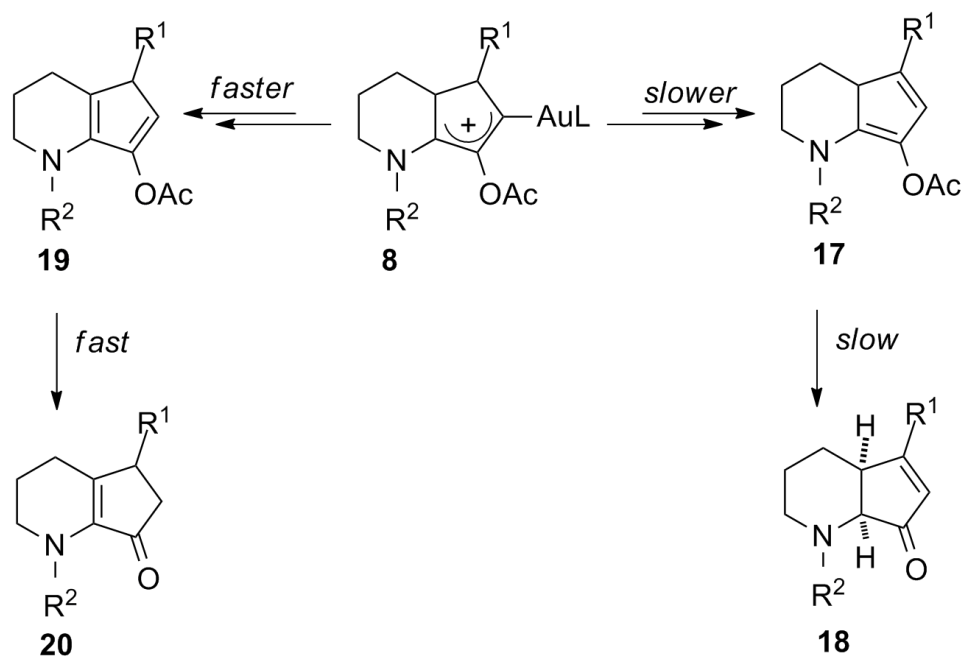


Figure 4.2.5: The Two Competing Pathways Towards the Cyclopentenone Products **18** and **20**.

4.2.2 COMPUTATIONAL METHODS

The structures were optimized by using density functional theory (DFT) using the B₃LYP hybrid density functional [101–103] combined with the 6-31G** and LANL2DZ [110–112] (for Au) basis set as implemented in Gaussian 09 [155]. The stationary points were characterized by frequency calculations in order to verify that they have the right number of imaginary frequencies.

4.2.3 RESULTS AND DISCUSSION

During the calculations, two model substrates were considered in which methyl was used at the propargylic position (R^1) and tosyl group or CO_2Me used as a N -protecting group (R^2) (Figure 4.2.6).

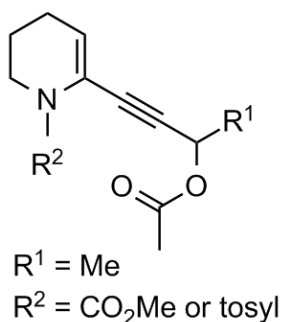
Model Substrates

Figure 4.2.6: Model Substrates Designed for Calculation Purposes.

The one with the tosyl group intended to mimic **16a**, while the CO_2Me containing structure allow us to mimic the carbamate containing compounds **16b-d**. The CO_2Me is conformatifonally simpler than the tosyl group, for this reason the following discussion will focus on the model reaction which involves this substituent (Figure 4.2.7).

The alkynyl-gold(I) cationic complex **I** (Figure 4.2.7) was considered as the starting point of the mechanism ($G = 0$ kcal/mol), and all reported energies in the following discussion are relative to it. The energy values correspond to ΔG Gibbs Free energies. The results with the corresponding N -tosyl derivative are very similar and reinforce the conclusions.

Initially, the coordination of the gold atom to the triple bond induces a rapid two step acetate rearrangement to form the pre-Nazarov cyclization complex **III** (Figure 4.2.7). The attack of the acetate carbonyl oxygen of **I** to the gold-activated alkyne leads to the formation of a cyclic intermediate **II**, and the subsequent C–O

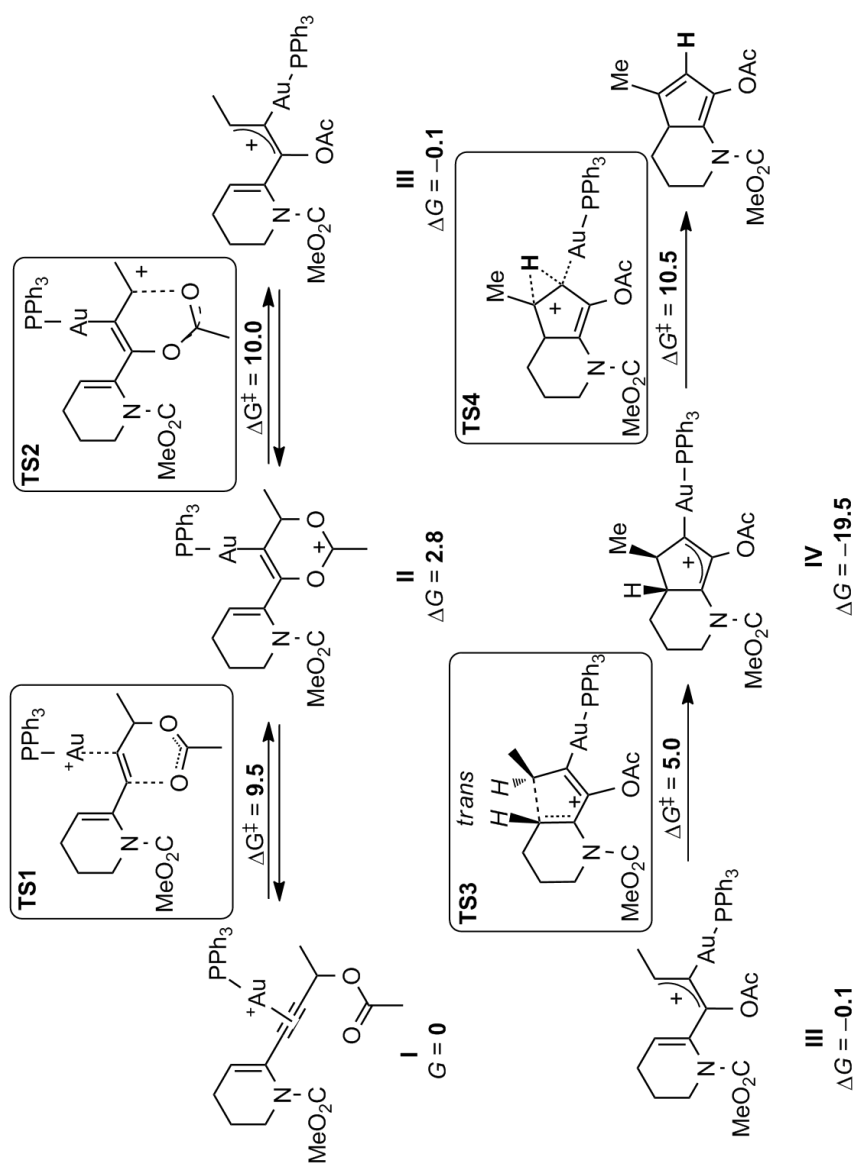


Figure 4.2.7: Reaction Mechanism. Top: Acetate Rearrangement in the Initial Steps of the Mechanism. Bottom: Cyclization Step from the pre-Nazarov cyclization complex **III** and Protodeauration. Gibbs Free Energy Changes (ΔG) and Barrier Heights (ΔG^\ddagger) are Given in kcal/mol.

bond breaking event renders an allylic cation (**III**), stabilized by the presence of the gold atom. This species could also be considered as a gold-carbene, although it should be more adequately described as a gold-stabilized carbocation [193].

Noteworthy, the computed energies indicate that **I** and **III** are isoenergetic (0.1 kcal/mol difference), and that the activation energies of both steps are fairly low, ca. 10 kcal/mol, meaning that in the absence of further evolution, **I** and **III** would be in an almost 1:1 fast equilibrium. However, complex **III** evolves through an easy cyclization to **IV**, a process that presents a very low barrier of 5.1 kcal/mol (**TS3**, Figure 4.2.7). In accordance to the conrotatory nature of the Nazarov reaction under thermal conditions, the reaction is predicted to be diastereoselective, with formation of the C–C bond that presents the two H atoms in a trans position. The alternative diastereoisomeric transition state, in which the two H are *cis* to each other is 3.9 kcal/mol higher in energy, and thus, not operative. The low activation barriers can explain the fast rate of a reaction that is completed at room temperature within 2-3 hours.

Although not shown in the Scheme, the results with the *N*-tosyl derivative are comparable, showing activation energies of 11.4 and 10.9 kcal/mol for the two step acetate rearrangement processes, a reaction energy of +0.7 kcal/mol in the formation of **III**, and a low activation barrier for the Nazarov cyclization (4.0 kcal/mol).

At this point, we attempted to explain the diene formation through a single-step intramolecular hydride shift with concomitant C–Au bond breaking. In fact, the corresponding transition structure **TS4** was located (Figure 4.2.7), but its accompanying activation energy (30 kcal/mol from **IV** to **TS4**) is too high to be feasible under the experimental reaction conditions. Interestingly, this [1,2]-H shift process has been postulated to be the rate-limiting step in the tandem [3,3]-rearrangement/Nazarov reaction of simpler enynyl acetates in the gas phase by Shi *et al* [194].

The [1,2]-H shift is not feasible in our case, because of which it is assumed that an external base is needed for the deprotonation, and it is important to highlight that several possible candidates exist in the reaction media, like the gold counterion in the gold(I) salt or the non-coordinating anion from the silver or copper

salt. Even some water molecules present in the reaction media could play a significant role and, in fact, the intervention of water molecules in the deprotonation/protodeauration steps has been suggested for the tandem process involving enynyl acetates **1** (Figure 4.2.2) in “wet” DCM [194].

We were particularly interested in the proton abstraction step since, based on the experimental findings, the regioselectivity of the reaction, which was not an issue with enynyl acetates **1** (only one type of final cyclopentenone product, Figure 4.2.2), seems to be determined with these substrates just at this point. Furthermore, Prof. Occhiato and his group showed that once the final diene-acetates **19** and **17** (models for acetates **VI** and **VIII**, respectively, Figure 4.2.8) are formed, there are not evident signs of significant equilibration between them during the reaction.

So, as a plausible approximation, and without knowing the exact nature of the molecule responsible for the abstraction, we decided to demonstrate that this is actually the regiodetermining stage, by computing the deprotonation step with triflate anion and water as a base (Figure 4.2.8).

Our computational results indicate that the triflate and water mediated hydrogen abstraction is, in fact, not highly regioselective, the difference between **TS5** and **TS6** being of only 0.8 kcal/mol and 0.6 kcal/mol, respectively, in favor of the formation of **VII** isomer (en route to **17**) when CO₂Me is the protecting group on the nitrogen. In the case of the triflate assisted deprotonation of the other model substrate bearing the *N*-tosyl group, the difference is even lower, only 0.4 kcal/mol (favoring **TS6**, (Figure 4.2.8)).

After the formation of **VI**- and **VIII**-type dienes (Figure 4.2.8), the most logical process would follow via hydrolysis to the final products (Figure 4.2.9).

There is a final interesting question at this point, regarding the very different experimental hydrolysis rates of the two diene types, **17** and **19** (see Figure 4.2.4). Once again, as the exact nature of the protonating species is unknown, we chose triflic acid and H₃O⁺ as simple models to study computationally this issue, and

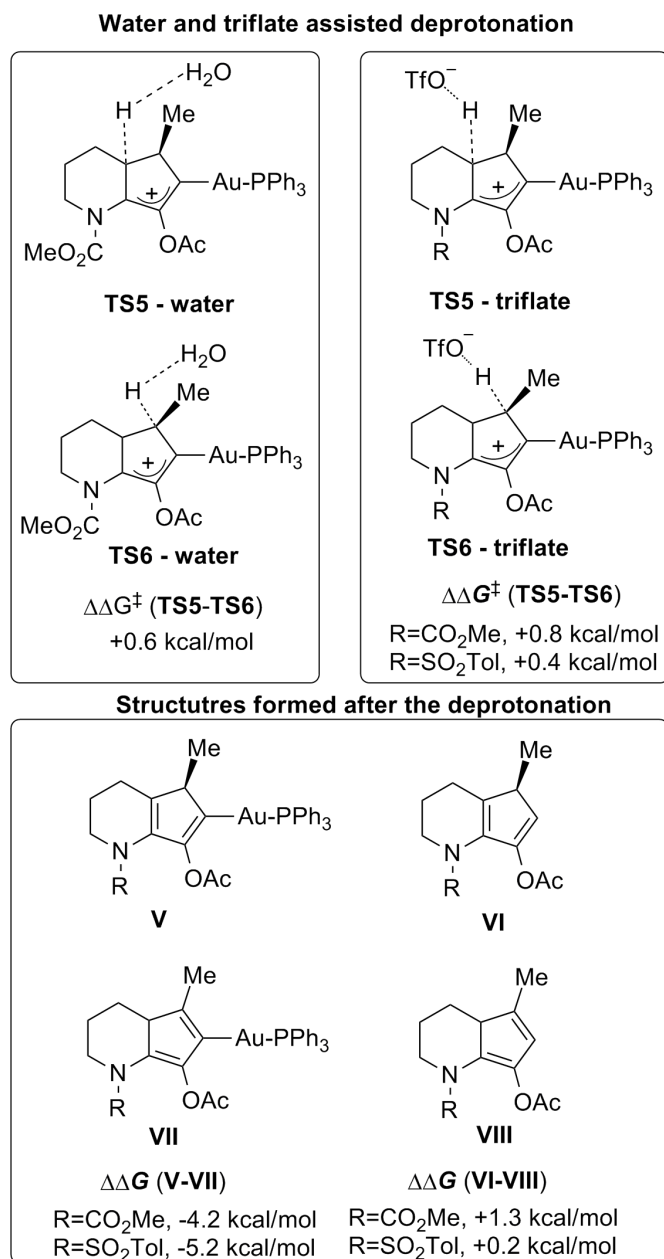


Figure 4.2.8: Relative Gibbs Free Energies of Transition States ($\Delta\Delta G^\ddagger$) **TS5** and **TS6** in the Presence of Triflate Anion and Relative Gibbs Free Energies of Compounds Formed afterwards ($\Delta\Delta G$).

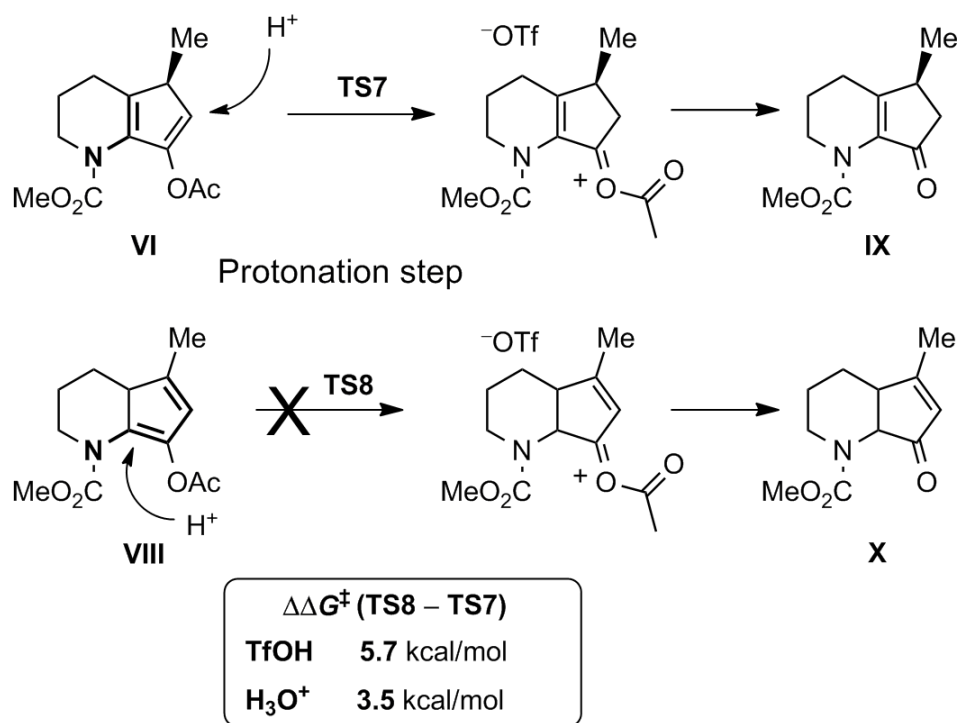


Figure 4.2.9: Hydrolysis of Diene-Acetates **VI** and **VIII** in the Presence of a Model Acid (TfOH or H₃O⁺).

the transition states for the proton transfer were located. Noteworthy, the protonation of **VI** (model of diene **19**) is predicted to be three or four orders of magnitude faster than the corresponding protonation of **VIII** (model of **17**), as derived from a 3.5 kcal/mol (H_3O^+) or 5.7 kcal/mol (TfOH) energy difference in favor of the former. These data easily explain why non-hydrolyzed **17** and hydrolyzed **20** are the final products of the reaction. The result can be understood in light of the dienamine structure of compound **17** (**VIII**, Figure 4.2.9), and the donor character of the nitrogen atom, which can induce a stabilization of that structure making it less prone to hydrolysis.

Concerning the lower reaction rates of *N*-alkoxycarbonyl protected substrates **16b–d**, the calculations predict the formation of a non-productive cyclized intermediate (**XI**), from carbonyl oxygen attack (Figure 4.2.10).

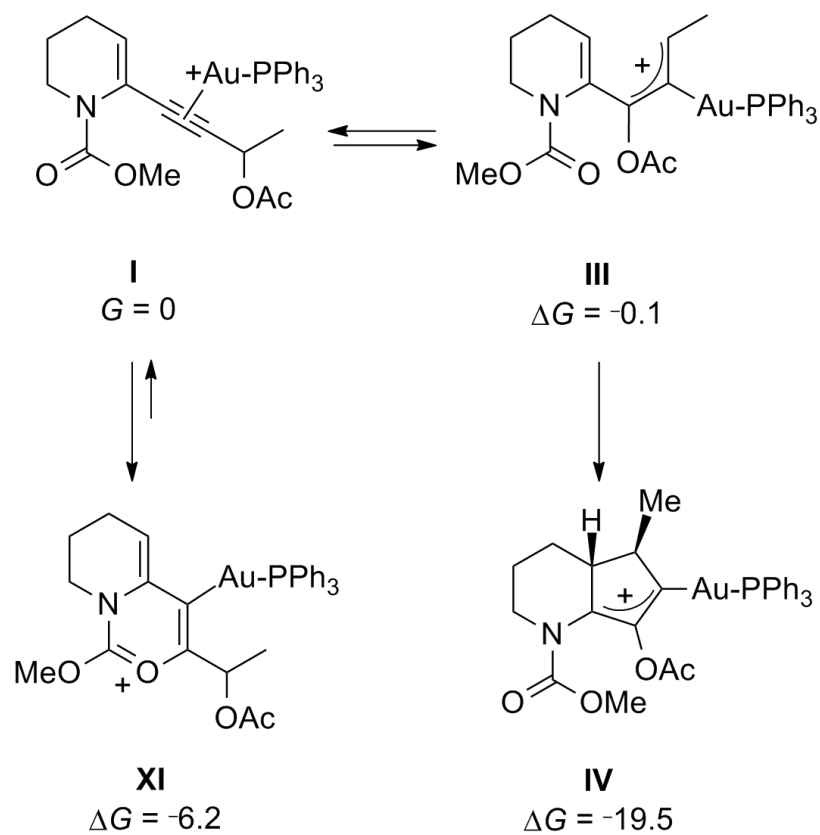


Figure 4.2.10: Predicted Formation of the Non-Productive **XI** Intermediate. Relative Gibbs Free Energies (ΔG) are Given in kcal/mol.

The starting compound **I** can proceed through acetate rearrangement to form **III** or through cyclization with the methyl ester to form **XI**. The three complexes **XI**, **I**, and **III** are in equilibrium, which is shifted towards the non-productive, but low in energy (-6.1 kcal/mol) side complex **XI**. Only the irreversible Nazarov cyclization from **III** to **IV** is finally able to displace this equilibrium towards the formation of the appropriate bicyclic adducts. Thus, **XI** is partially sequestering the gold catalyst and decreasing the reaction rate.

Additional experiments performed by Prof. Occhiato and his group shown that the torquoselectivity of the gold-catalyzed process is similar (*cis*) to the acid catalyzed Nazarov reaction, but lower than the corresponding classical reaction. It is not easy to address this issue, because the reason of the difference could be either kinetic (i.e. both clockwise and counterclockwise ring closures could take place at different rate in the putative intermediate) or related to the geometry of the oxalyl cation before ring closure.

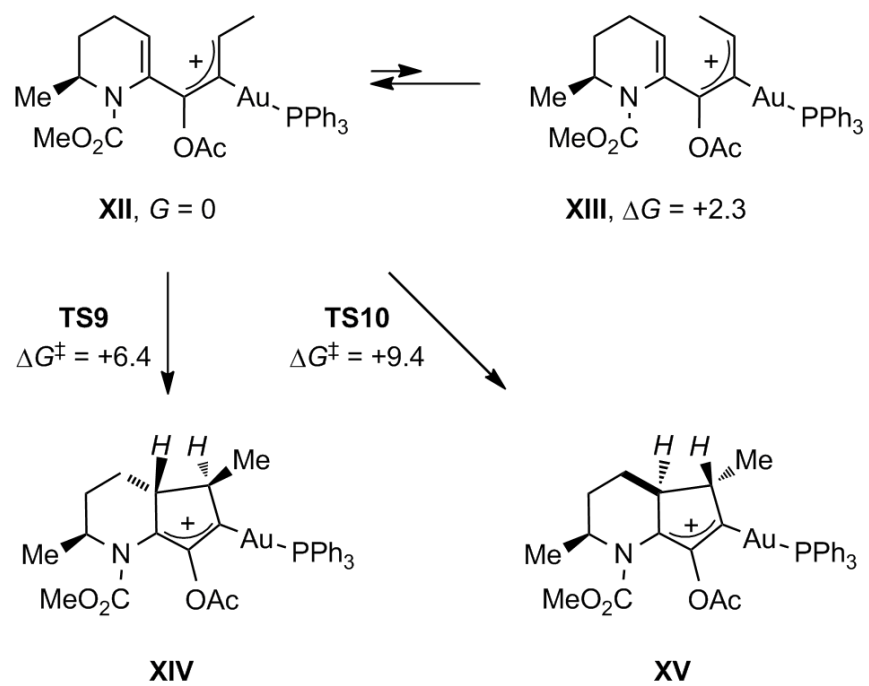


Figure 4.2.11: Study of the Torquoselectivity of the Ring Closure. Relative Gibbs Free Energies (ΔG) and Barrier Heights (ΔG^\ddagger) are Given in kcal/mol.

To study the torquoselectivity, an additional oxyallyl cation model compound was envisaged by adding a methyl group to **III** at the 2 position of the *N*-heterocycle and the two possible stable isomer (**XII** and **XIII**) were calculated (Figure 4.2.11).

The calculations revealed that the preference for **XII** is clear, with a difference of 2.3 kcal/mol over **XIII** because of steric reasons. Thus the major *cis* dimethyl diastereoisomer (**XIV**) is formed by a counterclockwise conrotatory ring closure of **XII**, with a low activation energy of 6.4 kcal/mol (**TS9**), whereas its *trans* diastereomer **XV** is formed by conrotatory clockwise ring closure from **XII** (**TS10**, 9.4 kcal/mol). Because of the predominance of intermediate **XII** it is likely that the alternative pathway from **XIII** to **XV** is never operative.

4.3 GOLD(I)-CATALYZED CYCLOISOMERIZATIONS

4.3.1 INTRODUCTION

IN 1926, LUDWIG CLAISEN INTRODUCED THE VINYLOGY PRINCIPLE: the transmission of electronic effects through a conjugate system [195–197]. He used this to explain the fact that the acidic properties of formylacetone is similar to acetic acid [198].

According to the evolved terminology, vinylogous derivative of any molecule can be designed if the insertion of a carbon-carbon double bond (vinyl moiety) is possible between two functional groups which were neighbours in the original structure (e.g. formylacetone - vinylogous carboxylic acid) [196, 197] (Figure 4.3.1).

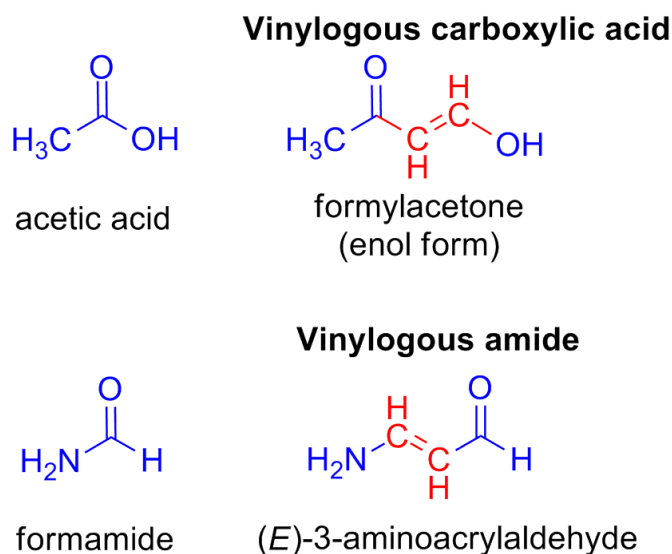


Figure 4.3.1: The Structure of Acetic Acid and Formamide along with their Vinylogous Derivatives Formylacetone and (*E*)-3-aminoacrylaldehyde, respectively.

Numerous application of vinyllogous structures are found in synthetic and medicinal chemistry [198]. For instance, vinyllogous amides are important synthetic intermediates of various natural products [170, 186].

Especially, the exocyclic vinyllogous amides, based on pyrrolidine or piperidine, form a precious group of compounds from which *N*-heterocycles and natural alkaloids (e.g. pinidinol [199], cassine [200], norallosedamine [201]) can be relatively easily prepared (Figure 4.3.2) [170, 186].

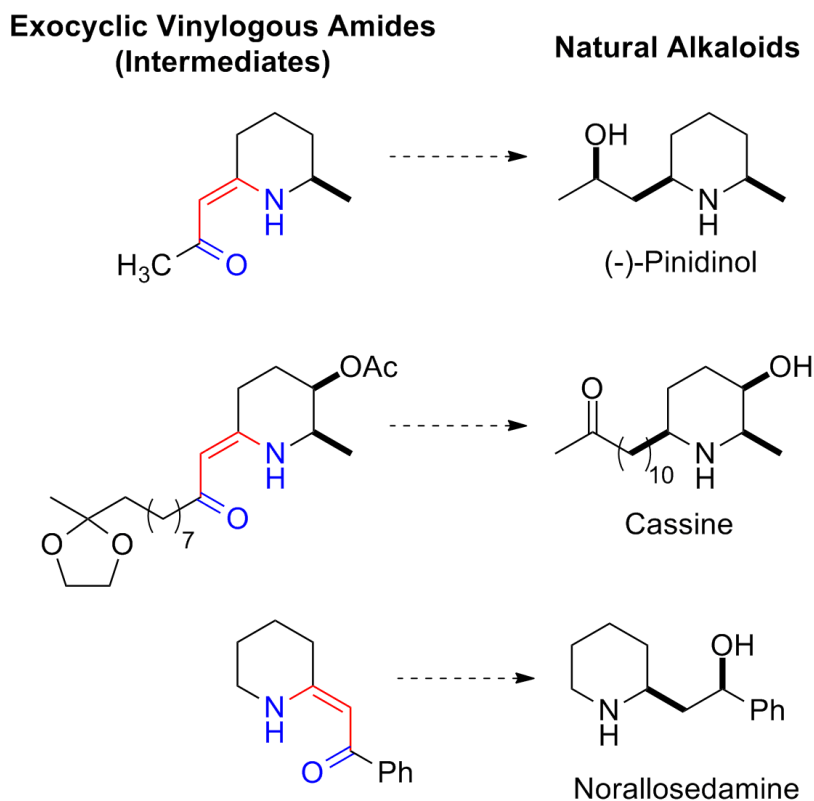


Figure 4.3.2: Synthetic Exocyclic Vinyllogous Amide Intermediates and the Corresponding Natural Alkaloids.

These exocyclic compounds are important in the pharmaceutical development and their therapeutic potential as antiepileptic drugs is also realized [202, 203].

For these reasons, the exocyclic vinylogous amides deserves special attention and their synthesis is of great interest to the chemical community in particular to medicinal and synthetic chemists.

Several methods have been developed to prepare exocyclic vinylogous amides [186]. Recently, Prof. Occhiato and his co-workers reported a new synthetic strategy based on gold(I)-catalyzed cyclization of *N*-Boc-protected 6-alkynyl-3,4-dihydro-2H-pyridines. By this method, cyclic intermediates produced which are easily convertible into the final vinylogous amide products (Figure 4.3.3) [186].

During the first stage of the process, gold(I)-catalyzed cyclization takes place within *N*-Boc protected enynes. The cationic gold(I) catalyst coordinating to the C-C triple bond and activating it, then the carbonyl moiety of the Boc, as a nucleophile, carry out a *6-endo-dig* attack on the activated bond forming neutral *endo* vinylgold species with *tert*-butyl fragmentation. Finally, the gold(I) catalyst is regenerated by protodeauration and cyclic carbamate intermediates produced. Then, these intermediates were hydrolyzed to achieve the final vinylogous amides (Figure 4.3.3) [186].

The Au(I)-catalyzed part of this process is similar to previously described examples in which *N*-Boc protected propargylamines were used to create oxazolidinones. However, the type of ring closure is different: it was *5-exo* in the previously reported cases [204–206] and exclusively *6-endo* in the above mentioned one.

These remarkably different results led our collaborators, Prof. Occhiato and his co-workers to carry out further experiments in this topic.

They attempted to extend the scope of the reaction by changing the protecting group (*N*-Boc to *N*-Cbz), the size and/or the substitution pattern of the heterocyclic ring and using saturated heterocyclic rings (piperidines) instead of unsaturated ones (3,4-dihydro-2H-pyridine) [170]. All the substrates which were studied before bear substituted alkyne groups, therefore they have tested structures with terminal alkyne moiety as well.

These experimental results pointed out the importance of the substitution of the alkyne group and that the *6-endo/5-exo-dig* selectivity depends on whether the

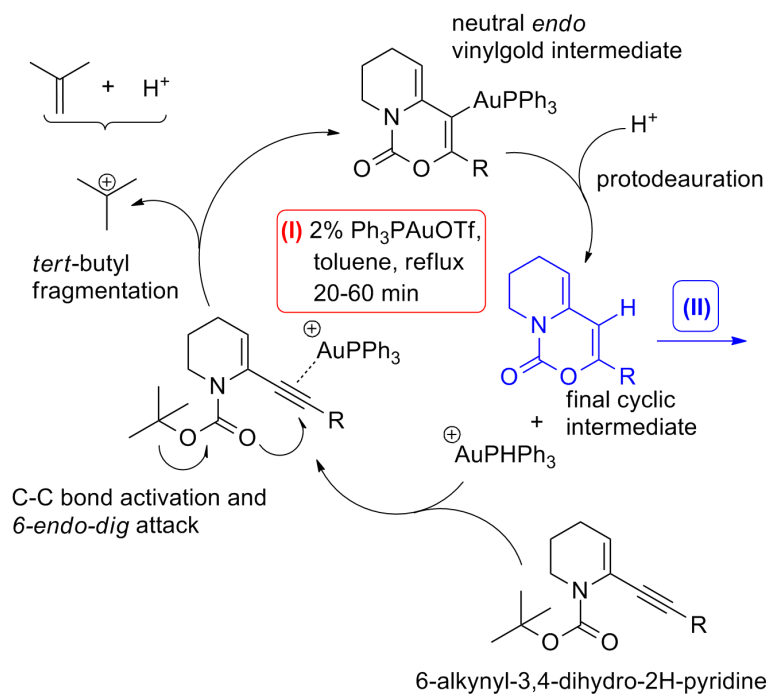
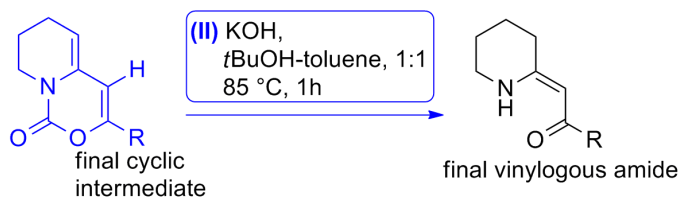
(I) Gold-catalyzed cyclization**(II) Hydrolysis**

Figure 4.3.3: (I) Gold(I)-Catalyzed Cyclization of *N*-Boc Protected Enynes and (II) Hydrolyzation to Produce Vinylogous Amides [186].

triple bond is internal or terminal (Figure 4.3.4).

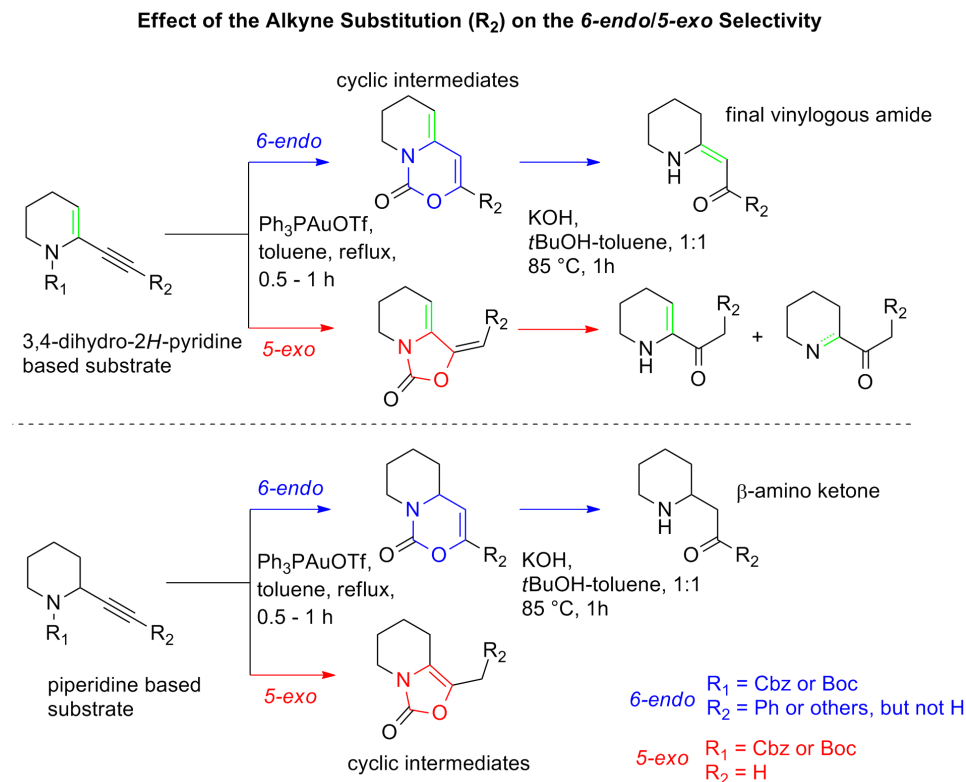


Figure 4.3.4: Test Reactions to Study the Effect of the Alkyne Substitution (R_2) on the 6-endo/5-exo Selectivity [170].

In collaboration with Prof. Occhiato and his group, we performed theoretical calculations to reveal what are the possible structural and/ or electronic features which lies behind the preference of 6-endo over 5-exo-dig attack during the gold-catalysed cyclization of enyne substrates with an internal triple bonds.

4.3.2 COMPUTATIONAL METHODS

The structures were optimized using density functional theory (DFT) with BHandHLYP [207] functional and the 6-31G* (LANL2DZ [110–112] for Au) basis set as implemented in Gaussian 09 [155]. The B3LYP functional was also evaluated [101–103]; it gave similar results to BHandHLYP, but some of the lowest-in-energy transition states did not converge properly when using B3LYP. Single point calculations were also performed using the Mo6-2X functional [100] combined with the 6-311++G**(SDD [108, 109]) basis set on the previously optimized structures, to better account for the dispersion forces of such large systems. The stationary points were characterized by frequency calculations in order to verify that they had the right number of imaginary frequencies. The intrinsic reaction coordinates (IRC) [156] were followed to verify the energy profiles connecting each TS to the correct associated local minima. Natural bond orbital (NBO) analysis [208] was carried out to evaluate the NPA atomic charges.

Since the *5-exo/6-endo-dig* selectivity trend does not depend on the alkoxy-carbonyl moiety [170], the *N*-Cbz protecting group was chosen, and compounds **1a**, **1b**, **2a**, and **2b** (Figure 4.3.5) were selected as model substrates for the cyclization reaction, as examples of the four possible combinations of saturated/unsaturated rings and substituted/unsubstituted alkynes.

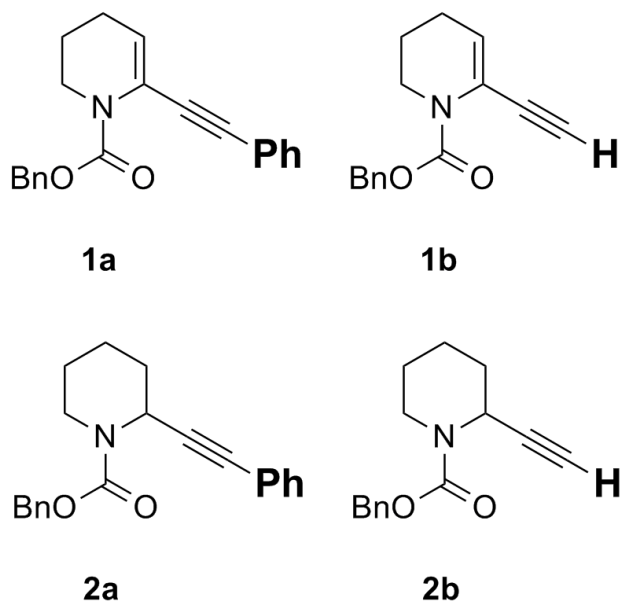


Figure 4.3.5: Selected Model Substrates for Calculations.

4.3.3 RESULTS AND DISCUSSION

Triphenylphosphine–gold(I) cation was used as the reaction catalyst, and the study focused on the cyclization, which is the regioselectivity-determining step. Given the very different degrees of steric hindrance at the two carbons of the triple bond in terminal alkynes (**1b** and **2b**), it would seem reasonable to hypothesize at first sight that steric effects were important for the observed *5-exo-dig* regioselectivity in these substrates, since the gold atom could preferably be placed at the least substituted terminal position during the attack of the oxygen atom. However, although this could be an important factor, this effect alone cannot explain the regioselectivity found in internal alkynes (**1a** and **2a**), since in those cases the two carbon atoms are sterically quite similar. Thus, calculations were carried out for the four alkyne–gold(I) complexes (only the unsaturated complexes, i.e., **1a-comp** and **1b-comp** are shown in Figure 4.3.6), and unsurprisingly, the complexes showed clear structural differences in terms of alkyne–gold complexation.

Specifically, in **1b-comp**, gold coordination induces a weakening of the triple bond [$\delta(C_a-C_b) = 1.23 \text{ \AA}$] and a strong asymmetry of the C–Au bonds [$\delta(C_a-Au) = 2.73 \text{ \AA}$, $\delta(C_b-Au) = 2.16 \text{ \AA}$]. The resulting complex can be considered to some extent as a vinyl cation. The calculated natural population atomic charges at the two carbon atoms are $+0.203 e (C_a)$ and $-0.480 e (C_b)$, which confirms that the positive charge of the complex is centred at C_a . These values are consistent with those calculated for a simple unsubstituted propargylic acetate,^[42b] although in our case the positive charge on C_a is even higher ($+0.203 e$ vs. $+0.063 e$), the C_a –Au bond length longer (2.73 vs. 2.514 \AA), and the C_b –Au bond length shorter (2.16 vs. 2.239 \AA). On the other hand, alkyne–gold complex **1a-comp** has a much more symmetrical structure, with nearly identical Au–C distances (Figure 4.3.6), and NPA (natural population analysis) charges ($C_a = -0.056 e$, $C_b = -0.002 e$). In this case, the positive charge is centred on the gold atom ($Au = +0.437 e$ in **1a-comp**, vs. $+0.365 e$ in **1b-comp**). As a result of the more positively-charged character of the internal C_a carbon atom in **1b-comp**, the attack of the oxygen atom takes place exclusively at that position. This experimental fact could be confirmed

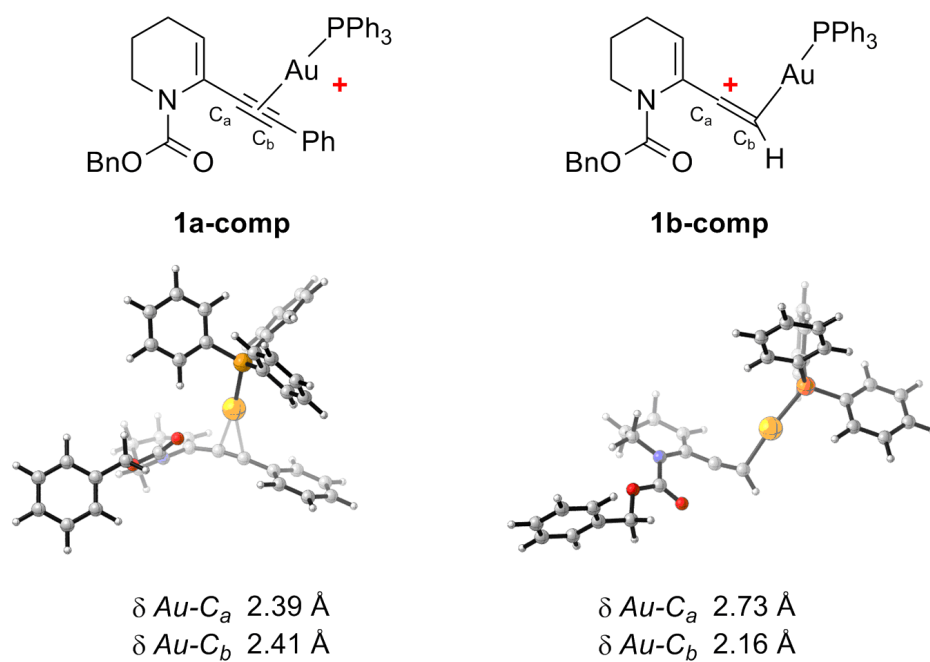


Figure 4.3.6: Structures and Structural Properties of 1a-comp and 1b-comp Complexes.

computationally with substrates **1b** and **2b**. We found that the *5-exo-dig* cyclization occurs with a very low barrier (3.9 kcal/mol for **TS1-H-5-exo**) or, in the case of the corresponding saturated compound **2a**, with essentially no activation barrier (**TS2-H-5-exo**, in Figure 4.3.7).

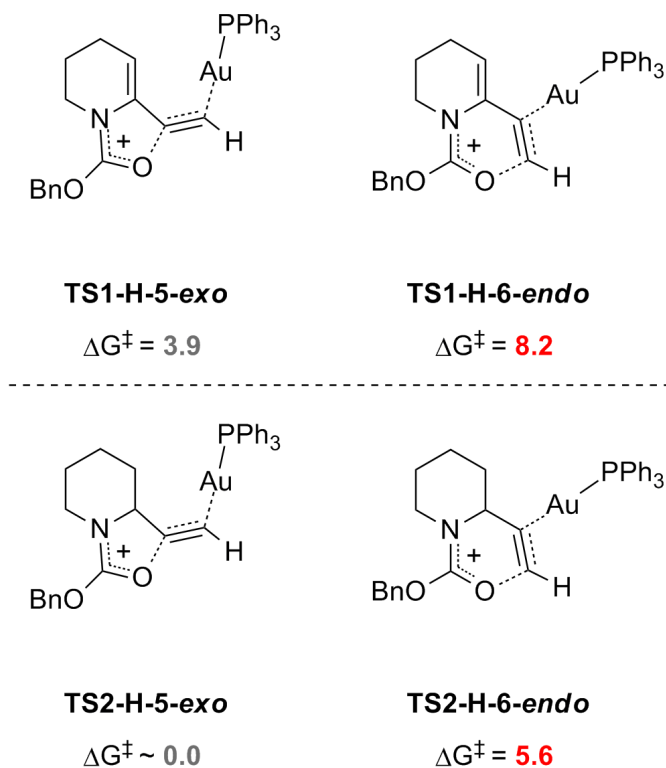


Figure 4.3.7: Transition State Structures and the Corresponding Barrier Heights for Terminal Alkynes. Barrier Heights (ΔG^\ddagger) are Given in kcal/mol.

In fact, no convergence or a convergence to the starting material was observed during the search for a transition state in the latter case, even though we tested different functionals (B3LYP, Mo6, BHandHLYP) and basis sets. To further analyse this issue, a potential scan for the O–C bond formation was carried out, and this confirmed that it is a downhill process without appreciable activation energy.

On the other hand, the transition states for the regioisomeric *6-endo* cyclizations were located, and were found to have low but measurable activation energies (8.2 and 5.6 kcal/mol, Figure 4.3.7), which are ca. 4–5 kcal/mol higher than those of the *5-exo* processes. This energy difference can explain the absolute experimental preference for the five-membered cyclic products. This is also consistent with the fact that a 1,2-acyl shift is preferred for propargylic acetates with an unsubstituted alkyne moiety.[42b] On the other hand, the transition-state structures for the reaction of the internal triple bonds are consistent with the experimental preference for the C_b attack. Thus, the lowest calculated activation energies were 7.8 kcal/mol for the unsaturated ring (**TS1-Ph-6-endo**, Figure 4.3.8), and 8.4 kcal/mol for **TS2-Ph-6-endo**.

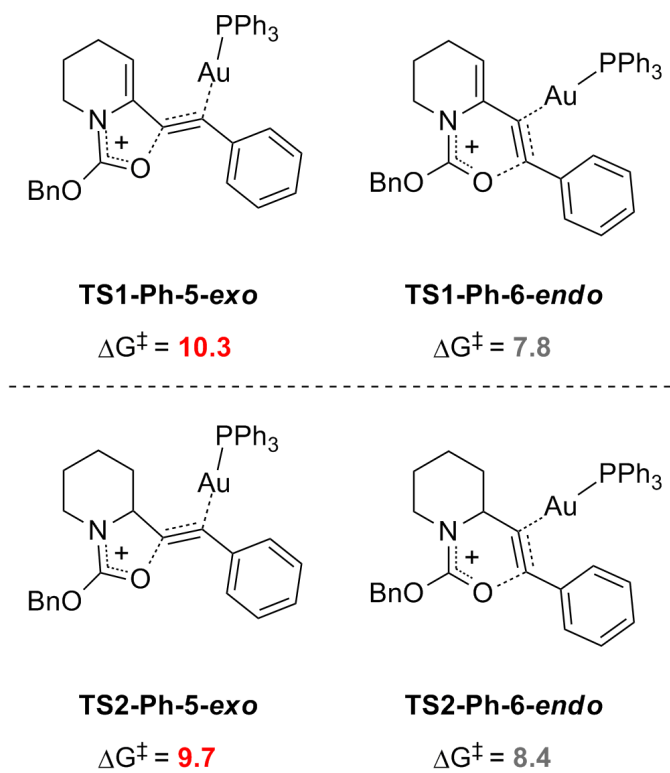


Figure 4.3.8: Transition State Structures and the Corresponding Barrier Heights for Internal Alkynes. Barrier Heights (ΔG^\ddagger) are Given in kcal/mol.

It is interesting to note that the *endo/exo* selectivity is predicted to be better for **1** ($\Delta\Delta G^\ddagger_{exo/endo} = 2.5$ kcal/mol) than for **2** ($\Delta\Delta G^\ddagger_{exo/endo} = 1.3$ kcal/mol). This effect can be attributed to the increase in the N-C-C_a angle induced by the presence of the double bond, from 113° (**16d**, N-C_{sp3}-C_a) to 119° (**1b**, N-C_{sp2}-C_a), a factor that plays against the formation of the smaller five-member ring.^[45] The data shown in Figure 4.3.6 and Figure 4.3.8 are not informative enough about the exact reason for the *6-endo* selectivity with internal alkynes, since C_a and C_b have very similar electronic properties, and their bonding distances with the gold atom are virtually equal (Figure 4.3.8).

Thus, we envisioned an indirect way to analyse the geometrical factors that determine the reactivity of the internal alkynes, by using symmetrical computational substrates (Figure 4.3.9).

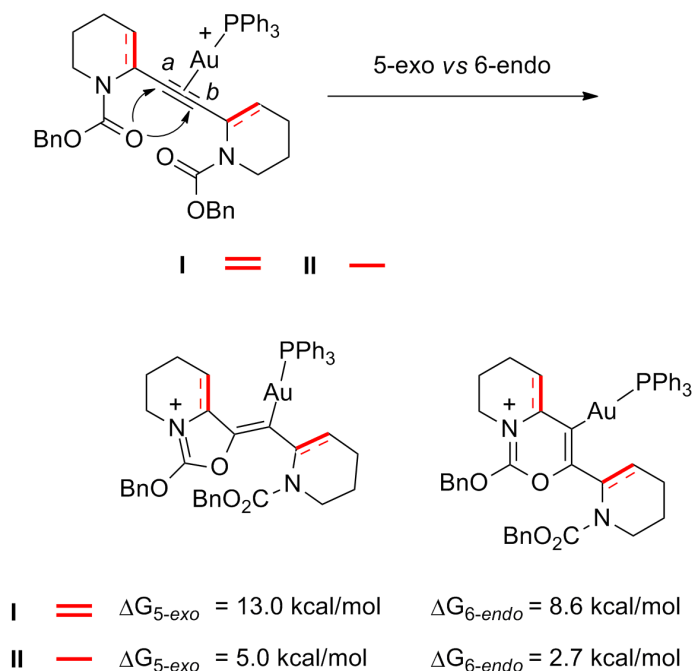


Figure 4.3.9: Comparison of the Activation Energies for the *5-exo* and *6-endo-dig* Pathways.

For example, in the model system **I**, the triple bond is symmetrically substituted, and the two carbons (C_a and C_b) are absolutely identical, which reduces the factors that affect the formation of one ring or the other to a simple geometrical preference. Interestingly, the activation energy is lower for the *6-endo* cyclization by 4.4 kcal/mol, indicating that in principle, the preference for the six-membered ring is purely geometrical, and could be generalized to any type of internal alkynes, irrespective of the substituent on the terminal position. It is worth mentioning that a similar preference, but to a lesser extent ($\Delta\Delta G^\ddagger = 2.3$ kcal/mol), was found for computational model compound **II**, with saturated rings, which is consistent with the generally lower selectivity of this type of substrates.

4.4 CONCLUSIONS

4.4.1 GOLD(I)-CATALYZED NAZAROV REACTION

Our collaborators demonstrated that the tandem gold(I)-catalyzed rearrangement/Nazarov reaction of propargylic ester derivatives is a useful strategy for the synthesis of cyclopenta-fused *N*-heterocyclic structures present in many natural compounds. This synthetic process has been studied in deeply computationally. The energetics and structural features of the reactants, intermediates, transition states and products involved in this process were computed and analyzed taken into account of the corresponding experimental findings. The calculations revealed the details of the reaction mechanism which allowed us to evaluate energetically the influence of the substrate structures on the reaction rate and on the regio- and stereoselectivity.

4.4.2 GOLD(I)-CATALYZED CYCLOISOMERIZATIONS

Prof. Occhiato and his co-workers reported a new synthetic strategy to produce exocyclic vinylogous amides based on gold(I)-catalyzed cyclization of *N*-Boc protected 6-alkynyl-3,4-dihydro-2H-pyridines. The first stage of this process is a gold(I)-catalyzed cyclization within *N*-Boc protected enynes. The cyclization can take place through *5-exo-* or *6-endo-dig* attack. The factors defining the preference of the processes were studied experimentally and computationally.

The calculations showed that the oxyuration step has a low barrier or almost no barrier at all when it involves the internal position of a terminal triple bond, resulting in a *5-exo-dig* process. In contrast, the *6-endo-dig* mechanism is always favoured with substituted alkynes, this preference being purely geometrical and irrespective of the type of substitution, thus providing either β -enaminones or their reduced equivalents, β -amino ketones, in a robust, reliable, and convenient way.

Time is an illusion. Lunchtime doubly so.

Douglas Adams, *The Hitchhiker's Guide to the Galaxy*

5

Baldwin Type Rules for Metal Catalyzed Cyclizations

5.1 INTRODUCTION

THE BASIC FRAMEWORK, of many complex and biologically interesting molecules and a plethora of natural products includes cyclic moieties [170, 192, 209]. Thus, most of the designed and developed small molecule inhibitors and drugs have also a cyclic skeleton [210]. Therefore, to predict or control the outcome of cycliza-

This chapter is based on the following manuscript: B. Fiser, J. M. Cuerva, E. Gómez-Bengoa, *Chemical Communications*, submitted in 2016.

tions is crucial in the design and implementation of synthetic procedures. One of the first key steps towards the applicable predictions was done by Sir Jack Baldwin in 1976, when his seminal work "Rules for Ring Closure" was published [211].

Prof. Baldwin used three parameters to describe and classify the ring forming reactions and these are still the basis of the nomenclature of cyclizations (Figure 5.1.1).

Terminology of Cyclizations

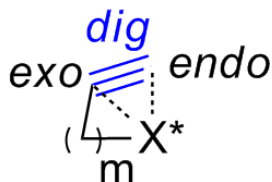
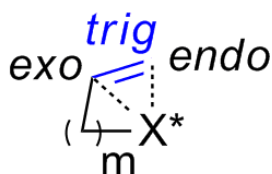
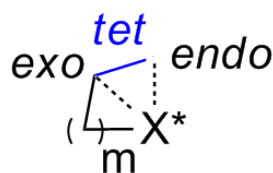


Figure 5.1.1: Baldwin's Terminology of Cyclizations. X^* must be a First Row Element According to the Original Paper. *exo*: $m = n - 2$; *endo*: $m = n - 3$, n - Number of Atoms in the Forming Ring; Hybridization of the Ring Closing Carbon: *tet* - sp^3 , *trig* - sp^2 , *dig* - sp [211].

The first parameter which was used to define the system is the size of the formed ring, which is nothing but the number of atoms (n) in the skeleton of the cycle ($n = 3 - 7$ in the original paper) (Figure 5.1.1).

Then, he referred to a process with the *exo* prefix if the breaking bond is exocyclic with respect to the formed ring and used the *endo* in the other way around (Figure 5.1.1).

Finally, the geometry of the ring closing carbon atom (hybridization) indicated by the *tet*, *trig* and *dig* suffixes, meaning tetrahedral (sp^3), trigonal (sp^2) and digonal (sp), respectively (Figure 5.1.1).

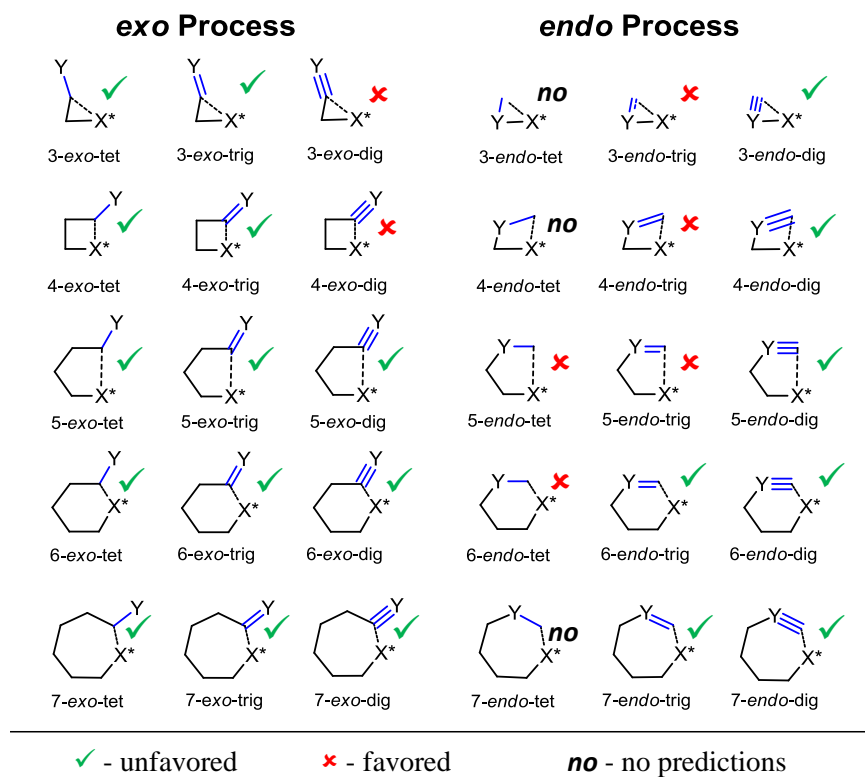
In his paper, Prof. Baldwin proposed three set of rules (Baldwin's rules) on an empirical basis to predict the relative easiness ("*relative facility*") of ring formations (ring closure/cyclization) [211].

"Ring-forming reactions are important and common processes in organic chemistry. I now adumbrate a set of simple rules which I have found useful in predicting the relative facility of different ring closures. I believe these will be useful to organic chemists, especially in planning syntheses."

— *Sir Jack Baldwin* [211]

The favored 3-7 member ring formations based on Baldwin's paper (original Baldwin's rules) and the corresponding classification are shown in Figure 5.1.2. In the case of *tet* and *trig* targets, there is a clear preference for *exo* processes, while in case of *dig* targets the other way around, mainly *endo* closures are favored and *exo* processes are only viable for larger cycles ($n = 5-7$). Originally nucleophilic ring closures were discussed, and the reactions were limited to involve first row elements (X), as a consequence of the larger atomic radii of heavier atoms, which can bypass the geometric restraints on disfavored ring closures (Figure 5.1.1). It was also noted that the rules applies to homolytic and cationic reactions as well [211]. However, a few years later, for radical involved cyclizations other guidelines were developed by Beckwith *et al.* [212].

The rules arise from the different stereochemical requirements which needs to be satisfied to form the transition states and thereafter the corresponding rings. A process is favored if the length and the nature of linking chain allows the terminal atoms to reach each other through a proper trajectory to close the cycle [211].



		Summary				
		Ring Size (n)				
		3	4	5	6	7
tet	exo	✓	✓	✓	✓	✓
	endo	no	no	✗	✗	no
trig	exo	✓	✓	✓	✓	✓
	endo	✗	✗	✗	✓	✓
dig	exo	✗	✗	✓	✓	✓
	endo	✓	✓	✓	✓	✓

Figure 5.1.2: Baldwin's Rules for Ring Closure. Green - Favorable; Red - Unfavorable; **no** - Prediction was not Made; According to Baldwin's Original Work [211].

Reactions are disfavored if the changes to achieve the ring forming configuration would lead to intense distortion within the structure and therefore, alternative reaction pathways may appear. All in all, the most favored trajectory of a cyclization is the one which accompanied with the least motion/distortion (least motion argument).

To find the ideal trajectory for the ring closing step is crucial, because the preference of the reaction is depends on the existence of such a reaction path. Three favorable reaction trajectories were suggested by Baldwin, one for each of the three hybridization of the attacked carbon (Figure 5.1.3).

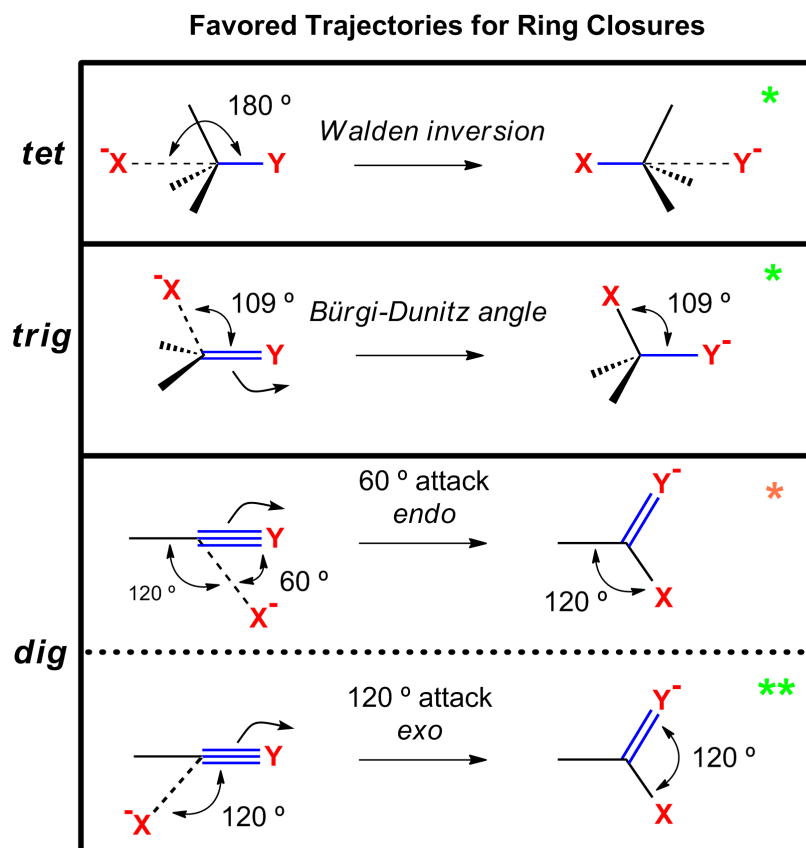


Figure 5.1.3: Favored Trajectories for Ring Closure Reactions in the Case of *tet*, *trig* and *dig* Systems. * - Baldwin's Prediction [211], ** - Revised Prediction [213].

Baldwin's suggestion for the preferred *tet* trajectory is associated with the Walden inversion process in S_N2 reactions. For the *trig* process, he proposed a trajectory based on the work of Bürgi and Dunitz *et al.*, who studied the reaction paths of the addition of various nucleophiles to carbonyl groups [214]. In digonal systems, two trajectories can be identified using the least motion argument, and maintain the angle between the three interacting atoms (-X-C-Y) during the cyclization. These trajectories can be easily associated with the *endo*- and *exo-dig* processes. Baldwin selected the *endo* path as overall preferred trajectory for digonal systems based on the available literature examples at that time (e. g. missing 4-*exo* product) [213]. However, contrary to this, several newer experimental and computational results supports that the *exo-dig* process is more preferred, which led to the re-evaluation of the original predictions [213].

Corrections and limitations of the Baldwin's rules have been reported since their publication [213, 215, 216], but they are still generally applied in many organic reactions, involving anions, cations, and radicals.

Furthermore, the rules, or at least the nomenclature, have been assumed to be applicable to transition metal-promoted reactions, especially in the context of the Palladium-catalyzed Heck-type reactions [217, 218].

However, a systematic comparative mechanistic study (activation energies) of their validity and selectivity in these metal-containing systems has not been reported. In this work, intramolecular carbometalations will be studied systematically by computational chemical tools and based on the results the extension of the Baldwin's rules for metal catalyzed ring closure reactions is proposed.

5.2 COMPUTATIONAL METHODS

The structures were calculated by using the Mo6 hybrid density functional [100] as implemented in Gaussian 09 [155]. Optimizations were carried out by using the 6-31+G(d,p) basis set for C, H, O, P and Li. For Ni, Pd and Pt, the Stuttgart-Dresden (SDD) energy-consistent effective core potentials (ECPs) [108, 109] were used. Solvent effects were taken into account in optimizations at the same levels of theory by applying the conductor-like polarizable continuum model (CPCM) [219, 220]. The solute cavity was constructed using radii from the UFF force field. The dielectric constant for the model solvent (dichloromethane) was 8.93 and the electrostatic scaling factor for the radius of the atoms was 1.1. Reported energy values correspond to Gibbs Free (G) energies. The critical stationary points were characterized by frequency calculations in order to verify that they have the right number of imaginary frequencies, and the intrinsic reaction coordinates (IRC) [156] were followed to verify the energy profiles connecting the key transition structures to the correct associated local minima.

Three type of reactions are differentiated within our calculations (favorable, borderline and unfavorable) and associated with certain reaction conditions and barrier heights. If the activation energy of a process is lower than 24 kcal/mol (reaction can complete within 12 h at room temperature) it is considered as a favorable reaction. If the activation energy is > 31 kcal/mol (reaction time longer than 36 h at 100°C) the process is unfavorable. Otherwise, if the barrier height is > 24 kcal/mol, but < 31 kcal/mol we are talking about a borderline process.

5.3 RESULTS AND DISCUSSION

5.3.1 GENERAL CONSIDERATIONS

To expand the undoubted utility of Baldwin's rules we have computationally studied a set of intramolecular carbometalations of alkenes and alkynes of alkyl metals of group 10 elements ($M = \text{Ni, Pd, Pt}$) with different chain lengths (3 - 7) (Figure 5.3.1). In all cases, the coordination sphere of the metal was saturated with phosphine ligands, PH_3 for simplicity, and PMe_3 for validation purposes (Figure 5.3.1).

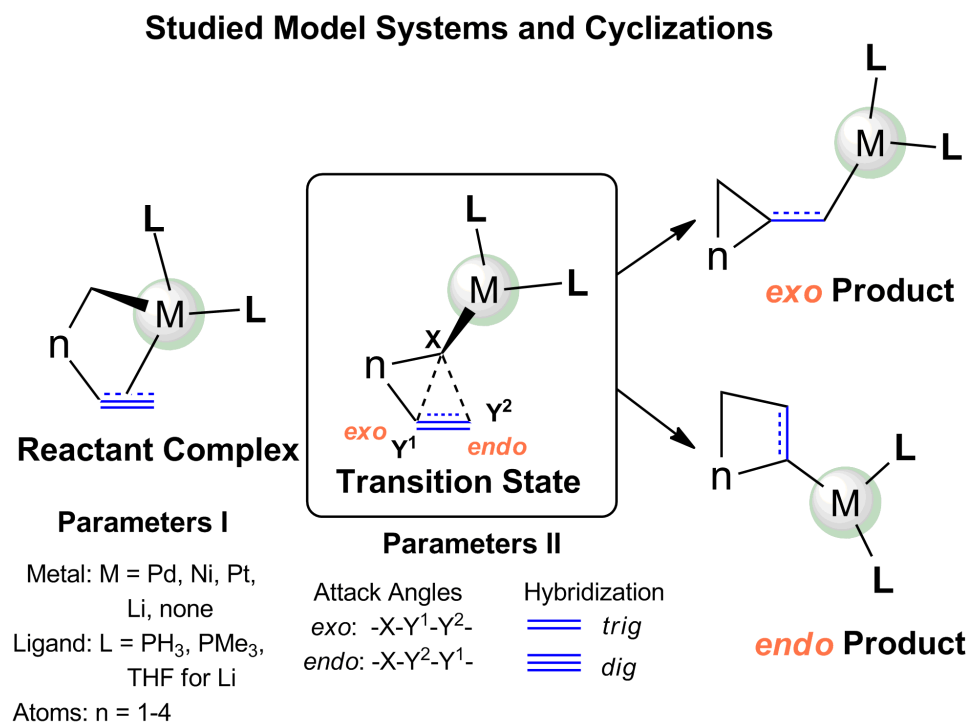


Figure 5.3.1: General Scheme of the Studied Model Systems and Cyclization Processes.

Within this context, carbometalations can be viewed as a special case of electrophile-promoted nucleophilic cyclizations, in which the electrophilic center, the metal, is strongly interacting with the carbanion.

5.3.2 PURE ANIONIC CYCLIZATIONS AND CARBOLITHIATIONS

For comparative purposes, the transition states of related carbolithiations ($M = \text{Li}$, Figure 5.3.1) were also calculated along with pure anionic species ($M = \text{none}$ (absence of any metal), Figure 5.3.1). Two tetrahydrofurans (THF) were used as ligands around the lithium in the calculations. In fact, carbolithiations are probably one of the most realistic mimic of pure anionic cyclizations, because lithium containing bases are widely used during such synthetic procedures [221, 222].

Regarding the carbolithiations, the activation energies for the *endo* channel are moderately higher in each case (up to 14.4 kcal/mol in 3-*endo-trig*) than predicted for pure anionic cyclizations, whereas *exo* cyclizations are only slightly affected (Figure 5.3.4 and Figure 5.3.3). For the *trigonal* compounds the difference is < 5 kcal/mol, but in different directions: the barrier height in 4-, and 5-*exo* increased by the introduction of lithium, thus pure anionic species are slightly more favored, while in 3-, and 6-*exo* the opposite. In the *digonal* species mostly the carbolithiations are more favored (in a range between 4.4 - 7.6 kcal/mol) than the anionic species except in the 5-*exo* cyclization in which the anionic transition state is preferred.

In general, *exo* cyclizations are always highly favored over the corresponding (n+1)-*endo* mode when lithium atom is present, the differences being very large for small ring sizes (3-*exo* vs 4-*endo* > 30 kcal/mol, Figure 5.3.2), and moderate as the size of the ring increases (6-*exo* vs 7-*endo* ca. 10 kcal/mol). The cases where an increment in the activation energy is noted from the pure anion to the organolithium derivative, can be rationalized by the lack of stabilization of the pure anionic starting material (Figure 5.3.2). Thus, the inclusion of the lithium atom decreases the energy of the starting point, increasing the activation energy (Figure 5.3.4 and Figure 5.3.3).

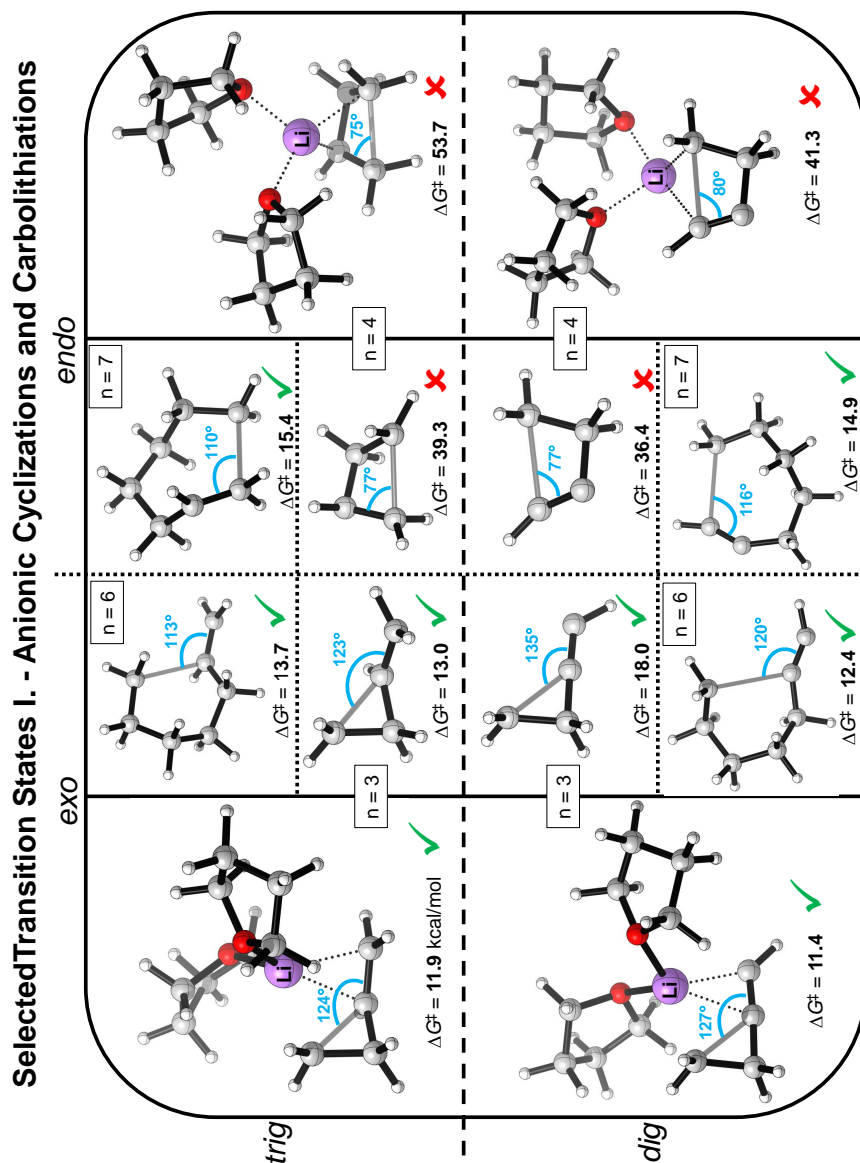


Figure 5.3.2: Selected Transition States I. - Anionic Cyclizations (middle) and Carbolithiations (edges). The Forming Bonds are Indicated with Faded Gray Lines. Corresponding Barrier Heights (ΔG^\ddagger , kcal/mol), Attack Angles and the Number of Atoms (n) in the Forming Cycles are also Shown. Green - Favorable; Red - Unfavorable. Calculated at the M06/6-31+G(d,p)/SDD Level of Theory in Dichloromethane.

The highest activation energy in the *exo-trig* and *-dig* set of carbolithiations and anionic cyclizations, corresponds to the *4-exo* compounds with 19.6 and 14.7 kcal/mol for *trig*, and 13.1 and 19.2 kcal/mol for *dig*, respectively (Figure 5.3.4 and Figure 5.3.3). These data clearly show that all *exo* cyclizations are attainable, and consistently under 20 kcal/mol (Figure 5.3.5).

Concerning the *endo* cyclizations, the *4-endo* species are consistently unfavorable and the barrier heights are over 35 kcal/mol for anionic and over 40 kcal/mol for the lithium containing cases (Figure 5.3.2). There are two borderline species within the *trig* set of carbolithiations, in which the activation energy for 5- and 6-*endo* are slightly higher than 24 kcal/mol.

The presented calculations for trigonal anionic and lithium containing species are in good agreement with Baldwin's original predictions (Figure 5.1.2 and Figure 5.3.5).

However, for digonal species Baldwin's rules predicted 3-*exo-dig* and 4-*exo-dig* to be prohibited while 3-*endo-dig* and 4-*endo-dig* to be favored. These predictions were revised by Alabugin *et al.* [216] and they ended up at a reverse situation predicting 3-, and 4-*exo* borderlines (these borderlines are defined in a different way than ours, for further details see [216]) and 3-, and 4-*endo* unfavorable reactions (Figure 5.3.5). Our calculations in the case of digonal species are in qualitative agreement with Alabugin's predictions [216] (Figure 5.3.5).

Furthermore, the similarities in the activation energies computed for *trig*- and *dig*-type anionic cyclizations and carbolithiation reactions also validate the computational approach used in this study (Figure 5.3.5, Figure 5.3.2).

On the other hand, the attacking angles defined by the nucleophilic carbon (X, Figure 5.3.1) and trigonal/digonal carbons (Y¹ and Y², Figure 5.3.1) also afford interesting data.

The presence of lithium widens the attacking angle by ca. 5° respecting the naked anion situation for *endo* processes (Figure 5.3.4, Figure 5.3.3 and Figure 5.3.2). Considering the *exo* approach for digonal compounds the anionic species

Activation Energies and Attack Angles – *trig* Cyclizations

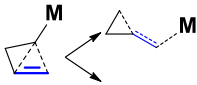
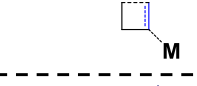
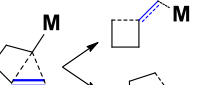

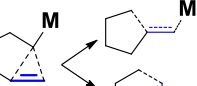
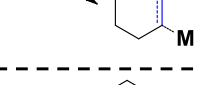
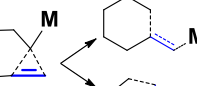
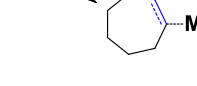
<i>trig</i>	none	Li	Ni	Pd	Pt
	3-exo ✓ 13.0 (123)	✓ 11.9 (124)	✓ 0.5 (112)	✓ 2.6 (114)	✓ 9.8 [†] (114) [†]
	4-endo ✗ 39.3 (77)	✗ 53.7 [†] (75) [†]	✗ 34.6 (76)	✗ 44.3 (76)	✗ 52.1 (77)
	4-exo ✓ 14.7 (128)	✓ 19.6 [†] (127) [†]	✓ 16.7 (122)	✓ 22.6 (123)	★ 27.5 (123)
	5-endo ✓ 16.3 (88)	★ 24.4 (97)	✓ 17.5 (89)	★ 26.7 (91)	✗ 33.9 (92)
	5-exo ✓ 8.7 (122)	✓ 10.4 (123)	✓ 9.3 (116)	✓ 11.9 (119)	✓ 18.9 (118)
	6-endo ✓ 18.9 (102)	★ 28.2 [†] (109) [†]	✓ 8.2 (100)	✓ 16.1 (102)	★ 25.5 (103)
	6-exo ✓ 13.7 (113)	✓ 11.3 (120)	✓ 9.8 (120)	✓ 15.6 (119)	✓ 21.6 (119)
	7-endo ✓ 15.4 (110)	✓ 21.6 (117)	✓ 16.1 (114)	✓ 18.4 (115)	★ 26.9 (115)

Figure 5.3.3: Activation Energies (kcal/mol) and Attack Angles for *trig* Cyclizations: M = none (Anionic), Li, Ni, Pd and Pt (Carbometalations). Green - Favorable; Orange - Borderline; Red - Unfavorable. Calculated at the M06/6-31+G(d,p)/SDD Level of Theory in Dichloromethane and in Some Cases (†) at the M06/6-31+G(d,p)/SDD//M06-2X/6-31+G(d,p)/SDD Level of Theory in Dichloromethane.

Activation Energies and Attack Angles – *dig* Cyclizations

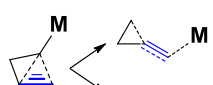
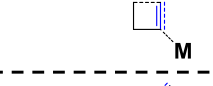
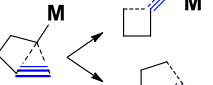
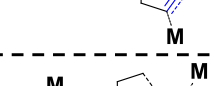
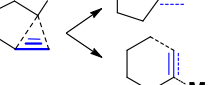
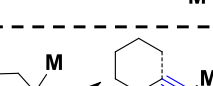
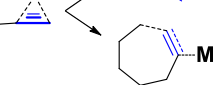
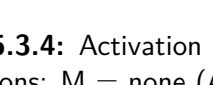
<i>dig</i>	none	Li	Ni	Pd	Pt
 3- <i>exo</i>	✓ 18.0 (135)	✓ 11.4 (127)	✓ 1.0 (126)	✓ 3.6 (125)	✓ 8.7 [†] (125) [†]
 4- <i>endo</i>	✗ 36.4 (77)	✗ 41.3 (80)	✗ 58.4 (88)	✗ 62.9 (86)	✗ 64.7 (90)
 4- <i>exo</i>	✓ 19.2 (132)	✓ 13.1 (127)	✓ 9.7 (124)	✓ 18.0 (125)	✓ 23.7 (125)
 5- <i>endo</i>	✓ 14.1 (85)	✓ 20.7 (90)	✗ 32.5 (103)	✗ 40.1 (103)	✗ 44.8 (105)
 5- <i>exo</i>	✓ 7.5 (124)	✓ 9.5 (117)	✓ 9.2 [†] (112) [†]	✓ 13.2 (116)	✓ 20.2 [†] (118) [†]
 6- <i>endo</i>	✓ 15.2 (101)	✓ 20.5 (107)	✓ 12.6 (84)	★ 25.9 (85)	✗ 31.8 (85)
 6- <i>exo</i>	✓ 12.4 (120)	✓ 8.0 (126)	✓ 9.6 (106)	✓ 21.2 (110)	✓ 19.7 (114)
 7- <i>endo</i>	✓ 14.9 (116)	✓ 18.1 (119)	✓ 8.4 (96)	★ 24.2 (103)	✓ 21.2 [†] (102) [†]

Figure 5.3.4: Activation Energies (kcal/mol) and Attack Angles for *dig* Cyclizations: M = none (Anionic), Li, Ni, Pd and Pt (Carbometalations). Green - Favorable; Orange - Borderline; Red - Unfavorable. Calculated at the M06/6-31+G(d,p)/SDD Level of Theory in Dichloromethane and in some Cases (†) at the M06/6-31+G(d,p)/SDD//M06-2X/6-31+G(d,p)/SDD Level of Theory in Dichloromethane.

have a wider attack angle by $5^\circ - 8^\circ$ than the corresponding lithium containing species, except the *6-exo* when the situation is reverse. In the trigonal transition states the attack angles are very close (1°) to each other comparing anionic and lithium containing species, except again the *6-exo*, in which the difference is 7° favoring the carbolithiation (Figure 5.3.4, Figure 5.3.3).

In general, larger angles have been found for the *exo* approaches, and within them the trigonal species varies in a range between $113^\circ - 128^\circ$, while for the digonal compounds the attack angles located in a slightly wider range between $117^\circ - 135^\circ$. In the *endo* processes, the attack angles are smaller than 120° in each case (Figure 5.3.4, Figure 5.3.3). The prohibitive activation energies appear when due to structural restrictions, the attacking angles are decreased to $75^\circ - 80^\circ$ (*4-endo* situations, Figure 5.3.2). In the two borderlines, which are appeared in the lithium set, the attack angles are 97° and 109° , for *5-endo-* and *6-endo-trig*, respectively. However, in the corresponding anionic species the angles are even smaller, 88° and 102° , respectively, while in the digonal species the angles are similar or a slightly smaller (Figure 5.3.4, Figure 5.3.3). Thus, the borderline status of these two carbolithiations are not explainable by the attack angles.

Regardless the type of approach (*endo/exo*) or the double/triple character of the reacting bond, there seems to be an ideal angle around $115^\circ - 125^\circ$ where activation energies are minimal.

Summary I - <i>trig</i>						Summary II - <i>dig</i>							
Ring Size (n)						Ring Size (n)							
Metal		3	4	5	6	7	Metal		3	4	5	6	7
none	<i>exo</i>	✓	✓	✓	✓	<i>no</i>	none	<i>exo</i>	✓	✓	✓	✓	<i>no</i>
	<i>endo</i>	<i>no</i>	✗	✓	✓	✓		<i>endo</i>	<i>no</i>	✗	✓	✓	✓
none ⁺	<i>exo</i>	✓	✓	✓	✓	✓	none ⁺	<i>exo</i>	✗	✗	✓	✓	✓
	<i>endo</i>	✗	✗	✗	✓	✓		<i>endo</i>	✓	✓	✓	✓	✓
						none [‡]	<i>exo</i>	★	★	✓	✓	<i>no</i>	
							<i>endo</i>	✗	✗	★	★	<i>no</i>	
Li	<i>exo</i>	✓	✓	✓	✓	<i>no</i>	Li	<i>exo</i>	✓	✓	✓	✓	<i>no</i>
	<i>endo</i>	<i>no</i>	✗	★	★	✓		<i>endo</i>	<i>no</i>	✗	✓	✓	✓
Ni	<i>exo</i>	✓	✓	✓	✓	<i>no</i>	Ni	<i>exo</i>	✓	✓	✓	✓	<i>no</i>
	<i>endo</i>	<i>no</i>	✗	✓	✓	✓		<i>endo</i>	<i>no</i>	✗	✗	✓	✓
Pd	<i>exo</i>	✓	✓	✓	✓	<i>no</i>	Pd	<i>exo</i>	✓	✓	✓	✓	<i>no</i>
	<i>endo</i>	<i>no</i>	✗	★	✓	✓		<i>endo</i>	<i>no</i>	✗	✗	★	★
Pt	<i>exo</i>	✓	★	✓	✓	<i>no</i>	Pt	<i>exo</i>	✓	✓	✓	✓	<i>no</i>
	<i>endo</i>	<i>no</i>	✗	✗	★	★		<i>endo</i>	<i>no</i>	✗	✗	✗	✓

✓ - Favorable ✗ - Unfavorable ★ - Borderline

★ - Borderline (Alabugin *et al.*) *no* - No Predictions

⁺ - Original Predictions by Baldwin [‡] - Corrected Predictions by Alabugin *et al.*

Figure 5.3.5: Summary of the Cyclization Rules for *trig* and *dig* Processes.

5.3.3 PALLADIUM PROMOTED CYCLIZATIONS

Carbometalations involving Ni, Pd and Pt were computed and they show some similarities and discrepancies with calculated values for carbolithiations and/or naked anions (Figure 5.3.3, Figure 5.3.4 and Figure 5.3.5).

The *exo* cyclizations are mostly favorable (up to 22.6 kcal/mol) with one borderline in the case of Pt-4-*exo-trig* (27.5 kcal/mol). In contrary, the *endo* processes are most likely unfavorable especially for carbopalladations and carboplatinations, up to 62.9 kcal/mol and 64.7 kcal/mol for Pd- and Pt-4-*endo-dig*, respectively (Figure 5.3.6 and Figure 5.3.12).

As expected, many examples of Palladium-mediated alkyl carbopalladations are known and fall into the 3- [223], 4- [224, 225], 5- [226, 227], and 6-*exo-trig* [226] cyclization modes (Figure 5.3.8).

The calculations revealed that, in general, 3- and 4-type Palladium-mediated alkylmetalations are slightly endergonic (Figure 5.3.7). In other words, these are not favored thermodynamically, which could explain their rare experimental occurrence and the necessity of a subsequent exergonic reaction in case of their appearance (i.e β -hydride elimination or coupling reaction, Figure 5.3.8, a).

However, for instance the 3-*exo-trig* is very competitive kinetically compare to the usually favored 5-*exo-trig* case with barriers as low as 2.6 kcal/mol and 11.9 kcal/mol, respectively (Figure 5.3.3). Consequently, competition between 3-*exo* and 5-*exo-trig* cyclizations has been described in literature [228, 229] (Figure 5.3.8, c), although a quantitative comparison with our results cannot be strictly made owing to the structural differences between the calculated and real structures.

Even for the more difficult alkyne substrates (*dig*), the computed values for the *exo* mode with Pd are low (≤ 21.2 kcal/mol). The fact that scarce examples have been described [230, 231], for this reactivity mode, can be attributed to the easiness of the competing β -elimination process that would become dominant in the presence of good donor ligands [230, 231] (Figure 5.3.9, a).

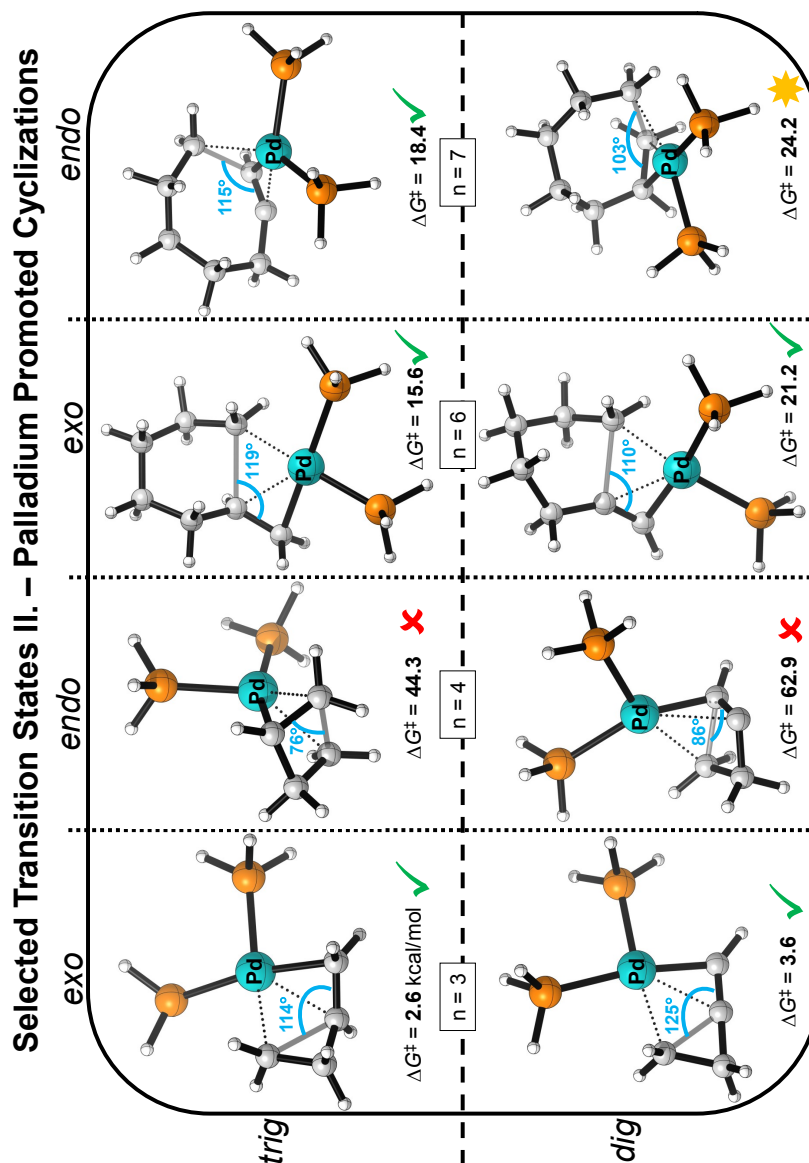


Figure 5.3.6: Selected Transition States III. - Palladium Promoted Cyclizations. The Forming Bonds are Indicated with Faded Gray Lines. Corresponding Barrier Heights (ΔG^\ddagger , kcal/mol), Attack Angles and the Number of Atoms (n) in the Forming Cycles are also Shown. Green - Favorable; Red - Unfavorable. Calculated at the M06/6-31+G(d,p)/SDD Level of Theory in Dichloromethane.

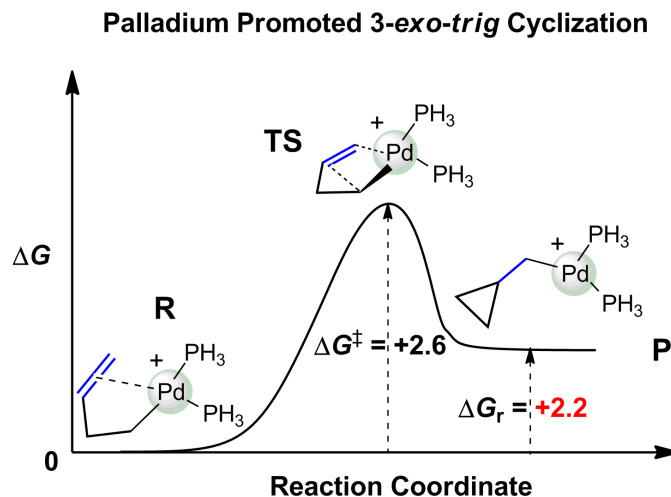


Figure 5.3.7: Reaction Energy Profile of the Palladium-Catalyzed 3-*exo-trig* Cyclization. ΔG^\ddagger and ΔG_r - Activation Energy and Reaction Energy (kcal/mol). R - Reactant; TS - Transition State; P - Product. Calculated at the M06/6-31+G(d,p)/SDD Level of Theory in Dichloromethane.

In any case, the main discrepancy between the computed carbopalladations and the original and revised Baldwin's rules is the low activation energy for 3-*exo-dig* (3.6 kcal/mol) and 4-*exo-dig* reactions (18.0 kcal/mol), which were previously reported as forbidden/borderline processes [211, 216] (Figure 5.3.5).

With respect to the less favored *endo* mode, the computed data show, high (> 40 kcal/mol) to exceedingly high activation energies (> 60 kcal/mol) for 4-*endo* (*trig* and *dig*) (Figure 5.3.6) and high barrier (> 40 kcal/mol) for 5-*endo-dig* cyclizations (Figure 5.3.4).

On the contrary, the most favored *endo* cases are the 6- and 7-*endo-trig* with barrier heights of 16.1 and 18.4 kcal/mol, respectively. They should be feasible in general, as the calculations shows and some experimental evidences also support this idea [232, 235] (Figure 5.3.9, **b**), whereas 5-*endo-trig* (26.7 kcal/mol) along with 6-, and 7-*endo-dig* (25.9 kcal/mol and 24.2 kcal/mol, respectively) should be also possible in certain circumstances.

It is worth noting that Baldwin's predictions considered 5-*endo-trig* cyclizations

Literature Examples of Pd-Catalyzed Cyclizations I.

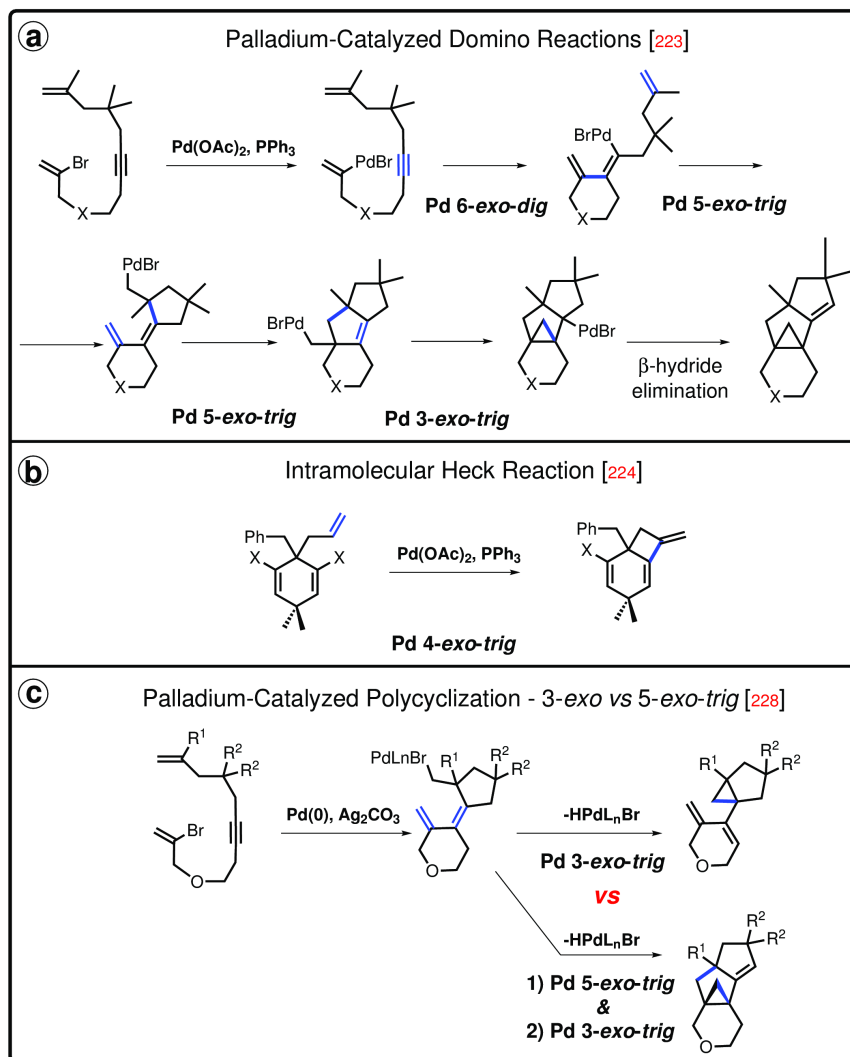


Figure 5.3.8: Literature Examples of Pd-Catalyzed Cyclizations I [223, 224, 228].

Literature Examples of Pd-Catalyzed Cyclizations II.

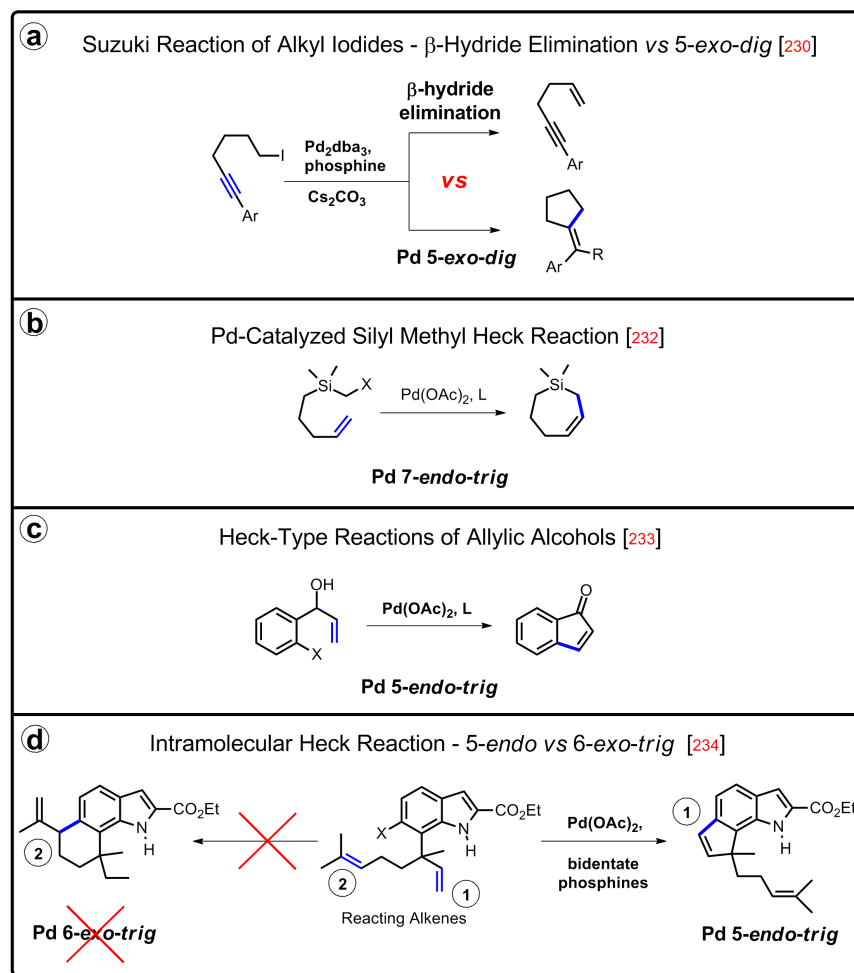


Figure 5.3.9: Literature Examples of Pd-Catalyzed Cyclizations II [230, 232–234].

to be unfavorable (Figure 5.3.5). Nevertheless, a few examples have been reported that follow the rule-breaking *5-endo-trig* cyclization [233, 236] (Figure 5.3.9, **c** and **d**). There is even a remarkable case, where the *5-endo-trig* product is regioselectively formed over the usually more favored *6-exo-trig* compound in a substrate containing two different reacting alkenes [234] (Figure 5.3.9, **d**). Nevertheless in these cases the carbon have sp^2 hybridation, somehow remembering the Baldwin's rules for alkylation of ketone enolates [237].

Nonetheless, there is a remarkable energy difference disfavoring the reactions of alkynes in comparison to alkenes, especially for the *endo* mode, in agreement with the scarcity of cyclization reactions for triple bonds. Again competing processes as β -hydride elimination could efficiently occur. Consequently, some *4-exo* and *5-exo-dig* reactions of alkenyl/aryl palladium intermediates have been described [238, 239].

These processes, especially the *4-exo-dig* were considered as forbidden [211] or borderline cases [216] for pure anionic reactions (Figure 5.3.5).

It is also of interest that the attacking angles for Pd-*exo* processes are in general very similar (slightly shorter) to those computed for the carbolithiations (Figure 5.3.3 and Figure 5.3.4). The angles for the *exo-trig* approaches range from 114° to 123° , whereas in the case of the *endo-trig* the restrictions imposed by the smallest cycles force the angles to be near 75° for the *4-endo-trig* transition state, widening up to 115° for *7-endo-trig* one (Figure 5.3.3, Figure 5.3.6).

Noteworthy, significant differences for the carbopalladations of alkynes were not found, in contradiction with previous beliefs. Moderate variations in the Tollman's cone value (θ) do not significantly affect the results, as one can see based on the similar results were obtained using PMe_3 ($\theta = 118^\circ$) as ligand instead of PH_3 ($\theta = 87^\circ$). In any case, calculations show that Baldwin's rules are basically of application for alkyl carbopalladations.

5.3.4 NICKEL PROMOTED CYCLIZATIONS

The barrier heights of the corresponding Ni derivatives were also calculated (Figure 5.3.3 and Figure 5.3.4). The cyclizations are consistently lower for Nickel than the previous ones for Palladium by 2.1 kcal/mol in the case of 3-*exo-trig* up to 15.8 kcal/mol in the case of 7-*endo-dig* (Figure 5.3.10), although the same trends in reactivity are maintained (Figure 5.3.3 and Figure 5.3.4).

All *exo*-cycles can be formed easily, with barrier heights ranging from 0.5 to 16.7 kcal/mol. Meanwhile, the decrease in the reaction barriers, affects positively some palladium-borderline cases, like 5-*endo-trig* or 6-, and 7-*endo-dig*, becoming feasible processes in theory with barrier heights of 17.7 kcal/mol, 12.6 kcal/mol and 8.4 kcal/mol, respectively (Figure 5.3.3 and Figure 5.3.4).

Also, the differences between the competing cyclization modes (*n-exo* vs *n+1-endo*) are much closer with nickel (Figure 5.3.10). Even a reversal in reactivity is observed in 6-*endo-trig* (8.2 kcal/mol) vs 5-*exo-trig* (9.3 kcal/mol), being regarded as non-selective (Figure 5.3.3 and Figure 5.3.4).

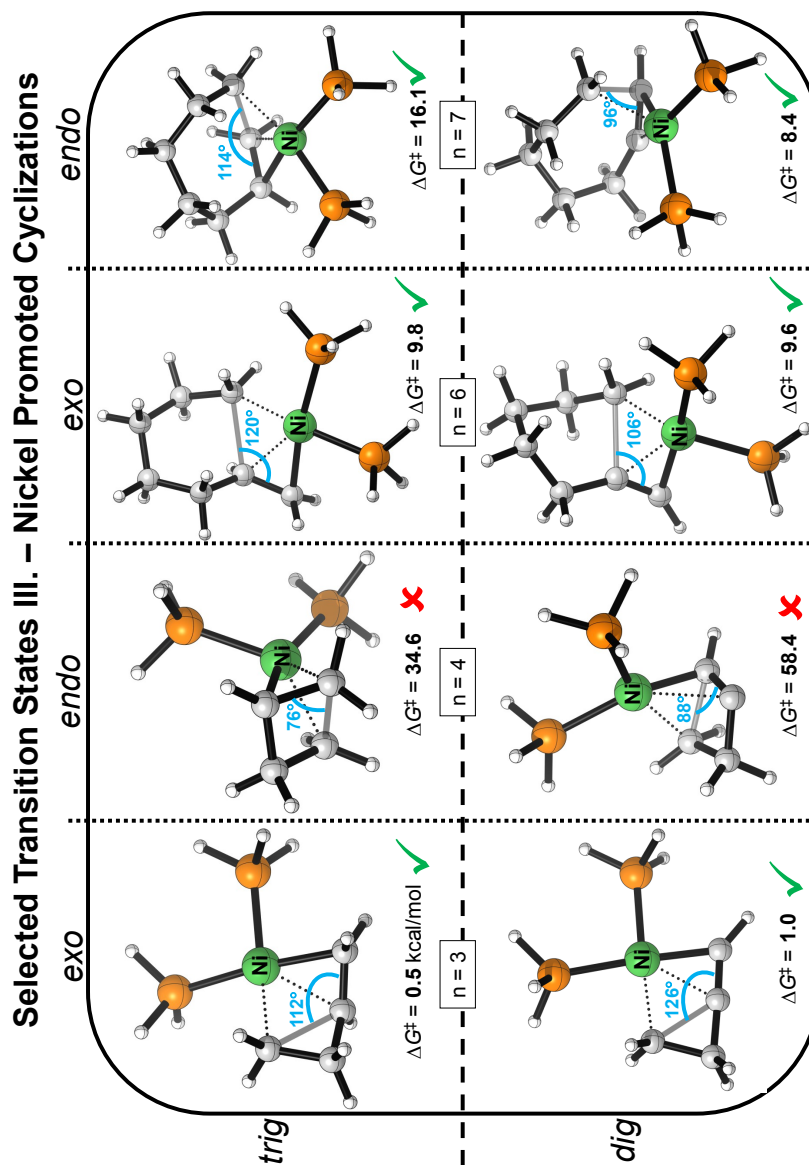


Figure 5.3.10: Selected Transition States III. - Nickel Promoted Cyclizations. The Forming Bonds are Indicated with Faded Gray Lines. Corresponding Barrier Heights (ΔG^\ddagger , kcal/mol), Attack Angles and the Number of Atoms (n) in the Forming Cycles are also Shown. Green - Favorable; Red - Unfavorable. Calculated at the M06/6-31+G(d,p)/SDD Level of Theory in Dichloromethane.

Noteworthy, in agreement with these findings, Cramer *et al.* have nicely shown that by the proper choice of the ligand of the nickel, the regiodivergent experimental formation of either 5-*exo* or 6-*endo* cycles from alkenyl nickel intermediates achievable from a single starting material [240] (Figure 5.3.11, **a**). Other authors have recently described Nickel-catalyzed 5-*exo-trig* [241] or 5-*exo-dig* [242] reactions of various substrates (Figure 5.3.11, **b** and **c**), in agreement with the computed activation energies (Figure 5.3.3 and Figure 5.3.4).

Surprisingly, we did not find significant differences in the attack angles between Pd and Ni in any case (it varies between 0° to 7°), in spite of the obvious different sizes of both atoms (Figure 5.3.3 and Figure 5.3.4). The maximum deviation we found was 7° for the case of 7-*endo-dig* cyclization (103° for Pd, 96° for Ni, Figure 5.3.10, Figure 5.3.6). Essentially, all the processes are favored with the exception of 4-*endo-trig*, 4-*endo-dig* and 5-*endo-dig* cases.

Literature Examples of Ni-Catalyzed Cyclizations

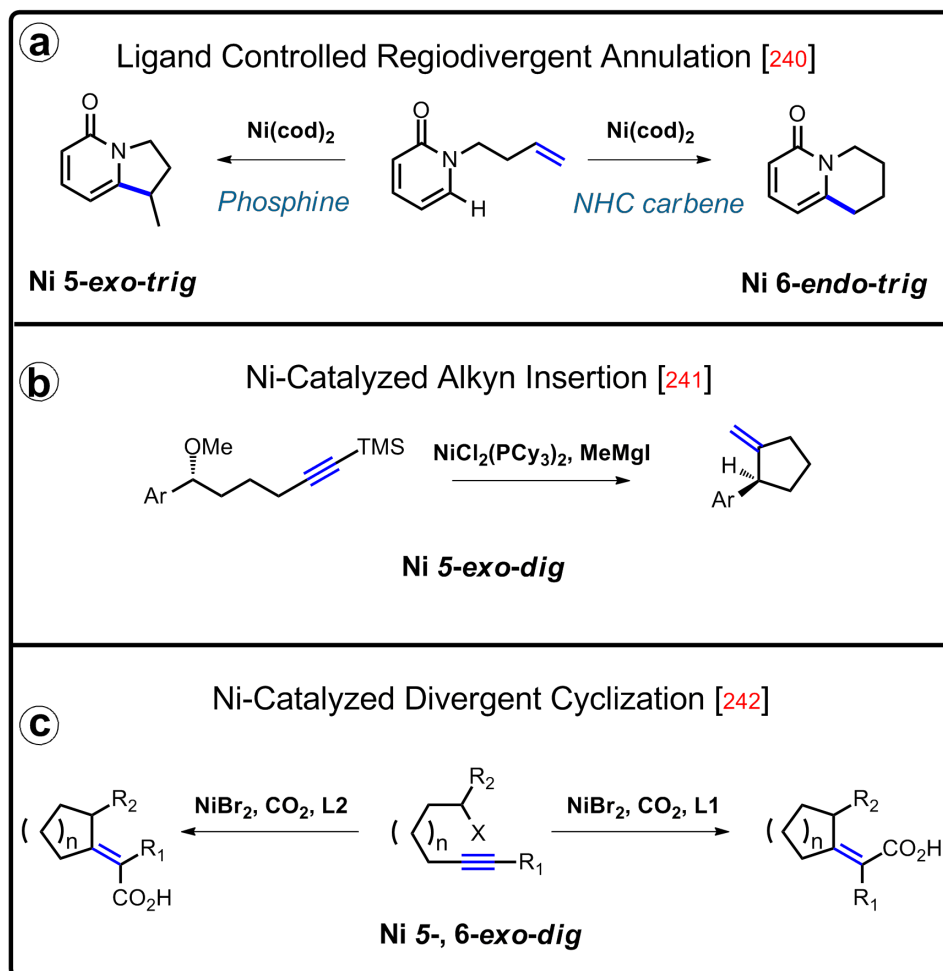


Figure 5.3.11: Literature Examples of Ni-Catalyzed Cyclizations [240–242].

5.3.5 PLATINUM PROMOTED CYCLIZATIONS

On the other hand, the opposite situation is observed with the larger Platinum atom (Figure 5.3.3 and Figure 5.3.4).

Whilst the reactivity trend is preserved, in close agreement with the palladium case, the activation energies are moderately higher, around 5 to 10 kcal/mol in most of the cases (Figure 5.3.3 and Figure 5.3.4). Two exceptions are the 6-*exo* and 7-*endo-dig* cyclizations in which the carbopalladations have higher barrier heights by 1.5 and 3.0 kcal/mol, respectively (Figure 5.3.6 and Figure 5.3.12). As a consequence of the higher activation energies, all *endo* modes become either borderline or forbidden (Figure 5.3.3 and Figure 5.3.4) except the Pt-7-*endo-dig* (21.2 kcal/mol, Figure 5.3.12), while the *exo* modes are close to 20 kcal/mol (5-*exo*, 6-*exo*) or even higher than 20 kcal/mol (Figure 5.3.3 and Figure 5.3.4) except 3-*exo-dig* and *trig* in which the activation energies are 9.8 and 8.7 kcal/mol, respectively (Figure 5.3.12).

All in all, the generally high activation energies are probably one of the reasons for the scarcity of cyclization methods employing Platinum catalysis [243, 244].

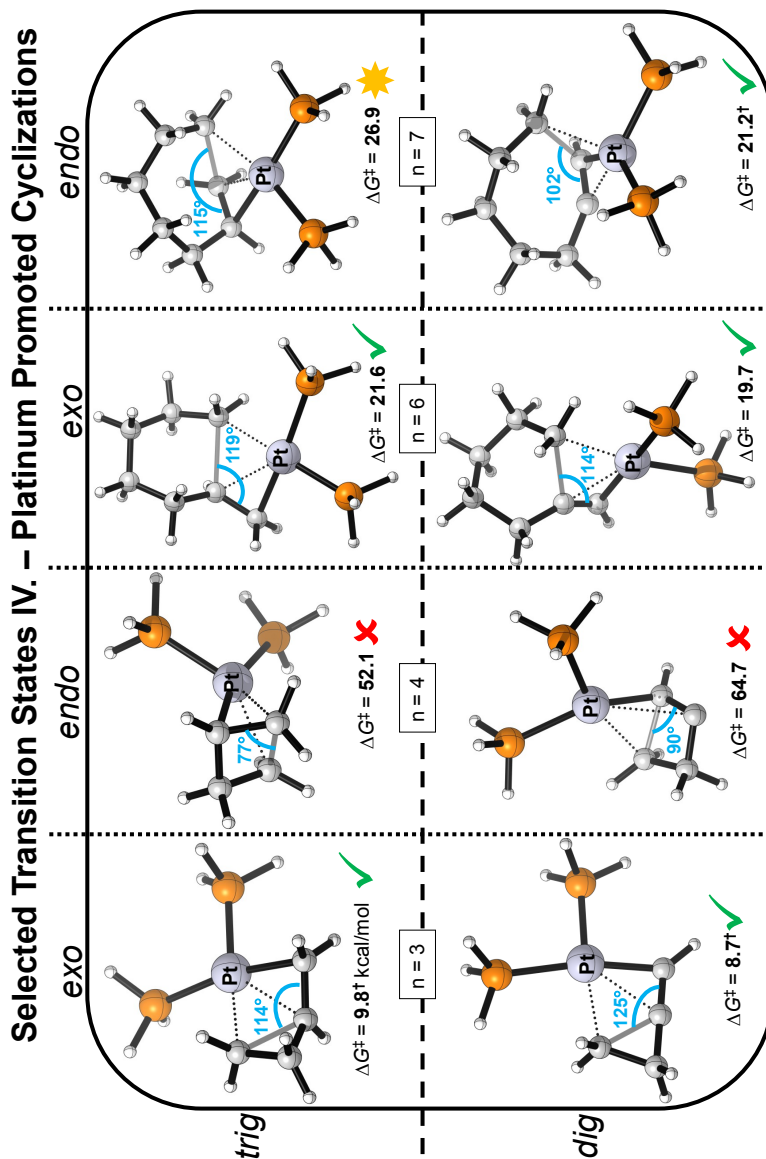


Figure 5.3.12: Selected Transition States IV. - Platinum Promoted Cyclizations. The Forming Bonds are Indicated with Faded Gray Lines. Corresponding Barrier Heights (ΔG^\ddagger , kcal/mol), Attack Angles and the Number of Atoms (n) in the Forming Cycles are also Shown. Green - Favorable; Orange - Borderline; Red - Unfavorable. Calculated at the M06/6-31+G(d,p)/SDD Level of Theory in Dichloromethane and in Some Cases (†) at the M06/6-31+G(d,p)/SDD//M06-2X/6-31+G(d,p)/SDD Level of Theory in Dichloromethane.

Noteworthy, the attacking angles (Figure 5.3.3 and Figure 5.3.4) do not vary significantly, the largest difference is 4° compare to the corresponding palladium species (4-*endo*- and 6-*exo-dig*). Not even when compared to the nickel promoted reactions, in this case the largest difference is 8° for the 6-*exo-dig* cyclizations (Figure 5.3.3 and Figure 5.3.4). These findings are clear indications that the structural requirements of the transition states are not dependent on the size of the transition metal, but only on the nature of the triple/double bond and the length of the alkyl chain to be cyclized.

5.3.6 SCOPE OF THE PREDICTIONS

After having compared the cyclizations of simple structures promoted by Ni, Pd and Pt-PH₃ complexes, other related systems were also investigated, which could be instructive for a wider understanding of the cyclizations. The 5-*exo*- and 6-*endo-trig* carbopalladation reaction pair were selected as reference processes. Three different type of modifications (ligand, functional group and metal, Figure 5.3.13) were made on the original system (Figure 5.3.1) to study the "scope" of the predictions.

As a first step, two trimethyl phosphine (PMe₃, **II**, Figure 5.3.13) ligands were used instead of the unsubstituted phosphine PH₃ (**I**, Figure 5.3.13) reduces the activation energy, especially for the *exo* case (2.1 kcal/mol lower, compare **I** vs **II**), while maintaining ca. 16 kcal/mol barrier for *endo*. If the carbon atom supporting the palladium has a sp² character (**III**), which is a very general situation in Heck type cyclizations, the barrier is fairly reduced in the *exo*-case to 7.8 kcal/mol, but increased to 18.7 kcal/mol for the *endo*. The introduction of an aryl moiety within the ring-forming chain (**IV**) originates an extra strain in the ring forming chain, increasing the barrier in both pathways (13.2 and 26.0 kcal/mol), but specially for the *endo* cycle formation, due to obvious increasing structural difficulties. More sterically encumbered starting materials, like **V**, where the terminal position of the alkene is occupied by two new methyl groups has a similar effect, increasing the cyclization barriers, but with a significant bias in disfavor of the *endo* mode. We can

Scope of the Predictions

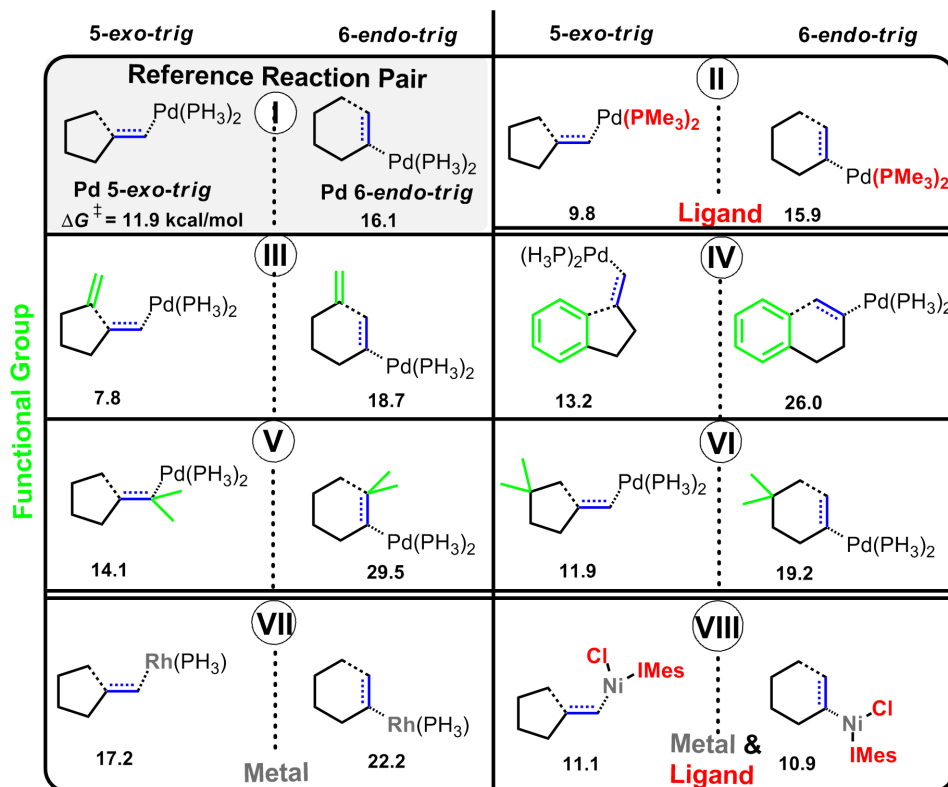


Figure 5.3.13: Scope of the Predictions. Comparison of 5-*exo-* and 6-*endo-trig* Cyclizations of More Complicated Structures. Calculated at the M06/6-31+G(d,p)/SDD Level of Theory in Dichloromethane.

say that the steric hindrance has a more pronounced effect on the formation of the C-C bond than on the Pd-C bond formation. On the other hand, no significant effect is observed by the introduction of two methyl groups in one of the carbons of the cycle forming chain (**VI**). The *exo* mode presents exactly the same energy as for **I** and a slight increase is predicted for the *endo* mode. It is usually considered that the introduction of substituents as a positive effect in any kind of cyclization process, through the Thorpe-Ingold effect, although the reasons are controversial. In our case, we do not appreciate a decrease in the energies, and we hypothesize that the effect could be related to the easier formation of the initial alkene-Palladium complex from the open chain precursor when substituents are present. When the metal was Rhodium (**VII**) the computed activation energies were 17.2 and 22.2 kcal/mol, which are in between of those of Palladium (11.9, 16.1 kcal/mol) and Platinum (18.9, 25.5 kcal/mol), closer indeed to Pt than to Pd (see Figure 5.3.3). Finally, a different coordination pattern was also considered for the Nickel complexes (**VIII**), in agreement with the type of ligands used in some experimental cases. A slight increase of ca. 2 kcal/mol in the activation energies was predicted in this case in comparison to its (Ni-PH₃)₂ analogue (see Figure 5.3.3), while the *exo/endo* energy gap is again very low. We can consider these two cases (original Ni *5-exo* & *6-endo-trig* and this reaction pair, **VIII**) as the only situations of the whole study where the *endo* reaction mode could compete with the *exo* one.

5.4 CONCLUSION

Baldwin's rules were proposed to be extended to group 10 alkyl metallations in terms of relative favorable/unfavorable processes. An intuitive summary of the qualitative results created (Figure 5.3.5).

The presence of the metal also affect the cyclizations, yielding relatively low activation energies for some of the calculated transition states involving different cycle sizes and metals.

The absolute values of the activation energies of cyclizations are highly dependent on the suitable orbitalic overlapping on carbonated substrates, being nickel the most favoured and platinum the less one.

Extremely low activation energies were found for 3-, and 4-*exo*-processes, which contradicts the fact that just a few experimental example exist. The calculations revealed that, despite the kinetic preference, the overall reaction is thermodynamically unfavorable in these cases. This is a reasonable explanation of the rare experimental occurrence of the processes and the necessity of a subsequent exergonic reaction in case of their appearance.

The calculations predicted the 4-, 5-*endo-dig* and 4-*endo-trig* metal promoted cyclizations to be forbidden which is in good agreement with the fact that they are unknown experimentally.

Furthermore, the 5-*endo-trig* reaction is predicted to be favourable with Ni or borderline with Pd, which is consistent with the fact, that there are experimental evidences of the Pd promoted process (*vide supra*).

Most of the 5-, 6- and 7-*exo/endo-dig* and *trig* cyclizations are favorable according to the computational results, which is also reflected by the number of known experimental results (*vide supra*).

The presented results could serve as a guide to explore not yet described cyclization processes based on the accessible computed activation energies and the qualitative comparison of the preferences.

Bernard of Chartres used to say that we were like dwarfs seated on the shoulders of giants. If we see more and further than they, it is not due to our own clear eyes or tall bodies, but because we are raised on high and upborne by their gigantic bigness.

John of Salisbury, *Metalogicon*

6

References

References

- [1] B. Lindström and L. J. Pettersson, “A brief history of catalysis,” *CATTECH*, vol. 7, no. 4, pp. 130–138, 2003.
- [2] E. Farnetti, R. Di Monte, and J. Kašpar, “Homogeneous and heterogeneous catalysis,” in *Inorganic and Bio-Inorganic Chemistry – Vol. II* (I. Bertini, ed.), Encyclopedia of Life Support Systems (EOLSS), 2009.
- [3] P. E. McGovern, J. Zhang, J. Tang, Z. Zhang, G. R. Hall, R. A. Moreau, A. Nuñez, E. D. Butrym, M. P. Richards, C.-s. Wang, G. Cheng, Z. Zhao, and C. Wang, “Fermented beverages of pre- and proto-historic China,” *Proceedings of the National Academy of Sciences of the United States of America*, vol. 101, no. 51, pp. 17593–17598, 2004.
- [4] L. Pasteur, “Mémoire sur la fermentation alcoolique,” *Comptes Rendus Séances de l’Academie des Sciences*, vol. 45, no. 913–916, pp. 1032–1036, 1857.
- [5] L. Pasteur, *Studies on Fermentation*. Macmillan (London), 1876.
- [6] L. Alba-Lois and C. Segal-Kischinevzky, “Beer & wine makers,” *Nature Education*, vol. 3, no. 9, p. 17, 2010.
- [7] G. B. Kauffman, “Johann Wolfgang Dobereiner’s Feuerzeug,” *Platinum Metals Review*, vol. 43, no. 3, pp. 122–128, 1999.
- [8] W. D. Williams, “Dobereiner’s hydrogen lighter,” *Bulletin for the History of Chemistry*, vol. 24, pp. 66–68, 1999.
- [9] J. Giordano, ed., *Maldynia: Multidisciplinary Perspectives on the Illness of Chronic Pain*. CRC Press, 2010.
- [10] J. Wisniak, “The history of catalysis. From the beginning to Nobel Prizes,” *Educación Química*, vol. 21, no. 1, pp. 60–69, 2010.

References

- [11] A. Libavius, *Alchemia*. Johannes Sautrius (Frankfurt), 1597.
- [12] J.J. Berzelius, "Quelques idées sur une nouvelle force agissant dans les combinaisons des corps organiques," *Annales de Chimie et de Physique*, vol. 61, pp. 146–151, 1836.
- [13] A. J. B. Robertson, "The early history of catalysis," *Platinum Metals Review*, vol. 19, no. 2, pp. 64–69, 1975.
- [14] D. Steinborn, *Fundamentals of Organometallic Catalysis*. Wiley, 2011.
- [15] "Nobel Lectures, Chemistry 1901-1921." Elsevier Publishing Company (Amsterdam), 1966.
- [16] W. Ostwald, "Abstract on catalysis," *Zeitschrift für Physikalische Chemie*, vol. 15, pp. 705–706, 1894.
- [17] A. D. McNaught and A. Wilkinson, eds., *IUPAC. Compendium of Chemical Terminology (the "Gold Book")*. Blackwell Scientific Publications (Oxford), 1997.
- [18] J. A. Osborn, F. H. Jardine, J. F. Young, and G. Wilkinson, "The preparation and properties of tris(triphenylphosphine)halogenorhodium(I) and some reactions thereof including catalytic homogeneous hydrogenation of olefins and acetylenes and their derivatives," *Journal of the Chemical Society A: Inorganic, Physical, Theoretical*, pp. 1711–1732, 1966.
- [19] R. Crabtree, "Iridium compounds in catalysis," *Accounts of Chemical Research*, vol. 12, no. 9, pp. 331–337, 1979.
- [20] S. Nishimura, *Handbook of Heterogeneous Catalytic Hydrogenation for Organic Synthesis*. Wiley, 2001.
- [21] M. Raney, "Method of preparing catalytic material." US Patent, 1563587, December 01, 1925.
- [22] M. Raney, "Method of producing finely divided Nickel." US Patent, 1628190, May 10, 1927.
- [23] A. Behr and P. Neubert, *Applied Homogeneous Catalysis*. Wiley, 2012.
- [24] R. H. Crabtree, *The Organometallic Chemistry of the Transition Metals, Fifth Edition*. Wiley, 2009.

References

- [25] D. Seyferth, "Cadet's fuming arsenical liquid and the cacodyl compounds of Bunsen," *Organometallics*, vol. 20, pp. 1488–1498, 2001.
- [26] G. Jaouen, ed., *Bioorganometallics: Biomolecules, Labeling, Medicine*. Wiley, 2006.
- [27] W. C. Zeise, "Von der Wirkung zwischen Platinchlorid und Alkohol, und von den dabei entstehenden neuen Substanzen," *Annalen der Physik*, vol. 97, pp. 497–541, 1831.
- [28] J. P. Griess and C. A. Martins, "Note sur l'éthylène-chlorure de platine," *Comptes Rendus Hebdomadaires des Séances de l'Académie des Sciences*, vol. 53, pp. 922–925, 1861.
- [29] K. Birnbaum, "Ueber die Verbindungen des Aethylens und seiner homologen mit dem Platinchlorür," *Justus Liebigs Annalen der Chemie*, vol. 145, pp. 67–77, 1868.
- [30] L. B. Hunt, "The first organometallic compounds: William Christopher Zeise and his platinum complexes," *Platinum Metals Review*, vol. 28, pp. 76–83, 1984.
- [31] E. Frankland, "On a new series of organic bodies containing metals," *Philosophical Transactions of the Royal Society of London*, vol. 142, pp. 417–444, 1852.
- [32] E. Frankland, "XIX.— On organo-metallic bodies. A discourse delivered to the members of the Chemical Society of London," *Quarterly Journal of the Chemical Society of London*, vol. 13, pp. 177–235, 1861.
- [33] L. Mond, C. Langer, and F. Quincke, "L.— Action of carbon monoxide on Nickel," *Journal of the Chemical Society, Transactions*, vol. 57, pp. 749–753, 1890.
- [34] W. C. Roberts-Austen, "The extraction of nickel from its ores by the Mond process," *Nature*, vol. 59, pp. 63–64, 1898.
- [35] V. Grignard, "Sur quelques nouvelles combinaisons organométalliques du magnésium et leur application à des synthèses d'alcools et d'hydrocarbures," *Comptes Rendus Hebdomadaires des Séances de l'Académie des Sciences*, vol. 130, pp. 1322–1324, 1900.

References

- [36] T. J. Kealy and P. L. Pauson, "A new type of organo-iron compound," *Nature*, vol. 168, pp. 1039–1040, 1951.
- [37] G. Wilkinson, M. Rosenblum, M. C. Whiting, and R. B. Woodward, "The structure of iron bis-cyclopentadienyl," *Journal of the American Chemical Society*, vol. 74, pp. 2125–2126, 1952.
- [38] H. Gilman, R. G. Jones, and L. A. Woods, "The preparation of methylcopper and some observations on the decomposition of organocopper compounds," *The Journal of Organic Chemistry*, vol. 17, pp. 1630–1634, 1952.
- [39] J. Boor, ed., *Ziegler–Natta Catalysts Polymerizations*. Academic Press, 1979.
- [40] W. S. Knowles, "Asymmetric hydrogenations." http://www.nobelprize.org/nobel_prizes/chemistry/laureates/2001/knowles-lecture.pdf, 2001. Nobel Lecture.
- [41] J. K. Stille, "The palladium-catalyzed cross-coupling reactions of organotin reagents with organic electrophiles," *Angewandte Chemie International Edition*, vol. 25, pp. 508–524, 1986.
- [42] J.-E. Bäckvall, "Scientific Background on the Nobel Prize in Chemistry 2010." http://www.nobelprize.org/nobel_prizes/chemistry/laureates/2010/advanced-chemistryprize2010.pdf, 2010. Nobel Media AB.
- [43] R. Parry, "Empedocles," in *The Stanford Encyclopedia of Philosophy* (E. N. Zalta, ed.), The Metaphysics Research Lab, Center for the Study of Language and Information (CSLI), Stanford University, fall 2012 ed., 2012.
- [44] N. Copernicus, *De Revolutionibus Orbium Coelestium*. Johannes Petreius (Nuremberg), 1543.
- [45] T. S. Kuhn, *The Structure of Scientific Revolutions*. University of Chicago Press, 1962.
- [46] R. Hooke, *Micrographia: or, Some Physiological Descriptions of Minute Bodies Made by Magnifying Glasses*. Royal Society, 1665. London: J. Martyn and J. Allestry.
- [47] F. Bacon, "Novum Organum Scientiarum," 1620. London.

References

- [48] J. M. McBride, “Freshman Organic Chemistry (CHEM 125).” <http://oyc.yale.edu/chemistry/chem-125a/lecture-1>, 2008. Yale University.
- [49] J. Klein, “Francis Bacon,” in *The Stanford Encyclopedia of Philosophy* (E. N. Zalta, ed.), The Metaphysics Research Lab, Center for the Study of Language and Information (CSLI), Stanford University, summer 2015 ed., 2015.
- [50] I. Newton, *Philosophiae Naturalis Principia Mathematica*. Royal Society, 1687. London.
- [51] T. Veszprémi and M. Fehér, *Quantum Chemistry - Fundamentals to Applications*. Springer US, 1999. New York.
- [52] F. Jensen, *Introduction to Computational Chemistry*. Wiley, 2007. Chichester, England.
- [53] T. A. Arias, “Practical DFT lecture series (2011 Phys 7654).” <https://www.youtube.com/watch?v=oyvGeQ8ehBM>, 2011. Cornell University.
- [54] E. C. Brewer, *Brewer’s Dictionary of Phrase and Fable*. Harper & Brothers, 1952. New York, US.
- [55] Food Standards Agency, “Food Additives Legislation Guidance to Compliance.” <http://www.food.gov.uk/sites/default/files/multimedia/pdfs/guidance/food-additives-legislation-guidance-to-compliance.pdf>, 2015.
- [56] H. von Helmholtz, “Robert Mayer’s Priorität,” in *Hermann von Helmholtz: Vorträge und Reden*, pp. 401–414, Braunschweig: Vieweg, 1896.
- [57] P. E. A. von Lenard, “On cathode rays.” http://www.nobelprize.org/nobel_prizes/physics/laureates/1905/lenard-lecture.pdf, 1906. Nobel Lecture.
- [58] M. Planck, “Zur theorie des gesetzes der energieverteilung im normal-spectrum,” *Verhandlungen der Deutschen Physikalische Gesellschaft*, vol. 2, pp. 237–245, 1900.

References

- [59] M. Planck, "Ueber die elementarquanta der materie und der elektricität," *Annalen der Physik*, vol. 309, pp. 564–566, 1901.
- [60] M. Planck, "Ueber eine verbesserung der wien'schen spectralgleichung," *Verhandlungen der Deutschen Physikalische Gesellschaft*, vol. 2, pp. 202–204, 1900.
- [61] H. Kangro, ed., *Planck's Original Papers in Quantum Physics, German and English edition*. Taylor & Francis Ltd., 1972. London, UK.
- [62] D. T. Haar, ed., *The Old Quantum Theory*. Pergamon Press Ltd, 1967. Glasgow, UK.
- [63] E. Rutherford, "The scattering of α and β particles by matter and the structure of the atom," *Philosophical Magazine Series 6*, vol. 21, pp. 669–688, 1911.
- [64] N. Bohr, "On the constitution of atoms and molecules," *Philosophical Magazine Series 6*, vol. 26, pp. 1–25, 1913.
- [65] N. Bohr, "On the constitution of atoms and molecules, Part II. - Systems containing only a single nucleus," *Philosophical Magazine Series 6*, vol. 26, pp. 476–502, 1913.
- [66] N. Bohr, "On the constitution of atoms and molecules, Part III. - Systems containing several nuclei," *Philosophical Magazine Series 6*, vol. 26, pp. 857–875, 1913.
- [67] L. de Broglie, "Recherches sur la théorie des quanta," 1924. Thesis, Paris.
- [68] M. Born, "Über quantenmechanik," *Zeitschrift für Physik*, vol. 26, pp. 379–395, 1924.
- [69] M. Born, *My life: Recollections of a Nobel laureate*. Scribner's Sons, 1978. New York, US.
- [70] W. Heisenberg, "Über quantentheoretische Umdeutung kinematischer und mechanischer Beziehungen," *Zeitschrift für Physik*, vol. 33, pp. 879–893, 1925.
- [71] M. Born and P. Jordan, "Zur Quantenmechanik," *Zeitschrift für Physik*, vol. 34, pp. 858–888, 1925.

References

- [72] M. Born, W. Heisenberg, and P. Jordan, “Zur Quantenmechanik II,” *Zeitschrift für Physik*, vol. 35, pp. 557–615, 1926.
- [73] E. Schrödinger, “Quantisierung als Eigenwertproblem,” *Annalen der Physik*, vol. 384, pp. 361–376, 1926.
- [74] E. Schrödinger, “Quantisierung als Eigenwertproblem,” *Annalen der Physik*, vol. 384, pp. 489–527, 1926.
- [75] E. Schrödinger, “Quantisierung als Eigenwertproblem,” *Annalen der Physik*, vol. 385, pp. 437–490, 1926.
- [76] E. Schrödinger, “An undulatory theory of the mechanics of atoms and molecules,” *Physical Review*, vol. 28, pp. 1049–1070, 1926.
- [77] F. Bloch, “Heisenberg and the early days of quantum mechanics,” *Physics Today*, vol. 29, pp. 23–27, 1976.
- [78] E. Schrödinger, “Über das Verhältnis der Heisenberg-Born-Jordanschen Quantenmechanik zu der meinem,” *Annalen der Physik*, vol. 384, pp. 734–756, 1926.
- [79] M. Born, “Zur Quantenmechanik der Stoßvorgänge,” *Zeitschrift für Physik*, vol. 37, pp. 863–867, 1926.
- [80] J. A. Wheeler and W. H. Zurek, eds., *Quantum Theory and Measurement*. Princeton University Press, 1983. Princeton, New Jersey, US.
- [81] W. Heisenberg, “Über den anschaulichen Inhalt der quantentheoretischen Kinematik und Mechanik,” *Zeitschrift für Physik*, vol. 43, pp. 172–198, 1927.
- [82] W. Heitler and F. London, “Wechselwirkung neutraler Atome und homöopolare Bindung nach der Quantenmechanik,” *Zeitschrift für Physik*, vol. 44, pp. 455–472, 1927.
- [83] P. Dirac, “The quantum theory of the electron,” *Proceedings of the Royal Society of London. Series A, Containing Papers of a Mathematical and Physical Character*, vol. 117, no. 778, pp. 610–624, 1928.
- [84] P. Dirac, *The Principles of Quantum Mechanics*. Oxford University Press, 1930. Oxford, UK.

References

- [85] J. von Neumann, *Mathematische Grundlagen der Quantenmechanik*. Springer, 1932. Berlin.
- [86] C. D. Sherrill, “A brief review of elementary quantum chemistry.” <http://vergil.chemistry.gatech.edu/notes/quantrev/>, 2001. Georgia Institute of Technology.
- [87] C. D. Sherrill, “An introduction to hartree-fock molecular orbital theory.” <http://vergil.chemistry.gatech.edu/notes/hf-intro/hf-intro.html>, 2000. Georgia Institute of Technology.
- [88] M. Born and R. Oppenheimer, “Zur Quantentheorie der Molekeln,” *Annalen der Physik*, vol. 389, pp. 457–484, 1927.
- [89] “On the Quantum Theory of Molecules.” http://www.ulb.ac.be/cpm/people/scientists/bsutclif/bornopn_corr.pdf. Translated by S. M. Blinder from M. Born and R. Oppenheimer, “Zur Quantentheorie der Molekeln,” *Annalen der Physik*, vol. 389, pp. 457–484, 1927.
- [90] J. C. Slater, “The theory of complex spectra,” *Physical Review*, vol. 34, pp. 1293–1322, 1929.
- [91] E. H. Lieb, “A brief review of Thomas-Fermi theory.” <http://physics.nyu.edu/LarrySpruch/Lieb.pdf>, 2000.
- [92] L. H. Thomas, “The calculation of atomic fields,” *Mathematical Proceedings of the Cambridge Philosophical Society*, vol. 23, pp. 542–548, 1927.
- [93] E. Fermi, “Un Metodo Statistico per la Determinazione di alcune Prioprietà dell’Atomo,” *Rendiconti dell’Accademia dei Lincei*, vol. 6, pp. 602–607, 1927.
- [94] J. C. Slater, “A simplification of the Hartree-Fock method,” *Physical Review*, vol. 81, pp. 385–390, 1951.
- [95] S. F. Sousa, P. A. Fernandes, and M. J. Ramos, “General performance of density functionals,” *The Journal of Physical Chemistry A*, vol. 111, pp. 10439–10452, 2007.
- [96] P. Hohenberg and W. Kohn, “Inhomogeneous electron gas,” *Physical Review*, vol. 136, pp. B864–B871, 1964.
- [97] W. Kohn and L. J. Sham, “Self-consistent equations including exchange and correlation effects,” *Physical Review*, vol. 140, pp. A1133–A1138, 1965.

References

- [98] J. P. Perdew and K. Schmidt, "Jacob's ladder of density functional approximations for the exchange-correlation energy," *AIP Conference Proceedings*, vol. 577, pp. 1–20, 2001.
- [99] "New american standard bible," 1971.
- [100] Y. Zhao and D. G. Truhlar, "The Mo6 suite of density functionals for main group thermochemistry, thermochemical kinetics, noncovalent interactions, excited states, and transition elements: two new functionals and systematic testing of four Mo6-class functionals and 12 other functionals," *Theoretical Chemistry Accounts*, vol. 120, pp. 215–241, 2008.
- [101] C. Lee, W. Yang, and R. G. Parr, "Development of the Colle-Salvetti correlation-energy formula into a functional of the electron density," *Phys. Rev. B*, vol. 37, pp. 785–789, 1988.
- [102] A. D. Becke, "Density-functional thermochemistry. III. The role of exact exchange," *The Journal of Chemical Physics*, vol. 98, no. 7, pp. 5648–5652, 1993.
- [103] W. Kohn, A. D. Becke, and R. G. Parr, "Density functional theory of electronic structure," *The Journal of Physical Chemistry*, vol. 100, no. 31, pp. 12974–12980, 1996.
- [104] Y. Zhao and D. G. Truhlar, "A new local density functional for main-group thermochemistry, transition metal bonding, thermochemical kinetics, and noncovalent interactions," *Journal of Chemical Physics*, vol. 125, pp. 194101–194118, 2006.
- [105] Y. Zhao, N. Schultz, and D. Truhlar, "Exchange-correlation functional with broad accuracy for metallic and nonmetallic compounds, kinetics, and noncovalent interactions," *Journal of Chemical Physics*, vol. 123, pp. 161103–4, 2005.
- [106] J. C. Slater, "Analytic atomic wave functions," *Physical Review*, vol. 42, pp. 33–43, 1932.
- [107] S. F. Boys, "Electronic wave functions. I. A general method of calculation for the stationary states of any molecular system," *Proceedings of the Royal Society of London. Series A, Mathematical and Physical Sciences*, vol. 200, pp. 542–554, 1950.

References

- [108] M. Dolg, U. Wedig, H. Stoll, and H. Preuß, "Energy-adjusted ab initio pseudopotentials for the first row transition elements," *The Journal of Chemical Physics*, vol. 86, pp. 866–872, 1987.
- [109] D. Andrae, U. Häußermann, M. Dolg, H. Stoll, and H. Preuß, "Energy-adjusted ab initio pseudopotentials for the second row and third row transition elements," *Theoretica Chimica Acta*, vol. 77, pp. 123–141, 1990.
- [110] P. J. Hay and W. R. Wadt, "Ab initio effective core potentials for molecular calculations. Potentials for the transition metal atoms Sc to Hg," *The Journal of Chemical Physics*, vol. 82, no. 1, pp. 270–283, 1985.
- [111] W. R. Wadt and P. J. Hay, "Ab initio effective core potentials for molecular calculations. Potentials for main group elements Na to Bi," *The Journal of Chemical Physics*, vol. 82, no. 1, pp. 284–298, 1985.
- [112] P. J. Hay and W. R. Wadt, "Ab initio effective core potentials for molecular calculations. Potentials for K to Au including the outermost core orbitals," *The Journal of Chemical Physics*, vol. 82, no. 1, pp. 299–310, 1985.
- [113] C. Reichardt, *Solvents and Solvent Effects in Organic Chemistry*. Wiley, 2004.
- [114] J. Tomasi, B. Mennucci, and R. Cammi, "Quantum mechanical continuum solvation models," *Chemical Reviews*, vol. 105, pp. 2999–3093, 2005.
- [115] S. Miertus, E. Scrocco, and J. Tomasi, "Electrostatic interaction of a solute with a continuum. A direct utilization of ab initio molecular potentials for the prevision of solvent effects," *Chemical Physics*, vol. 55, pp. 117–129, 1981.
- [116] A. Klamt and G. Schüürmann, "COSMO: a new approach to dielectric screening in solvents with explicit expressions for the screening energy and its gradient," *Journal of the Chemical Society, Perkin Transactions 2*, pp. 799–805, 1993.
- [117] E. Cancès, B. Mennucci, and J. Tomasi, "A new integral equation formalism for the polarizable continuum model: Theoretical background and applications to isotropic and anisotropic dielectrics," *The Journal of Chemical Physics*, vol. 107, pp. 3032–3041, 1997.

References

- [118] B. Mennucci, E. Cancès, and J. Tomasi, "Evaluation of solvent effects in isotropic and anisotropic dielectrics and in ionic solutions with a unified integral equation method: Theoretical bases, computational implementation, and numerical applications," *The Journal of Physical Chemistry B*, vol. 101, pp. 10506–10517, 1997.
- [119] E. Cancès and B. Mennucci, "New applications of integral equations methods for solvation continuum models: ionic solutions and liquid crystals," *Journal of Mathematical Chemistry*, vol. 23, pp. 309–326, 1998.
- [120] L. Pasteur, "Mémoire sur la relation qui peut exister entre la forme cristalline et la composition chimique, et sur la cause de la polarisation rotatoire," *Comptes rendus de l'Académie des sciences (Paris)*, vol. 26, pp. 535–538, 1848.
- [121] L. Pasteur, "Sur les relations qui peuvent exister entre la forme cristalline, la composition chimique et le sens de la polarisation rotatoire," *Annales de Chimie et de Physique*, vol. 24, no. 6, pp. 442–459, 1848.
- [122] H. D. Flack, "Louis Pasteur's discovery of molecular chirality and spontaneous resolution in 1848, together with a complete review of his crystallographic and chemical work," *Acta Crystallographica Section A*, vol. 65, no. 5, pp. 371–389, 2009.
- [123] P. Ahlberg, "The Nobel Prize in Chemistry 2001 - Advanced Information." http://www.nobelprize.org/nobel_prizes/chemistry/laureates/2001/advanced.html, 2001. Nobel Media AB.
- [124] C. A. Challener, ed., *Chiral Drugs*. Wiley, 2004.
- [125] L. A. Nguyen, H. He, and C. Pham-Huy, "Chiral drugs: An overview," *International Journal of Biomedical Science*, vol. 2, no. 2, pp. 85–100, 2006.
- [126] G. H. Christie and J. Kenner, "LXXI. — The molecular configurations of polynuclear aromatic compounds. Part I. The resolution of γ -6 : 6'-dinitro- and 4 : 6 : 4' : 6'-tetranitro-diphenic acids into optically active components," *Journal of the Chemical Society, Transactions*, vol. 121, pp. 614–620, 1922.
- [127] I. G. Csizmadia, *Basic Principles for Introductory Organic Chemistry*. Quirk Press, 1997.

References

- [128] W. S. Knowles and M. J. Sabacky, "Catalytic asymmetric hydrogenation employing a soluble, optically active, rhodium complex," *Chemical Communications (London)*, pp. 1445–1446, 1968.
- [129] O. Yun, "Profile of William S. Knowles," *Proceedings of the National Academy of Sciences of the United States of America*, vol. 102, no. 47, pp. 16913–16915, 2005.
- [130] B. D. Vineyard, W. S. Knowles, M. J. Sabacky, G. L. Bachman, and D. J. Weinkauff, "Asymmetric hydrogenation. Rhodium chiral bisphosphine catalyst," *Journal of the American Chemical Society*, vol. 99, no. 18, pp. 5946–5952, 1977.
- [131] W. S. Knowles, "Asymmetric hydrogenation," *Accounts of Chemical Research*, vol. 16, no. 3, pp. 106–112, 1983.
- [132] H. Nozaki, S. Moriuti, H. Takaya, and R. Noyori, "Asymmetric induction in carbenoid reaction by means of a dissymmetric copper chelate," *Tetrahedron Letters*, vol. 7, no. 43, pp. 5239–5244, 1966.
- [133] H. Nozaki, H. Takaya, S. Moriuti, and R. Noyori, "Homogeneous catalysis in the decomposition of diazo compounds by copper chelates: Asymmetric carbenoid reactions," *Tetrahedron*, vol. 24, no. 9, pp. 3655–3669, 1968.
- [134] R. Noyori, "Asymmetric catalysis: Science and opportunities." http://www.nobelprize.org/nobel_prizes/chemistry/laureates/2001/noyori-lecture.pdf, 2001. Nobel Lecture.
- [135] A. Miyashita, A. Yasuda, H. Takaya, K. Toriumi, T. Ito, T. Souchi, and R. Noyori, "Synthesis of 2,2'-bis(diphenylphosphino)-1,1'-binaphthyl (BINAP), an atropisomeric chiral bis(triaryl)phosphine, and its use in the rhodium(I)-catalyzed asymmetric hydrogenation of α -(acylamino)acrylic acids," *Journal of the American Chemical Society*, vol. 102, no. 27, pp. 7932–7934, 1980.
- [136] T. Ohta, H. Takaya, and R. Noyori, "Bis(diarylphosphino)-1,1 binaphthyl (BINAP)-ruthenium(II) dicarboxylate complexes: new, highly efficient catalysts for asymmetric hydrogenations," *Inorganic Chemistry*, vol. 27, no. 3, pp. 566–569, 1988.

References

- [137] M. Kitamura, T. Ohkuma, S. Inoue, N. Sayo, H. Kumobayashi, S. Akutagawa, T. Ohta, H. Takaya, and R. Noyori, "Homogeneous asymmetric hydrogenation of functionalized ketones," *Journal of the American Chemical Society*, vol. 110, no. 2, pp. 629–631, 1988.
- [138] R. Noyori and H. Takaya, "BINAP: an efficient chiral element for asymmetric catalysis," *Accounts of Chemical Research*, vol. 23, no. 10, pp. 345–350, 1990.
- [139] T. Ohkuma, H. Ooka, S. Hashiguchi, T. Ikariya, and R. Noyori, "Practical enantioselective hydrogenation of aromatic ketones," *Journal of the American Chemical Society*, vol. 117, no. 9, pp. 2675–2676, 1995.
- [140] E. N. Jacobsen, A. Pfaltz, and H. Yamamoto, eds., *Comprehensive Asymmetric Catalysis I-III*. Springer, New York, 1999.
- [141] T. P. Yoon and E. N. Jacobsen, "Privileged chiral catalysts," *Science*, vol. 299, no. 5613, pp. 1691–1693, 2003.
- [142] N. W. Alcock, J. M. Brown, and D. I. Hulmes, "Synthesis and resolution of 1-(2-diphenylphosphino-1-naphthyl)isoquinoline; a P–N chelating ligand for asymmetric catalysis," *Tetrahedron: Asymmetry*, vol. 4, no. 4, pp. 743–756, 1993.
- [143] M. P. Carroll and P. J. Guiry, "P,N ligands in asymmetric catalysis," *Chemical Society Reviews*, vol. 43, pp. 819–833, 2014.
- [144] E. Fernández, P. J. Guiry, K. P. T. Connole, and J. M. Brown, "Quinap and congeners: Atropis PN ligands for asymmetric catalysis," *The Journal of Organic Chemistry*, vol. 79, no. 12, pp. 5391–5400, 2014.
- [145] M. McCarthy, R. Goddard, and P. J. Guiry, "The preparation and resolution of 2-phenyl-Quinazolinap, a new atropisomeric phosphinamine ligand for asymmetric catalysis," *Tetrahedron: Asymmetry*, vol. 10, no. 14, pp. 2797–2807, 1999.
- [146] F. Y. Kwong, Q. Yang, T. C. W. Mak, A. S. C. Chan, and K. S. Chan, "A new atropisomeric P,N ligand for Rhodium-catalyzed asymmetric hydroboration," *The Journal of Organic Chemistry*, vol. 67, no. 9, pp. 2769–2777, 2002.

References

- [147] T. F. Knöpfel, P. Aschwanden, T. Ichikawa, T. Watanabe, and E. M. Carreira, "Readily available biaryl P,N ligands for asymmetric catalysis," *Angewandte Chemie International Edition*, vol. 43, no. 44, pp. 5971–5973, 2004.
- [148] F. S. P. Cardoso, K. A. Abboud, and A. Aponick, "Design, preparation, and implementation of an imidazole-based chiral biaryl P,N-ligand for asymmetric catalysis," *Journal of the American Chemical Society*, vol. 135, no. 39, pp. 14548–14551, 2013.
- [149] R. W. Baker, S. O. Rea, M. V. Sargent, E. M. Schenkelaars, T. S. Tjahjandarie, and A. Totaro, "Enantioselective synthesis of axially chiral 1-(1-naphthyl)isoquinolines and 2-(1-naphthyl)pyridines through sulfoxide ligand coupling reactions," *Tetrahedron*, vol. 61, no. 15, pp. 3733–3743, 2005.
- [150] T. Thaler, F. Geittner, and P. Knochel, "A novel synthetic approach towards chiral QUINAP via diastereomeric sulfoxide intermediates," *Synlett*, no. 17, pp. 2655–2658, 2007.
- [151] J. Clayden, S. P. Fletcher, J. J. W. McDouall, and S. J. M. Rowbottom, "Controlling axial conformation in 2-arylpiperidines and 1-arylisoquinolines: Application to the asymmetric synthesis of QUINAP by dynamic thermodynamic resolution," *Journal of the American Chemical Society*, vol. 131, no. 14, pp. 5331–5343, 2009.
- [152] A. Ros, B. Estepa, P. Ramírez-López, E. Álvarez, R. Fernández, and J. M. Lassaletta, "Dynamic kinetic cross-coupling strategy for the asymmetric synthesis of axially chiral heterobiaryls," *Journal of the American Chemical Society*, vol. 135, no. 42, pp. 15730–15733, 2013.
- [153] J. M. Lassaletta, A. Ros, R. Fernández, B. Estepa, and P. Ramírez-López, "Procedimiento de síntesis de compuestos heterobiarílicos con quiralidad axial, compuestos obtenidos y uso." ES Patent, P201331068, July 12, 2013.
- [154] V. Bhat, S. Wang, B. M. Stoltz, and S. C. Virgil, "Asymmetric synthesis of QUINAP via dynamic kinetic resolution," *Journal of the American Chemical Society*, vol. 135, no. 45, pp. 16829–16832, 2013.
- [155] M. J. Frisch, G. W. Trucks, H. B. Schlegel, G. E. Scuseria, M. A. Robb, J. R. Cheeseman, G. Scalmani, V. Barone, B. Mennucci, G. A. Petersson, H. Nakatsuji, M. Caricato, X. Li, H. P. Hratchian, A. F. Izmaylov, J. Bloino, G. Zheng, J. L. Sonnenberg, M. Hada, M. Ehara, K. Toyota, R. Fukuda,

References

- J. Hasegawa, M. Ishida, T. Nakajima, Y. Honda, O. Kitao, H. Nakai, T. Vreven, J. A. Montgomery, Jr., J. E. Peralta, F. Ogliaro, M. Bearpark, J. J. Heyd, E. Brothers, K. N. Kudin, V. N. Staroverov, R. Kobayashi, J. Normand, K. Raghavachari, A. Rendell, J. C. Burant, S. S. Iyengar, J. Tomasi, M. Cossi, N. Rega, J. M. Millam, M. Klene, J. E. Knox, J. B. Cross, V. Bakken, C. Adamo, J. Jaramillo, R. Gomperts, R. E. Stratmann, O. Yazyev, A. J. Austin, R. Cammi, C. Pomelli, J. W. Ochterski, R. L. Martin, K. Morokuma, V. G. Zakrzewski, G. A. Voth, P. Salvador, J. J. Dannenberg, S. Dapprich, A. D. Daniels, Ö. Farkas, J. B. Foresman, J. V. Ortiz, J. Cioslowski, and D. J. Fox, "Gaussian 09, Revision D.01." Gaussian Inc. Wallingford CT 2009.
- [156] C. Gonzalez and H. B. Schlegel, "Reaction path following in mass-weighted internal coordinates," *The Journal of Physical Chemistry*, vol. 94, no. 14, pp. 5523–5527, 1990.
- [157] J. Ogden, "Gold in antiquity," *Interdisciplinary Science Reviews*, vol. 17, pp. 261–270, 1992.
- [158] A. S. K. Hashmi and M. Rudolph, "Gold catalysis in total synthesis," *Chemical Society Reviews*, vol. 37, pp. 1766–1775, 2008.
- [159] A. S. K. Hashmi, L. Schwarz, J.-H. Choi, and T. M. Frost, "A new gold-catalyzed C-C bond formation," *Angewandte Chemie International Edition*, vol. 39, pp. 2285–2288, 2000.
- [160] M. Jia and M. Bandini, "Counterion effects in homogeneous gold catalysis," *ACS Catalysis*, vol. 5, pp. 1638–1652, 2015.
- [161] X.-Z. Shu, D. Shu, C. M. Schienebeck, and W. Tang, "Rhodium-catalyzed acyloxy migration of propargylic esters in cycloadditions, inspiration from the recent "gold rush"," *Chemical Society Reviews*, vol. 41, pp. 7698–7711, 2012.
- [162] W. Zi and F. D. Toste, "Recent advances in enantioselective gold catalysis," *Chemical Society Reviews*, 2016.
- [163] Z. Zheng, Z. Wang, Y. Wang, and L. Zhang, "Au-catalysed oxidative cyclisation," *Chemical Society Reviews*, 2016.
- [164] A. S. K. Hashmi, "Homogeneous catalysis by gold," *Gold Bulletin*, vol. 37, pp. 51–65, 2004.

References

- [165] E. Jimenez-Nunez and A. M. Echavarren, "Gold-catalyzed cycloisomerizations of enynes: A mechanistic perspective," *Chemical Society Reviews*, vol. 108, pp. 3326–3350, 2008.
- [166] M. Rudolph and A. S. K. Hashmi, "Gold catalysis in total synthesis—an update," *Chemical Society Reviews*, vol. 41, pp. 2448–2462, 2012.
- [167] D. Pflasterer and A. S. K. Hashmi, "Gold catalysis in total synthesis – recent achievements," *Chemical Society Reviews*, vol. 45, pp. 1331–1367, 2016.
- [168] P. Schwerdtfeger, H. L. Hermann, and H. Schmidbaur, "Stability of the gold(I)–phosphine bond. A comparison with other group 11 elements," *Inorganic Chemistry*, vol. 42, pp. 1334–1342, 2003.
- [169] D. J. Gorin and F. D. Toste, "Relativistic effects in homogeneous gold catalysis," *Nature*, vol. 446, pp. 395–403, 2007.
- [170] D. Scarpi, S. Begliomini, C. Prandi, A. Oppedisano, A. Deagostino, E. Gómez-Bengoa, B. Fiser, and E. G. Occhiato, "Gold-catalysed synthesis of exocyclic vinylogous amides and β -amino ketones: A detailed study on the 5-exo/6-endo-dig selectivity, methodology and scope," *European Journal Organic Chemistry*, vol. 2015, p. 3251–3265, 2015.
- [171] I. N. Nazarov and I. I. Zaretskaya, "Structure of products of hydration of divinylethynyl hydrocarbons," *Zhurnal Obshchei Khimii*, vol. 27, pp. 693–713, 1957.
- [172] I. N. Nazarov, I. I. Zaretskaya, and T. I. Sorkina, "Cyclopentanones from the cyclization of divinyl ketones," *Zhurnal Obshchei Khimii*, vol. 30, pp. 746–754, 1960.
- [173] D. J. Aitken, H. Eijsberg, A. Frongia, J. Ollivier, and P. P. Piras, "Recent progress in the synthetic assembly of 2-cyclopentenones," *Synthesis*, vol. 46, pp. 1–24, 2014.
- [174] I. N. Nazarov and I. I. Zaretskaya, "Acetylene derivatives. xvii. Hydration of hydrocarbons of the divinylacetylene series," *Akademiia Nauk SSSR. Izvestiia. Seriia kóKhimicheskaiia*, pp. 211–224, 1941.
- [175] K. L. Habermas, S. E. Denmark, and T. K. Jones, *The Nazarov Cyclization. Organic Reactions*, vol. 45:1, pp. 1–158. John Wiley & Sons, Inc., 2004.

References

- [176] E. A. Braude and J. A. Coles, "Syntheses of polycyclic systems. Part iii. Some hydroindanones and hydrofluorenones. The mechanism of the Nazarov cyclisation reaction," *Journal of the Chemical Society*, pp. 1430–1433, 1952.
- [177] "Nazarov cyclization." <http://www.rsc.org/publishing/journals/prospect/ontology.asp?id=RXNO:0000209>. Reaction ID: RXNO:0000209.
- [178] M. A. Tius, "Allene ether Nazarov cyclization," *Chemical Society Reviews*, vol. 43, pp. 2979–3002, 2014.
- [179] T. Vaidya, R. Cheng, P. N. Carlsen, A. J. Frontier, and R. Eisenberg, "Cationic cyclizations and rearrangements promoted by a heterogeneous gold catalyst," *Organic Letters*, vol. 16, pp. 800–803, 2014.
- [180] M. Hoffmann, J.-M. Weibel, P. de Frémont, P. Pale, and A. Blanc, "Gold(I)/(III)-catalyzed rearrangement of divinyl ketones and acyloxyalkynyloxiranes into cyclopentenones," *Organic Letters*, vol. 16, pp. 908–911, 2014.
- [181] L. Zhang and S. Wang, "Efficient synthesis of cyclopentenones from enynyl acetates via tandem Au(I)-catalyzed 3,3-rearrangement and the Nazarov reaction," *Journal of the American Chemical Society*, vol. 128, pp. 1442–1443, 2006.
- [182] W. Zi, H. Wu, , and F. D. Toste, "Gold(I)-catalyzed dearomative rautenstrauch rearrangement: Enantioselective access to cyclopenta[b]indoles," *Journal of the American Chemical Society*, vol. 137, pp. 3225–3228, 2015.
- [183] E. G. Occhiato, C. Prandi, A. Ferrali, A. Guarna, and P. Venturello, "New synthetic approach to cyclopenta-fused heterocycles based upon a mild Nazarov reaction," *The Journal of Organic Chemistry*, vol. 68, pp. 9728–9741, 2003.
- [184] P. Larini, A. Guarna, and E. G. Occhiato, "The Lewis acid-catalyzed Nazarov reaction of 2-(N-methoxycarbonylamino)-1,4-pentadien-3-ones," *Organic Letters*, vol. 8, pp. 781–784, 2006.
- [185] A. Cavalli, A. Pacetti, M. Recanatini, C. Prandi, D. Scarpi, and E. G. Occhiato, "Predicting reactivity and stereoselectivity in the Nazarov reaction: A combined computational and experimental study," *Chemistry – A European Journal*, vol. 14, pp. 9292–9304, 2008.

References

- [186] A. Oppedisano, C. Prandi, P. Venturello, A. Deagostino, G. Goti, D. Scarpi, and E. G. Occhiato, "Synthesis of vinylogous amides by gold(I)-catalyzed cyclization of N-boc-protected 6-alkynyl-3,4-dihydro-2H-pyridines," *The Journal of Organic Chemistry*, vol. 78, pp. 11007–11016, 2013.
- [187] B. M. Trost, C. K. Chung, and A. B. Pinkerton, "The structure of abikoviomycin," *Angewandte Chemie International Edition*, vol. 43, pp. 4327–4329, 2004.
- [188] A. I. Gurevich, M. N. Kolosov, V. G. Korobko, and V. V. Onoprienko, "Stereocontrolled total synthesis of (+)-streptazolin by a palladium-catalyzed reductive diyne cyclization," *Tetrahedron Letters*, vol. 9, pp. 2209–2212, 1968.
- [189] R. A. Ramli, W. Lie, and S. G. Pyne, "Alkaloids from the roots of *Stichoneuron caudatum* and their acetylcholinesterase inhibitory activities," *Journal of Natural Products*, vol. 77, pp. 894–901, 2014.
- [190] N. Isono and M. Mori, "Total synthesis of (-)-cephalotaxine," *The Journal of Organic Chemistry*, vol. 60, pp. 115–119, 1995.
- [191] S.-H. Kim and J. K. Cha, "Synthetic studies toward cephalotaxine: Functionalization of tertiary N-acylhemiaminals by Nazarov cyclization," *Synthesis*, vol. 2000, pp. 2113–2116, 2000.
- [192] M. Petrović, D. Scarpi, B. Fiser, E. Gómez-Bengoa, and E. G. Occhiato, "Annulated N-heterocycles by tandem gold(I)-catalyzed [3,3]-rearrangement/Nazarov reaction of propargylic ester derivatives: an experimental and computational study," *European Journal Organic Chemistry*, vol. 2015, pp. 3943–3956, 2015.
- [193] A. Fürstner and L. Morency, "On the nature of the reactive intermediates in gold-catalyzed cycloisomerization reactions," *Angewandte Chemie International Edition*, vol. 120, pp. 5030–5033, 2008.
- [194] F. Q. Shi, X. Li, Y. Xia, L. Zhang, and Z. X. Yu, "DFT study of the mechanisms of in water Au(I)-catalyzed tandem [3,3]-rearrangement/Nazarov reaction/[1,2]-hydrogen shift of enynyl acetates: A proton-transport catalysis strategy in the water-catalyzed [1,2]-hydrogen shift," *Journal of the American Chemical Society*, vol. 129, pp. 15503–15512, 2007.

References

- [195] L. Claisen, "Zu den O-Alkylderivaten des Benzoyl-acetons und den aus ihnen entstehenden Isoxazolen. (Entgegnung an Hrn. O. Weygand.)," *Berichte der Deutschen Chemischen Gesellschaft (A and B Series)*, vol. 59, pp. 144–153, 1926.
- [196] R. C. Fuson, "The principle of vinylogy," *Chemical Reviews*, vol. 16, pp. 1–27, 1935.
- [197] S. Krishnamurthy, "The principle of vinylogy," *Journal of Chemical Education*, vol. 59, pp. 543–547, 1982.
- [198] C. G. Wermuth, ed., *The Practice of Medicinal Chemistry*. Academic Press, 2011.
- [199] S. Fréville, P. Delbecq, V. M. Thuy, H. Petit, J. P. Célérier, and G. Lhommet, "Diastereocontrolled reduction of cyclic β -enaminones. A new diastereoselective route to 2,6-disubstituted piperidines," *Tetrahedron Letters*, vol. 42, pp. 4609–4611, 2001.
- [200] C. Herdeis, P. Küpper, and S. Plé, "An expeditious stereoselective synthesis of natural (–)-cassine via cascade HWE [3 + 2]-cycloaddition process," *Organic & Biomolecular Chemistry*, vol. 4, pp. 524–529, 2006.
- [201] B. A. D. Neto, A. A. M. Lapis, A. B. Bernd, and D. Russowsky, "Studies on the Eschenmoser coupling reaction and insights on its mechanism. application in the synthesis of norallosedamine and other alkaloids," *Tetrahedron*, vol. 65, pp. 2484–2496, 2009.
- [202] N. N. Salama, N. D. Eddington, D. Payne, T. L. Wilson, and K. R. Scott, "Multidrug resistance and anticonvulsants: New studies with some enaminones," *Current Medicinal Chemistry*, vol. 11, pp. 2093–2103, 2004.
- [203] I. O. Edafioho, S. B. Kombian, K. V. Ananthalakshmi, N. N. Salama, N. D. Eddington, T. L. Wilson, M. S. Alexander, P. L. Jackson, C. D. Hanson, and K. Scott, "Enaminones: Exploring additional therapeutic activities," *Journal of Pharmaceutical Sciences*, vol. 96, pp. 2509–2531, 2007.
- [204] R. Robles-Machín, J. Adrio, and J. C. Carretero, "Gold-catalyzed synthesis of alkylidene 2-oxazolidinones and 1,3-oxazin-2-ones," *The Journal of Organic Chemistry*, vol. 71, pp. 5023–5026, 2006.

References

- [205] A. Buzas and F. Gagosz, "Gold(I)-catalyzed formation of 5-methylene-1,3-oxazolidin-2-ones," *Synlett*, vol. 2006, pp. 2727–2730, 2006.
- [206] E.-S. Lee, H.-S. Yeom, J.-H. Hwang, and S. Shin, "A practical gold-catalyzed route to 4-substituted oxazolidin-2-ones from N-boc propargylamines," *European Journal of Organic Chemistry*, vol. 2007, pp. 3503–3507, 2007.
- [207] http://www.gaussian.com/g_tech/g_ur/k_dft.htm.
BHandHLYP was used as implemented in Gaussian 09.
- [208] J. P. Foster and F. Weinhold, "Natural hybrid orbitals," *Journal of the American Chemical Society*, vol. 102, pp. 7211–7218, 1980.
- [209] M. A. Koch, A. Schuffenhauer, M. Scheck, S. Wetzel, M. Casaulta, A. Odermatt, P. Ertl, and H. Waldmann, "Charting biologically relevant chemical space: A structural classification of natural products (SCONP)," *Proceedings of the National Academy of Sciences of the United States of America*, vol. 102, pp. 17272–17277, 2005.
- [210] R. S. Bon and H. Waldmann, "Bioactivity-guided navigation of chemical space," *Accounts of Chemical Research*, vol. 43, pp. 1103–1114, 2010.
- [211] J. E. Baldwin, "Rules for ring closure," *Journal of the Chemical Society, Chemical Communications*, pp. 734–736, 1976.
- [212] A. L. J. Beckwith, C. J. Easton, and A. K. Serelis, "Some guidelines for radical reactions," *Journal of the Chemical Society, Chemical Communications*, pp. 482–483, 1980.
- [213] K. Gilmore, R. K. Mohamed, and I. V. Alabugin, "The Baldwin rules: revised and extended," *Wiley Interdisciplinary Reviews: Computational Molecular Science*, 2016.
- [214] H. Bürgi, J. Dunitz, J. Lehn, and G. Wipff, "Stereochemistry of reaction paths at carbonyl centres," *Tetrahedron*, vol. 30, pp. 1563–1572, 1974.
- [215] C. D. Johnson, "Stereochemical effects in the formation of 5- and 6-membered rings: the role of Baldwin's rules," *Accounts of Chemical Research*, vol. 26, pp. 476–482, 1993.
- [216] K. Gilmore and I. V. Alabugin, "Cyclizations of alkynes: Revisiting Baldwin's rules for ring closure," *Chemical Reviews*, vol. 111, pp. 6513–6556, 2011.

References

- [217] I. P. Beletskaya and A. V. Cheprakov, "The Heck reaction as a sharpening stone of palladium catalysis," *Chemical Reviews*, vol. 100, pp. 3009–3066, 2000.
- [218] G. Zeni and R. C. Larock, "Synthesis of heterocycles via palladium-catalyzed oxidative addition," *Chemical Reviews*, vol. 106, pp. 4644–4680, 2006.
- [219] V. Barone and M. Cossi, "Quantum calculation of molecular energies and energy gradients in solution by a conductor solvent model," *The Journal of Physical Chemistry A*, vol. 102, pp. 1995–2001, 1998.
- [220] M. Cossi, N. Rega, G. Scalmani, and V. Barone, "Energies, structures, and electronic properties of molecules in solution with the C-PCM solvation model," *Journal of Computational Chemistry*, vol. 24, pp. 669–681, 2003.
- [221] K. Rathwell and M. A. Brimble, "Use of stabilized phthalide anion annulation reactions in synthesis: An update," *Synthesis*, no. 5, pp. 643–662, 2007.
- [222] D. Mal and P. Pahari, "Recent advances in the Hauser annulation," *Chemical Reviews*, vol. 107, pp. 1892–1918, 2007.
- [223] A. de Meijere, P. von Zezschwitz, and S. Bräse, "The virtue of palladium-catalyzed domino reactions – diverse oligocyclizations of acyclic 2-bromoynes and 2-bromoenediynes," *Accounts of Chemical Research*, vol. 38, pp. 413–422, 2005.
- [224] S. Bräse, "Synthesis of bis(enolnonaflates) and their 4-exo-trig-cyclizations by intramolecular Heck reactions," *Synlett*, vol. 1999, pp. 1654–1656, 1999.
- [225] B. Salem, P. Klotz, and J. Suffert, "Cyclocarbopalladation: Formation of bicyclic 1,2-cyclobutanediols through a rare 4-exo-dig cyclization," *Organic Letters*, vol. 5, pp. 845–848, 2003.
- [226] R. Grigg, V. Santhakumar, and V. Sridharan, "Palladium catalysed cascade cyclisation - cyanide ion capture," *Tetrahedron Letters*, vol. 34, pp. 3163–3164, 1993.
- [227] D. M. Schultz and J. P. Wolfe, "Synthesis of polycyclic nitrogen heterocycles via alkene aminopalladation/carbopalladation cascade reactions," *Organic Letters*, vol. 12, pp. 1028–1031, 2010.

References

- [228] F. E. Meyer, P. J. Parsons, and A. D. Meijere, "Palladium-catalyzed poly-cyclization of dienyne: surprisingly facile formation of tetracyclic systems containing a three-membered ring," *The Journal of Organic Chemistry*, vol. 56, pp. 6487–6488, 1991.
- [229] Y. Zhanga and E. Negishi, "Palladium-catalyzed cascade carbometalation of alkynes and alkenes as an efficient route to cyclic and polycyclic structures," *Journal of the American Chemical Society*, vol. 111, pp. 3454–3456, 1989.
- [230] B. M. Monks and S. P. Cook, "Palladium-catalyzed alkyne insertion/Suzuki reaction of alkyl iodides," *Journal of the American Chemical Society*, vol. 134, pp. 15297–15300, 2012.
- [231] B. M. Trost and Y. Shi, "Palladium-catalyzed cyclizations of polyenyne. A palladium zipper," *Journal of the American Chemical Society*, vol. 115, pp. 9421–9438, 1993.
- [232] M. Parasram, V. O. Iaroshenko, and V. Gevorgyan, "Endo-selective Pd-catalyzed silyl methyl Heck reaction," *Journal of the American Chemical Society*, vol. 136, pp. 17926–17929, 2014.
- [233] A. M. Zawisza, B. Ganchegui, I. González, S. Bouquillon, A. Roglans, F. Hénin, and J. Muzart, "Heck-type reactions of allylic alcohols: Part IV: (2-substituted)-1-indanones via 5-endo-trig cyclizations," *Journal of Molecular Catalysis A: Chemical*, vol. 283, pp. 140–145, 2008.
- [234] P. Vital, P.-O. Norrby, and D. Tanner, "An intramolecular Heck reaction that prefers a 5-endo- to a 6-exo-trig cyclization pathway," *Synlett*, vol. 2006, pp. 3140–3144, 2006.
- [235] S. P. Maddaford, N. G. Andersen, W. A. Cristofoli, and B. A. Keay, "Total synthesis of (+)-xestoquinone using an asymmetric palladium-catalyzed polyene cyclization," *Journal of the American Chemical Society*, vol. 118, pp. 10766–10773, 1996.
- [236] D. Ray, S. Paul, S. Brahma, and J. K. Ray, "Palladium-catalyzed intramolecular 5-endo-trig oxidative Heck cyclization: A facile pathway for the synthesis of some sesquiterpene precursors," *Tetrahedron Letters*, vol. 48, pp. 8005–8008, 2007.

References

- [237] J. E. Baldwin and L. I. Kruse, "Approach vector analysis: A stereochemical approach to reactivity," *Journal of the Chemical Society, Chemical Communications*, pp. 233–235, 1977.
- [238] B. Salem and J. Suffert, "A 4-exo-dig cyclocarbopalladation/ 8π electrocyclization cascade: Expeditious access to the tricyclic core structures of the ophiobolins and aleurodiscal," *Angewandte Chemie International Edition*, vol. 43, pp. 2826–2830, 2004.
- [239] C. Bour and J. Suffert, "Cyclocarbopalladation: Sequential cyclization and C–H activation/Stille cross-coupling in the Pd-5-exo-dig reaction," *Organic Letters*, vol. 7, pp. 653–656, 2005.
- [240] P. A. Donets and N. Cramer, "Ligand-controlled regiodivergent nickel-catalyzed annulation of pyridones," *Angewandte Chemie International Edition*, vol. 54, pp. 633–637, 2015.
- [241] M. R. Harris, M. O. Konev, and E. R. Jarvo, "Enantiospecific intramolecular Heck reactions of secondary benzylic ethers," *Journal of the American Chemical Society*, vol. 136, pp. 7825–7828, 2014.
- [242] X. Wang, Y. Liu, and R. Martin, "Ni-catalyzed divergent cyclization/carboxylation of unactivated primary and secondary alkyl halides with CO_2 ," *Journal of the American Chemical Society*, vol. 137, pp. 6476–6479, 2015.
- [243] M. P. M. noz, J. Adrio, J. C. Carretero, and A. M. Echavarren, "Ligand effects in gold- and platinum-catalyzed cyclization of enynes: Chiral gold complexes for enantioselective alkoxy cyclization," *Organometallics*, vol. 24, pp. 1293–1300, 2005.
- [244] M. Gruit, A. Pews-Davtyan, and M. Beller, "Platinum-catalyzed cyclization reaction of alkynes: synthesis of azepino[3,4-b]indol-1-ones," *Organic & Biomolecular Chemistry*, vol. 9, pp. 1148–1159, 2011.

I love deadlines. I love the whooshing noise they make as they go by.

Douglas Adams, *The Salmon of Doubt*

7

Appendix

A Dynamic Kinetic C–P Cross–Coupling for the Asymmetric Synthesis of Axially Chiral P,N Ligands

Pedro Ramírez-López,[†] Abel Ros,^{*,†} Beatriz Estepa,[‡] Rosario Fernández,^{*,‡} Béla Fiser,[§] Enrique Gómez-Bengo,^{*,§} and José M. Lassaletta^{*,†}

[†]Instituto Investigaciones Químicas (CSIC-US), C/Américo Vespucio, 49, 41092 Sevilla, Spain

[‡]Departamento de Química Orgánica, Universidad de Sevilla—Campus Reina Mercedes, C/Prof. García González, 1, 41012 Sevilla, Spain

[§]Departamento de Química Orgánica I, Universidad del País Vasco, UPV/EHU, Apdo. 1072, 20080 San Sebastián, Spain

Supporting Information

ABSTRACT: The Pd-catalyzed enantioselective C–P cross-coupling between racemic, configurationally stable heterobiaryl triflates and trialkylsilyldiaryl(dialkyl)phosphines has been used for the synthesis of several families of enantiomerically enriched heterobiaryl phosphines including QUINAP, PINAP, and QUINAZOLINAP analogues, which can be performed with good yields and enantioselectivities using JOSIPHOS-type bidentate phosphines. The strategy relies on two key assumptions: (I) The N atom of the heterocycle is a better ligand than triflate, and upon oxidative addition, it incorporates into the coordination sphere of the Pd^{II} center to form cationic cyclic intermediates. (II) The geometry of the palladacycle results in a widening of the angles involved in the stabilization of the stereogenic axis, facilitating a fast interconversion of diastereomeric structures and, hence, a dynamic kinetic C–P cross-coupling reaction. These starting hypotheses are supported by experimental and computational studies.

KEYWORDS: P,N-ligands, QUINAP, DYKAT, asymmetric catalysis, C–P coupling, silylphosphines, heterobiaryls

1. INTRODUCTION

Axially chiral P,N-ligands have found important applications in the field of asymmetric catalysis. Since the pioneering developments by Brown and co-workers on Rh^I-catalyzed asymmetric hydroboration/oxidation of styrenes,¹ the original ligand QUINAP I and related axially chiral P,N-ligands have found many other applications in asymmetric catalysis, including Rh^I-catalyzed hydroboration/amination,² Rh^I-catalyzed diboration of alkenes,³ Cu^I-catalyzed conjugate boration,⁴ Ag^I-catalyzed 1,3-dipolar cycloadditions,⁵ Ni⁰-catalyzed cycloaddition of 1,2,3,4-benzothiazine-1,1(2H)-dioxides with allenes,⁶ Cu^I-catalyzed 1,2-addition of alkynes to enamines⁷ or iminium ions,⁸ or Cu^I-catalyzed conjugate addition to alkylidene Meldrum's acids⁹ (Scheme 1).

In spite of the excellent ligand properties exhibited by QUINAP, its resolution via stoichiometric Pd^{II} complexes¹⁰ has been a serious drawback that has hampered its application by the chemical industry. Even being commercially available, its high price has probably excluded its structure from being a common candidate in many exploratory screenings at average research laboratories. A second aspect that has retarded the development of applications for axially chiral P,N-ligands has been the lack of structural variability, as for years QUINAP itself and a few analogues differing in the diarylphosphino group^{9b} have been the only available option. These problems have motivated the development of alternative axially chiral P,N ligands, on one hand, and studies directed to improve the

efficiency and economy of the synthetic methods, on the other. Thus, the groups of Guiry, Carreira, Apponik, Chan, and others have approached the problem by introducing alternative ligands such as QUINAZOLINAP II,¹¹ PINAP III,¹² PyPHOS IV,¹³ and StackPHOS V¹⁴ (Figure 1). These ligands have also been successfully applied in asymmetric catalysis, matching or improving in some cases the results collected with QUINAP in previously developed or new catalytic reactions. However, the methods required for their synthesis are still far from practical: in the best cases, the synthesis requires resolution of diastereomers by chromatography or crystallization (PINAP),¹² while most of them (QUINAZOLINAP,¹⁰ PyPHOS,¹² and StackPHOS¹³) have to be prepared by crystallization of stoichiometric amounts of Pd(II) complexes.

Alternative approaches to the synthesis of QUINAP have also been reported. The first practical synthesis avoiding the use of half-equivalents of Pd salts was reported in 2007 by Knochel and co-workers, who exploited the easy chromatographic separation of diastereomeric sulfoxide intermediates and their easy transformation into enantiopure QUINAP after sulfoxide–lithium exchange, quenching with Ph₃PCl and sulfur, and reduction with Raney-Ni.¹⁵ Two years later, Clayden and co-workers¹⁶ went a step further and, taking advantage of the

Received: March 17, 2016

Revised: May 9, 2016

Scheme 1. Selected Applications of Axially Chiral P,N-Ligands

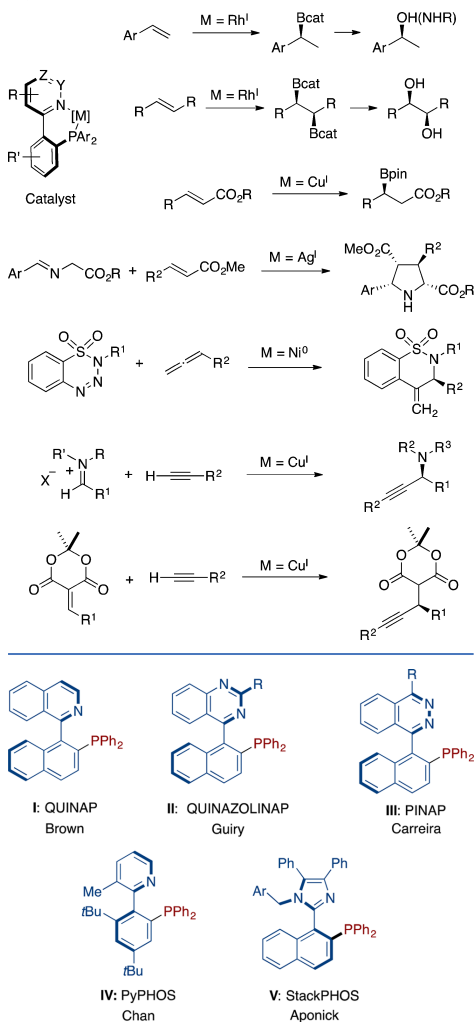


Figure 1. Families of axially chiral P,N-ligands.

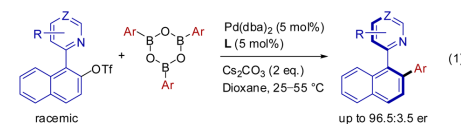
stereochemical control by the sulfinyl group in heterobiaryl sulfoxides, succeeded in the development of a “dynamic thermodynamic resolution” leading to QUINAP after the functional group transformations mentioned above. This constitutes the first asymmetric synthesis of QUINAP but still requires the introduction of an enantiopure sulfinyl group as a sacrificial auxiliary.

Therefore, there is still demand for a general methodology for the synthesis of axially chiral heterobiaryls, ideally based on a catalytic asymmetric procedure enabling the introduction of

structural variability at both the heterocycle and the diaryl-(dialkyl)phosphino group. The direct construction of the stereogenic axis by a cross-coupling reaction might appear as the most straightforward approach to these systems. However, in spite of the great progress achieved during the past years in asymmetric Suzuki–Miyaura cross-couplings,¹⁷ the reaction using heterocyclic substrates remains an unsolved synthetic challenge, presumably due to the interferences caused by the coordination of the heteroatoms located on the substrate, the limitations associated with the availability and poor stability of heteroaromatic organometallics, and the lower configurational stability of the products compared to standard biaryls.¹⁸ In the frame of our research program in asymmetric cross-coupling reactions, we recently developed an alternative methodology for the asymmetric synthesis of axially chiral heterobiaryls consisting of a dynamic asymmetric Suzuki–Miyaura coupling (DYKAT) between racemic, configurationally stable heterobiaryl triflates and arylboroxines (Scheme 2, eq 1).¹⁹ In a

Scheme 2. DYKAT Techniques for the Asymmetric Synthesis of Heterobiaryls

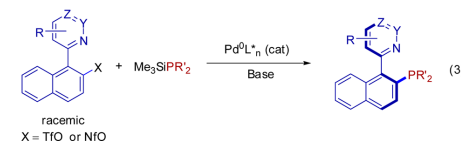
Dynamic kinetic asymmetric Suzuki–Miyaura coupling (ref. 19)



Preliminary results on dynamic kinetic asymmetric C–P bond formation (refs. 20 & 21)



This work



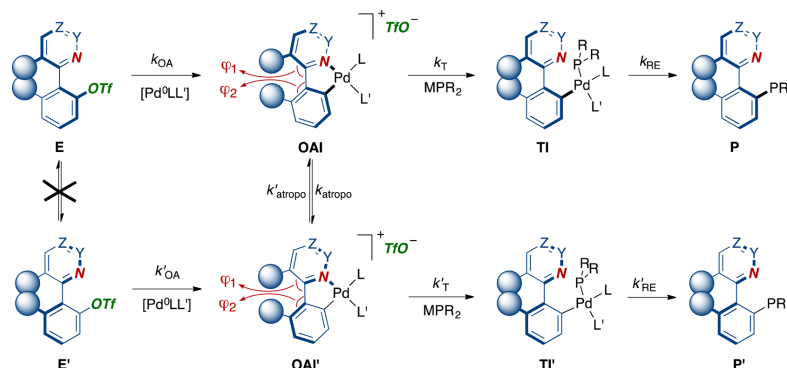
parallel work, we started investigations to apply this strategy for C–P bond forming reactions²⁰ while, simultaneously, Virgil et al. also reported the enantioselective synthesis of QUINAP according to a similar procedure²¹ (eq 2). In both cases, a single example (QUINAP itself) was reported, and different mechanisms involved in the dynamic kinetic cross-coupling were invoked. In this paper, an expanded, general procedure for the synthesis of enantiomerically enriched isoquinoline, 3-methylpyridine, quinazoline, and phtalazine derivatives is reported (eq 3), along with experimental and computational support for a mechanism based on the labilization of cyclic, cationic oxidative addition intermediates.

RESULTS AND DISCUSSION

Starting Hypothesis and Method Development.

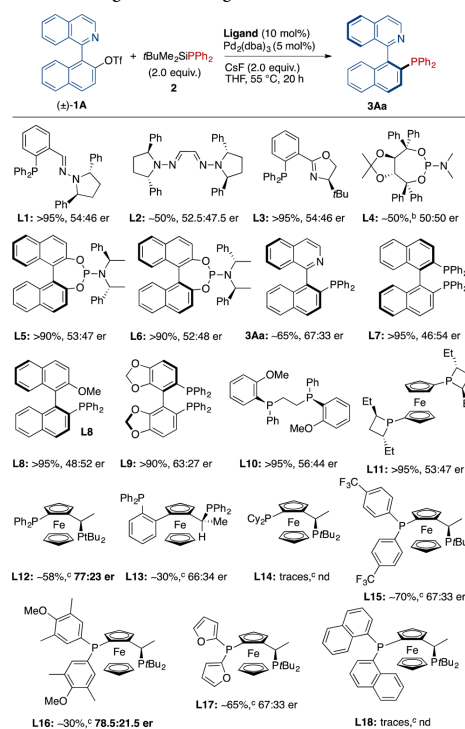
Basically, our strategy is based on two key assumptions: (1) Thanks to the poor coordinating ability of the triflate anion, the oxidative addition of Pd⁰LL' catalysts [LL' = chiral ligand(s)]

Scheme 3. Starting Mechanistic Hypothesis



should generate cyclic cationic intermediates **OAI** and **OAI'** incorporating the isoquinoline/pyridine N atom as a ligand (Scheme 3). (2) A widening of the angles φ_1 and φ_2 would compromise the configurational stability of the stereogenic axis, facilitating an easy equilibration of atropisomeric intermediates **OAI** and **OAI'**. In this scenario, two additional conditions are required to achieve a highly enantioselective dynamic kinetic C–P coupling to products **P** or **P'**. (3) The transmetalation step from both **OAI** and **OAI'** into intermediates **TI** and **TI'** should be relatively slow with respect to the interconversion between **OAI** and **OAI'**. (4) The chiral ligand(s) **LL'** should provide a substantial energy gap between the diastereomeric transmetalation transition states.

Our initial ligand screening was performed using the coupling of triflate **1A** and *t*BuMe₂SiPPh₂ (**2**)²² as a model reaction, with CsF as the base,²³ dry THF at 55 °C as the solvent, and 5 mol % Pd₂(dba)₃/10 mol % ligand as the catalyst system (Scheme 4). The use of silylphosphine reagents,²⁴ whose reactivities can be tuned by adjusting the steric and/or electronic properties of the silyl group, was envisaged as a potentially useful method to modulate the rate of release of the phosphine fragment: according with our strategy, a relatively slow transmetalation step is necessary to facilitate the equilibration of the oxidatively added intermediates. Bishydrazone and phosphino–hydrazone ligands **L1** and **L2**, which showed very good enantioselectivities and activities in asymmetric Suzuki–Miyaura cross-couplings,²⁵ and a privileged ligand such as the phosphino oxazoline **L3**, were chosen as candidates and tested in the model reaction. These ligands provided moderate to excellent conversions into the desired product **3Aa**, although low enantioselectivities were observed. Motivated by the excellent performance of these type of ligands in dynamic asymmetric (DYKAT) Suzuki–Miyaura couplings,¹⁹ we also examined TADDOL-derived phosphoramidite ligand **L4** and related binaphthol-derivatives **L5** and **L6**. **L5** and **L6** afforded **3Aa** in >90% conversions but with low enantioselectivities. Axially chiral, commercially available ligands such as BINAP, MeO-MOP, and SEGPHOS **L7**–**L9** also provided high catalytic activity, but only in the last case was a low yet significant 63:37 er observed. Additionally, a kind of “autocatalytic” reaction promoted by QUINAP **3Aa** formed during the reaction was also considered. Using commercially available (S)-QUINAP as the ligand, a moderate ~65%

Scheme 4. Ligand Screening^a

^aReactions performed at 0.1 mmol scale in dry THF (2 mL). Conversions estimated by ¹H NMR. Enantiomeric ratios were determined by HPLC on chiral stationary phases after oxidation of **3Aa** to the corresponding phosphine oxide. ^bReaction time was 38 h. ^cReaction time was 6 h.

optimized conditions, the model reaction was analyzed at approximately 50% conversion, leading to the product **3Aa** in 96:4 er, while the unreacted material **1A** had a 68:32 er. This result rules out a mechanism relying on a fast racemization of **1A** (dynamic kinetic resolution).

Further efforts were directed to extend the scope of the methodology to related systems. To this aim, silylphosphines **5a–5e** were synthesized by a modified protocol of the described procedure²⁹ and reacted with heterobiaryl triflates **1A–1D** or nonaflates **8C** and **8D** in the presence of Pd(dba)₂/L12 as the catalytic system and CsF as the base. Heterobiaryl phosphines **3** were obtained in excellent yields and good enantiomeric excesses (Table 2). Silylphosphines **5b–5d**, which bear electron-withdrawing and electron-donating groups on the aryl fragment, afforded the corresponding chiral phosphines **3Ab–3Ad** in 74–88% isolated yields and er's from 78:22 to 92:8. Pyridine-derived phosphines **3Ba–3Bd** were also obtained in excellent yields and enantioselectivities (er 85.5:14.5–95.5). Additionally, the heterobiaryl dialkylphosphine **3Be** could also be obtained in 93% yield and a good 85:15 er when **L16** was used as the ligand. Reproducibility problems were observed when triflate **1C** was employed as the substrate, due presumably to some undetected impurity. In this case, we resorted to using nonaflate **8C**,³⁰ which allowed obtaining of the desired products **3Ca–3Cd** in excellent yields and enantioselectivities of 74–90%. Dialkyl heterobiarylphosphine **3Ce** was obtained in 72% yield and a moderate 72.5:27.5 er. Phthalazine-derived triflate **1D** was also tested in the C–P coupling reaction, giving the corresponding biarylphosphines **3Da** and **3Db** in 71 and 73% yield, and 85.5:14.5 and 91:9 er, respectively. The enantiomeric purity of products **3** could be increased by crystallization in some cases. As representative examples, QUINAP itself (**3Aa**) and **3Ca** were obtained in 99.5:0.5 er after a single recrystallization or washing with cold acetone, respectively. In the case of **3Ac**, the crystallization of a small amount of the racemate served to increase the optical purity of the remaining mother liquors (up to 97.5:2.5 er after a single crystallization).

Mechanism and Computational Studies. In the preliminary investigations mentioned above, two different mechanisms were postulated to explain the observed dynamic asymmetric cross-coupling. On one hand, our group assumed that the nitrogen atom of the isoquinoline coordinates to the Pd center, leading to diastereomeric, cyclic **OAI** and **OAI'** intermediates, displacing the poorly coordinating triflate anion. The geometry of these **OAI** intermediates suggests that the equilibration proceeds via a transition state **TS_{rot}–OAI** in which the angles φ_1 and φ_2 are just slightly wider to allow hydrogen atoms H(8) and H(8') to reach coplanarity with the stereogenic axis (Scheme 5, path a). On the other hand, Virgil et al.²¹ suggested that unsaturated T-shaped **OAI_b** and **OAI'_b** intermediates equilibrate via a square planar transition state **TS_{rot}–OAI_b**, stabilized by an agostic Pd–H(8) interaction (path b).

In this last proposal, the presence of a coordinating nitrogen atom on the heteroaryl moiety does not play any role, and the DYKAT process should work with triflate **9**. However, no C–P coupling products were observed from the reaction of **9** with **5a**, which afforded an incomplete conversion into hydrolysis product **10** after overnight heating at 40 °C (Scheme 6).

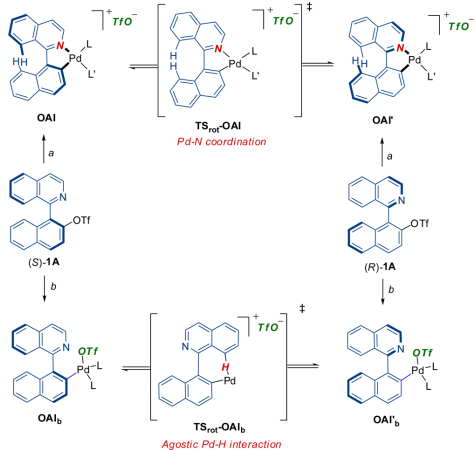
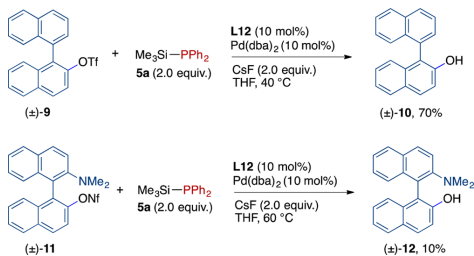
This experiment reveals that the presence of a coordinating isoquinolyl/pyridinyl nitrogen is not only necessary to favor the formation of the cationic and configurationally labile pallada-

Table 2. Dynamic Kinetic Asymmetric C–P Couplings: Scope^{a,f}

Series	A	B	C	D
3Aa	3Ab	3Ac	3Ad	3Ba
94%, er 95.5:4.5 ^b (99.5:0.5) ^c	88%, er 90:10 ^b	84%, er 92.8 ^b (97.5:2.5) ^d	74%, er 78:22 ^{b,e}	89%, er 95:5 ^b
3Bc	3Bd	3Be	3Ca	3Cb
81%, er 93:7 ^b	77%, er 85:15 ^{b,e}	93%, er 85:15 ^{b,f,g}	90%, er 95:5 ^b (99.5:0.5) ⁱ	87%, er 93:7 ^b
3Cd	3Ce	3Da	3Db	
74%, er 89.5:10.5 ^{b,e}	72%, er 73:27 ^{b,g}	71%, er 85.5:14.5 ^b	73%, er 91:9 ^b	

^aReactions performed on a 0.1 mmol scale. Synthetic and phosphine-free silylphosphines **5a–5e** were used in all cases. Isolated yields and er's determined by HPLC on chiral stationary phases are shown. ^bTriflate **1** was used as a starting material. ^cer after recrystallization (toluene/CH₂Cl₂). ^der of mother liquor after crystallization of minor amounts of racemate (*n*-hexane/AcOEt). ^eAir-sensitive compounds: fast flash chromatography under nitrogen was required for purification. ^f**L16** was used instead of **L12**. ^gReaction time 40 h. ^hNonaflate **8** was used as a starting material. ⁱer after washing with cold acetone.

cycle but also to facilitate the chelate-assisted oxidative addition of the racemic triflate/nonaflate to the Pd⁰ center. Similarly, the

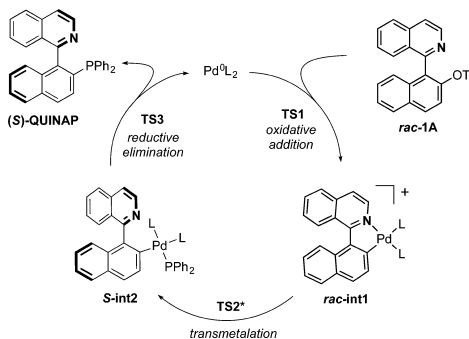
Scheme 5. Proposed Mechanisms for the Epimerization of Diastereomeric Oxidative Addition Intermediates**Scheme 6. Experiments with Triflate **9** and Nonaflate **11****

reaction of NOBIN-derived nonaflate **11** with **5a** afforded a low conversion into hydrolysis product **12**, even at a higher temperature (60 °C), indicating that the formation of a *five-membered* cationic palladacycle is essential to reactivity.

In order to gain further insight into the mechanism of the reaction, we decided to set out an in depth DFT computational investigation of the process. According to the aforementioned data, the optimal experimental conditions involved the use of aromatic triflates or nonaflates as substrates, a Pd catalytic center bound to **L12** or **L16** as chiral ligands (both containing a second metal center, Fe), and the combination of $\text{Me}_3\text{SiPPh}_2$ and CsF as a phosphide transfer system. The sum of all these species would produce transition structures too large and complex to be computed by the current computational methods, if desirable accuracy has to be achieved. In order to maintain the system as close as possible to the experimental system, however, only a few simplifications were included in our study. We thus chose the model containing triflate **1A** and the Pd^0 -**L12** chiral system, which has shown good performance in the reaction (Tables 1 and 2), and the symmetrical triphenyl phosphine (PPh_3) as a model for the incoming nucleophilic phosphide during the transmetalation (vide infra). The calculations were performed at the B3LYP/6-31G** (LANL2DZ for Pd and Fe) level with the Gaussian 09 suite of

programs.^{31,32} In this way, we were able to maintain the computational model as similar to the experimental one as possible, without compromising the accuracy of the method of choice.

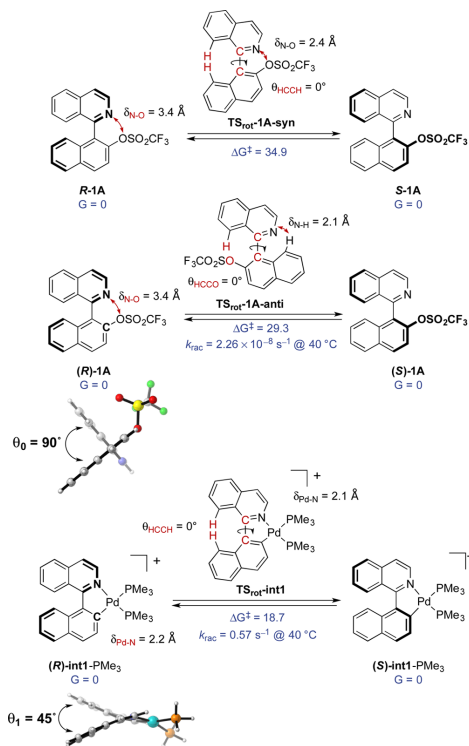
We anticipated that the general mechanism to transform the initial racemic triflate **1A** into the final enantioenriched QUINAP product would involve the three classical coupling steps, namely, oxidative addition, transmetalation, and reductive elimination (Scheme 7). Our model is based on two central

Scheme 7. General Mechanism for the Pd-Catalyzed QUINAP Formation

ideas: (i) The starting triflates **R-1A** and **S-1A** are configurationally stable, whereas the oxidative addition to $\text{Pd}(0)$ leads to the formation of configurationally labile $\text{Pd}(II)$ intermediates (**int1**), which are prone to epimerization. (ii) The present DYKAT transformation is taking place under typical Curtin-Hammett conditions, meaning that the epimerization rate of the interconverting $\text{Pd}(II)$ complexes (**int1**, pro-*R*, and pro-*S*) is faster than their further evolution to **int-2** through transmetalation. Thus, the transmetalation step (**TS2**) is the stereodetermining one, and the two diastereomeric transmetalations must occur at sufficiently different rates as to induce enough selectivity in the formation of the final *R* and *S* products. Another important issue is that the reductive elimination process (**TS3**) must be fast again, making the transmetalation step irreversible.

We found computational evidence supporting our working hypothesis based on the following results. The interconversion of the two enantiomeric triflates **R-1A** and **S-1A** is predicted to be an extremely slow process in the absence of palladium, since its activation energy is as high as 29.3 kcal/mol (**TSrot-1A-anti**, Scheme 8). There is a clear difficulty for the substrate to adopt the necessary conformation for the rotation. In the ground state, the angle formed by the planes of the two aromatic rings θ_0 is ca. 90°, but it must approach 0° during the transition state **TS_rot-1A-syn** (34.9 kcal/mol, Scheme 8), with the accompanying energetic cost. The rotation is easier through the *anti* approach³³ but still too high to be feasible at room temperature (29.3 kcal/mol, **TS_rot-1A-anti**). Meanwhile, after the oxidative addition of $\text{Pd}(0)$ to the C-OTf bond, the chelation complex **R-int1-PMe3** presents drastic geometrical changes in the right direction to facilitate the rotation/epimerization process, like the reduction of the q_1 angle to 45° (Scheme 8). Furthermore, the N-Pd distance, which is a favorable, bonding interaction, is

Scheme 8. Activation Energies for the Axial Rotation of Initial Triflates and Palladacyclic Intermediates



similar (ca. 2.1 Å) in the ground states of *R*- or *S*-int1-PMe₃ and during the transition state for the rotation (TS_{rot-int1}). Thus, the energy barrier is dramatically reduced to 18.7 kcal/mol, explaining the fast interconversion of both enantiomeric complexes under the experimental conditions. These results are the confirmation that the palladacyclic intermediates can easily racemize, whereas the initial triflates can not.

The use of an achiral phosphine (PMe₃) as a first approximation implies that *R*-int1-PMe₃ and *S*-int1-PMe₃ are isoenergetic (Scheme 8), but the computation of the experimental chiral ligand L12 makes the corresponding complexes *R*-int1-L12 and *S*-int1-L12 diastereomeric (Figure 2), differentiating their energies. Both complexes can still interconvert, and the equilibrium is clearly shifted toward the *pro-R* complex *R*-int1-L12, which is 4.3 kcal/mol lower in energy than its *pro-S* counterpart. The two complexes in Figure 2 are actually the lowest in energy intermediates of a total of eight possible diastereomeric species, the rest of them being remarkably higher in energy (between 5.3 to 13.4 kcal/mol) than *R*-int1-L12. Four of these species are a result of the fact that the palladium center is not forming a perfect square planar structure. The two cycles around the palladium atom are not coplanar and form a pseudotetrahedral geometry with two different configurations. Also, the relative disposition of the two

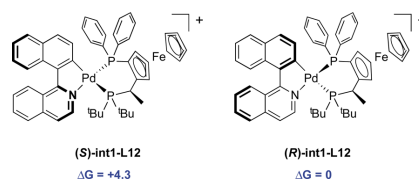
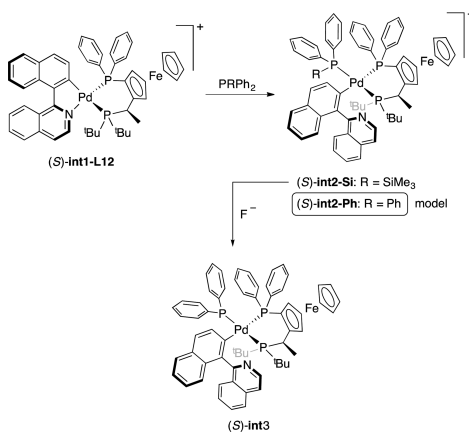


Figure 2. Structures of the two most stable palladacyclic intermediates (int1) computed at M06/6-31+G(d,p) (iefcm,THF)//B3LYP/6-31G(d,p).

phosphorus atoms in the asymmetric diphosphine (L12) with respect to the C and N atoms of the aromatic rings leads to the formation of the other four diastereoisomers.

It is important to note that the overall lowest in energy intermediate (*R*-int1-L12) corresponds to the *minor* experimental enantiomer *R*. However, this fact is irrelevant in the present Curtin–Hammett conditions, since all possible isomers are involved in a fast equilibrium, and the final outcome of the reaction is determined by the relative activation energy of the different transmetalation transition states. At this point, attention must be drawn to the fact that the transmetalation step is not in fact a *classical* transmetalation, since it actually consists on a isoquinoline/Me₃SiPPh₂ ligand exchange, with subsequent abstraction of the silyl moiety by the CsF salt (Scheme 9). This system is difficult to compute, but a slightly

Scheme 9. Two-Step Transmetalation Process and the Computed PPh₃ Model

altered model was envisioned, consisting of the replacement of the actual Me₃SiPPh₂ ligand by PPh₃ (int2-Si vs int2-Ph). This alternative has the great advantage that triphenylphosphine is conformationally much simpler than Me₃SiPPh₂, while maintaining a similar steric hindrance.

Thus, all possible transition structures for the approach of the nucleophilic phosphine were computed, maintaining in all cases similar distances for the coordination of the phosphine to palladium and decoordination of the isoquinoline-nitrogen from the metal (Figure 3). As mentioned before, there are eight main isomers for the int-1 type complexes, and for each of

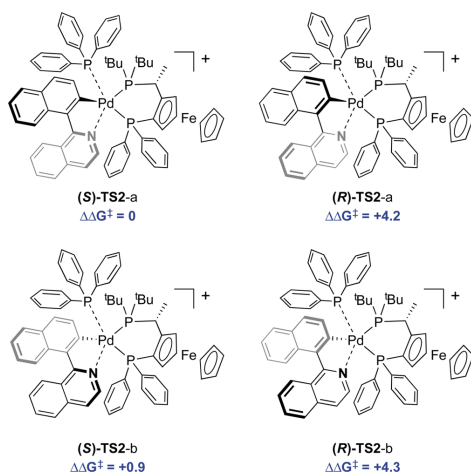


Figure 3. Most stable transition states for the approach of PPh_3 to the Pd center, computed at M06/6-31+G(d,p) (iefpcm,THF)//B3LYP/6-31G(d,p).

them we found at least two different transition structures, depending on the departing trajectory followed by the isoquinoline. Compare for example the two lowest in energy structures for the *S* enantiomer (*S*-TS2-a, *S*-TS2-b), in which the isoquinoline ligand leaves the palladium sphere toward the lower or upper face, respectively. All of the possible alternatives were computed, resulting in a large range of activation energies (ca. 10 kcal/mol), but only the most stable ones are shown in Figure 3. To our delight, the most favored approach (*S*-TS2-a) is in agreement with the formation of the experimental *major S* enantiomer, and the difference with the lowest *pro-R* structure (*R*-TS2-a) is 4.2 kcal/mol, large enough to explain a high selectivity in the process. Even more, the second favored structure also corresponds to the *S*-enantiomer (*S*-TS2-b, +0.9 kcal/mol). Taking the results of Schemes 8 and Figure 3 together, we are facing the typical situation where the minor, less stable isomer (*S*-int1-L12) reacts faster than the major unreactive one (*R*-int1-L12), nicely explaining the experimental stereoselectivity results (Figure 4). It is also important to note that the computed activation energy of the (*S*)-TS2-a is $\Delta G^\ddagger = 25.2$ kcal/mol from the separate PPh_3 and (*R*)-int1-L12 and can be safely considered the rate limiting step, as it is much larger than either isomerization or reductive elimination.³⁴

The final C–P reductive elimination step was also computed (Scheme 10), affording interesting data. First, the activation barrier for TS3 is very low comparing to the rest of energies found in this study ($\Delta G^\ddagger = 12.5$ kcal/mol), making the whole process after transmetalation irreversible. Second, the rotation barrier for the int3-type intermediates and for the final QUINAP-type products increase to 34.7 and 32.5 kcal/mol, respectively. Racemization processes at the final stages of the reaction are, thus, unfeasible, confirming that the formation of palladacycles by chelation with the nitrogen of the isoquinoline (like in int1) is a mandatory condition to allow the epimerization of the substrates.

Finally, we also checked the possible involvement of the palladium center in a Pd–H agostic bond (int4, Figure 5),

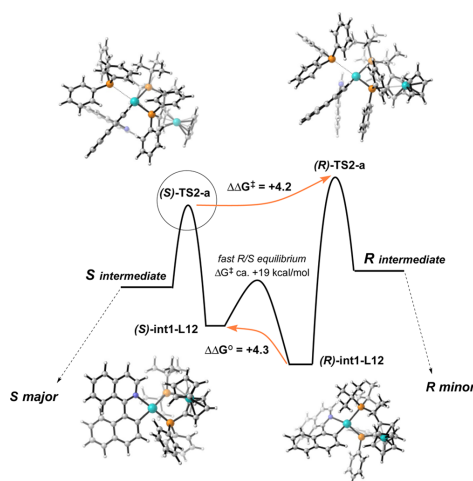


Figure 4. Energy diagram for the transmetalation step.

Scheme 10. Structure and Activation Energy of the C–P Reductive Elimination Step

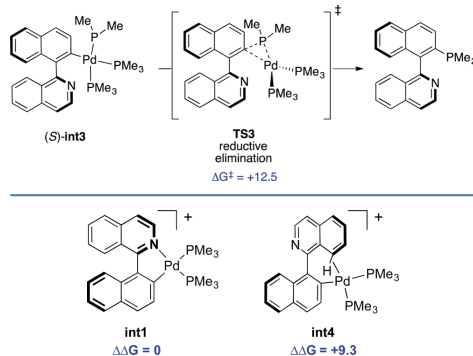


Figure 5. Comparison of Virgil–Stolz proposal (int4) and palladacycle int1.

which has been proposed by Virgil and co-workers²¹ to explain the epimerization of the oxidative addition intermediates without the intervention of the nitrogen atom. Our calculations show that the model complex int4 is remarkably more unstable ($\Delta G = +9.3$ kcal/mol) than the simple int1-type palladacycle. This large energy difference is enough to completely discard the participation of int4 in the mechanism.

CONCLUSION

In summary, the dynamic kinetic asymmetric C–P coupling between heterobiaryl triflates or nonaflates and trimethylsilylphosphines appears as an efficient, general methodology for the asymmetric synthesis of QUINAP, PyPHOS, QUINAZOLINAP, and PINAP analogues. The collected experimental evidence and the results of the performed computational

- (18) (a) Pedersen, J. R.; et al. *Acta Chem. Scand.* **1972**, *26*, 929–936. (b) Brunner, H.; Olschewski, G.; Nuber, B. *Synthesis* **1999**, 429–434. (c) Tucker, S. C.; Brown, J. M.; Oakes, J.; Thornthwaite, D. *Tetrahedron* **2001**, *57*, 2545–2554. (d) Baker, R. W.; Rea, S. O.; Sargent, M. V.; Schenkelaars, E. M. C.; Tjahjandarie, T. S.; Totaro, A. *Tetrahedron* **2005**, *61*, 3733–3743. (e) Tanaka, S.; Suzuki, Y.; Matsushita, M.; Kitamura, M. *Bull. Chem. Soc. Jpn.* **2015**, *88*, 1726–1734.
- (19) Ros, A.; Estepa, B.; Ramírez-López, P.; Álvarez, E.; Fernández, R.; Lassaletta, J. M. *J. Am. Chem. Soc.* **2013**, *135*, 15730–15733.
- (20) Lassaletta, J. M.; Ros, A.; Fernández, R.; Estepa, B.; Ramírez-López, P. (CSIC, Universidad de Sevilla). Procedimiento de Síntesis de Compuestos Heterobifilícos con Quiralidad Axial, Compuestos Obtenidos y Uso. ES Patent P201331068, July 12, 2013.
- (21) Bhat, V.; Wang, S.; Stoltz, B. M.; Virgil, S. C. *J. Am. Chem. Soc.* **2013**, *135*, 16829–16832.
- (22) *t*BuMe₂SiPPh₂ (2) and *i*Pr₃SiPPh₂ (4) were synthesized following previously described procedures, see: (a) Hayashi, M.; Matsuura, Y.; Watanabe, Y. *Tetrahedron Lett.* **2004**, *45*, 1409–1411. (b) Trepohl, V. T.; Oestreich, M. *Chem. Commun.* **2007**, 3300–3302.
- (23) Other bases such as Ba(OH)₂, K₃PO₄, KF, Cs₂CO₃, and K₂CO₃ were tested using L1 as the ligand, but lower conversions were observed.
- (24) For a review on the synthetic utility of silylphosphines, see: (a) Hayashi, M. *Chem. Rec.* **2009**, *9*, 236–245. Pd-catalyzed synthesis of triarylphosphines from aryl iodides and silylphosphines: (b) Tunney, S. E.; Stille, J. K. *J. Org. Chem.* **1987**, *52*, 748–753. Enantioselective arylation of silylphosphines: (c) Chan, V. S.; Bergman, R. G.; Toste, F. D. *J. Am. Chem. Soc.* **2007**, *129*, 15122–15123. Nickel-catalyzed synthesis of triarylphosphines from aryl nitriles or aryl chlorides: (d) Sun, M.; Zhang, H.-Y.; Han, Q.; Yang, K.; Yang, S.-D. *Chem. - Eur. J.* **2011**, *17*, 9566–9570. (e) Sun, M.; Zang, Y.-S.; Hou, L.-K.; Chen, X.-X.; Sun, W.; Yang, S.-D. *Eur. J. Org. Chem.* **2014**, *2014*, 6796–6801.
- (25) (a) Bermejo, A.; Ros, A.; Fernández, R.; Lassaletta, J. M. *J. Am. Chem. Soc.* **2008**, *130*, 15798–15799. (b) Ros, A.; Estepa, B.; Bermejo, A.; Álvarez, E.; Fernández, R.; Lassaletta, J. M. *J. Org. Chem.* **2012**, *77*, 4740–4750.
- (26) (a) Tappe, M. J. F.; Trepohl, V. T.; Oestreich, M. *Synthesis* **2010**, 3037–3062. (b) Li, Y.-M.; Yang, S.-D. *Synlett* **2013**, *24*, 1739–1744. (c) Wauters, L.; Debrouwer, W.; Stevens, C. V. *Beilstein J. Org. Chem.* **2014**, *10*, 1064–1096. (d) Glueck, D. S. *Top. Organomet. Chem.* **2010**, *31*, 65–100.
- (27) The S configuration was assigned by chemical correlation. See the Supporting Information for details.
- (28) Triflates were stored in the fridge for months to prevent the formation of triflic acid traces, affording reproducible enantiomeric excesses throughout this study without the need of further purifications.
- (29) Trepohl, V. T.; Fröhlich, R.; Oestreich, M. *Tetrahedron* **2009**, *65*, 6510–6518. The deprotonation at –78 °C of commercially available phosphines, followed by trapping of the corresponding phosphide with ClSiMe₃, gave the silylphosphine crudes with purity higher than 90%. Further purification by distillation *in vacuo* (see SI) afforded the pure silylphosphines 5a–5e in 71–92% isolated yields.
- (30) Nonaflates (nonafluorobutanesulfonates) have been broadly used in synthesis as an alternative to triflates due to their higher stability and similar reactivity: Högermeier, J.; Reissig, H.-U. *Adv. Synth. Catal.* **2009**, *351*, 2747–2763.
- (31) Frisch, M. J.; Trucks, G. W.; Schlegel, H. B.; Scuseria, G. E.; Robb, M. A.; Cheeseman, J. R.; Scalmani, G.; Barone, V.; Mennucci, B.; Petersson, G. A.; Nakatsuji, H.; Caricato, M.; Li, X.; Hratchian, H. P.; Izmaylov, A. F.; Bloino, J.; Zheng, G.; Sonnenberg, J. L.; Hada, M.; Ehara, M.; Toyota, K.; Fukuda, R.; Hasegawa, J.; Ishida, M.; Nakajima, T.; Honda, Y.; Kitao, O.; Nakai, H.; Vreven, T.; Montgomery, J. A., Jr.; Peralta, J. E.; Ogliaro, F.; Bearpark, M.; Heyd, J. J.; Brothers, E.; Kudin, K. N.; Staroverov, V. N.; Keith, T.; Kobayashi, R.; Normand, J.; Raghavachari, K.; Rendell, A.; Burant, J. C.; Iyengar, S. S.; Tomasi, J.; Cossi, M.; Rega, N.; Millam, J. M.; Klene, M.; Knox, J. E.; Cross, J. B.;

Annulated N-Heterocycles by Tandem Gold(I)-Catalyzed [3,3]-Rearrangement/ Nazarov Reaction of Propargylic Ester Derivatives: an Experimental and Computational Study

Martina Petrović,^[a] Dina Scarpi,^[a] Béla Fiser,^[b] Enrique Gómez-Bengoá,^[b] and
Ernesto G. Occhiato*^[a]

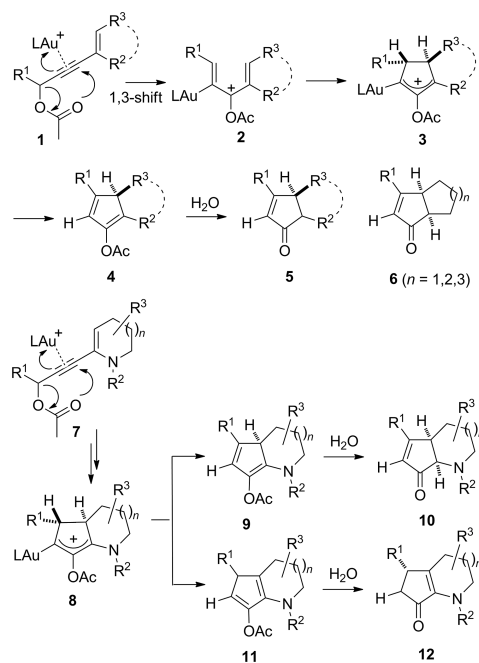
Keywords: Homogeneous catalysis / Gold / Annulation / Enynes / Nitrogen heterocycles

The gold(I)-catalyzed tandem rearrangement/Nazarov reaction of propargylic ester derivatives is a useful strategy for the synthesis of cyclopenta-fused N-heterocyclic structures present in many natural compounds. Readily available lactams are converted into enol phosphates and triflates and coupled to propargyl alcohols under Sonogashira conditions. After acetylation, the gold-catalyzed rearrangement of the enynyl acetates readily occurs when using 3–5 mol-% of a gold(I) catalyst. The rearrangement generates a divinyl cat-

ion which undergoes a 4π electrocyclization (Nazarov reaction) leading to the target compound in good to excellent yield. This process has been studied in details both experimentally and computationally to understand the influence of both the reaction conditions and substrate structural features on the reaction rate and regioselectivity, as well as the torquoselectivity in the ring closure step. A series of examples illustrates at the end the scope of the reaction.

Introduction

The widespread presence of the 2-cyclopentenone moiety in natural products has always been a stimulus for synthetic organic chemists to find new methods for efficiently building this structure, with a varying degree of substitution and control of the stereochemistry.^[1] Among the many approaches to 2-cyclopentenones, the Nazarov reaction ranks as one of the most important and versatile since the requisite 4π electron pentadienyl cation can be generated not only from classical dienones but also from a steadily increasing variety of unconventional substrates or processes,^[2] including gold-catalyzed transformations.^[3–4] Suitably assembled propargylic esters are particularly useful as substrates for the Nazarov reaction, since the transition metal-catalyzed migration of the carboxylic group to any of the two unsaturated positions leads to competent pentadienyl cations. 5-Acyloxy-1,3-enynes **1** in particular (Scheme 1), undergo – under remarkably mild conditions – a gold(I)-catalyzed [3,3]-rearrangement to pentadienyl cations **2** which, after Nazarov reaction and eventual protodeauration, provide acetyloxy-substituted cyclopentadiene products **4**. Hydrolysis (in situ or after work-up) of the latter leads to the target cyclopentenones **5**.^[5] This strategy



Scheme 1. Sequential gold(I)-catalyzed [3,3]-rearrangement/Nazarov reaction of 5-acyloxy-1,3-enynes **1** (above) and **7** (below).

[a] Dipartimento di Chimica “U. Schiff”, Università degli Studi di Firenze,
Via della Lastruccia 13, 50019 Sesto Fiorentino (FI), Italy
E-mail: ernesto.occhiato@unifi.it
www.egocch.it/

[b] Departamento de Química Orgánica I, Universidad del País Vasco/UPV-EHU,
Manuel de Lardizabal 3, 20018 Donostia-San Sebastián, Spain
Supporting information for this article is available on the
WWW under http://dx.doi.org/10.1002/ejoc.201500462.

FULL PAPER

E. G. Occhiato et al.

successfully provides cyclopenta-fused carbacycles **6** when the enyne double bond is embedded in a five-, six- and seven-membered ring (Scheme 1).^[5a,5b,6] Our interest in the synthesis of cyclopenta-fused heterocycles by the Nazarov reaction,^[7] as well as in gold-catalysis,^[8a] prompted us to investigate if the same approach could still furnish annulated systems when embodying the same double bond into *N*-heterocycles as **7** (Scheme 1).

This in fact would represent a new synthetic approach to molecular structures (e.g. [1]pyridines, annulated pyrrolines and azepines) present in many natural compounds (Figure 1),^[9] some of which (e.g. cephalotaxine and roseophilin) already synthesized via some of the Nazarov reaction variants.^[10]

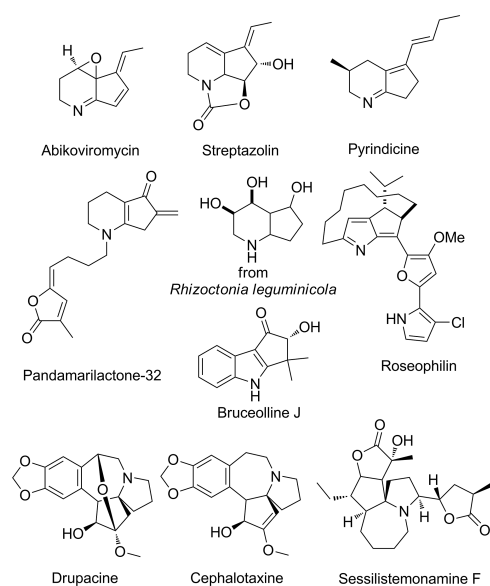


Figure 1. Natural compounds containing a cyclopenta-fused *N*-heterocyclic ring.

To accomplish this, however, a few issues have to be dealt with. First, because of the likely contribution of the *N* atom in stabilizing positively charged intermediates, whether and how the presence of the heteroatom influences the rate and the regiochemical outcome of the reaction had to be assessed. In our previous studies on the Brønsted acid-catalyzed Nazarov reaction of masked and classical dienones,^[7] deprotonation of the oxyallyl cation exclusively led to compounds of type **12** having the more substituted double bond and not to even traces of its regioisomer **10**, in strong contrast with the outcome of the gold-catalyzed reaction of the corresponding carbacyclic systems (Scheme 1). Moreover, the choice of the *N* protecting group is not of secondary importance, as its involvement in gold-catalyzed rearrangement of closely related *N*-Boc enynes has been shown,^[8]

thus posing a concern about a possible competition in the nucleophilic attack to the activated triple bond. Because the cyclization leading to intermediate **8** involves a vinylgold species, a further question arises about the conservation of the high torquoselectivity we have previously observed in Brønsted acid-catalyzed Nazarov reactions, which led to *cis* disubstituted cyclopenta-fused *N*-heterocycles.^[7a,7b,7d,7g] and which we have exploited for the formal enantioselective synthesis of roseophilin.^[10] Finally, to establish this approach as a reliable synthetic strategy for cyclopenta-annulated *N*-heterocycles, the scope of the reaction had to be assessed on the alkyne chain *R*¹ and the heterocycle ring size and substituents. In this paper we demonstrate that the tandem gold(I)-catalyzed propargylic rearrangement/Nazarov reaction of propargylic esters **7** is a useful strategy for the synthesis of annulated *N*-heterocycles but, also, that the picture for this process is much more complex than that previously reported for non-heterocyclic systems, with a whole series of elements [*N*-protecting group, heterocycle ring size, gold(I) counterion, etc.] all influencing reaction rate and selectivity (regio- and stereoselectivity) in one way or another. To assist us in the comprehension of the experimental results, the energies and structures of the intermediates and transition states involved in this process were determined by a computational study, the results of which are well in accordance with the experimental data and which we present in this paper.

Results and Discussion

Evaluating the Reactivity of Model Compounds

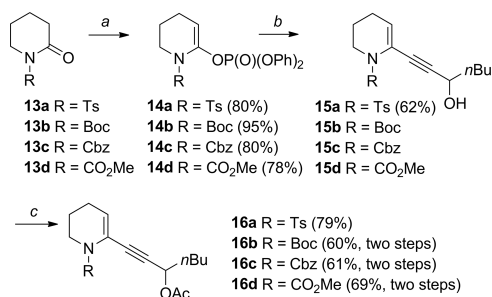
We have recently shown that *N*-Boc-protected enynes closely related to **7** (but lacking the acetoxy group) are excellent substrates for a gold(I)-catalyzed oxyauration involving the *N*-Boc carbonyl oxygen which eventually affords exocyclic vinylogous amides.^[8a] Thus, in order to avoid any possible interference by a *N*-alkoxycarbonyl group, we decided to find the best reaction conditions for the sequential [3,3]-rearrangement/Nazarov cyclization with compound **16a**, bearing a *N*-Tosyl protecting group. The synthesis of this model compound (Scheme 2) was carried by converting the *N*-Ts-substituted δ -valerolactam **13a** into the corresponding enol phosphate **14a** which was immediately subjected to Sonogashira coupling^[11] with 1-heptyn-3-ol to give alcohol **15a** in 62% after chromatography. This was eventually treated with acetic anhydride to provide acetate **16a** in 79% yield.^[12]

To find the best catalyst, we first screened a series of silver and copper salts as sources of the non-coordinating anion with 3 mol-% of Ph_3PAuCl in CH_2Cl_2 at room temperature (Table 1).^[13] The reactions were monitored by TLC and, after consumption of **16a**, they were left whilst stirring (usually 16 h at room temperature) to allow hydrolysis (if occurred) of the acetate intermediate(s) to the final Nazarov product(s). With all screened catalysts, compound **16a** was a competent substrate. However, the expected acetate **17a**^[14] was always obtained in mixture with cyclopentenone **20a**,

Appendix: Publications - Chapter 4 - Gold(I)-Catalyzed Nazarov Reaction

Gold(I)-Catalyzed Synthesis of Annulated N-Heterocycles

EurJOC
European Journal
of Organic Chemistry



Scheme 2. [a] KHMDS, -78°C , 1.5 h; then $(\text{PhO})_2\text{POCl}$, -78°C , 1 h. [b] heptyn-3-ol, 15 mol-% CuI, 6 mol-% $(\text{Ph}_3\text{P})_2\text{PdCl}_2$, $\text{CHCl}_3/\text{Et}_3\text{N}$, 1:2, 55°C , 5–7 h. [c] Ac_2O , Et_3N , DMAP, DCM, 0°C to room temp., 1–7 h.

possessing the more substituted double bond in 4a–7a position and possibly deriving from the hydrolysis in situ of its acetate precursor **19a**. Intriguingly, we never isolated this acetate.^[14] With AgOTf ^[15] (entry 1) complete conversion was observed in less than 1.5 hours, whereas hydrolysis occurred only partially in 16 hours, providing acetate **17a** in 51% yield and cyclopentenone **20a** in 35% yield after chromatography. Trying to increase the relative amount of acetate **17a**, the reaction was carried out in different solvents (THF, 1,4-dioxane, acetonitrile, dichloroethane). The best result was achieved in toluene which provided pure

acetate **17a** in 61% yield and **20a** in 18% yield after chromatography. Decreasing the reaction temperature to 0°C the ratio between **17a** and **20a** was further improved (4:1), but the yield of **17a** was not changed much (60%) as degradation took place during the reaction.

In sharp contrast with the results obtained by using AgOTf and even more with those reported for the corresponding carbocyclic systems **1** (Scheme 1),^[5a,5b] with all of the other silver salts the major product was always cyclopentenone **20a** (entries 4–6) accompanied by lower amounts of acetate **17a** and only traces (less than 5%) of cyclopentenone **18a**. The best silver salt was AgSbF_6 (entry 6) as the reaction provided cyclopentenone **20a** in 70% yield after chromatography together with some residual acetate **17a** (14%). Again contrarily to expectations, the reaction was much slower when using “wet” CH_2Cl_2 .^[5a] In this case, only after 5 h the conversion was complete.^[16] Instead, the concurrent hydrolysis of acetate **19a** was faster to provide **20a** again as the major product but in a lower ratio with residual acetate **17a** (55% and 30% respectively after chromatography) than in commercial CH_2Cl_2 . Similarly, a lower ratio between **20a** and **17a** was obtained when the reaction was carried out with AgSbF_6 in chloroform (entry 10).

To demonstrate that the formation of ketone **20a** occurs via hydrolysis in situ of acetate intermediate **19a**, we set up one experiment in CDCl_3 and monitored the progress of the reaction by ^1H NMR spectroscopy (Figure 2). Aliquots of the reaction mixture were filtered through a Celite layer and diluted after 0.5, 1 and 2.5 h from the addition of the

Table 1. Sequential gold(I)-catalyzed rearrangement/Nazarov reaction of acetate **16a**.^[a]

Entry	Catalyst ^[b]	Conditions ^[c]	Time [h] ^[d,e]	Yield ^[f]			
				17a	18a	19a	20a
1	$\text{Ph}_3\text{PAuCl}/\text{AgOTf}$	CH_2Cl_2	1.5	51	– ^[g]	–	35
2		toluene	1	61	–	–	18
3		toluene, 0°C	5	60	–	–	15
4	$\text{Ph}_3\text{PAuCl}/\text{AgBF}_4$	CH_2Cl_2	3	18	5	–	62
5	$\text{Ph}_3\text{PAuCl}/\text{AgNTf}_2\cdot\text{ACN}$	CH_2Cl_2	6	18	5	–	50
6	$\text{Ph}_3\text{PAuCl}/\text{AgSbF}_6$	CH_2Cl_2	2.5	14	3	–	70
7		wet CH_2Cl_2	5 (0)	30	–	–	55
8		dry CH_2Cl_2	5 ^[i] (0)	18 ^[h]	–	22 ^[h]	19 ^[h]
9	$\text{Ph}_3\text{PAuSbF}_6$ ^[j]	CH_2Cl_2	3	18	–	–	64
10	$\text{Ph}_3\text{PAuCl}/\text{AgSbF}_6$	CHCl_3	2 (0.5)	30	–	–	60
11	$\text{Ph}_3\text{PAuCl}/\text{Cu}(\text{OTf})_2$	CH_2Cl_2	6 ^[k]	–	19	–	29
12		CH_2Cl_2 , reflux	0.7 (3)	–	58 ^[h]	–	42 ^[h]
13	AgOTf	CH_2Cl_2	3	–	–	–	< 5 ^[h]
14	AgSbF_6	CH_2Cl_2	3	–	–	–	< 5 ^[h]
15	$\text{Cu}(\text{OTf})_2$	CH_2Cl_2	16 (0)	–	–	–	–

[a] Reactions were carried out on 0.1–0.15 mmol scale, at 25°C and left standing whilst stirring 16 h after consumption of the starting material. An aqueous work-up was carried out to recover the products from the reaction mixture. [b] Catalysts were prepared by adding the silver salt to a 0.004 M solution of the gold(I) chloride in the reaction solvent. [c] Solvents were not dried before use unless otherwise indicated. [d] Time to reach complete conversion of the starting material. [e] In brackets, time left for hydrolysis. [f] Yield after chromatography unless otherwise indicated. [g] Not detected by ^1H NMR analysis of the crude reaction mixture. [h] By ^1H NMR analysis of the crude reaction mixture. [i] The reaction stopped at a 70% conversion. [j] The reaction was carried out with 6 mol-% of catalyst and after filtration of AgCl . [k] The conversion was not complete and degradation of the starting material occurred.

FULL PAPER

E. G. Occhiato et al.

catalyst. After 30 min, ^1H NMR analysis actually showed three new sets of signals, of which one for cyclopentenone **20a** and two for the two acetates (**17a** and **19a**). As we could anticipate from our previous results, the ratio between intermediates **19a** and **17a** decreased during the reaction concurrently to a relative increase of **20a**. At the end of the reaction, only the signals of **20a** and acetate **17a** were present in the spectrum.

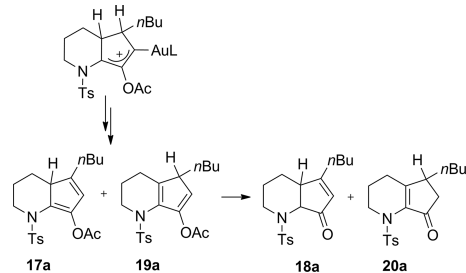


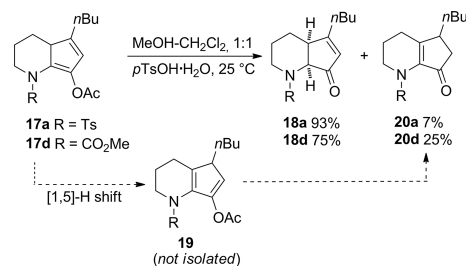
Figure 2. Monitoring by ^1H NMR of the reaction of **16a** in CDCl_3 .

Having in mind to prevent hydrolysis of the acetate intermediates and to isolate **19a** we also carried out one experiment in anhydrous CH_2Cl_2 (entry 8) but the reaction was slower and, after 5 h, only reached an approximately 50% conversion into the acetates (roughly in a 1:1 ratio between **17a** and **19a**) by ^1H NMR analysis of the crude reaction mixture.^[17] Degradation of enynyl acetate **16a** occurred to a great extent under these conditions, though, and we observed the formation also of a small amount of final product **20a** (19% by ^1H NMR of the crude reaction mixture) probably due to the presence of adventitious water.^[18]

Given the role that silver can have in gold-catalyzed reaction,^[19] we carried out an experiment with a catalyst obtained after filtration through a Celite layer (entry 9), in order to exclude AgCl from the reaction medium. Since decomposition of the catalyst during such an operation has been reported^[20] we opted for a larger amount of initial catalyst (6 mol-%). We were glad to see that the reaction occurred as usual, thus demonstrating that the silver halide does not affect neither the reaction rate nor the selectivity.^[21] On the other hand, AgOTf alone (entry 13) as well as AgSbF_6 (entry 14) did catalyze the reaction, albeit to a very low extent (less than 5% conversion after 3 h).^[22]

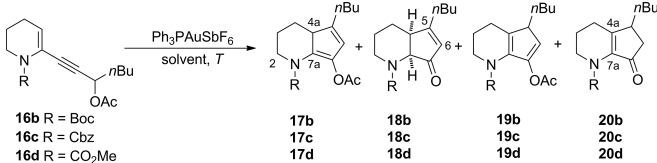
Finally, when the reaction was carried out using $\text{Cu}(\text{OTf})_2$ to generate the active gold(I) catalyst (entry 11),^[23] both isomers **18a** and **20a** were obtained in a 1.5:1 ratio and 48% yield (degradation of the starting material was observed under these conditions). Repeating the reaction in refluxing dichloromethane, consumption of the starting material was complete in 40 min and hydrolysis in 3 h, providing again a mixture of the two isomers in a 1:1.4 ratio. It is interesting to note here that only with $\text{Cu}(\text{OTf})_2$ we observe hydrolysis of acetate **17a**. Unlike AgOTf , copper triflate remains in solution and due to its Lewis acid character it can accelerate the hydrolysis of the acetates. Also, with

triflate as a counterion from both AgOTf and $\text{Cu}(\text{OTf})_2$, there is an appreciable increase of the relative amount of either acetate **17a** or its product of hydrolysis **18a**. A [1,5]-H shift in **19a** to form **17a** triggered by triflic acid (as $\text{H}_3\text{O}^+\text{TfO}^-$) generated in situ can be excluded because by acidic treatment we instead observe some conversion of **17a** into **19a**. In fact, when acetate **17a** was dissolved in dichloromethane/MeOH and treated with a catalytic amount of monohydrate *p*TsOH (Scheme 3), it slowly (16 h) provided the corresponding *cis* fused (see later) cyclopentenone **18a** as the main product and in a 13:1 ratio with **20a**, the formation of which could be accounted for by an acid catalyzed [1,5]-H shift in **17a**.^[24] On the contrary, attempts at basic hydrolysis (K_2CO_3 in MeOH) led to decomposition of the starting material.^[25] Similarly, we observed decomposition of cyclopentenone **18a** when we tried to convert it into its isomer **20a** upon treatment with bases.^[26]



Scheme 3. Hydrolysis of acetates **17a** and **17d**.

The best reaction conditions (3 mol-% $\text{Ph}_3\text{PAuCl}/\text{AgSbF}_6$, in DCM at room temperature) found for enyne **16a** were then extended to the corresponding substrates protected as *N*-Boc (**16b**), *N*-Cbz (**16c**) and *N*- CO_2Me (**16d**), all prepared in good overall yield as described for **16a** starting from the corresponding protected lactams (Scheme 2). Given our previous results on the gold-catalyzed oxyauration of simple *N*-Boc protected enynes,^[8a] we anticipated a possible interaction of the carbamate carbonyl group with the activated triple bond before the acetate rearrangement and so we were not surprised by the much lower reactivity of substrates **16b–d**. The reaction of *N*-Boc derivative **16b** (Table 2, entries 1–3) only provided degradation products plus a minor amount of the oxyauration product (about 20%) when the reaction was carried out in toluene.^[27] The formation of this byproduct, in particular, is consistent with our hypothesis of a carbamate carbonyl group competing for the activated triple bond (see later for DFT calculation on this issue). Better results, but only with 8 mol-% of catalyst, were obtained with *N*-Cbz derivative **16c** (entry 5) which provided cyclopentenone **20c** (61% yield after chromatography) as the sole product. In this case, both consumption of the starting material and hydrolysis were complete after 3 h in refluxing DCM. Also in this case, some degradation of the starting material occurred, albeit in a much lower extent than with *N*-Boc compound **16b**. Similarly, with the *N*- CO_2Me protected compound the

Table 2. Sequential gold(I)-catalyzed rearrangement/Nazarov reaction of acetates **16b-d**.^[a,b]


Entry	Substrate	Conditions ^[c]	Time [h] ^[d]	Yield ^[e]			
				17	18	19	20
1	16b	CH ₂ Cl ₂ , 25 °C	1 ^[f]	– ^[g]	–	–	–
2		toluene, 25 °C to reflux	3 ^[f]	–	–	–	–
3		acetone, 25 °C to reflux	3 ^[f]	–	–	–	–
4 ^[h]	16c	CH ₂ Cl ₂ , 25 °C	20 ^[f]	–	–	–	48
5 ^[h,i]		CH ₂ Cl ₂ , reflux	3	–	–	–	61
6	16d	CH ₂ Cl ₂ , 25 °C	2	–	–	–	–
7		CH ₂ Cl ₂ , reflux	2 ^[k]	14	–	–	64
8		toluene, reflux	1.5 ^[k]	11	–	–	50
9		THF, reflux	1.5 ^[k]	15	–	–	45

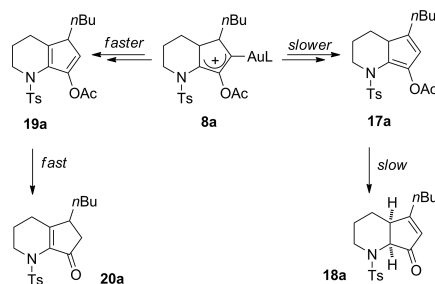
[a] Reactions carried out on 0.15–0.2 mmol, with 5 mol-% of catalyst unless otherwise indicated. [b] Catalysts were prepared by adding the silver salt to a 0.004 M solution of the gold(I) chloride in the reaction solvent. [c] Solvents were not dried before use unless otherwise indicated. [d] Time to reach complete conversion of the starting material. [e] Yield after chromatography unless otherwise indicated. [f] Complete degradation of the starting material occurred. [g] Not detected by ¹H NMR analysis of the crude reaction mixture. [h] Reaction carried out with 8 mol-% of catalyst. [i] Reaction carried out on a 0.075 mmol scale. [j] Degradation occurred to a certain extent. [k] Then left standing for 16 h at room temperature.

reaction did not take place if not by heating in refluxing dichloromethane (entry 7) with 5 mol-% of catalyst. Again, Nazarov compound **20d** with the double bond at 4a-7a position was the major product after chromatography (64%) and in this case we isolated also a smaller amount of acetate **17d** (14%).^[28] Similarly to acetate **17a**, when we subjected acetate **17d** to hydrolysis in DCM/MeOH (1:1) and in the presence of catalytic amount of monohydrate *p*TsOH (Scheme 3), its quantitative conversion into the corresponding Nazarov product **18d** was slow (16 h) and this was obtained in a 4:1 mixture with its isomer **20d**.

Mechanistic Considerations and DFT Calculations

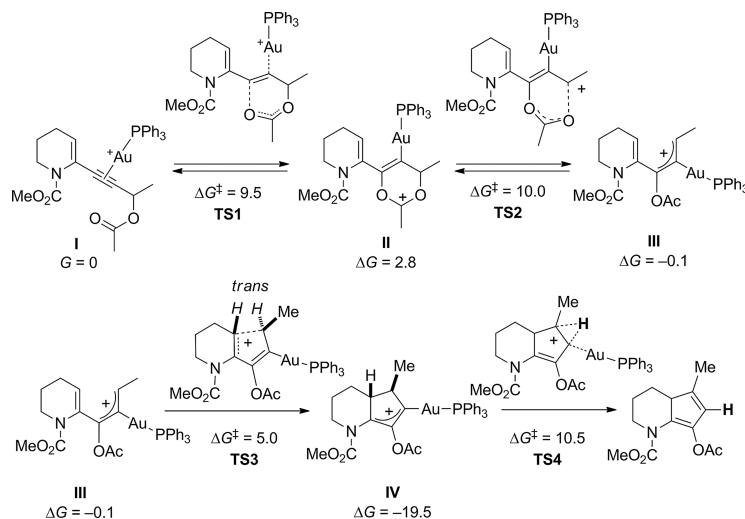
The fact that we could in most cases isolate acetates **17a** and **17d** and never their isomers (**19a** and **19d**) from the crude reaction mixtures of the gold-catalyzed reactions, together with the observation that acetates **17** are very slowly converted into the corresponding cyclopentenones when subjected to hydrolytic conditions (Scheme 3), suggests that acetates **17**, after their formation in the protodeauration step involving oxyallyl cation **8** (Scheme 4), only slowly hydrolyze under the conditions of the gold-catalyzed reaction. Instead, isomers **19** are quickly converted into the corresponding cyclopentenones **20** and so we never isolated them (see the NMR study above, Figure 2). Since cyclopentenone **20** is the major or only product in the reactions carried out in DCM when using AgSbF₆ as the anion source we can hypothesize that, under these conditions, formation of acetate **19** from oxyallyl cation **8** is faster than formation of its isomer **17** and that then a fast hydrolysis of **19** under the reaction conditions occurs. It is interesting to compare here

this result with those reported by Zhang et al. on the corresponding carbacyclic systems **1** (Scheme 1), in which the formation of a unique cyclopentenone (**6**) with the less substituted double bond was observed.^[5a]

Scheme 4. The two competing pathways to **18a** and **20a**.

In order to understand this process in more detail, and help identifying the structures and energies of the critical steps of the mechanism, we studied the potential reaction coordinates computationally. The structures were located using the B3LYP^[29] density functional theory method as implemented in the Gaussian suite of programs.^[30]

For the sake of simplicity, two model complexes were considered for the computational studies, that is **1** (Scheme 5), which contains the smallest substituent (methyl) in the propargylic position and a *N*-CO₂Me moiety; and the corresponding one with the *N*-tosyl group. In the former case, the methyl carbamate is conformationally simpler than the tosylate group, and would allow us to

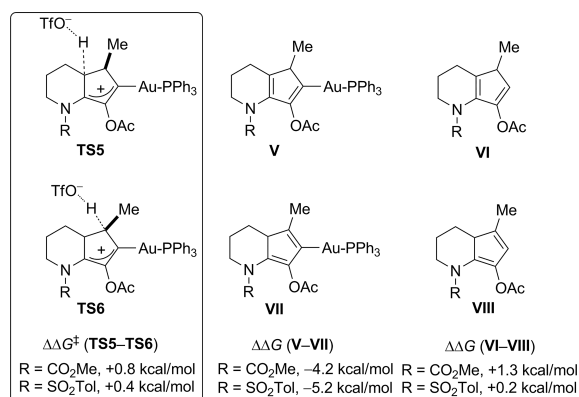
Scheme 5. Top: acetate rearrangement in the initial steps of the mechanism. Bottom: cyclization step from **III** and protodeauration step.

mimic also compound **16d** and related carbamates **16b–c**. The alkynyl-gold(I) cationic complex **I** (Scheme 5) was thus considered as the starting point of the mechanism ($G = 0$ kcal/mol), and all reported energies in the following discussion are relative to it. The energy values correspond to ΔG Gibbs Free energies, computed at B3LYP/6-31G** level (LANL2DZ^[31] for gold atom). The overall discussion is based on model **I**. The results with the corresponding *N*-tosyl derivative are very similar and reinforce the conclusions.

Initially, the coordination of the gold atom to the triple bond induces a rapid two step acetate rearrangement to form the pre-Nazarov cyclization complex **III** (Scheme 5). The attack of the acetate carbonyl oxygen of **I** to the gold-activated alkyne leads to the formation of a cyclic intermediate **II**, and the subsequent C–O bond breaking event renders an allylic cation (**III**), stabilized by the presence of the gold atom.^[32] Noteworthy, the computed energies indicate that **I** and **III** are isoenergetic (0.1 kcal/mol difference), and that the activation energies of both steps are fairly low, ca. 10 kcal/mol, meaning that in the absence of further evolution, **I** and **III** would be in an almost 1:1 equilibrium. However, complex **III** evolves through an easy cyclization to **IV**, a process that presents a very low barrier of 5.1 kcal/mol (**TS3**, Scheme 5). In accordance to the conrotatory nature of the Nazarov reaction under thermal conditions, the reaction is predicted to be diastereoselective, with formation of the C–C bond that presents the two H atoms in a *trans* relationship. The alternative diastereoisomeric transition state, in which the two H are *cis* to each other is 3.9 kcal/mol higher in energy, and thus, not operative. The low activation barriers can explain the fast rate of a reaction that is completed at room temperature in less than two hours.

Although not shown in the Scheme the results with the *N*-tosyl derivative are comparable, showing activation energies of 11.4 and 10.9 kcal/mol for the two step acetate rearrangement processes, a reaction energy of +0.7 kcal/mol in the formation of **III**, and a low activation barrier for the Nazarov cyclization (4.0 kcal/mol).

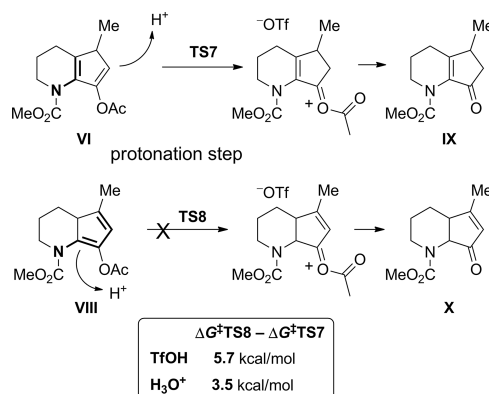
At this point, we attempted to explain the diene formation through a single-step intramolecular hydride shift with concomitant C–Au bond breaking. In fact, the corresponding transition structure **TS4** was located (Scheme 5), but its accompanying activation energy (30 kcal/mol from **IV** to **TS4**) is too high to be feasible under the experimental reaction conditions.^[33] Therefore, an external base is needed for the deprotonation, and it is important to highlight that several possible candidates exist in the reaction media, like the gold counterion in the gold(I) salt or the anion forming the silver or copper salt. Even some water molecules present in the reaction media could play a significant role and, in fact, the intervention of water molecules in the deprotonation/protodeauration steps has been suggested for the tandem process involving enynyl acetates **1** (Scheme 1) in “wet” CH_2Cl_2 .^[5b,34] We were particularly interested in the proton abstraction step since, based on our experimental findings, the regioselectivity of the reaction, which was not an issue with enynyl acetates **1**, seems to be determined with our substrates just at this stage. We have in fact shown (vide supra) that once the final diene-acetates **VI** and **VIII** (models for acetates **19** and **17**, respectively, Figure 3) are formed, there are not evident signs of significant equilibration between them during the reaction. So, as a plausible approximation, and without knowing the exact nature of the molecule responsible for the abstraction, to demonstrate that this is actually the regiodetermining stage, we decided to


 Figure 3. Transition states **TS5** and **TS6** in the presence of triflate anion and compounds formed thereafter.

compute the deprotonation step by using the triflate anion as the base (Figure 3 and Figure S2 in Supporting Information).^[3,5]

Our computational results indicate that the triflate mediated hydrogen abstraction is, in fact, not highly regioselective, the difference between **TS5** and **TS6** being of only 0.8 kcal/mol in favor of the formation of **VII** isomer (en route to **17**). In the case of the *N*-tosyl group, the difference is 0.4 kcal/mol (favoring **TS6**). The experimental data (Table 1) show a regioselectivity that ranges from 4:1 (**17a** over **20a**, entry 3), when using AgOTf as the source of the non-coordinating anion, to 1:5 (**20a** over **17a**, entry 6), when instead using AgSbF₆, which computationally accounts for a difference of less than 1 kcal/mol in each sense. As we will show later, with different types of substrates the regioselectivity we observed when using AgSbF₆ was instead complete in favour of ketones derived from hydrolysis of acetate **VI** (i.e. **19**).

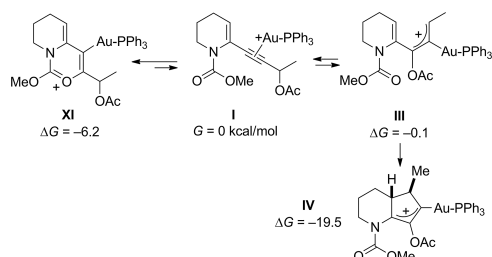
After the formation of **VI**- and **VIII**-type dienes (Figure 3), the most logical process would follow via hydrolysis to the final products (Scheme 6). There is a final interesting question at this point, regarding the very different experimental hydrolysis rates of the two diene types, **17** and **19**. Once again, as the exact nature of the protonating species is unknown, we chose triflic acid and H₃O⁺ as simple models to study computationally this issue, and the transition states for the hydrogen transfer were located. Noteworthy, the protonation of **VI** (model of diene **19**) is predicted to be three or four orders of magnitude faster than the corresponding protonation of **VIII** (model of **17**), as derived from a 3.5 kcal/mol (H₃O⁺) or 5.7 kcal/mol (TfOH) energy difference in favor of the former. These data easily explain why non-hydrolyzed **17** and hydrolyzed **20** are the final products of the reaction. The result can be understood in light of the dienamine structure of compound **17** (**VIII**), and the donor character of the nitrogen atom, which can induce a stabilization of that structure making it less prone to hydrolysis.


 Scheme 6. Hydrolysis of diene-acetates **VI** and **VIII** in the presence of a model acid (TfOH or H₃O⁺).

Concerning the lower reaction rates of *N*-alkoxycarbonyl protected substrates **16b–d**, as we have hypothesized, DFT calculations predict the formation of a non-productive cyclized intermediate (from carbonyl oxygen attack), which is more stable than the starting material, thus sequestering the gold catalyst for a while and reducing the reaction rate (Scheme 7). The starting compound **I** can proceed through acetate rearrangement to form **III** or through cyclization with the methyl ester to form **XI**. The three complexes **XI**, **I**, and **III** are in equilibrium, which is shifted towards the non-productive, but low in energy (–6.1 kcal/mol) side complex **XI**. Only the irreversible Nazarov cyclization from **III** to **IV** is finally able to displace this equilibrium towards the formation of the bicyclic adducts. Thus, **XI** is partially sequestering the gold catalyst and decreasing the reaction rate.

FULL PAPER

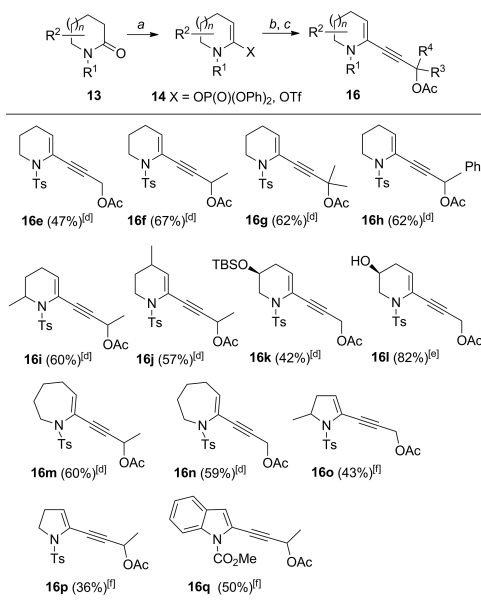
E. G. Occhiato et al.



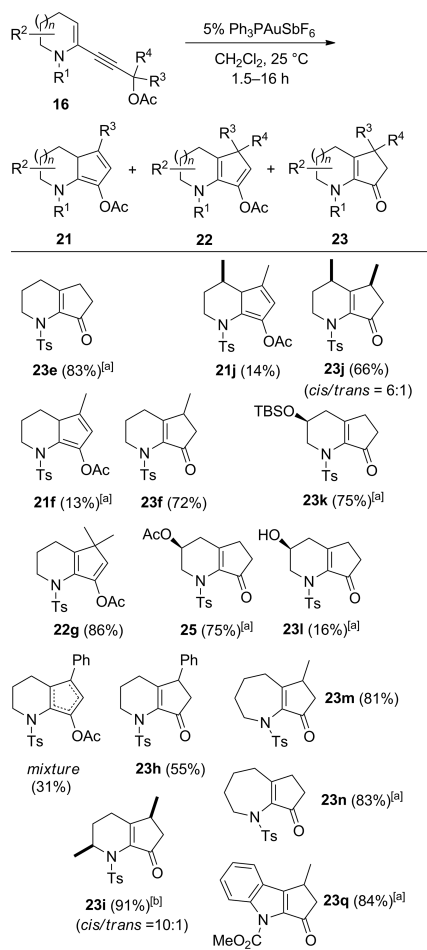
Scheme 7. DFT predicted formation of the non-productive XI intermediate.

The Torquoselectivity

To evaluate the torquoselectivity^[36] in the ring closure we synthesized model compounds **16i** and **16j** (Scheme 8) from the corresponding lactams^[37] which should provide Nazarov compounds with defined stereochemistry we had already prepared in the past.^[7a] The reaction of enyne **16i** was first carried out in DCM at room temperature in the presence of 5 mol-% of $\text{Ph}_3\text{PAuSbF}_6$ as the catalyst and provided, quite interestingly, only cyclopentenone **23i** in 78% yield after chromatography (Scheme 9) with no traces of the acetate **21i**.



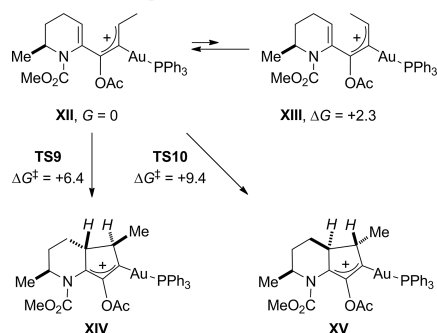
Scheme 8. Reagents and conditions: [a] KHMDs , -78°C , 1.5 h; then $(\text{PhO})_2\text{POCl}$ or PhNTf_2 , -78°C , 1 h. [b] alkyne, 15 mol-% CuI , 6 mol-% $(\text{Ph}_3\text{P})_2\text{PdCl}_2$, $\text{CHCl}_3/\text{Et}_3\text{N}$, 1:2, 55°C , 5–7 h. [c] Ac_2O , Et_3N , DMAP , DCM , 0°C to room temp., 1–7 h. [d] Yield over two steps. [e] Prepared from **16k**. [f] Yield over three steps.



Scheme 9. [a] Reaction carried out under reflux. [b] 83% yield, pure *cis* after chromatography. Reaction carried out with $(c\text{-Hex})_3\text{PAuSbF}_6$.

^1H NMR analysis of **23i** revealed that a 6:1 mixture of diastereomers was present, with the *cis* compound being predominant. As the pre-Nazarov complex is a vinylgold species, a few ligands with different properties were screened to evaluate their possible role in the ring closure selectivity. Best results were obtained with the electron-rich ligand $(c\text{-hex})_3\text{P}$ (10:1 *cis/trans* ratio, separable mixture, 91% yield) whereas with electron-poor $[(p\text{CF}_3\text{C}_6\text{H}_4)_3\text{P}]$ and NHC-carbene ligands [1,3-bis(2,6-diisopropylphenyl)imidazol-2-ylidene], not only the selectivity did not ameliorate but the reaction provided a mixture of cyclopentenones, acetates and degradation products. Moreover, the reaction with 5 mol-% $(c\text{-hex})_3\text{PAuSbF}_6$ was much cleaner than with

Ph_3P .^[38] These results are consistent with our previous observations on the torquoselectivity in the Nazarov reaction,^[7a,7b,7d,7g] although the *cis* selectivity was in those cases complete.^[7a] For stereoelectronic reasons, the ring closure occurs in a way to form the new bond on the opposite side of the axially oriented 6-Me group.^[7d,7g] The bases for the lower torquoselectivity in the gold-catalyzed process are not easy to understand, and could be either kinetic (i.e. both clockwise and counterclockwise ring closures could take place at different rate in the putative intermediate **XII**, Scheme 10) or related to the geometry of the oxallyl cation before ring closure. In the latter case a counterclockwise ring closure of the isomer **XIII** would lead to the *trans* compound. However, DFT calculations revealed that the preference for **XII** is clear, with a difference over **XIII** of 2.3 kcal/mol because of steric reasons.^[38] Thus the major *cis* dimethyl diastereoisomer (**XIV**) is formed by a counterclockwise conrotatory ring closure of **XII**, with a low activation energy of 6.4 kcal/mol (**TS9**), whereas its *trans* diastereomer **XV** is formed by conrotatory clockwise ring closure from **XII** (**TS10**, 9.4 kcal/mol). Because of the predominance of intermediate **XII** it is likely that the alternative pathway from **XIII** is never operative.^[39]



Scheme 10. DFT study on the torquoselectivity of the ring closure.

The torquoselectivity with 4-methyl substituted enyne **16j** was in line (6:1) with that observed for **16i**, as this substrate provided a separable 6:1 mixture of *cis* (major) and *trans* (minor) compounds **23j** (66% after chromatography) when using $\text{Ph}_3\text{PAuSbF}_6$ as the catalyst, together with some acetate **21j** (14% after chromatography). In this case, the use of other ligands did not improve the torquoselectivity and, moreover, caused the formation of a complex mixture of all acetates and cyclopentenone isomers.

Assessing the Scope of the Reaction

To assess the scope of the reaction, a series of enynyl acetates (Scheme 8) was prepared by varying the substituents on the alkyne moiety and on the piperidine ring as well as the heterocycle. All acetates **16** were prepared in good yield over two or three steps from lactam-derived enol phosphates **14**, with the exception of pyrrolidin-2-one deriv-

atives **16o** and **16p**, and enyne **16q**, which were obtained from the corresponding lactam-derived enol triflates.^[7a,7b,40,41] The results are shown in Scheme 9.

The number of alkyl groups at 3' position seems to affect the reaction outcome and reactivity. Unsubstituted acetate **16e** reacted slower at room temperature and it required higher temperature (refluxing DCM) to be completely converted into **23e** (83%) only. This could be due to a slower rearrangement of the propargyl acetate moiety as a positive charge develops on a primary C atom (C3') in the transition state. Interestingly, no traces of acetate **21e** (or the corresponding ketone) were found in the crude reaction mixture, meaning that proton abstraction is much more favored if occurs at the more substituted position to generate the most substituted double bond. The calculated energy difference between the two competing transition state is 1.2 kcal/mol (as usually using triflate as the base) which corresponds to a 7:1 selectivity (Figure 4).

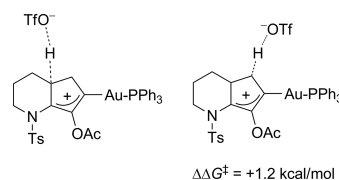


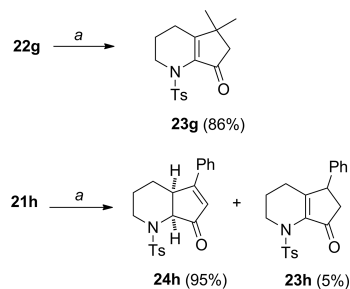
Figure 4. DFT study on the competing proton abstraction pathway in the reaction of **16e**.

The results obtained with 3'-methyl-substituted **16f** were in line with those for our model compound **16a** whereas, curiously, dimethyl-substituted acetate **22g** (86%) only, which did not hydrolyze spontaneously. This was later done by treatment with *p*TsOH (Scheme 11) which furnished Nazarov compound **23g** in 86% yield. With the 3'-phenyl-substituted enyne **16h** the reaction provided expected cyclopentenone **23h** in 55% after chromatography. Acetate **21h**, formed during the reaction in mixture with **23h** in ca. 1:1 ratio, during the purification underwent [1,5]-H shift giving a complex mixture of few acetate isomeric products. A small amount of pure **21h** was treated with *p*TsOH (Scheme 11), and it was converted into a mixture of **24h** (95%) and **23h**. With compound **24h** it was possible to demonstrate by ¹H NMR studies the *cis* fusion of the rings (in analogy to the corresponding carbocyclic systems)^[55a] and the structure of most populated conformer. 7a-H is a doublet with a low coupling constant (6.8 Hz) with 4a-H indicating its equatorial orientation, further confirmed by the lack of any NOE of 7a-H with 2-H_{ax} and 4-H_{ax}. Consequently, 4a-H is axially oriented. Similarly, in compound **18a** (Scheme 3) 7a-H is a doublet with a low coupling constant (6.9 Hz) with 4a-H confirming the *cis* fusion also for this compound. Hydroxy-substituted piperidine derivatives, both protected (**16k**) and unprotected (**16l**) on the OH group, were compatible with the reaction conditions. However, while **16k** provided cyclopentenone **23k** as the sole products in 75% yield after chromatography, substrate **16l** furnished the acetylated derivatives **25** as the

FULL PAPER

E. G. Occhiato et al.

major compound (75%), accompanied by a minor amount of the corresponding alcohol **23i** (16%). Clearly, the free OH group acts a nucleophile by trapping the acyl cation which is released in the final step of the process (Scheme 6).



a: *p*TsOH (cat.), DCM-MeOH, 1:1, r.t., 16 h.

Scheme 11. [a] *p*TsOH (cat.), DCM-MeOH, 1:1, room temp., 16 h.

Also seven-membered rings as in **16m** and **16n** were compatible as these substrates provided, after complete hydrolysis of the corresponding acetate intermediates, Nazarov compounds **23m** (81%) and **23n** (83%) only and in excellent yield after chromatography. As in the case of **16e**, the reaction of **16n** required refluxing conditions, too. In both cases, disappearance of the starting material was faster than with the corresponding six-membered heterocycles and no traces of acetate isomers were detected by ¹H NMR analysis of the crude reaction mixture. Not unexpectedly,^[7a] the ring closure of five-membered derivatives **16o** and **16p** did not occur both at room temperature and in refluxing CH₂Cl₂, but we only recovered residual starting material with a certain amount of unidentified degradation compounds. The reaction of **16p** was also carried out in refluxing toluene, but to no avail. We have already reported the greater difficulty in the ring closure to give a 5–5 fused system, presumably due to ring strain in the intermediate azabicyclo[3.3.0]octenyl cation.^[7a] On the other hands, we were very glad to observe that propargyl acetate **16q** containing a *N*-CO₂Me-protected indole nucleus reacted smoothly in refluxing CH₂Cl₂, to provide the corresponding cyclopenta-fused aromatic system **23q** in 84% yield after 1.5 h, thus paving a new way for the synthesis of natural compounds containing the cyclopenta[*b*]indole nucleus.

Conclusions

In this paper we have demonstrated that the tandem gold(I)-catalyzed rearrangement/Nazarov reaction of propargylic ester derivatives is a useful strategy for the synthesis, in just four steps, of cyclopenta-fused N-heterocyclic structures present in many natural compounds. First, readily available lactams are converted into the corresponding enol phosphates and triflates and coupled to propargyl alcohols

under Sonogashira conditions. After acetylation, the gold-catalyzed rearrangement of the enynyl acetates readily (and best) occurs when using hexafluoroantimonate as the non-coordinating anion. This generates a divinyl cation which undergoes a 4 π electrocyclic cyclization forming the target annulated N-heterocyclic compound in good to excellent yield. This process has been studied in details both experimentally and computationally, and the influence of the reaction conditions and the structure of the substrates on the reaction rate, regio- and stereoselectivity have been evaluated. The main features can be summarized as follows: (a) compared to the tandem process of carbacyclic enynyl acetates, the presence of the N atom clearly favors the nearly exclusive formation of the Nazarov product having the most substituted double bond, i.e. at the 4a-7a position. This is true with most catalysts we used, although its isomer (i.e. with the double bond at the 5–6 position) was the major product when triflate was the gold(I) counterion. (b) In contrast to similar cases in literature, suitably prepared “wet” dichloromethane seems to be not necessary to have a complete hydrolysis of the acetate intermediates. However the presence of some water in the solvent seems in any case essential for the process to occur properly, as in dry CH₂Cl₂ the conversion into the Nazarov product mixture was much lower. Under the best conditions (with Ph₃PAuSbF₆) the hydrolysis of only one of the two regioisomeric acetates occurs, leading to the 4a-7a unsaturated compound. (c) All N-protecting groups are compatible with the propargyl acetate rearrangement, with exception of the *N*-Boc group, and with the *N*-Ts being the best. The other *N*-alkoxycarbonyl groups somehow interfere, though, and heating is necessary to achieve complete conversion. (d) With piperidine rings substituted at 4 or 6 position, moderate to high torquoselectivity in the ring closure in favor of the *cis* diastereomers is observed when the propargyl moiety bears a substituent at C3'. This is in accordance to the results previously reported by us for the classical Nazarov reaction, meaning that the gold atom on the divinyl cation has a little effect on the stereoelectronically preferred conrotation mode. (e) The scope of the reaction ranges from six to seven-membered N-heterocyclic rings and various substituents at C3' on the propargyl moiety, but is not extended to pyrroline derivatives which proved unsuitable for this approach. Instead, an indole containing enynyl acetate reacted smoothly to provide the cyclopenta[*b*]indole nucleus. Because of the combination of easily accessible propargyl alcohols and readily available lactams in the assemblage of the substrates required for the tandem process, this methodology is surely suited for the preparation of natural and biologically active compounds possessing a cyclopenta-annulated N-heterocyclic nucleus.

Experimental Section

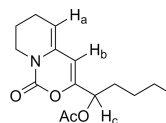
General: Anhydrous solvents were prepared according to the standard techniques. Commercially available reagents were used without further purification. Chromatographic separations were per-

Appendix: Publications - Chapter 4 - Gold(I)-Catalyzed Nazarov Reaction

Gold(I)-Catalyzed Synthesis of Annulated N-Heterocycles

EurJOC
European Journal
of Organic Chemistry

3706. A plethora of natural, cyclopentannulated indole alkaloids exist; for example Brucecolline J, isolated from *Brucea mollis*, see: o) H. Chen, J. Bai, Z.-F. Fang, S.-S. Yu, S.-G. Ma, S. Xu, Y. Li, J. Qu, J.-H. Ren, L. Li, Y.-K. Si, X.-G. Chen, *J. Nat. Prod.* **2011**, *74*, 2438–2445.
- [10] Cephalotaxine synthesis: a) S. H. Kim, J. K. Cha, *Synthesis* **2000**, 2113–2116. For formal and total syntheses of roseophilin by the Nazarov reaction, see: b) D. J. Kerr, L. B. Flynn, *Org. Lett.* **2012**, *14*, 1740–1743; c) C. Song, H. Liu, M. Hong, Y. Liu, F. Jia, L. Sun, Z. Pan, J. Chang, *J. Org. Chem.* **2012**, *77*, 704–706; d) M. Hong, H. Liu, L. Sun, F. Jia, Y. Liu, Q. Jiang, C. Song, *Synlett* **2011**, 2995–2996; e) A. Y. Bitar, A. J. Frontier, *Org. Lett.* **2009**, *11*, 49–52; f) E. G. Occhiato, C. Prandi, A. Ferrali, A. Guarna, *J. Org. Chem.* **2005**, *70*, 4542–4545; g) P. E. Harrington, M. A. Tius, *J. Am. Chem. Soc.* **2001**, *123*, 8509–8514.
- [11] We used the procedure reported by us in ref.^[8a] for simple alkynes.
- [12] As with simpler enynes,^[8a] compounds **16** decompose when neat, but they can be stored for months in solution of the chromatographic eluant containing 1% Et₃N. Because of their instability when neat, we cannot provide elemental analysis for these compounds.
- [13] This was the best solvent for the corresponding carbocyclic substrates, see ref.^[5a]
- [14] Monitoring the reaction by TLC we observed the formation of only one spot which corresponded to both acetates. Acetate **17a** and **19a** are easily distinguished by ¹H NMR as in **17a** the bridgehead proton 4a-H can be identified at 2.21–2.30 ppm and the olefinic 6-H proton resonates at $\delta = 6.03$ ppm as a singlet. In **19a** this proton is more shielded and resonates at $\delta = 5.88$ ppm as a doublet (with a very low coupling constant) because of the coupling with 5-H (which is a multiplet at 2.98–3.92 ppm).
- [15] The Ph₃PAuOTf catalyst was the best in the oxyuration of the triple bond in *N*-Boc-protected 6-alkynyl-3,4-dihydro-2H-pyridines, see ref.^[8a]
- [16] Degradation of the active gold(I) catalyst has been reported to increase with the relative amount of water in organic solvents. M. Kumar, J. Jasinski, G. B. Hammond, B. Xu, *Chem. Eur. J.* **2014**, *20*, 3113–3119.
- [17] No aqueous work up, only filtration through Celite.
- [18] Adventitious water was also responsible for the hydrolysis of acetate **4** in carbocyclic systems (Scheme 1), see ref.^[5a]
- [19] D. Wang, R. Cai, S. Sharma, J. Jirak, S. K. Thummanapelli, N. G. Akhmedov, H. Zhang, X. Liu, J. L. Petersen, X. Shi, *J. Am. Chem. Soc.* **2012**, *134*, 9012–9019.
- [20] M. Kumar, G. B. Hammond, B. Xu, *Org. Lett.* **2014**, *16*, 3452–3455.
- [21] An opposite result has been recently reported for the [3,3]-rearrangement of propargyl ester derivatives, see: L.-J. Wang, H.-T. Zhu, A.-Q. Wang, Y.-F. Qiu, X.-Y. Liu, Y.-M. Liang, *J. Org. Chem.* **2014**, *79*, 204–212.
- [22] For the silver-catalyzed [3,3]-rearrangement of propargyl esters see: *Silver in Organic Chemistry* (Ed.: M. Harmata), John Wiley & Sons, **2010**, p. 402.
- [23] A. Guérinot, W. Fang, M. Sircoglou, C. Bour, S. Bezzenine-Lafollée, V. Gandon, *Angew. Chem. Int. Ed.* **2013**, *52*, 5848–5852; *Angew. Chem.* **2013**, *125*, 5960.
- [24] In the hydrolysis of **17a** with 1% TfOH the shift was more pronounced as we obtained a mixture of **18a** and **20a** in 2:1 ratio.
- [25] This degradation could be due to the acidity of the bridgehead proton in acetates **17**. Deprotonation at that position leads to an aromatic cyclopentadienyl anion and from this, probably, to various unidentified byproducts during work-up.
- [26] Two experiments were performed in MeOH with 0.8 equiv. of MeONa and with 2 equiv. of DBU in THF. Isomerization has been instead successfully performed with the corresponding carbocyclic systems (see ref.^[5a]) and it has been reported for five-membered N-heterocycles. See: M. M. Domostoj, E. Irwing, F. Scheimann, K. J. Hale, *Org. Lett.* **2004**, *6*, 2615–2618.
- [27] The cyclic urethane intermediate was not isolated. Diagnostic signals are the triplet at $\delta = 4.71$ ppm and the singlet at $\delta = 5.56$ ppm assigned to protons H_a and H_b, respectively. Proton H_c resonates at $\delta = 5.15$ ppm as a triplet:



- [28] In this particular case, monitoring the reaction by TLC revealed the formation of two spots corresponding to the two acetate isomers and only one of this disappeared to form a more polar spot corresponding to Nazarov product **20**.
- [29] a) C. Lee, W. Yang, R. G. Parr, *Phys. Rev. B* **1988**, *37*, 785–789; b) A. D. Becke, *J. Chem. Phys.* **1993**, *98*, 5648–5652; c) W. Kohn, A. D. Becke, R. G. Parr, *J. Phys. Chem.* **1996**, *100*, 12974–12980.
- [30] M. J. Frisch, G. W. Trucks, H. B. Schlegel, G. E. Scuseria, M. A. Robb, J. R. Cheeseman, G. Scalmani, V. Barone, B. Mennucci, G. A. Petersson, H. Nakatsuji, M. Caricato, X. Li, H. P. Hratchian, A. F. Izmaylov, J. Bloino, G. Zheng, J. L. Sonnenberg, M. Hada, M. Ehara, K. Toyota, R. Fukuda, J. Hasegawa, M. Ishida, T. Nakajima, Y. Honda, O. Kitao, H. Nakai, T. Vreven, J. A. Montgomery Jr., J. E. Peralta, F. Ogliaro, M. Bearpark, J. J. Heyd, E. Brothers, K. N. Kudin, V. N. Staroverov, T. Keith, R. Kobayashi, J. Normand, K. Raghavachari, A. Rendell, J. C. Burant, S. S. Iyengar, J. Tomasi, M. Cossi, N. Rega, J. M. Millam, M. Klene, J. E. Knox, J. B. Cross, V. Bakken, C. Adamo, J. Jaramillo, R. Gomperts, R. E. Stratmann, O. Yazyev, A. J. Austin, R. Cammi, C. Pomelli, J. W. Ochterski, R. L. Martin, K. Morokuma, V. G. Zakrzewski, G. A. Voth, P. Salvador, J. J. Dannenberg, S. Dapprich, A. D. Daniels, O. Farkas, J. B. Foresman, J. V. Ortiz, J. Cioslowski, D. J. Fox, *Gaussian 09*, revision D.01, Gaussian, Inc., Wallingford CT, **2013**.
- [31] a) P. J. Hay, W. R. Wadt, *J. Chem. Phys.* **1985**, *82*, 270–283; b) W. R. Wadt, P. J. Hay, *J. Chem. Phys.* **1985**, *82*, 284–298; c) P. J. Hay, W. R. Wadt, *J. Chem. Phys.* **1985**, *82*, 299–310.
- [32] This species could also be considered as a gold-carbene, although it should be more adequately described as a gold-stabilized carbocation, see: a) A. Fürstner, L. Morency, *Angew. Chem. Int. Ed.* **2008**, *47*, 5030–5033; *Angew. Chem.* **2008**, *120*, 5108. See also ref.^[3a] and references cited therein.
- [33] Interestingly, this [1,2]-H shift process has been postulated to be the rate-limiting step in the tandem [3,3]-rearrangement/Nazarov reaction of simpler enynyl acetates in the gas phase.^[5b]
- [34] Interestingly, when the reaction of **16a** was carried out in anhydrous DCM, we observed a significant decrease in the conversion rate of the substrate into any of the acetate intermediates accompanied by the formation of degradation products.
- [35] The results for the water assisted process are shown in the Supporting Information, and the conclusions are in total agreement with the ones withdrawn from Figure 3. With water as a base, the process leading to **VII** is favoured by 0.6 kcal/mol.
- [36] For the most recent studies on the torquoselectivity in Nazarov reactions, see: a) T. D. R. Morgan, L. M. LeBlanc, G. H. Ardagh, R. J. Boyd, D. J. Burnell, *J. Org. Chem.* **2015**, *80*, 1042–1051; b) B. L. Flynn, N. Manchala, E. H. Krenske, *J. Am. Chem. Soc.* **2013**, *135*, 9156–9163, and references cited therein, see also ref.^[2b]
- [37] See Supporting Information for the preparation of all lactams.
- [38] We noticed that the solution maintains its initial orange colour (whereas it turns blackish when Ph₃P is used as the ligand), which is probably accounted for by a greater stability of the

FULL PAPER

E. G. Occhiato et al.

- cationic gold complex. The same ligand was tested with model compound **16a** but the regioisomeric ratio did not change compared to Ph₃P ligand.
- [39] Clearly our calculations overestimate the kinetic preference for **XIV** (by 3 kcal/mol), which is not experimentally so high.
- [40] T. Luker, H. Hiemstra, W. N. Speckamp, *J. Org. Chem.* **1997**, *62*, 8131–8140.
- [41] X.-H. Xu, X. Wang, G.-K. Liu, E. Tokunaga, N. Shibata, *Org. Lett.* **2012**, *14*, 2544–2547.

Received: April 10, 2015
Published Online: May 15, 2015

Gold-Catalysed Synthesis of Exocyclic Vinylogous Amides and β -Amino Ketones: A Detailed Study on the 5-*exo*/6-*endo-dig* Selectivity, Methodology and Scope

Dina Scarpi,^{*[a]} Stefano Begliomini,^[a] Cristina Prandi,^[b] Alberto Oppedisano,^[b] Annamaria Deagostino,^[b] Enrique Gómez-Bengoa,^[c] Béla Fiser,^[c] and Ernesto G. Occhiato^{*[a]}

Dedicated to Professor Antonio Guarna on the occasion of his retirement

Keywords: Homogeneous catalysis / Gold / Enynes / Nitrogen heterocycles / Amides / Regioselectivity

The gold(I)-catalysed reaction of *N*-Boc-protected 6-alkynyl-3,4-dihydro-2*H*-pyridines, which gives synthetically useful vinylogous amides (β -enaminones), has been studied in detail, in order to optimize the reaction conditions, enlarge the scope and gain insight into the mechanism and the structural features that selectively favour the 6-*endo-dig* oxyauration of the triple bond. Experimental studies and DFT calculations demonstrate that the 6-*endo-dig* approach is exclusive with

substituted alkynes, whereas with terminal alkynes the 5-*exo-dig* cyclization prevails, despite the large angle (120°) at C-6. The same selectivity was observed with *N*-Cbz-protected 2-alkynylpiperidines. With these compounds, β -amino ketones are obtained as a consequence of the 6-*endo-dig* attack onto a substituted triple bond. Sedamine alkaloids are easily obtained by this approach.

Introduction

Vinylogous amides (β -enaminones) constitute an important class of valuable intermediates in the synthesis of heterocyclic and natural compounds.^[1] They also have important therapeutic potential against the multidrug resistance (MDR) of cancer cells,^[2] and against epilepsy.^[3] For these reasons, much effort has been put into the search for new methods for their efficient synthesis.^[3,4] Exocyclic vinylogous amides built on a piperidine ring are versatile intermediates for the preparation of many *N*-heterocycles^[5] and natural alkaloids (Figure 1), such as desoxoprosophylline,^[6] cassine,^[7] pinidinone,^[8] deoxyfebrifugine,^[9] norallosedamine,^[10] and others.^[11] The synthesis of other related alkaloids such as sedamine,^[12] 5-hydroxy-sedamine,^[13] halosaline,^[14] and pelletierine^[15] could also be easily envisaged by exploiting the reactivity of such vinylogous amides.

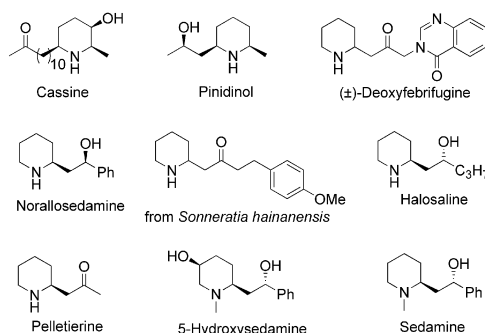


Figure 1. Naturally occurring alkaloids prepared from vinylogous amides, and some related compounds.

[a] Dipartimento di Chimica "U. Schiff", Università degli Studi di Firenze, Via della Lastruccia 13, 50019 Sesto Fiorentino (FI), Italy
E-mail: dina.scarpi@unifi.it
ernesto.occhiato@unifi.it
www.egocch.it

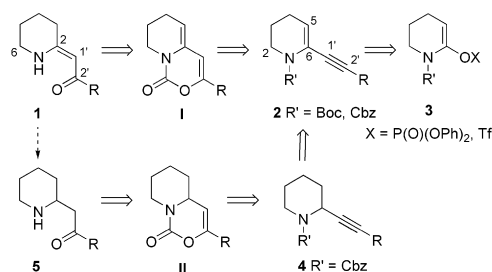
[b] Dipartimento di Chimica, Università degli Studi di Torino, Via P. Giuria 7, 10125 Torino, Italy

[c] Departamento de Química Orgánica I, Universidad del País Vasco/UPV-EHU, Manuel de Lardizabal 3, 20018 Donostia-San Sebastián, Spain
Supporting information for this article is available on the WWW under <http://dx.doi.org/10.1002/ejoc.201500205>.

We recently reported a new approach to the synthesis of exocyclic vinylogous amides **1** in which the key step was a gold(I)-catalysed rearrangement of *N*-Boc (*tert*-butoxycarbonyl) enynes **2** (Scheme 1).^[11] *N*-Boc enynes **2** were obtained by the Sonogashira coupling of lactam-derived enol phosphates and triflates **3** with a variety of terminal alkynes.^[11]

FULL PAPER

D. Scarpi, E. G. Occhiato et al.



Scheme 1. Retrosynthetic analysis.

The gold(I)-catalysed step, which was carried out in the presence of Ph_3PAuOTf (2–3 mol-%) in refluxing toluene, included a 6-*endo-dig* attack onto the activated triple bond by the Boc carbonyl oxygen of the enyne to form a labile cyclic urethane intermediate (I). Because of its instability, this intermediate could not be isolated, and thus its hydrolysis was carried out in situ to give the corresponding vinylogous amide (i.e., **1**) in good yields (generally no less than 70%, irrespective of the R residue), and as the *Z* isomer only.

In view of possible applications of this method to large-scale synthesis, we wanted to further decrease the catalyst loading. Moreover, the scope of the reaction had only been explored in terms of the alkyne chain, so we decided to explore the compatibility of various functional groups on the piperidine ring with the reaction conditions, as well as to explore the reactivity of 7-alkynyl-2,3,4,5-tetrahydroazepine derivatives. Furthermore, we envisaged that the method could be extended further by replacing the *N*-Boc protection with an *N*-Cbz (benzyloxycarbonyl) group; in theory, this would result in *C*-1'-substituted vinylogous amides deriving from a carbodeauration step.^[16]

A key point of our previous work was that with substrates such as *N*-Boc enynes **2**, the exclusive formation of products derived from a 6-*endo-dig* oxyauration step was observed, whereas for *N*-Boc propargylamines and 2-alkynyl *N*-Boc-substituted pyrrolidines and piperidines^[17–19] only a 5-*exo-dig* cyclization has been reported.^[20] Also, based on other reports from the literature, it seemed reasonable to us that in our case the alternative 5-*exo-dig* mechanism was disfavoured by the larger bond angle at C-6 (due to the presence of the endocyclic double bond), which also caused substrates **2** to have a much lower reactivity than the corresponding saturated compounds.^[18,19] Therefore, the strikingly different results obtained with substrates **2** prompted us to carry out further investigations, including theoretical calculations, to reveal the role of the hybridization of C-6, and also other possible structural features, in the 6-*endo/5-exo-dig* preference during the gold-catalysed cyclization of enynes **2**. Finally, since all of the natural compounds potentially derived from exocyclic vinylogous amides (Figure 1) are β -amino ketones (or alcohols obtained from β -amino ketones), we decided to also explore

the gold(I)-catalysed cycloisomerization of 2-alkynylpiperidines **4** (Scheme 1) as an alternative synthetic route in which reduction of the double bond to give the β -amino ketone **5** is carried out before (as opposed to after) the gold-catalysed step.

Results and Discussion

In gold(I)-catalysed processes, the catalyst is generally used at a catalyst loading between 1 and 5 mol-%,^[21] although some exceptions to this have been reported.^[22] The active gold(I) catalysts are generally prepared in situ by anion exchange between LAuX ($\text{X} = \text{Cl}, \text{Br}$) and a silver salt (AgY) so that the highly coordinating anion X^- can be eliminated as AgX . Besides the fact that silver does play a role in some gold(I)-catalysed processes,^[23] issues related to the decay/decomposition of the active gold catalyst have recently been pointed out.^[24,25] This is what we actually observed in our previous study of the gold(I)-catalysed rearrangement of *N*-Boc-protected 6-alkynyl-3,4-dihydro-2*H*-pyridines, and for this reason we then used 2–3 mol-% of the catalyst to achieve complete conversion within a reasonable time.^[11] In a study by Bezenine-Lafollée and Gandon on anion metathesis,^[24] it was found that by slowing down the rate of the anion exchange, for example by changing the source of the weakly coordinating anion from silver to copper salts, the decomposition of the catalyst could be prevented. This was a result of slow release of the active LAu^+ species in the solution over a longer period of time.^[26] Among the various catalytic systems, $\text{Cu}(\text{OTf})_2$ proved to be the best, and so we decided to evaluate these new conditions, aiming for a lower catalyst loading (Table 1).

Table 1. Gold(I)-catalysed reaction of enyne **2** in the presence of $\text{Cu}(\text{OTf})_2$.^[a]

Entry	Ph_3PAuCl [mol-%]	$\text{Cu}(\text{OTf})_2$ [mol-%]	Time [h]	I [%] ^[b]	1 [%] ^[c]
1	0.5	10	0.5	100	70
2	0.5	5	0.5	100	72
3	0.2	5	3.5	76	–
4	0.1	5	6.5	70	–
5	0	10	2.5	40	–

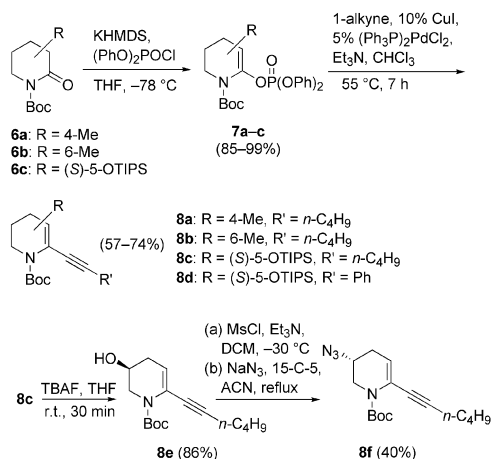
[a] Reactions were run on a 0.5 mmol scale under an inert atmosphere. [b] Conversion was measured by ^1H NMR spectroscopy. [c] Yield after chromatographic purification.

Using compound **2** as a model substrate, we carried out the reaction in refluxing toluene, and lowered the amount of gold(I) to 0.5 mol-% and added $\text{Cu}(\text{OTf})_2$ in a 20:1 molar ratio (Table 1, entry 1). We were delighted to find out that

after just 30 min, the starting material had been completely consumed, and the corresponding vinylogous amide (i.e., **1**) was obtained after alkaline hydrolysis of intermediate **I** in the usual 70% yield after purification. The same result was obtained using a 10:1 molar ratio by lowering the quantity of $\text{Cu}(\text{OTf})_2$ to 5 mol-% (Table 1, entry 2). However, with lower amounts of Ph_3PAuCl , the reaction did not go to completion (Table 1, entries 3 and 4), even when the reaction time was prolonged to 6.5 h (Table 1, entry 4). Not unexpectedly, $\text{Cu}(\text{OTf})_2$ used alone at a catalyst loading of 10 mol-% did have some catalytic properties,^[24,27] but the reaction required 2.5 h to reach a conversion of 40% (Table 1, entry 5), so the cationic gold(I) species is the true catalyst. Based on these results, we decided to use Ph_3PAuCl at 0.5 mol-% together with 5 mol-% of $\text{Cu}(\text{OTf})_2$ as the new catalytic system for the next gold(I)-catalysed experiments.

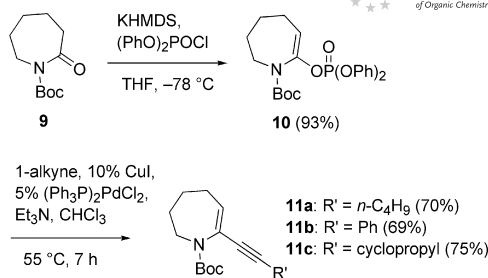
The synthesis of substrates bearing functional groups on the piperidine ring, and also of larger heterocyclic rings, was carried out in order to expand the scope of the reaction.

Enynes **8a–8f** and **11a–11c** were all prepared by Sonogashira coupling of lactam-derived enol phosphates **7a–7c** and **10**,^[34] respectively (Schemes 2 and 3).^[11] Lactams **6a**^[28] and **6b**^[29] were obtained by oxidation of the corresponding racemic *N*-Boc-protected methylpiperidines,^[30,31] whereas lactam **6c** (Scheme 2) was prepared from (*S*)-(+)- γ -hydroxymethyl- γ -butyrolactone,^[32,33] using standard chemistry for the final two protection steps of the 5-hydroxy- δ -valerolactam.^[33] As we have already reported for analogous substrates, enynes **8** and **11** were unstable when neat, and so they were stored in solution in the presence of Et_3N (1% v/v).^[11]



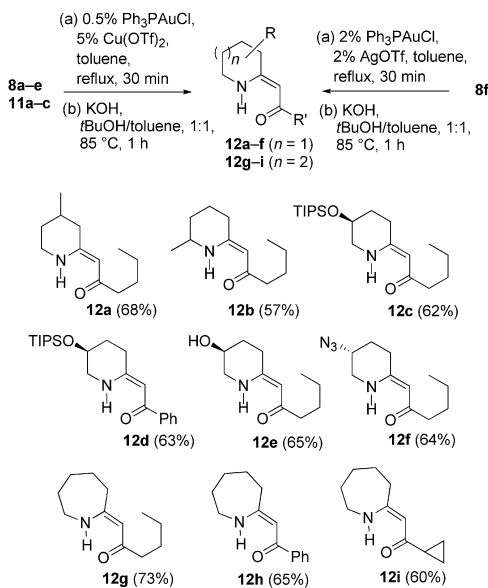
Scheme 2. Synthesis of compounds **8a–8f**; KHMDS = potassium hexamethyldisilazide; TIPS = triisopropylsilyl.

Enynes **8a–8f** and **11a–11c** were all successfully used for the synthesis of the corresponding vinylogous amides with



Scheme 3. Synthesis of compounds **11a–11c**.

the gold–copper catalytic system (Scheme 4). Only in the case of **8f** was the reaction best carried out by using the $\text{Ph}_3\text{PAuCl}/\text{AgOTf}$ system^[11] to give the corresponding vinylogous amide (i.e., **12f**, which contains a masked amino group on the piperidine ring) in good yield after purification. As we reported in our previous work, the cyclic intermediates were unstable, and thus the hydrolysis was carried out in situ at 80 °C by addition of KOH and *tert*-butanol.^[35] In all cases, the vinylogous amides were obtained in good yields over the two steps (57–73%).



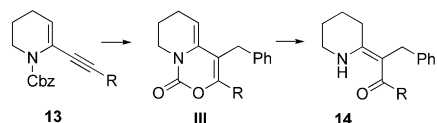
Scheme 4. Synthesis of compounds **12a–12i**.

To further expand the scope of the reaction, we then decided to focus our attention on different substrates in which a benzyloxycarbonyl group replaces the *tert*-butoxycarbonyl group. According to the reaction mechanism, in the case of *N*-Boc-protected substrates, once the carbonyl oxygen of the Boc group attacks the gold-activated triple

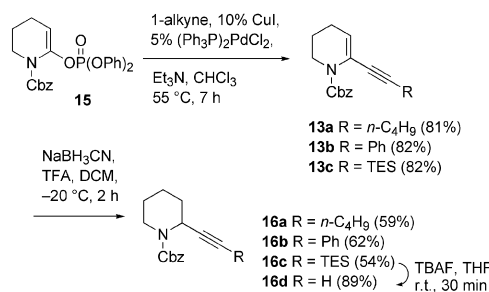
FULL PAPER

D. Scarpi, E. G. Occhiato et al.

bond, the resulting *tert*-butyl cation decomposes to give isobutylene and H^+ , generating the proton necessary for the protodeauration step. Since carbodeauration has been demonstrated with substrates that are able to generate a carbocation (mainly allylic),^[16] we decided to verify whether this process would be possible in our case with a benzylic carbocation derived from an *N*-Cbz protecting group. This would lead to vinylogous amides **14** bearing a C-1' substituent (Scheme 5).

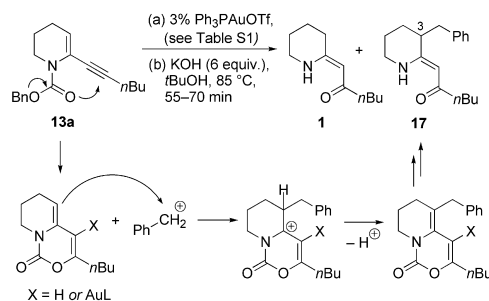
Scheme 5. Planned synthesis of **14**.

The synthesis of *N*-Cbz enyne **13a** (Scheme 6), a model substrate, was carried out by Sonogashira coupling between *N*-Cbz enol phosphate **15**^[36] and 1-hexyne. As was seen for the analogous *N*-Boc compound, **13a** also proved to be unstable when neat, and was stored in solution in the presence of Et_3N .

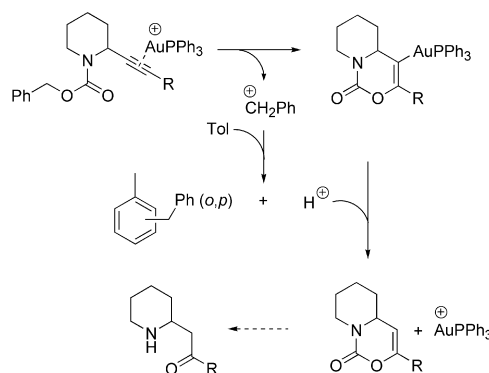
Scheme 6. Synthesis of compounds **13a–13c** and **16a–16d**; TFA = trifluoroacetic acid; TES = triethylsilyl.

Compound **13a** was then tested in the gold(I)-catalysed process under the usual conditions, but the reaction failed to go to completion even when the reaction time was prolonged to 4.5 h, and it did not provide, after hydrolysis, compound **14** deriving from carbodeauration. With this *N*-Cbz derivative, the reaction was best carried out with 3 mol-% of $Ph_3PAuOTf$ (Scheme 7), but whatever conditions were used, the reaction took place by a 6-*endo-dig* oxyauration mechanism and, together with unreacted starting material, we obtained only a mixture of vinylogous amides **1** and **17** (Table S1 in the Supporting Information). Compound **1** derives from a protodeauration process, and compound **17** from an electrophilic addition of the benzylic carbocation onto the piperidine double bond (before or after the protodeauration step), with subsequent release of a proton. Moreover, *o*-benzyltoluene and *p*-benzyltoluene were detected in the 1H NMR spectrum of the crude mixture, both deriving from an electrophilic aromatic substitution reaction on toluene, which thus represents an additional proton

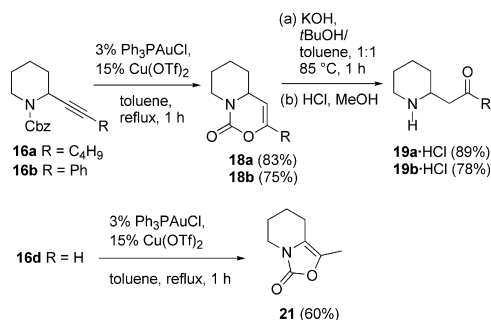
source. Compounds **1** and **17** were not separated by chromatography, but the structure of **17** was easily assigned by 1H NMR spectroscopic analysis of the mixture, which showed a diagnostic ABX system that was assigned to the two benzylic protons (dd at $\delta = 3.06$ ppm, $J = 13.5, 4.7$ Hz; and dd at $\delta = 2.73$ ppm, $J = 13.5, 10.2$ Hz), and 3-H (m at $\delta = 2.64–2.58$ ppm).

Scheme 7. Au^I -catalysed reaction of **13a**.

Based on these results, we decided to reduce the double bond of **13a** (to obtain **16a**) so that no benzylic addition could occur, and, by exploiting toluene as a proton source, products formally derived from double-bond reduction of vinylogous amides **1** (i.e., β -amino ketones) could be obtained instead (Scheme 8).

Scheme 8. Planned synthesis of β -amino ketones.

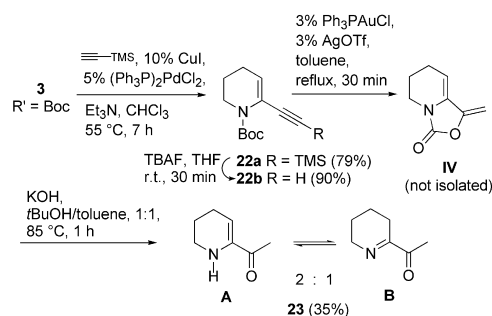
As mentioned above, this would represent an alternative synthetic route to β -amino ketones in which reduction of the double bond is carried out before the gold-catalysed step. For example, a series of natural products, including various Sedamine alkaloids, has been obtained from β -amino ketone **19b** (Scheme 9),^[10] which is itself a natural product (norsedaminone).^[37] The selective reduction was carried out at low temperature with $NaBH_3CN$ under acidic conditions,^[38] and gave compound **16a** in good yield (Scheme 6).

Scheme 9. Synthesis of compounds **19a**, **19b**, and **21**.

We were glad to observe that the subsequent gold-catalysed step [best catalysed by 3 mol-% of the gold(I) salt together with 15 mol-% of $\text{Cu}(\text{OTf})_2$] gave only compound **18a**, which was derived from a 6-*endo-dig* approach; we were instead unable to find any signal in the ^1H NMR spectrum of the crude reaction mixture that could be assigned to the 5-*exo-dig* isomer (Scheme 9).^[39] To confirm our findings, we decided to synthesize compound **16b** through Sonogashira coupling of **15** with phenylacetylene followed by reduction of the double bond of **13b** as already described (Scheme 6). Compound **18b** is a known compound,^[40] and since it was synthesized by a [4+2] cycloaddition of *N*-acyliminium ion with phenylacetylene, its structure was assigned unambiguously. Treatment of **16b** with Ph_3PAuCl and $\text{Cu}(\text{OTf})_2$ under the usual conditions gave only **18b** (Scheme 9), with spectroscopic data identical to those reported in the literature.^[41] Further confirmation of the structures of both **18a** and **18b** came from hydrolysis under basic conditions, which gave β -amino ketones **19a** and **19b**, which, being quite volatile, were converted into their HCl salts in good overall yield (89 and 78%, respectively).

These results seemed to be in contrast with data previously reported in the literature for *N*-Boc-protected propargylamines, in which only 5-*exo-dig* products were obtained, even though a 6-*endo-dig* mechanism was equally possible. Also, when heterocyclic substrates were used, i.e., *N*-Boc-2-ethynylpyrrolidine,^[18,19] *N*-Boc-2-ethynylpiperidine,^[19] and *N*-Boc-2-ethynylazepane,^[19] 5-*exo-dig* products were obtained,^[20] but all of these compounds had a terminal alkyne moiety. Since all the substrates we tested had substituted alkyne groups, we wondered whether a situation analogous to the gold(I)-catalysed propargylic ester migration could exist. In this process, the 1,2-rearrangement is favoured for terminal alkynes, whereas the 1,3-rearrangement becomes a competing, or even the major, pathway for internal alkynes.^[42] The synthesis of a substrate with a terminal alkyne was therefore necessary; this was carried out by Sonogashira coupling of phosphate **15** with triethylsilylacetylene (to give **13c**), followed by reduction of the double bond (to give **16c**), and deprotection with TBAF (tetrabutylammonium fluoride; to give **16d**; Scheme 6). It

should be highlighted that if our hypothesis was correct, treatment of **16d** with the gold catalyst would give the same product previously obtained by Gagosz and Buzas starting from the analogous *N*-Boc substrate.^[19] We were delighted to verify that **16d**, under the usual gold catalysis conditions, gave only compound **21** (Scheme 9), which derives from a 5-*exo-dig* reaction followed by isomerization of the double bond to the endocyclic position.^[43] Furthermore, an experiment carried out with unsaturated *N*-Boc compound **22** (Scheme 10) gave known compound **23**,^[44] derived from the 5-*exo-dig* intermediate. Taken together, these results show that the 6-*endo/5-exo-dig* selectivity we observe with our substrates depends on whether the triple bond is internal or terminal.

Scheme 10. Synthesis of compound **23**. TMS = trimethylsilyl.

To get further insight into the reason for the different selectivities for terminal and internal alkynes, and to ascertain whether the large $\text{N}-\text{C}_{\text{sp}^2}-\text{C}_{\text{sp}}$ angle has a role in the high 6-*endo-dig* preference with those substrates with an internal triple bond, DFT calculations were carried out with the Gaussian 09 suite of programs (see Computational Methods section). Since the 5-*exo/6-endo-dig* selectivity trend does not depend on the alkoxy-carbonyl moiety, the *N*-Cbz protecting group was chosen, and compounds **13b**, **13d**, **16b**, and **16d** (Figure 2) were selected as model substrates for the cyclization reaction, as examples of the four possible combinations of saturated/unsaturated rings and substituted/unsubstituted alkynes. Triphenylphosphine-gold(I) cation was used as the reaction catalyst, and the

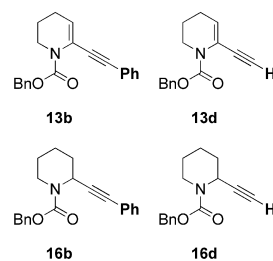


Figure 2. Model substrates for DFT studies.

FULL PAPER

D. Scarpi, E. G. Occhiato et al.

study focussed on the cyclization step, which is the regioselectivity-determining step.

Given the very different degrees of steric hindrance at the two carbons of the triple bond in terminal alkynes (**13d** and **16d**), it would seem reasonable to hypothesize at first sight that steric effects were important for the observed 5-*exo-dig* regioselectivity in these substrates, since the gold atom could preferably be placed at the least substituted terminal position during the attack of the oxygen atom. However, although this could be an important factor, this effect alone cannot explain the regioselectivity found in internal alkynes (**13b** and **16b**), since in those cases the two carbon atoms are sterically quite similar. Thus, calculations were carried out for the four alkyne-gold(I) complexes (only the unsaturated complexes, i.e., **V-Ph** and **V-H** are shown in Figure 3), and unsurprisingly, the complexes showed clear structural differences in terms of alkyne-gold complexation.

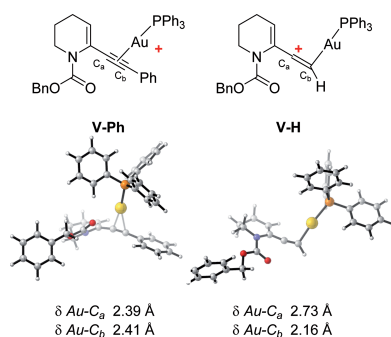


Figure 3. Structures of complexes **V-Ph** and **V-H**.

Specifically, in **V-H**, gold coordination induces a weakening of the triple bond [$\delta(C_a-C_b) = 1.23 \text{ \AA}$] and a strong asymmetry of the C–Au bonds [$\delta(C_a-Au) = 2.73 \text{ \AA}$, $\delta(C_b-Au) = 2.16 \text{ \AA}$]. The resulting complex can be considered to some extent as a vinyl cation. The calculated natural population atomic charges at the two carbon atoms are $+0.203 \text{ e}$ (C_a) and -0.480 e (C_b), which confirms that the positive charge of the complex is centred at C_a . These values are consistent with those calculated for a simple unsubstituted propargylic acetate,^[42b] although in our case the positive charge on C_a is even higher ($+0.203 \text{ e}$ vs. $+0.063 \text{ e}$), the C_a –Au bond length longer (2.73 vs. 2.514 \AA), and the C_b –Au bond length shorter (2.16 vs. 2.239 \AA). On the other hand, alkyne-gold complex **V-Ph** has a much more symmetrical structure, with nearly identical Au–C distances (Figure 3), and NPA (natural population analysis) charges ($C_a = -0.056 \text{ e}$, $C_b = -0.002 \text{ e}$). In this case, the positive charge is centred on the gold atom (Au = $+0.437 \text{ e}$ in **V-Ph**, vs. $+0.365 \text{ e}$ in **V-H**).

As a result of the more positively-charged character of the internal C_a carbon atom in **V-H**, the attack of the oxygen atom takes place exclusively at that position. This ex-

perimental fact could be confirmed computationally with substrates **13d** and **16d**. We found that the 5-*exo-dig* cyclization occurs with a very low barrier (3.9 kcal/mol for TS13-H-5-*exo*) or, in the case of the corresponding saturated compound **16b**, with essentially no activation barrier (TS16-H-5-*exo*, Figure 4).

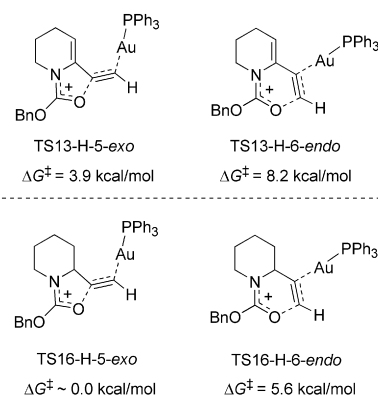


Figure 4. Transition-state structures and energies for terminal alkynes.

In fact, no convergence or a convergence to the starting material was observed during the search for a transition state in the latter case, even though we tested different functionals (B3LYP, M06, BHandHLYP) and basis sets. To further analyse this issue, a potential scan for the O–C bond formation was carried out, and this confirmed that it is a downhill process without appreciable activation energy. On the other hand, the transition states for the regioisomeric 6-*endo* cyclizations were located, and were found to have low but measurable activation energies (8.2 and 5.6 kcal/mol, Figure 4), which are ca. 4–5 kcal/mol higher than those of the 5-*exo* processes. This energy difference can explain the absolute experimental preference for the five-membered cyclic products. This is also consistent with the fact that a 1,2-acyl shift is preferred for propargylic acetates with an unsubstituted alkyne moiety.^[42b]

On the other hand, the transition-state structures for the reaction of the internal triple bonds are consistent with the experimental preference for the C_b attack. Thus, the lowest calculated activation energies were 7.8 kcal/mol for the unsaturated ring (TS13-Ph-6-*endo*, Figure 5 and Figure S1 in Supporting Information), and 8.4 kcal/mol for TS16-Ph-6-*endo*. It is interesting to note that the *endo/exo* selectivity is predicted to be better for **13** ($\Delta\Delta G^\ddagger_{exo-endo} = 2.5 \text{ kcal/mol}$) than for **16** ($\Delta\Delta G^\ddagger_{exo-endo} = 1.3 \text{ kcal/mol}$). This effect can be attributed to the increase in the N–C– C_a angle induced by the presence of the double bond, from 113° (**16d**, N– C_{sp^3} – C_a) to 119° (**13d**, N– C_{sp^2} – C_a), a factor that plays against the formation of the smaller five-membered ring.^[45]

The data shown in Figures 3 and 5 are not informative enough about the exact reason for the 6-*endo* selectivity

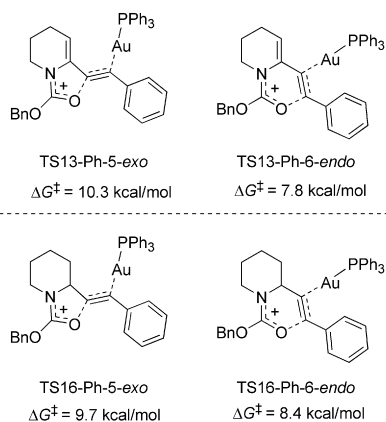


Figure 5. Transition-state structures and energies for internal alkynes.

with internal alkynes, since C_a and C_b have very similar electronic properties, and their bonding distances with the gold atom are virtually equal (Figure 3). Thus, we envisioned an indirect way to analyse the geometrical factors that determine the reactivity of the internal alkynes, by using symmetrical computational substrates (Figure 6).

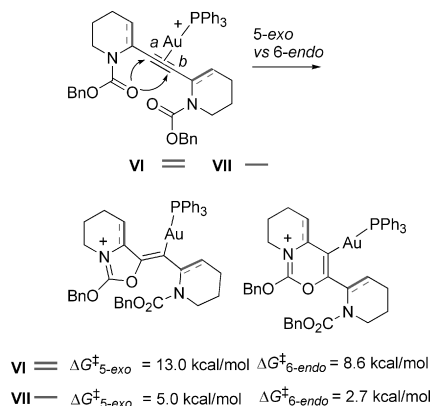


Figure 6. Comparison of the activation energies for the 5-*exo* and 6-*endo-dig* pathways.

For example, in the model system **VI**, the triple bond is symmetrically substituted, and the two carbons (C_a and C_b) are absolutely identical, which reduces the factors that affect the formation of one ring or the other to a simple geometrical preference. Interestingly, the activation energy is lower for the 6-*endo* cyclization by 4.4 kcal/mol, indicating that in principle, the preference for the six-membered ring is purely geometrical, and could be generalized to any type of internal alkynes, irrespective of the substituent on the

terminal position. It is worth mentioning that a similar preference, but to a lesser extent ($\Delta\Delta G^\ddagger = 2.3$ kcal/mol), was found for computational model compound **VII**, with saturated rings, which is consistent with the generally lower selectivity of this type of substrates (vide supra).

Conclusions

In this work, we have studied in detail the gold(I)-catalysed cyclization of *N*-Boc-protected 6-alkynyl-3,4-dihydro-2*H*-pyridines to give synthetically useful exocyclic vinyllogous amides, with three objectives in mind. First, bearing in mind possible large-scale applications of the method, we wanted to optimize the reaction conditions to reduce the amount of the gold catalyst as far as possible. This was realized by using $\text{Cu}(\text{OTf})_2$ as the triflate source, which allowed us to use 0.5 mol-% of Au^{I} without affecting the reaction rate. Secondly, we expanded the scope of the reaction to substituted piperidines and different nitrogen heterocycles to assess the tolerance to the reaction conditions of some functional groups often present in natural products that could easily be prepared from the vinyllogous amide products. Our third goal was to assess the structural features that selectively favour the 6-*endo-dig* oxyauration of the triple bond. We found that a 6-*endo-dig* mechanism operates exclusively with substituted alkynes, whereas with terminal alkynes a 5-*exo-dig* cyclization prevails, despite the large angle (120°) at C-6. An analogous selectivity was observed with *N*-Cbz-protected 2-alkynylpiperidines. These compounds, after gold-catalysed cyclisation and hydrolysis of the cyclic intermediates, give β -amino ketones as a result of a 6-*endo-dig* attack onto the internal triple bond. DFT calculations showed that with both types of substrates, the oxyauration step has a low barrier or almost no barrier at all when it involves the internal position of a terminal triple bond, resulting in a 5-*exo-dig* process. In contrast, the 6-*endo-dig* mechanism is always favoured with substituted alkynes, this preference being purely geometrical and irrespective of the type of substitution, thus providing either β -enamminones or their reduced equivalents, β -amino ketones, in a robust, reliable, and convenient way.

Experimental Section

General Remarks: Chromatographic separations were carried out under pressure on silica gel using flash-column techniques. R_f values refer to TLC carried out on 0.25 mm silica gel plates (F_{254}) with the same eluent as indicated for the column chromatography. ^1H NMR spectra were recorded at 200 or 400 MHz, and ^{13}C NMR spectra were recorded at 50.33 or 100.4 MHz, both in CDCl_3 solution, unless otherwise specified. The solvent reference line was set at $\delta = 7.26$ (CDCl_3) or 4.79 (D_2O) ppm. Mass spectra were either recorded at an ionizing voltage of 70 eV, or measured with an LCQ FleetTM Ion-Trap LC-MS system with an electrospray ionization (ESI) interface in positive-ion mode by direct inlet of a 10 ppm solution in CH_3OH . Microanalyses were carried out with an elemental analyser. Compounds **6a**,^[28] **6b**,^[29] **10**,^[34] **15**,^[36] and 5-hy-

droxy- δ -valerolactam^[32] were prepared as reported. All enynes **2**, **8**, **11**, **13**, and **22**, as well as intermediates **16** decompose when neat and must be stored in solution in the presence of Et₃N (1% v/v).

Computational Methods: The structures were optimized using density functional theory (DFT) with BHandHLYP^[46] functional and the 6-31G* (LANL2DZ for Au) basis set as implemented in Gaussian 09.^[47] The B3LYP functional was also evaluated; it gave similar results to BHandHLYP, but some of the lowest-in-energy transition states (TS13-H-5-*exo* and TS16-H-5-*exo*) did not converge properly when using B3LYP. The energy values shown in Figures 3^[48] and 4 also include single-point refinements at the M06-2X/6-311++G**(SDD) level of theory^[49] on the previously optimized structures, to better account for the dispersion forces of such large systems. The stationary points were characterized by frequency calculations in order to verify that they had the right number of imaginary frequencies. The intrinsic reaction coordinates (IRC)^[50] were followed to verify the energy profiles connecting each TS to the correct associated local minima. Natural bond orbital (NBO) analysis^[51] was carried out to evaluate the NPA atomic charges.

tert-Butyl (5S)-2-Oxo-5-(triisopropylsilyloxy)piperidine-1-carboxylate (6c): 5-Hydroxy- δ -valerolactam^[32] (680 mg, 5.9 mmol) was dissolved in anhydrous DMF (12 mL), Imidazole (1.21 g, 17.7 mmol) and triisopropylsilyl chloride (1.27 mL, 5.9 mmol) were added, and then the resulting mixture was warmed to 40 °C. A second equivalent of triisopropylsilyl chloride (1.27 mL, 5.9 mmol) was added in portions over 8 h, and the reaction was stirred at 40 °C overnight. The mixture was cooled to room temperature, then water was added (120 mL), and the mixture was extracted with Et₂O (4 × 50 mL). The combined organic phases were dried with anhydrous Na₂SO₄ and filtered, and the solvent was evaporated. The residue was purified by flash chromatography (EtOAc; R_f = 0.27) to give pure 5-(triisopropylsilyloxy)piperidin-2-one (1.36 g, 85%) as a colourless oil. $[\alpha]_D^{25} = -11.3$ (*c* = 1.12, CHCl₃). ¹H NMR (400 MHz): δ = 7.05 (br. s, 1 H, NH), 4.17–4.12 (m, 1 H, 5-H), 3.41–3.37 (m, 1 H, 6-H), 3.23–3.19 (m, 1 H, 6-H'), 2.56 (dt, *J* = 17.6, 7.6 Hz, 1 H, 3-H), 2.27 (dt, *J* = 17.6, 6.1 Hz, 1 H, 3-H'), 1.90–1.86 (m, 2 H, 4-H), 1.05–0.98 (m, 21 H, TIPS) ppm. ¹³C NMR (100.4 MHz): δ = 172.1 (s, C-2), 64.1 (d, C-5), 49.4 (t, C-6), 29.0 (t, C-3), 27.5 (t, C-4), 17.9 (q, 6 C, CH₃ TIPS), 12.1 (d, 3 C, CH TIPS) ppm. MS (ESI): *m/z* (%) = 565 [2M + Na]⁺ (100), 543 [2M + 1]⁺ (16). C₁₄H₂₉NO₂Si (271.47): calcd. C 61.94, H 10.77, N 5.16; found C 61.72, H 10.50, N 4.91.

5-(Triisopropylsilyloxy)piperidin-2-one (1.3 g, 4.79 mmol) was dissolved in anhydrous CH₂Cl₂ (30 mL), Et₃N (740 μ L, 5.27 mmol), di-*tert*-butyl dicarbonate (1.1 g, 4.79 mmol), and DMAP (4-dimethylaminopyridine; 59 mg, 0.48 mmol) were added, and the resulting mixture was heated under reflux. After 2 h, a second equivalent of di-*tert*-butyl dicarbonate (1.1 g, 4.79 mmol) was added. When the reaction was complete (TLC; 5 h), the mixture was cooled to room temperature, water (40 mL) was added, and the layers were separated. The aqueous phase was extracted with CH₂Cl₂ (3 × 20 mL), and the combined organic extracts were washed with KHSO₄ (5% aq.; 40 mL), satd. NaHCO₃ (40 mL), water (40 mL), and brine (40 mL), and finally dried with anhydrous Na₂SO₄. The mixture was filtered, and the solvent was evaporated. The residue was purified by flash chromatography (*n*-hexane/EtOAc, 8:1; R_f = 0.12) to give pure **6c** (1.44 g, 81%) as a colourless oil. $[\alpha]_D^{25} = +10.0$ (*c* = 0.92, CHCl₃). ¹H NMR (400 MHz): δ = 4.26–4.21 (m, 1 H, 5-H), 3.73 (dd, *J* = 13.1, 4.7 Hz, 1 H, 6-H), 3.62 (dd, *J* = 13.1, 3.5 Hz, 1 H, 6-H'), 2.75–2.67 (m, 1 H, 3-H), 2.40 (dt, *J* = 17.2, 5.9 Hz, 1 H, 3-H'), 1.98–1.92 (m, 1 H, 4-H), 1.91–

1.84 (m, 1 H, 4-H'), 1.48 [s, 9 H, C(CH₃)₃], 1.10–0.95 (m, 21 H, TIPS) ppm. ¹³C NMR (100.4 MHz): δ = 170.8 (s, C-2), 152.3 (s, C=O), 82.7 [s, C(CH₃)₃], 64.4 (d, C-5), 52.5 (t, C-6), 31.0 (t, C-3), 29.1 (t, C-4), 27.9 (q, 3 C, CH₃ Boc), 17.8 (q, 6 C, CH₃ TIPS), 12.0 (d, 3 C, CH TIPS) ppm. MS (ESI): *m/z* (%) = 766 (33), 765 [2M + Na]⁺ (100), 394 [M + Na]⁺ (7). C₁₉H₃₇NO₄Si (371.59): calcd. C 61.41, H 10.04, N 3.77; found C 61.25, H 9.98, N 3.91.

tert-Butyl (±)-6-(Diphenoxyphosphoryloxy)-4-methyl-3,4-dihydro-2H-pyridine-1-carboxylate (7a): KHMDs (0.5 M solution in toluene; 6.4 mL, 3.2 mmol) was diluted with anhydrous THF (18 mL), and the solution was cooled to –78 °C. A solution of **6a**^[28] (455 mg, 2.13 mmol) in anhydrous THF (10 mL) was then added dropwise, keeping the temperature below –70 °C, and the resulting mixture was stirred for 1.5 h. Diphenylchlorophosphate (663 μ L, 3.2 mmol) was slowly added. After 1 h, the mixture was warmed to 0 °C, and the reaction was quenched by the addition of NaOH (10% aq.; 50 mL). The mixture was extracted with Et₂O (3 × 40 mL), and the combined organic extracts were washed once with NaOH (10% aq.; 28 mL), and dried with anhydrous K₂CO₃. The mixture was filtered, and the solvent was evaporated. The residue was purified over a short pad of silica gel (*n*-hexane/EtOAc, 7:1 + 1% Et₃N; R_f = 0.13) to give pure **7a** (800 mg, 85%) as a colourless oil. ¹H NMR (400 MHz): δ = 7.37–7.31 (m, 4 H, Ar), 7.25–7.17 (m, 6 H, Ar), 5.01–4.99 (m, 1 H, 5-H), 3.61–3.50 (m, 2 H, 2-H), 2.45–2.38 (m, 1 H, 4-H), 1.87–1.79 (m, 1 H, 3-H), 1.43 [s, 9 H, C(CH₃)₃], 1.41–1.33 (m, 1 H, 3-H'), 1.01 (d, *J* = 6.0 Hz, 3 H, CH₃) ppm. ¹³C NMR (100.4 MHz): δ = 153.1 (s, C=O), 150.6 (s, Ph), 150.5 (s, Ph), 140.0 (s, C-6), 129.7 (d, 4 C, C_{Ar}), 125.4 (d, Ph), 125.3 (d, Ph), 120.09 (d, Ph), 120.08 (d, Ph), 120.04 (d, Ph), 120.03 (d, Ph), 105.3 (d, C-5), 81.7 [s, C(CH₃)₃], 44.1 (t, C-2), 31.1 (d, C-4), 28.1 [q, 3 C, C(CH₃)₃], 27.8 (t, C-3), 21.3 (q, CH₃) ppm. MS (ESI): *m/z* (%) = 913 [2M + Na]⁺ (100), 468 [M + Na]⁺ (20), 446 [M + 1]⁺ (35).

tert-Butyl (±)-6-(Diphenoxyphosphoryloxy)-2-methyl-3,4-dihydro-2H-pyridine-1-carboxylate (7b): Prepared as described for **7a**, starting from **6b**^[29] (362 mg, 1.7 mmol), to give, after purification (*n*-hexane/EtOAc, 6:1 + 1% Et₃N; R_f = 0.12), pure **7b** (658 mg, 87%) as a clear yellowish oil. ¹H NMR (400 MHz): δ = 7.38–7.28 (m, 4 H, Ph), 7.26–7.12 (m, 6 H, Ph), 5.11 (q, *J* = 3.5 Hz, 1 H, 5-H), 4.67–4.53 (m, 1 H, 2-H), 2.21–2.10 (m, 2 H, 4-H), 1.77–1.66 (m, 1 H, 3-H), 1.63–1.57 (m, 1 H, 3-H'), 1.43 [s, 9 H, C(CH₃)₃], 1.15 (d, *J* = 6.9 Hz, 3 H, CH₃) ppm. ¹³C NMR (100.4 MHz): δ = 153.2 (s, C=O), 150.5 (s, Ph), 150.4 (s, Ph), 138.3 (s, C-6), 129.7 (d, 4 C, Ph), 125.4 (d, Ph), 125.3 (d, Ph), 120.12 (d, Ph), 120.10 (d, Ph), 119.98 (d, Ph), 119.93 (d, Ph), 99.3 (d, C-5), 81.6 [s, C(CH₃)₃], 49.2 (d, C-2), 28.1 [q, 3 C, C(CH₃)₃], 27.1 (t, C-4), 18.6 (t, C-3), 15.7 (q, CH₃) ppm. MS (ESI): *m/z* (%) = 913 [2M + Na]⁺ (100), 468 [M + Na]⁺ (41), 446 [M + 1]⁺ (27).

tert-Butyl (3S)-6-(Diphenoxyphosphoryloxy)-3-(triisopropylsilyloxy)-3,4-dihydro-2H-pyridine-1-carboxylate (7c): Prepared as described for **7a**, starting from **6c** (1.44 g, 3.87 mmol), to give, after purification (*n*-hexane/EtOAc, 5:1 + 1% Et₃N; R_f = 0.50), pure **7c** (2.33 g, 99%) as a pale yellow oil. ¹H NMR (400 MHz): δ = 7.37 (m, 4 H, Ph), 7.27–7.25 (m, 4 H, Ph), 7.21–7.18 (m, 2 H, Ph), 5.06–5.04 (m, 1 H, 5-H), 4.11–4.06 (m, 1 H, 3-H), 3.71 (dd, *J* = 12.9, 3.1 Hz, 1 H, 2-H), 3.51 (dd, *J* = 12.9, 7.4 Hz, 1 H, 2-H'), 2.51–2.43 (m, 1 H, 4-H), 2.16–2.08 (m, 1 H, 4-H'), 1.44 [s, 9 H, C(CH₃)₃], 1.13–1.01 (m, 21 H, TIPS) ppm. ¹³C NMR (100.4 MHz): δ = 153.0 (s, C=O), 150.5 (s, 2 C, C_{Ar}), 140.0 (s, C-6), 129.7 (d, 4 C, C_{Ar}), 125.4 (d, 2 C, C_{Ar}), 120.0 (d, 4 C, C_{Ar}), 97.8 (d, C-5), 81.6 [s, C(CH₃)₃], 65.2 (d, C-3), 51.2 (t, C-2), 32.4 (t, C-4), 28.0 (q, 3 C, CH₃ Boc), 17.9 (q, 6 C, CH₃ TIPS), 12.1 (d, 3 C, CH TIPS) ppm. MS (ESI): *m/z* (%) = 1229 [2M + Na]⁺ (100), 792 [M + Na]⁺ (7).

General Procedure for Sonogashira Coupling: Phosphate (**7a–7c**, **10**)^[34] **15**)^[36] was dissolved in an anhydrous mixture of Et₃N and CHCl₃ (3:1; 0.13 M), and the alkyne (1 mmol), CuI (0.1 mmol), and (Ph₃P)₂PdCl₂ (0.05 mmol) were added. The resulting solution was heated at 55 °C (external) for 2 h, after which time further alkyne (0.5 mmol), CuI (0.05 mmol), and (Ph₃P)₂PdCl₂ (0.025 mmol) were added, if necessary. The mixture was heated at 55 °C until the reaction was complete (TLC, usually after 4–7 h). The mixture was cooled to room temperature, then water (12 mL) was added, and the mixture was extracted with Et₂O (3 × 12 mL). The combined organic extracts were dried with anhydrous K₂CO₃ and filtered, and the solvent was evaporated. The crude enyne (**8a–8d**, **11a–11c**, **13a–13c**) was purified by flash chromatography (eluent containing 1% Et₃N), and stored at 4 °C as a 0.1 M solution in the eluent until use.

tert-Butyl (±)-6-(Hex-1-ynyl)-4-methyl-3,4-dihydro-2H-pyridine-1-carboxylate (8a): Pale yellow oil (205 mg, 74%). *R*_f = 0.12 (*n*-hexane/EtOAc, 30:1 + 1% Et₃N). ¹H NMR (400 MHz): δ = 5.34 (d, *J* = 3.5 Hz, 1 H, 5-H), 3.59 (ddd, *J* = 12.9, 7.0, 3.1 Hz, 1 H, 2-H), 3.46 (ddd, *J* = 12.9, 8.2, 2.7 Hz, 1 H, 2-H'), 2.36–2.30 (m, 1 H, 4-H), 2.30 (t, *J* = 7.0 Hz, 2 H, 3'-H), 1.88–1.83 (m, 1 H, 3-H'), 1.55–1.46 (m, 2 H, 4'-H), 1.49 [s, 9 H, C(CH₃)₃], 1.44–1.36 (m, 3 H, 5'-H, 3-H), 1.00 (d, *J* = 7.0 Hz, 3 H, CH₃), 0.90 (t, *J* = 7.4 Hz, 3 H, 6'-H) ppm. ¹³C NMR (100.4 MHz): δ = 153.1 (s, C=O), 126.7 (d, C-5), 121.4 (s, C-6), 88.3 (s, C-1'), 80.7 [s, C(CH₃)₃], 77.6 (s, C-2'), 42.2 (t, C-2), 30.9 (d, C-4), 30.7 (t, C-4'), 29.0 (t, C-3), 28.3 (q, 3 C, CH₃ Boc), 22.0 (q, CH₃), 21.0 (t, C-5'), 19.1 (t, C-3'), 13.6 (q, C-6') ppm. MS (ESI): *m/z* (%) = 577 [2M + Na]⁺ (100), 300 [M + Na]⁺ (30). MS/MS (ESI of [M + Na]⁺): *m/z* (%) = 300 (4), 244 (100).

tert-Butyl (±)-6-(Hex-1-ynyl)-2-methyl-3,4-dihydro-2H-pyridine-1-carboxylate (8b): Yellow oil (160 mg, 58%). *R*_f = 0.18 (*n*-hexane/EtOAc, 30:1 + 1% Et₃N). ¹H NMR (400 MHz): δ = 5.44 (t, *J* = 3.7 Hz, 1 H, 5-H), 4.56–4.49 (m, 1 H, 2-H), 2.30 (t, *J* = 7.0 Hz, 2 H, 3'-H), 2.15–2.09 (m, 2 H, 4-H), 1.83–1.73 (m, 1 H, 3-H), 1.62–1.55 (m, 1 H, 3-H'), 1.49 [s, 9 H, C(CH₃)₃], 1.55–1.38 (m, 4 H, 4'-H, 5'-H), 1.11 (d, *J* = 6.7 Hz, 3 H, CH₃), 0.90 (t, *J* = 7.3 Hz, 3 H, 6'-H) ppm. ¹³C NMR (100.4 MHz): δ = 153.0 (s, C=O), 119.9 (d, C-5), 119.8 (s, C-6), 87.6 (s, C-1'), 80.6 [s, C(CH₃)₃], 78.3 (s, C-2'), 46.8 (d, C-2), 30.7 (t, C-4'), 28.3 (q, 3 C, CH₃ Boc), 27.0 (t, C-4), 22.1 (t, C-5'), 19.8 (t, C-3), 19.1 (t, C-3'), 15.9 (q, CH₃), 13.6 (q, C-6') ppm. MS/MS (ESI of [M + Na]⁺): *m/z* (%) = 300 (3), 244 (100).

tert-Butyl (3S)-6-(Hex-1-ynyl)-3-(triisopropylsilyloxy)-3,4-dihydro-2H-pyridine-1-carboxylate (8c): Yellow oil (279 mg, 64%). *R*_f = 0.36 (*n*-hexane/EtOAc, 20:1 + 1% Et₃N). [α]_D²⁰ = +37.9 (*c* = 0.77, CHCl₃). ¹H NMR (400 MHz): δ = 5.40 (t, *J* = 4.0 Hz, 1 H, 5-H), 4.05–3.99 (m, 1 H, 3-H), 3.84 (dd, *J* = 12.4, 3.0 Hz, 1 H, 2-H), 3.21 (dd, *J* = 12.4, 8.4 Hz, 1 H, 2-H'), 2.44 (dt, *J* = 18.9, 5.2 Hz, 1 H, 4-H), 2.31 (t, *J* = 7.0 Hz, 2 H, 3'-H), 2.08 (ddd, *J* = 18.9, 6.3, 4.0 Hz, 1 H, 4-H'), 1.53–1.46 (m, 2 H, 4'-H), 1.48 [s, 9 H, C(CH₃)₃], 1.44–1.39 (m, 2 H, 5'-H), 1.07–1.04 (m, 21 H, TIPS), 0.90 (t, *J* = 7.3 Hz, 3 H, 6'-H) ppm. ¹³C NMR (100.4 MHz): δ = 152.9 (s, C=O), 122.2 (s, C-6), 119.2 (d, C-5), 88.7 (s, C-1'), 80.7 [s, C(CH₃)₃], 77.3 (s, C-2'), 65.2 (d, C-3), 49.8 (t, C-2), 34.5 (t, C-4), 30.7 (t, C-4'), 28.1 (q, 3 C, CH₃ Boc), 22.0 (t, C-5'), 19.1 (t, C-3'), 18.0 (q, 6 C, CH₃ TIPS), 13.6 (q, C-6'), 12.1 (d, 3 C, CH TIPS) ppm. MS (ESI): *m/z* (%) = 909 [2M + K]⁺ (43), 893 [2M + Na]⁺ (100), 458 [M + Na]⁺ (26).

tert-Butyl (3S)-6-(Phenylethynyl)-3-(triisopropylsilyloxy)-3,4-dihydro-2H-pyridine-1-carboxylate (8d): Yellow oil (314 mg, 69%). *R*_f = 0.13 (*n*-hexane/EtOAc, 20:1 + 1% Et₃N). [α]_D²⁰ = +22.5 (*c* = 2.03,

CHCl₃). ¹H NMR (400 MHz): δ = 7.45–7.32 (m, 2 H, Ph), 7.33–7.27 (m, 3 H, Ph), 5.60 (t, *J* = 4.1 Hz, 1 H, 5-H), 4.13–4.08 (m, 1 H, 3-H), 3.87 (dd, *J* = 12.5, 2.7 Hz, 1 H, 2-H), 3.36 (dd, *J* = 12.5, 8.0 Hz, 1 H, 2-H'), 2.53 (dt, *J* = 19.1, 5.3 Hz, 1 H, 4-H), 2.18 (ddd, *J* = 19.1, 5.6, 4.1 Hz, 1 H, 4-H'), 1.49 [s, 9 H, C(CH₃)₃], 1.11–1.02 (m, 21 H, TIPS) ppm. ¹³C NMR (100.4 MHz): δ = 153.0 (s, C=O), 131.3 (d, 2 C, Ph), 128.3 (d, 2 C, Ph), 128.0 (d, Ph), 123.3 (s, C-6), 122.1 (s, Ph), 120.5 (d, C-5), 87.8 (s, C-1'), 86.3 (s, C-2'), 81.1 [s, C(CH₃)₃], 65.1 (d, C-3), 50.0 (t, C-2), 34.7 (t, C-4), 28.2 (q, 3 C, CH₃ Boc), 18.0 (q, 6 C, CH₃ TIPS), 12.3 (d, 3 C, CH TIPS) ppm. MS (ESI): *m/z* (%) = 933 [2M + Na]⁺ (100), 478 [M + Na]⁺ (12), 456 [M + 1]⁺ (11).

tert-Butyl 6-(Trimethylsilyl-ethynyl)-3,4-dihydro-2H-pyridine-1-carboxylate (22a): Colourless oil (229 mg, 82%). *R*_f = 0.63 (petroleum ether/EtOAc, 9:1 + 1% Et₃N). ¹H NMR (200 MHz): δ = 5.63 (t, *J* = 4.0 Hz, 1 H, 5-H), 3.57–3.52 (m, 2 H, 2-H), 2.16 (td, *J* = 6.9, 4.1 Hz, 2 H, 4-H), 1.83–1.71 (m, 2 H, 3-H), 1.52 [s, 9 H, C(CH₃)₃], 0.19 [s, 9 H, Si(CH₃)₃] ppm. ¹³C NMR (50.33 MHz): δ = 153.2 (s, C=O), 124.0 (s, C-6), 122.5 (d, C-5), 101.9 (s, C-2'), 91.9 (s, C-1'), 81.4 [s, C(CH₃)₃], 43.2 (t, C-2), 28.3 (q, 3 C, CH₃ Boc), 23.7 (t, C-4), 22.7 (t, C-3), –0.1 [q, 3 C, Si(CH₃)₃] ppm. MS: *m/z* (%) = 279 [M]⁺ (23), 223 (92), 206 (15), 179 (87), 178 (100), 164 (72), 57 (56).

Benzyl 6-(Hex-1-ynyl)-3,4-dihydro-2H-pyridine-1-carboxylate (13a): Colourless oil (720 mg, 81%). *R*_f = 0.11 (*n*-hexane/EtOAc, 20:1 + 1% Et₃N). ¹H NMR (400 MHz): δ = 7.42–7.27 (m, 5 H), 5.52 (t, *J* = 3.9 Hz, 1 H, 3-H), 5.20 (s, 2 H, CH₂Ph), 3.65–3.62 (m, 2 H, 6-H), 2.21–2.13 (m, 4 H, 4-H, 3'-H), 1.82–1.75 (m, 2 H, 5-H), 1.45–1.31 (m, 4 H, 4'-H, 5'-H), 0.87 (t, *J* = 7.0 Hz, 3 H, 6'-H) ppm. ¹³C NMR (100.4 MHz): δ = 153.9 (s, C=O), 136.4 (s, Ph), 128.3 (d, 2 C, Ph), 127.9 (d, 2 C, Ph), 127.8 (d, Ph), 122.2 (s, C-6), 121.9 (d, C-5), 89.1 (s, C-1'), 77.1 (s, C-2'), 67.5 (t, CH₂Ph), 44.0 (t, C-2), 30.6 (t, C-4'), 23.5 (t, C-4), 22.6 (t, C-3), 22.0 (t, C-5'), 18.9 (t, C-3'), 13.6 (q, C-6') ppm. MS (ESI): *m/z* (%) = 617 [2M + Na]⁺ (100), 320 [M + Na]⁺ (12), 298 [M + 1]⁺ (31).

Benzyl 6-(Phenylethynyl)-3,4-dihydro-2H-pyridine-1-carboxylate (13b): Pale yellow oil (260 mg, 82%). *R*_f = 0.21 (*n*-hexane/EtOAc, 20:1 + 1% Et₃N). ¹H NMR (400 MHz): δ = 7.42–7.39 (m, 2 H, Ph), 7.29–7.23 (m, 8 H, Ph), 5.73 (t, *J* = 4.1 Hz, 1 H, 5-H), 5.24 (s, 2 H, CH₂Ph), 3.73–3.70 (m, 2 H, 2-H), 2.25 (td, *J* = 6.8, 4.1 Hz, 2 H, 4-H), 1.88–1.83 (m, 2 H, 3-H) ppm. ¹³C NMR (100.4 MHz): δ = 153.9 (s, C=O), 136.2 (s, Ph), 131.4 (d, 2 C, Ph), 128.4 (d, 2 C, Ph), 128.1 (d, 2 C, Ph), 128.04 (d, 2 C, Ph), 128.02 (d, Ph), 127.9 (d, Ph), 123.4 (d, C-5), 123.1 (s, C-6), 122.0 (s, Ph), 88.1 (s, C-1'), 86.1 (s, C-2'), 67.8 (t, CH₂Ph), 44.0 (t, C-2), 23.7 (t, C-4), 22.5 (t, C-3) ppm. MS (ESI): *m/z* (%) = 657 [2M + Na]⁺ (100), 318 [M + 1]⁺ (30).

Benzyl 6-(Triethylsilyl-ethynyl)-3,4-dihydro-2H-pyridine-1-carboxylate (13c): Colourless oil (709 mg, 82%). *R*_f = 0.25 (*n*-hexane/EtOAc, 20:1 + 1% Et₃N). ¹H NMR (400 MHz): δ = 7.42–7.40 (m, 2 H, Ph), 7.39–7.28 (m, 3 H, Ph), 5.70 (t, *J* = 4.1 Hz, 1 H, 5-H), 5.21 (s, 2 H, CH₂Ph), 3.65–3.62 (m, 2 H, 2-H), 2.18 (td, *J* = 6.6, 4.1 Hz, 2 H, 4-H), 1.82–1.72 (m, 2 H, 3-H), 1.24 (s, 9 H, Si(CH₂CH₃)₃), 0.57 [q, *J* = 8.0 Hz, 6 H, Si(CH₂CH₃)₃] ppm. ¹³C NMR (100.4 MHz): δ = 153.9 (s, C=O), 136.5 (s, Ph), 128.3 (d, 2 C, Ph), 127.8 (d, 2 C, Ph), 127.7 (d, Ph), 124.5 (s, C-6), 122.0 (d, C-5), 102.2 (s, C-2'), 90.6 (s, C-1'), 67.3 (t, CH₂Ph), 43.8 (t, C-2), 23.6 (t, C-4), 22.5 (t, C-3), 7.4 [q, 3 C, Si(CH₂CH₃)₃], 4.3 [t, 3 C, Si(CH₂CH₃)₃] ppm. MS (ESI): *m/z* (%) = 733 [2M + Na]⁺ (100), 356 [M + 1]⁺ (30).

tert-Butyl 7-(Hex-1-ynyl)-2,3,4,5-tetrahydroazepine-1-carboxylate (11a): Colourless oil (194 mg, 70%). *R*_f = 0.24 (*n*-hexane/EtOAc, 20:1 + 1% Et₃N). ¹H NMR (200 MHz): δ = 5.81 (t, *J* = 6.6 Hz, 1

FULL PAPER

D. Scarpi, E. G. Occhiato et al.

H, 6-H), 3.42 (t, $J = 5.3$ Hz, 2 H, 2-H), 2.28 (t, $J = 6.8$ Hz, 2 H, 3'-H), 2.19–2.10 (m, 2 H, 5-H), 1.78–1.66 (m, 2 H, 4-H), 1.66–1.35 (m, 6 H, 3-H, 4'-H, 5'-H), 1.46 [s, 9 H, C(CH₃)₃], 0.89 (t, $J = 6.9$ Hz, 3 H, 6'-H) ppm. ¹³C NMR (50.33 MHz): $\delta = 153.6$ (s, C=O), 131.0 (s, C-7), 127.8 (d, C-6), 87.3 (s, C-2'), 80.0 [s, C(CH₃)₃], 78.5 (s, C-1'), 47.2 (t, C-2), 30.7 (t, C-4'), 29.6 (t, C-5), 28.3 [q, 3 C, C(CH₃)₃], 27.5 (t, C-4), 23.8 (t, C-3), 22.0 (t, C-5'), 19.0 (t, C-3'), 13.5 (q, C-6') ppm. MS: m/z (%) = 277 [M]⁺ (4), 221 (61), 179 (68), 162 (65), 148 (57), 135 (87), 57 (100).

tert-Butyl 7-(Phenylethynyl)-2,3,4,5-tetrahydroazepine-1-carboxylate (11b): Yellow oil (205 mg, 69%). $R_f = 0.21$ (*n*-hexane/EtOAc, 20:1 + 1% Et₃N). ¹H NMR (200 MHz): $\delta = 7.44$ –7.37 (m, 2 H, Ph), 7.32–7.28 (m, 3 H, Ph), 6.02 (t, $J = 6.6$ Hz, 1 H, 6-H), 3.54–3.49 (m, 2 H, 2-H), 2.29–2.20 (m, 2 H, 5-H), 1.83–1.72 (m, 2 H, 4-H), 1.58–1.45 (m, 2 H, 3-H), 1.48 [s, 9 H, C(CH₃)₃] ppm. ¹³C NMR (50.33 MHz): $\delta = 153.3$ (s, C=O), 132.4 (d, Ph), 131.1 (d, 2 C, Ph), 128.1 (d, 2 C, Ph), 127.8 (d, C-6), 127.3 (s, Ph), 123.0 (s, C-7), 87.5 (s, C-2'), 86.4 (s, C-1'), 80.1 [s, C(CH₃)₃], 47.2 (t, C-2), 29.4 (t, C-5), 28.2 [q, 3 C, C(CH₃)₃], 27.6 (t, C-4), 23.6 (t, C-3) ppm. MS: m/z (%) = 297 [M]⁺ (3), 241 (100), 197 (67), 196 (99), 182 (47), 169 (54).

tert-Butyl 7-(Cyclopropylethynyl)-2,3,4,5-tetrahydroazepine-1-carboxylate (11c): Colourless oil (196 mg, 75%). $R_f = 0.30$ (*n*-hexane/EtOAc, 20:1 + 1% Et₃N). ¹H NMR (200 MHz): $\delta = 5.81$ (t, $J = 6.5$ Hz, 1 H, 6-H), 3.44–3.39 (m, 2 H, 2-H), 2.18–2.09 (m, 2 H, 5-H), 1.77–1.66 (m, 2 H, 4-H), 1.52–1.40 (m, 2 H, 3-H), 1.47 [s, 9 H, C(CH₃)₃], 1.37–1.24 (m, 1 H, 3'-H), 0.83–0.64 (m, 4 H, 4'-H) ppm. ¹³C NMR (50.33 MHz): $\delta = 153.5$ (s, C=O), 131.0 (d, C-6), 127.7 (s, C-7), 90.2 (s, C-2'), 80.0 [s, C(CH₃)₃], 73.9 (s, C-1'), 47.3 (t, C-2), 29.6 (t, C-5), 28.4 [q, 3 C, C(CH₃)₃], 27.5 (t, C-4), 23.8 (t, C-3), 8.2 (t, 2 C, C-4'), -0.1 (d, C-3') ppm. MS: m/z (%) = 261 [M]⁺ (10), 205 (100), 204 (41), 160 (44), 57 (43).

tert-Butyl (3S)-6-(Hex-1-ynyl)-3-hydroxy-3,4-dihydro-2H-pyridine-1-carboxylate (8e): TBAF (1 M solution in THF; 1.94 mL, 1.94 mmol) was slowly added to a solution of **8c** (740 mg, 1.7 mmol) in anhydrous THF (82 mL), under a nitrogen atmosphere. After 30 min, the solvent was evaporated under vacuum, and the residue was dissolved in Et₂O (82 mL). The solvent was evaporated again, and the residue was purified by flash chromatography (*n*-hexane/EtOAc, 2:1 + 1% Et₃N; $R_f = 0.24$) to give pure **8e** (410 mg, 86%). $[\alpha]_D^{25} = -10.6$ ($c = 0.97$, CHCl₃). ¹H NMR (400 MHz): $\delta = 5.40$ (t, $J = 3.9$ Hz, 1 H, 5-H), 4.07–4.02 (m, 1 H, 3-H), 3.56 (AB system, $J_{AB} = 12.8$ Hz, 1 H, 2-H), 3.54 (AB system, $J_{AB} = 12.8$ Hz, 1 H, 2-H'), 2.53 (br. s, 1 H, OH), 2.44 (dt, $J = 19.1$, 4.3 Hz, 1 H, 4-H), 2.29 (t, $J = 7$ Hz, 2 H, 3'-H), 2.09 (dt, $J = 19.1$, 4.7 Hz, 1 H, 4-H'), 1.54–1.45 (m, 2 H, 4'-H), 1.47 [s, 9 H, C(CH₃)₃], 1.44–1.36 (m, 2 H, 5'-H), 0.89 (t, $J = 7.4$ Hz, 3 H, 6'-H) ppm. ¹³C NMR (100.4 MHz): $\delta = 153.8$ (s, C=O), 122.4 (s, C-6), 118.6 (d, C-5), 88.8 (s, C-1'), 81.2 [s, C(CH₃)₃], 77.0 (s, C-2'), 64.3 (d, C-3), 49.2 (t, C-2), 32.8 (t, C-4), 30.6 (t, C-4'), 28.2 (q, 3 C, CH₃ Boc), 22.0 (t, C-5'), 19.0 (t, C-3'), 13.6 (q, C-6') ppm. MS (ESI): m/z (%) = 597 [2M + K]⁺ (24), 581 [2M + Na]⁺ (100), 302 [M + Na]⁺ (21).

tert-Butyl 6-Ethynyl-3,4-dihydro-2H-pyridine-1-carboxylate (22b): Prepared as described for **8e**, starting from **22a** (279 mg, 1.0 mmol), to give, after purification by flash chromatography (petroleum ether/EtOAc, 9:1; $R_f = 0.50$), pure **22b** (205 mg, 99%) as a colourless oil. ¹H NMR (200 MHz): $\delta = 5.65$ (t, $J = 4.0$ Hz, 1 H, 5-H), 3.59–3.54 (m, 2 H, 2-H), 2.93 (s, 1 H, 2'-H), 2.21–2.12 (m, 2 H, 4-H), 1.84–1.72 (m, 2 H, 3-H), 1.50 [s, 9 H, C(CH₃)₃] ppm. ¹³C NMR (50.33 MHz): $\delta = 152.9$ (s, C=O), 123.8 (s, C-6), 121.5 (d, C-5), 81.5 (s, C-1'), 80.6 [s, C(CH₃)₃], 75.9 (d, C-2'), 43.4 (t, C-2), 28.3 (q, 3 C, CH₃ Boc), 23.6 (t, C-4), 22.5 (t, C-3) ppm. MS: m/z (%) =

207 [M]⁺ (22), 151 (65), 134 (29), 107 (81), 106 (71), 92 (41), 79 (12), 57 (100), 41 (26).

tert-Butyl (3R)-3-Azido-6-(hex-1-ynyl)-3,4-dihydro-2H-pyridine-1-carboxylate (8f): Compound **8e** (280 mg, 1.00 mmol) and triethylamine (180 μ L, 1.3 mmol) were dissolved in anhydrous CH₂Cl₂ (1.44 mL), and the solution was cooled to –30 °C. MsCl (103 μ L, 1.3 mmol) was added dropwise. After 5 min, the cooling bath was removed, and the reaction mixture was stirred for 2 h at room temperature. Then KHSO₄ (5% aq.; 6 mL) was added dropwise, and after 10 min, the mixture was extracted with CH₂Cl₂ (3 \times 5 mL). The combined organic layers were washed with water (3 \times 10 mL), dried with Na₂SO₄, and filtered, and the solvent was evaporated. The residue was purified by flash chromatography (*n*-hexane/EtOAc, 4:1 + 1% Et₃N; $R_f = 0.20$) to give the mesylate (307 mg, 86%) as a pale yellow oil. ¹H NMR (400 MHz): $\delta = 5.36$ (t, $J = 3.9$ Hz, 1 H, 5-H), 5.01–4.98 (m, 1 H, 3-H), 4.06 (dd, $J = 13.7$, 5.9 Hz, 1 H, 2-H), 3.43 (dd, $J = 13.7$, 1.9 Hz, 1 H, 2-H'), 2.99 (s, 3 H, CH₃ Ms), 2.56 (dm, $J = 19.9$ Hz, 1 H, 4-H), 2.38 (dm, $J = 19.9$ Hz, 1 H, 4-H'), 2.28 (t, $J = 7.0$ Hz, 2 H, 3'-H), 1.52–1.43 (m, 2 H, 4'-H), 1.46 [s, 9 H, C(CH₃)₃], 1.42–1.36 (m, 2 H, 5'-H), 0.87 (t, $J = 7.0$ Hz, 3 H, 6'-H) ppm.

The intermediate mesylate (301 mg, 0.84 mmol) was dissolved in anhydrous CH₃CN (2 mL), and 15-crown-5 (34 μ L, 0.17 mmol) and NaN₃ (82 mg, 1.26 mmol) were added under a nitrogen atmosphere. The mixture was heated at reflux for 6 h, and then stirred at room temperature for a further 12 h. The mixture was filtered through a pad of silica/Celite (1:1), and the filtrate was concentrated under vacuum. The residue was purified by flash chromatography (*n*-hexane/EtOAc, 30:1 + 1% Et₃N; $R_f = 0.14$) to give pure **8f** (120 mg, 47%) as a pale yellow oil. $[\alpha]_D^{25} = -21.0$ ($c = 1.16$, CHCl₃). ¹H NMR (400 MHz): $\delta = 5.37$ (t, $J = 3.9$ Hz, 1 H, 5-H), 3.80–3.74 (m, 1 H, 3-H), 3.66–3.57 (m, 2 H, 2-H), 2.47 (ddd, $J = 19.5$, 6.2, 3.9 Hz, 1 H, 4-H), 2.86 (t, $J = 7$ Hz, 2 H, 3'-H), 2.15 (dt, $J = 19.5$, 4.7 Hz, 1 H, 4-H'), 1.53–1.44 (m, 2 H, 4'-H), 1.48 [s, 9 H, C(CH₃)₃], 1.43–1.35 (m, 2 H, 5'-H), 0.88 (t, $J = 7.0$ Hz, 3 H, 6'-H) ppm. ¹³C NMR (100.4 MHz): $\delta = 153.0$ (s, C=O), 122.9 (s, C-6), 117.2 (d, C-5), 89.2 (s, C-1'), 81.4 [s, C(CH₃)₃], 76.7 (s, C-2'), 54.4 (d, C-3), 46.3 (t, C-2), 30.5 (t, C-4), 29.4 (t, C-4'), 28.1 (q, 3 C, CH₃ Boc), 21.9 (t, C-5'), 18.9 (t, C-3'), 13.5 (q, C-6') ppm. MS (ESI): m/z (%) = 631 [2M + Na]⁺ (100), 343 [M + K]⁺ (8), 327 [M + Na]⁺ (35).

Gold-Catalysed Rearrangement and Hydrolysis Procedure: A volume of the enyne solution containing 1 mmol of substrate was concentrated and dried under vacuum (no heating) for 30 min, and then the enyne was dissolved in anhydrous toluene (5 mL). Ph₃PAuCl (0.005 mmol) was dissolved in anhydrous toluene (5 mL) in a two-necked round-bottomed flask, and then Cu(OTf)₂ (0.05 mmol) was added to this solution under a nitrogen atmosphere. After 15 min, the solution of the enyne was added, and the resulting mixture was heated at reflux until the starting material had disappeared (TLC, usually 30 min.). The mixture was cooled to 85 °C (external), and *tert*-butyl alcohol (10 mL) was added, followed by powdered KOH (6 mmol). The mixture was heated at 85 °C until the reaction was complete (TLC, usually 15 min.). The mixture was then cooled to room temp., water (15 mL) was added, and the mixture was extracted with EtOAc (3 \times 10 mL). The combined organic extracts were washed once with brine (15 mL), dried with anhydrous Na₂SO₄, and filtered, and the solvent was evaporated. The crude vinylogous amide (**12a–12e**, **12g–12i**) was purified by flash chromatography to give the pure compound.

(±)-1-(4-Methylpiperidin-2-ylidene)hexan-2-one (12a): Pale yellow solid (133 mg, 68%). $R_f = 0.23$ (*n*-hexane/EtOAc, 7:1). Mp 52.6–

54.1 °C. $^1\text{H NMR}$ (400 MHz): δ = 11.09 (br. s, 1 H, *NH*), 4.81 (s, 1 H, 1'-H), 3.39–3.34 (m, 1 H, 6-H), 3.28–3.21 (m, 1 H, 6'-H), 2.33–2.79 (m, 1 H, 3-H'), 2.15 (t, J = 7.4 Hz, 2 H, 3'-H), 1.98 (dd, J = 17.1, 10.5 Hz, 1 H, 3-H'), 1.82–1.73 (m, 2 H, 4-H, 5-H'), 1.55–1.48 (m, 2 H, 4'-H), 1.40–1.24 (m, 3 H, 5-H, 5'-H), 0.96 (d, J = 6.3 Hz, 3 H, CH_3), 0.85 (t, J = 7.0 Hz, 3 H, 6'-H) ppm. $^{13}\text{C NMR}$ (100.4 MHz): δ = 197.4 (s, C-2'), 163.6 (s, C-2), 92.8 (d, C-1'), 41.5 (t, C-6), 40.7 (t, C-3'), 36.7 (d, C-4), 30.1 (t, C-5), 28.5 (t, C-3), 25.8 (t, C-4'), 22.6 (t, C-5'), 21.2 (q, CH_3), 13.8 (q, C-6') ppm. IR (KBr): $\tilde{\nu}$ = 1611 (CO), 1572 (C=C) cm^{-1} . MS (ESI): m/z (%) = 413 [2M + Na] $^+$ (100), 196 [M + 1] $^+$ (44). MS/MS (ESI of [M + 1] $^+$): m/z (%) = 178 (5), 112 (100). $\text{C}_{12}\text{H}_{21}\text{NO}$ (195.30): calcd. C 73.80, H 10.84, N 7.17; found C 73.75, H 10.97, N 7.30.

(\pm)-1-(6-Methylpiperidin-2-ylidene)hexan-2-one (12b): Orange oil (111 mg, 57%). R_f = 0.13 (*n*-hexane/EtOAc, 7:1). $^1\text{H NMR}$ (400 MHz): δ = 11.06 (br. s, 1 H, *NH*), 4.81 (s, 1 H, 1'-H), 3.45–3.37 (m, 1 H, 6-H), 2.31–2.26 (m, 2 H, 3-H), 2.17 (t, J = 7.5 Hz, 2 H, 3'-H), 1.91–1.84 (m, 1 H, 5-H), 1.80–1.72 (m, 1 H, 4-H), 1.63–1.49 (m, 3 H, 4-H', 4'-H), 1.36–1.24 (m, 3 H, 5-H', 5'-H), 1.20 (d, J = 6.5 Hz, 3 H, CH_3), 0.86 (t, J = 7.4 Hz, 3 H, 6'-H) ppm. $^{13}\text{C NMR}$ (100.4 MHz): δ = 197.3 (s, C-2'), 163.6 (s, C-2), 92.5 (d, C-1'), 47.3 (d, C-6), 41.5 (t, C-3'), 30.6 (t, C-5), 28.3 (t, C-3), 28.1 (t, C-4'), 22.6 (t, C-5'), 22.5 (t, C-4), 18.9 (q, CH_3), 13.9 (q, C-6') ppm. MS (ESI): m/z (%) = 413 [2M + Na] $^+$ (100), 218 [M + Na] $^+$ (17), 196 [M + 1] $^+$ (65). MS/MS (ESI of [M + 1] $^+$): m/z (%) = 111 (100), 94 (3). $\text{C}_{12}\text{H}_{21}\text{NO}$ (195.30): calcd. C 73.80, H 10.84, N 7.17; found C 73.61, H 10.93, N 7.14.

(5S)-1-(5-Triisopropylsilyloxy piperidin-2-ylidene)hexan-2-one (12c): Yellow oil (219 mg, 62%). R_f = 0.24 (*n*-hexane/EtOAc, 10:1). $[\alpha]_D^{20}$ = -25.4 (c = 0.98, CHCl_3). $^1\text{H NMR}$ (400 MHz): δ = 11.02 (br. s, 1 H, *NH*), 4.99 (br. s, 1 H, 1'-H), 4.17–4.12 (m, 1 H, 5-H), 3.48 (dd, J = 13.2, 4.0 Hz, 1 H, 6-H), 3.21 (dd, J = 13.2, 5.8 Hz, 1 H, 6-H'), 2.64 (ddd, J = 17.5, 7.8, 5.9 Hz, 1 H, 3-H), 2.31 (ddd, J = 17.5, 7.1, 5.9 Hz, 1 H, 3-H'), 2.21–2.18 (m, 2 H, 3'-H), 1.91–1.84 (m, 1 H, 4-H), 1.80–1.71 (m, 1 H, 4-H'), 1.57–1.55 (m, 2 H, 4'-H), 1.37–1.25 (m, 2 H, 5'-H), 1.10–0.96 (m, 21 H, TIPS), 0.88 (t, J = 7.4 Hz, 3 H, 6'-H) ppm. $^{13}\text{C NMR}$ (100.4 MHz): δ = 197.9 (s, C-2'), 163.0 (s, C-2), 93.1 (d, C-1'), 64.7 (d, C-5), 48.3 (t, C-6), 41.6 (t, C-3'), 28.4 (t, C-4'), 28.3 (t, C-3), 25.4 (t, C-4), 22.6 (t, C-5'), 17.9 (q, 6 C, CH_3 TIPS), 13.9 (q, C-6'), 12.1 (d, 3 C, CH TIPS) ppm. IR (neat): $\tilde{\nu}$ = 1610 (CO), 1574 (C=C) cm^{-1} . MS (ESI): m/z (%) = 729 [2M + Na] $^+$ (69), 707 [2M + 1] $^+$ (14), 706 [2M] $^+$ (33), 354 [M + 1] $^+$ (100). MS/MS (ESI of [M + 1] $^+$): m/z (%) = 354 (4), 270 (5), 180 (100), 162 (9). $\text{C}_{20}\text{H}_{39}\text{NO}_2\text{Si}$ (353.61): calcd. C 67.93, H 11.12, N 3.96; found C 67.63, H 11.21, N 3.77.

(5S)-1-Phenyl-2-(5-triisopropylsilyloxy piperidin-2-ylidene)ethanone (12d): Yellow oil (119 mg, 63%). R_f = 0.10 (*n*-hexane/EtOAc, 10:1). $[\alpha]_D^{20}$ = -12.3 (c = 1.49, CHCl_3). $^1\text{H NMR}$ (400 MHz): δ = 11.61 (br. s, 1 H, *NH*), 7.85–7.83 (m, 2 H, Ph), 7.40–7.35 (m, 3 H, Ph), 5.62 (s, 1 H, 1'-H), 4.23–4.20 (m, 1 H, 5-H), 3.56 (dt, J = 13.3, 2.9 Hz, 1 H, 6-H), 3.30 (ddd, J = 13.3, 5.3, 2.0 Hz, 1 H, 6-H'), 2.80 (ddd, J = 17.4, 8.0, 6.1 Hz, 1 H, 4-H), 2.45 (dt, J = 17.4, 6.2 Hz, 1 H, 4-H'), 1.95–1.89 (m, 1 H, 3-H), 1.88–1.81 (m, 1 H, 3-H'), 1.12–1.04 (m, 21 H, TIPS) ppm. $^{13}\text{C NMR}$ (100.4 MHz): δ = 187.2 (s, C-2'), 165.0 (s, C-2), 140.5 (s, Ph), 130.2 (d, Ph), 128.1 (d, 2 C, Ph), 126.8 (d, 2 C, Ph), 90.1 (d, C-1'), 64.6 (d, C-5), 48.6 (t, C-6), 28.3 (t, C-3), 25.9 (t, C-4), 18.0 (q, 6 C, CH_3 TIPS), 12.2 (d, 3 C, CH TIPS) ppm. IR (CHCl_3): $\tilde{\nu}$ = 1604 (CO), 1538 (C=C) cm^{-1} . MS (ESI): m/z (%) = 769 [2M + Na] $^+$ (100), 746 [2M] $^+$ (72), 374 [M + 1] $^+$ (66). $\text{C}_{22}\text{H}_{35}\text{NO}_2\text{Si}$ (373.60): calcd. C 70.73, H 9.44, N 3.75; found C 70.59, H 9.72, N 3.91.

(5S)-1-(5-Hydroxypiperidin-2-ylidene)hexan-2-one (12e): Yellow oil (128 mg, 65%). R_f = 0.19 (*n*-hexane/EtOAc, 3:1). $[\alpha]_D^{20}$ = -16.5 (c

= 1.34, CHCl_3). $^1\text{H NMR}$ (400 MHz): δ = 10.95 (br. s, 1 H, *NH*), 4.89 (s, 1 H, 1'-H), 4.29 (br. s, 1 H, *OH*), 4.08–4.02 (m, 1 H, 5-H), 3.44 (br. d, J = 13.3 Hz, 1 H, 6-H), 3.17 (dd, J = 13.3, 5.5 Hz, 1 H, 6-H'), 2.57 (ddd, J = 17.5, 7.4, 5.8 Hz, 1 H, 3-H), 2.30 (dt, J = 17.5, 6.6 Hz, 1 H, 3-H'), 2.13 (t, J = 7.8 Hz, 2 H, 3'-H), 1.89–1.83 (m, 1 H, 4-H), 1.76–1.69 (m, 1 H, 4-H'), 1.53–1.45 (m, 2 H, 4'-H), 1.32–1.22 (m, 2 H, 5'-H), 0.85 (t, J = 7.4 Hz, 3 H, 6'-H) ppm. $^{13}\text{C NMR}$ (100.4 MHz): δ = 197.5 (s, C-2'), 163.8 (s, C-2), 92.8 (d, C-1'), 63.3 (d, C-5), 47.6 (t, C-6), 41.5 (t, C-3'), 28.6 (t, C-3), 27.2 (t, C-4'), 25.4 (t, C-4), 22.5 (t, C-5'), 13.8 (q, C-6') ppm. IR (neat): $\tilde{\nu}$ = 3346 (br., OH), 1607 (CO), 1548 (C=C) cm^{-1} . MS (ESI): m/z (%) = 417 [2M + Na] $^+$ (100), 220 [M + Na] $^+$ (14), 198 [M + 1] $^+$ (17). MS/MS (ESI of [M + 1] $^+$): m/z (%) = 198 (22), 180 (100), 162 (34), 113 (58), 95 (21). $\text{C}_{11}\text{H}_{19}\text{NO}_2$ (197.27): calcd. C 66.97, H 9.71, N 7.10; found C 67.37, H 10.00, N 7.03.

1-Azepan-2-ylidenehexan-2-one (12g): Colourless oil (142 mg, 73%). R_f = 0.25 (*n*-hexane/EtOAc, 3:1). $^1\text{H NMR}$ (200 MHz): δ = 11.0 (br. s, 1 H, *NH*), 4.96 (s, 1 H, 1'-H), 3.36–3.28 (m, 2 H, 7-H), 2.32–2.19 (m, 4 H, 3-H, 3'-H), 1.68–1.28 (m, 10 H, 4-H, 5-H, 6-H, 4'-H, 5'-H), 0.90 (t, J = 7.2 Hz, 3 H, 6'-H) ppm. $^{13}\text{C NMR}$ (50.33 MHz): δ = 198.7 (s, C-2'), 169.6 (s, C-2), 93.6 (d, C-1'), 44.2 (t, C-7), 41.9 (t, C-3'), 34.9 (t, C-3), 30.6 (t, C-6), 29.5 (t, C-5), 28.5 (t, C-4'), 26.0 (t, C-4), 22.7 (t, C-5'), 14.0 (q, C-6') ppm. MS: m/z (%) = 195 [M] $^+$ (23), 138 (100), 111 (35). $\text{C}_{12}\text{H}_{21}\text{NO}$ (195.30): calcd. C 73.80, H 10.84, N 7.17; found C 74.01, H 10.90, N 7.03.

2-Azepan-2-ylidene-1-phenylethanone (12h): Yellow oil (140 mg, 65%). R_f = 0.22 (*n*-hexane/EtOAc, 3:1). $^1\text{H NMR}$ (200 MHz): δ = 11.54 (br. s, 1 H, *NH*), 7.90–7.82 (m, 2 H, Ph), 7.42–7.35 (m, 3 H, Ph), 5.67 (s, 1 H, 1'-H), 3.45–3.37 (m, 2 H, 7-H), 2.47–2.42 (m, 2 H, 3-H), 1.80–1.60 (m, 6 H, 4-H, 5-H, 6-H) ppm. $^{13}\text{C NMR}$ (50.33 MHz): δ = 188.1 (s, C-2'), 171.3 (s, C-2), 140.6 (s, Ph), 130.3 (d, Ph), 128.0 (d, 2 C, Ph), 126.8 (d, 2 C, Ph), 91.0 (d, C-1'), 44.4 (t, C-7), 35.3 (t, C-3), 30.5 (t, C-6), 29.3 (t, C-5), 25.8 (t, C-4) ppm. MS: m/z (%) = 215 [M] $^+$ (81), 214 (100), 186 (22), 105 (24). $\text{C}_{14}\text{H}_{17}\text{NO}$ (215.29): calcd. C 78.10, H 7.96, N 6.51; found C 77.92, H 7.90, N 6.24.

2-Azepan-2-ylidene-1-cyclopropylethanone (12i): Colourless oil (108 mg, 60%). R_f = 0.31 (*n*-hexane/EtOAc, 3:1). $^1\text{H NMR}$ (200 MHz): δ = 10.89 (br. s, 1 H, *NH*), 5.12 (s, 1 H, 1'-H), 3.34–3.26 (m, 2 H, 7-H), 2.34–2.29 (m, 2 H, 3-H), 1.78–1.54 (m, 7 H, 4-H, 5-H, 6-H, 3'-H), 0.99–0.90 (m, 2 H, 4'-H), 0.82–0.66 (m, 2 H, 4'-H') ppm. $^{13}\text{C NMR}$ (50.33 MHz): δ = 197.1 (s, C-2'), 168.7 (s, C-2), 93.6 (d, C-1'), 44.2 (t, C-7), 35.0 (t, C-3), 30.6 (t, C-6), 29.5 (t, C-5), 26.0 (t, C-4), 19.8 (d, C-3'), 8.61 (t, 2 C, C-4') ppm. MS: m/z (%) = 179 [M] $^+$ (80), 138 (100). $\text{C}_{11}\text{H}_{17}\text{NO}$ (179.26): calcd. C 73.70, H 9.56, N 7.81; found C 73.44, H 9.82, N 8.05.

1-(1,4,5,6-Tetrahydropyridin-2-yl)ethanone (23):^[44] Pale yellow oil (22 mg, 35%). $^1\text{H NMR}$ (200 MHz): 2:1 mixture of isomers A and B): δ = 5.61 (t, J = 4.4 Hz, 1 H, 2-H, A), 4.19 (br. s, 1 H, NH, A), 3.84–3.79 (m, 2 H, 5-H, B), 3.14 (t, J = 5.3 Hz, 2 H, 5-H, A), 2.38–2.31 (m, 2 H, 2-H, B), 2.33 (s, 3 H, CH_3 , B), 2.31–2.20 (m, 2 H, 3-H, A), 2.26 (s, 3 H, CH_3 , A), 1.85–1.73 (m, 2 H, 4-H, A), 1.73–1.54 (m, 4 H, 3-H, 4-H, B) ppm.

(5R)-1-(5-Azidopiperidin-2-ylidene)hexan-2-one (12f): A volume of the enyne solution containing 1 mmol of substrate was concentrated and dried under vacuum (no heating) for 30 min, and then the enyne was dissolved in anhydrous toluene (5 mL). Separate solutions in anhydrous toluene of AgOTf (0.2 m) and of Ph_3PAuCl (4 mM) were prepared. The AgOTf solution (100 μL , 0.02 mmol) was added at room temp. to the Ph_3PAuCl solution (5 mL, 0.02 mmol) while stirring under a nitrogen atmosphere, and a white precipitate immediately formed. The solution of enyne 8f

FULL PAPER

D. Scarpi, E. G. Occhiato et al.

(1.0 mmol) in anhydrous toluene (5 mL) was then added, and the resulting mixture was heated at reflux until the starting material had disappeared (TLC, 30 min). The mixture was cooled to 85 °C (external), and *tert*-butyl alcohol (10 mL) was added, followed by powdered KOH (6 mmol). The mixture heated at 85 °C until the reaction was complete (TLC, 10 min.). The mixture was cooled to room temperature, then water (15 mL) was added, and the mixture was extracted with EtOAc (3 × 10 mL). The combined organic extracts were washed once with brine (15 mL), dried with anhydrous Na₂SO₄, and filtered, and the solvent was evaporated. The residue was purified by flash chromatography (*n*-hexane/EtOAc, 3:1; *R_f* = 0.24) to give pure vinylogous amide **12f** (142 mg, 64%) as a colourless oil. $[\alpha]_D^{25} = -11.5$ ($c = 0.92$, CHCl₃). ¹H NMR (400 MHz): $\delta = 10.99$ (br. s, 1 H, NH), 4.93 (s, 1 H, 1'-H), 3.89–3.83 (m, 1 H, 5-H), 3.49 (ddd, $J = 13.3, 4.7, 2.3$ Hz, 1 H, 6-H), 3.23 (ddd, $J = 13.3, 6.2, 1.9$ Hz, 1 H, 6'-H), 2.55 (ddd, $J = 17.6, 7.8, 5.9$ Hz, 1 H, 3-H), 2.36 (ddd, $J = 17.6, 7.4, 6.3$ Hz, 1 H, 3'-H), 2.22–2.18 (m, 2 H, 3'-H), 2.03–1.95 (m, 1 H, 4-H), 1.85–1.76 (m, 1 H, 4'-H), 1.57–1.50 (m, 2 H, 4'-H), 1.35–1.28 (m, 2 H, 5'-H), 0.88 (t, $J = 7.4$ Hz, 3 H, 6'-H) ppm. ¹³C NMR (100.4 MHz): $\delta = 198.5$ (s, C-2'), 161.4 (s, C-2), 93.5 (d, C-1'), 54.4 (d, C-5), 44.5 (t, C-6), 41.7 (t, C-3'), 28.3 (t, C-3), 25.4 (t, C-4), 24.6 (t, C-4'), 22.6 (t, C-5'), 13.9 (q, C-6') ppm. IR (neat): $\tilde{\nu} = 2106$ (N₃), 1614 (CO), 1574 (C=C) cm⁻¹. MS (ESI): m/z (%) = 467 [2M + Na]⁺ (100), 245 [M + Na]⁺ (38), 223 [M + 1]⁺ (18). MS/MS (ESI of [M + 1]⁺): m/z (%) = 166 (94), 110 (32), 93 (100), 81 (93). C₁₁H₁₈N₄O (222.29): calcd. C 59.44, H 8.16, N 25.20; found C 59.83, H 7.82, N 24.98.

Benzyl 2-(Hex-1-ynyl)piperidine-1-carboxylate (16a): Enyne **13a** (217 mg, 0.73 mmol) was dissolved in anhydrous CH₂Cl₂ (36 mL), and NaBH₃CN (275 mg, 4.37 mmol) was added. The mixture was vigorously stirred at r.t. for 20 min, and then it was cooled to -50 °C. A solution of TFA (561 μ L, 7.28 mmol) in anhydrous CH₂Cl₂ (4.9 mL) was added dropwise, keeping the temperature constant during the addition. The mixture was then warmed to -20 °C, and then stirred at that temperature until the reaction was complete (TLC; 2–3 h). The reaction was then quenched by addition of satd. aq. NaHCO₃ (40 mL). The phases were separated, and the aqueous phase was extracted with CH₂Cl₂ (2 × 20 mL). The combined organic extracts were washed once with satd. aq. NaHCO₃ (40 mL), dried with anhydrous Na₂SO₄, and filtered, and the solvent was evaporated. The residue was purified by flash chromatography (*n*-hexane/EtOAc, 20:1; *R_f* = 0.11) to give pure **16a** (129 mg, 59%) as a colourless oil. ¹H NMR (400 MHz): $\delta = 7.36$ –7.28 (m, 5 H, Ph), 5.18–5.08 (m, 1 H, 2-H), 5.14 (s, 2 H, CH₂Ph), 3.98 (br. d, $J = 12.5$ Hz, 1 H, 6-H), 3.11 (br. t, $J = 12.3$ Hz, 1 H, 6'-H), 2.19 (td, $J = 6.8, 2.0$ Hz, 2 H, 3'-H), 1.81–1.56 (m, 5 H, 3-H, 4-H, 5-H), 1.51–1.36 (m, 5 H, 4'-H, 5'-H, 5-H'), 0.91 (t, $J = 7.2$ Hz, 3 H, 6'-H) ppm. ¹³C NMR (100.4 MHz): $\delta = 155.1$ (s, C=O), 136.9 (s, Ph), 128.4 (d, 2 C, Ph), 127.9 (d, 2 C, Ph), 127.7 (d, Ph), 84.8 (s, C-1'), 77.7 (s, C-2'), 67.1 (t, CH₂Ph), 44.6 (t, C-6), 40.5 (d, C-2), 31.0 (t, C-3), 30.9 (t, C-4'), 25.4 (t, C-5), 21.9 (t, C-5'), 19.9 (t, C-4), 18.3 (t, C-3'), 13.6 (q, C-6') ppm. MS (ESI): m/z (%) = 621 [2M + Na]⁺ (100), 322 [M + Na]⁺ (17), 300 [M + 1]⁺ (4). C₁₉H₂₅NO₂ (299.41): calcd. C 76.22, H 8.42, N 4.68; found C 76.33, H 8.82, N 4.40.

Benzyl 2-(Phenylethynyl)piperidine-1-carboxylate (16b): Prepared as described for **16a**, starting from **13b** (151 mg, 0.47 mmol), to give, after purification by flash chromatography (*n*-hexane/EtOAc, 20:1; *R_f* = 0.21), pure **16b** (93 mg, 62%) as a pale yellow oil. ¹H NMR (400 MHz): $\delta = 7.43$ –7.29 (m, 10 H, Ph), 5.38 (br. s, 1 H, 2-H), 5.17 (s, 2 H, CH₂Ph), 4.05 (br. d, $J = 12.3$ Hz, 1 H, 6-H), 3.21 (br. t, $J = 11.9$ Hz, 1 H, 6'-H), 1.90–1.83 (m, 2 H, 3-H), 1.77–1.67 (m, 3 H, 5-H, 4-H), 1.51–1.42 (m, 1 H, 5-H') ppm. ¹³C NMR

(100.4 MHz): $\delta = 155.0$ (s, C=O), 136.7 (s, Cbz), 131.7 (d, 2 C, Ph), 128.5 (d, Ph), 128.2 (d, 2 C, Ph), 128.1 (d, 2 C, Cbz), 127.9 (d, 2 C, Cbz), 127.7 (d, Cbz), 122.9 (s, Ph), 84.4 (s, C-1'), 77.2 (s, C-2'), 67.2 (t, CH₂Ph), 45.0 (t, C-6), 40.7 (d, C-2), 30.8 (t, C-3), 25.3 (t, C-5), 20.0 (t, C-4) ppm. MS (ESI): m/z (%) = 661 [2M + Na]⁺ (100), 342 [M + Na]⁺ (10), 320 [M + 1]⁺ (3). C₂₁H₂₁NO₂ (319.40): calcd. C 78.97, H 6.63, N 4.39; found C 78.79, H 6.41, N 4.84.

Benzyl 2-(Triethylsilyl)ethylpiperidine-1-carboxylate (16c): Prepared as described for **16a**, starting from **13c** (702 mg, 1.97 mmol), to give, after purification by flash chromatography (*n*-hexane/EtOAc, 20:1; *R_f* = 0.31), pure **16c** (383 mg, 54%) as a colourless oil. ¹H NMR (400 MHz): $\delta = 7.36$ –7.28 (m, 5 H, Ph), 5.25–5.09 (m, 1 H, 2-H), 5.14 (s, 2 H, CH₂Ph), 4.01 (br. d, $J = 11.3$ Hz, 1 H, 6-H), 3.20–3.05 (br. m, 1 H, 6'-H), 1.90–1.74 (m, 2 H, 3-H), 1.70–1.60 (m, 3 H, 5-H, 4-H), 1.48–1.33 (m, 1 H, 5-H'), 0.97 [t, $J = 7.8$ Hz, 9 H, Si(CH₂CH₃)₃], 0.59 [q, $J = 7.8$ Hz, 6 H, Si(CH₂CH₃)₃] ppm. ¹³C NMR (100.4 MHz): $\delta = 155.0$ (s, C=O), 136.8 (s, Ph), 128.4 (d, 2 C, Ph), 127.9 (d, 2 C, Ph), 127.6 (d, Ph), 104.8 (s, C-2'), 86.3 (s, C-1'), 67.1 (t, CH₂Ph), 45.2 (t, C-6), 40.5 (d, C-2), 30.7 (t, C-3), 25.3 (t, C-5), 19.8 (t, C-4), 7.4 [q, 3 C, Si(CH₂CH₃)₃], 4.4 [t, 3 C, Si(CH₂CH₃)₃] ppm. MS (ESI): m/z (%) = 737 [2M + Na]⁺ (100), 380 [M + Na]⁺ (10), 358 [M + 1]⁺ (3). C₂₁H₃₁NO₂Si (357.56): calcd. C 70.54, H 8.74, N 3.92; found C 70.24, H 8.46, N 4.24.

Benzyl 2-Ethynylpiperidine-1-carboxylate (16d): Prepared as described for **8e**, starting from **16c** (341 mg, 0.95 mg), to give, after purification by flash chromatography (*n*-hexane/EtOAc, 20:1; *R_f* = 0.18), pure **16d** (207 mg, 89%) as a colourless oil. ¹H NMR (400 MHz): $\delta = 7.39$ –7.29 (m, 5 H, Ph), 5.18–5.12 (m, 1 H, 2-H), 5.15 (s, 2 H, CH₂Ph), 4.03 (br. d, $J = 11.7$ Hz, 1 H, 6-H), 3.12 (br. t, $J = 12.3$ Hz, 1 H, 6'-H), 2.30 (d, $J = 2.3$ Hz, 1 H, 2'-H), 1.83–1.74 (m, 2 H, 3-H), 1.71–1.65 (m, 3 H, 5-H, 4-H), 1.46–1.35 (m, 1 H, 5-H') ppm. ¹³C NMR (100.4 MHz): $\delta = 155.0$ (s, C=O), 136.6 (s, Ph), 128.4 (d, 2 C, Ph), 127.9 (d, 2 C, Ph), 127.8 (d, Ph), 81.6 (s, C-1'), 72.3 (d, C-2'), 67.2 (t, CH₂Ph), 44.2 (t, C-6), 40.5 (d, C-2), 30.3 (t, C-3), 25.1 (t, C-5), 19.7 (t, C-4) ppm. MS (ESI): m/z (%) = 509 [2M + Na]⁺ (100), 266 [M + Na]⁺ (37), 244 [M + 1]⁺ (7). C₁₅H₁₇NO₂ (243.30): calcd. C 74.05, H 7.04, N 5.76; found C 73.79, H 7.41, N 5.84.

3-Butyl-5,6,7,8-tetrahydro-4*H*-pyrido[1,2-*c*]1,3,5-oxazin-1-one (18a): Ph₃PAuCl (5.4 mg, 0.011 mmol) was dissolved in toluene (1.8 mL) in a two-necked round-bottomed flask, and Cu(OTf)₂ (20 mg, 0.055 mmol) was added under a nitrogen atmosphere. A solution of alkyne **16a** (108 mg, 0.36 mmol) in toluene (1.8 mL) was added, and the resulting mixture was heated at reflux until the starting material had disappeared (TLC, 1.5–2 h). The mixture was cooled, then water (5 mL) was added, and the mixture was extracted with EtOAc (3 × 5 mL). The combined organic extracts were washed once with brine (5 mL), dried with anhydrous Na₂SO₄, and filtered, and the solvent was evaporated. The residue was purified by flash chromatography (*n*-hexane/EtOAc, 5:1; *R_f* = 0.23) to give pure **18a** (63 mg, 83%) as a colourless oil. ¹H NMR (400 MHz): $\delta = 4.64$ (d, $J = 2.8$ Hz, 1 H, 4-H), 4.43 (dd, $J = 13.2, 1.6$ Hz, 1 H, 8-H), 3.78 (d, $J = 11.2$ Hz, 1 H, 4a-H), 2.67 (td, $J = 12.8, 2.8$ Hz, 1 H, 8'-H), 2.07 (t, $J = 7.6$ Hz, 2 H, 1'-H), 1.89–1.85 (m, 1 H, 7-H), 1.75–1.72 (m, 2 H, 6-H, 7'-H), 1.58–1.41 (m, 4 H, 5-H, 6-H', 2'-H), 1.39–1.27 (m, 3 H, 5-H', 3'-H), 0.89 (t, $J = 7.2$ Hz, 3 H, 4'-H) ppm. ¹³C NMR (100.4 MHz): $\delta = 150.2$ (s, C-1), 150.0 (s, C-3), 98.6 (d, C-4), 55.0 (d, C-4a), 45.1 (t, C-8), 34.2 (t, C-5), 32.0 (t, C-1'), 28.0 (t, C-2'), 25.0 (t, C-7), 24.2 (t, C-6), 22.0 (t, C-3'), 13.7 (q, C-4') ppm. MS (ESI): m/z (%) = 441 [2M + Na]⁺ (100), 419 [2M + 1]⁺ (25), 210 [M + 1]⁺ (9). C₁₂H₁₉NO₂ (209.28): calcd. C 68.87, H 9.15, N 6.69; found C 69.05, H 9.13, N 6.54.

3-Phenyl-5,6,7,8-tetrahydro-4aH-pyrido[1,2-c][1,3]oxazin-1-one (18b):^[40] Prepared as described for **18a**, starting from **16b** (90 mg, 0.28 mmol), to give, after purification by flash chromatography (*n*-hexane/EtOAc, 5:1; R_f = 0.19), pure **18b** (48 mg, 75%) as a colourless oil. ¹H NMR (400 MHz): δ = 7.63–7.61 (m, 2 H, Ph), 7.39–7.32 (m, 3 H, Ph), 5.42 (d, J = 3.2 Hz, 1 H, 4-H), 4.50 (d, J = 13.6 Hz, 1 H, 8-H), 3.99 (d, J = 10.4 Hz, 1 H, 4a-H), 2.76 (td, J = 12.5, 2.9 Hz, 1 H, 8-H'), 1.95–1.92 (m, 1 H, 6-H), 1.83–1.80 (m, 1 H, 5-H), 1.75–1.72 (m, 1 H, 7-H), 1.64–1.46 (m, 3 H, 5-H', 6-H', 7-H') ppm. ¹³C NMR (100.4 MHz): δ = 149.6 (s, C-1), 147.3 (s, C-3), 131.8 (s, Ph), 129.2 (d, Ph), 128.4 (d, 2 C, Ph), 124.5 (d, 2 C, Ph), 98.7 (d, C-4), 55.3 (d, C-4a), 45.2 (t, C-8), 33.9 (t, C-5), 25.0 (t, C-7), 24.2 (t, C-6) ppm. MS (ESI): m/z (%) = 481 [2M + Na]⁺ (100), 459 [2M + 1]⁺ (36), 230 [M + 1]⁺ (32).

1-(Piperidin-2-yl)hexan-2-one (19a): Compound **18a** (60 mg, 0.29 mmol) was dissolved in toluene (2.9 mL). *tert*-Butanol (2.9 mL) was added, followed by powdered KOH (65 mg, 1.16 mmol). The mixture was heated at 85 °C (external) for 45 min. The mixture was then cooled to r.t., and water (6 mL) was added. The mixture was extracted with EtOAc (3 \times 6 mL). The combined organic extracts were dried with anhydrous Na₂SO₄ and filtered, and the solvent was evaporated under vacuum (caution! The product is volatile!). The residue was purified by flash chromatography (EtOAc/MeOH, 1:1; R_f = 0.13). The fractions were concentrated to a small volume under vacuum. Due to the volatility of the product, only a small portion was dried under vacuum for characterization as the free amine. Colourless oil. R_f = 0.13 (EtOAc/MeOH, 1:1). ¹H NMR (400 MHz): δ = 3.01 (d, J = 11.7 Hz, 1 H, 6-H), 2.98–2.91 (m, 1 H, 2-H), 2.66 (td, J = 11.7, 2.7 Hz, 1 H, 6-H'), 2.48 (d, J = 5.9 Hz, 2 H, 1'-H), 2.38 (t, J = 7.4 Hz, 2 H, 3'-H), 2.33 (br. s, 1 H, NH), 1.78–1.72 (m, 1 H, 5-H), 1.63–1.49 (m, 3 H, 3-H, 4'-H), 1.47–1.24 (m, 5 H, 4-H, 5-H', 5'-H), 1.21–1.12 (m, 1 H, 3-H'), 0.89 (t, J = 7.4 Hz, 3 H, 6'-H) ppm. ¹³C NMR (100.4 MHz): δ = 210.9 (s, C=O), 52.4 (t, C-1'), 49.5 (t, C-3'), 46.7 (t, C-6), 43.2 (d, C-2), 32.4 (t, C-3), 25.9 (t, C-4'), 25.8 (t, C-5), 24.6 (t, C-4), 22.3 (t, C-5'), 13.8 (q, C-6') ppm. MS (ESI): m/z (%) = 184 [M + 1]⁺ (100).

The larger portion was cooled in an ice-bath, and HCl (1.25 M in MeOH; 500 μ L) was added while stirring. After 30 min, the solvent was evaporated. The residue was dissolved in a small volume of acetone, and the product was precipitated by the addition of Et₂O. The white solid was filtered, washed with cold Et₂O, and dried under vacuum to give pure **19a** hydrochloride (57 mg, 89%) as a white solid, m.p. 115.2–116.6 °C. ¹H NMR (400 MHz, D₂O): δ = 3.52–3.43 (m, 1 H, 2-H), 3.34 (dm, J = 13.2 Hz, 1 H, 6-H), 3.01–2.91 (m, 2 H, 6-H', 1'-H), 2.87–2.80 (m, 1 H, 1'-H'), 2.50 (t, J = 7.6 Hz, 2 H, 3'-H), 1.87–1.77 (m, 3 H, 3-H, 5-H), 1.65–1.38 (m, 5 H, 3'-H, 4-H, 4'-H), 1.24 (sextuplet, J = 7.2 Hz, 2 H, 5'-H), 0.82 (t, J = 7.2 Hz, 3 H, 6'-H) ppm. C₁₁H₂₂ClNO (219.75): calcd. C 60.12, H 10.09, N 6.37; found C 60.05, H 9.98, N 6.51.

1-Phenyl-2-(piperidin-2-yl)ethanone (19b):^[10] Prepared as described for **19a** and **19a**·HCl, starting from **18b** (45 mg, 0.19 mmol), to give, after purification by flash chromatography (EtOAc/MeOH, 1:1; R_f = 0.07), a small sample of free amine **19b** and pure **19b**·HCl (36 mg, 78%) as a white solid, after treatment with HCl (1.25 M in MeOH).

Data for **19b**:^[10] R_f = 0.05 (EtOAc/MeOH, 2:1). ¹H NMR (400 MHz): δ = 7.96–7.93 (m, 2 H, Ph), 7.59–7.54 (m, 1 H, Ph), 7.47–7.43 (m, 2 H, Ph), 3.38 (br. s, NH), 3.24–3.04 (m, 4 H, 3-H, 6-H), 2.74 (td, J = 11.7, 2.7 Hz, 1 H, 2-H), 1.86–1.80 (m, 1 H, 5-H), 1.73–1.62 (m, 2 H, 1'-H), 1.59–1.38 (m, 3 H, 4-H, 5-H') ppm. ¹³C NMR (100.4 MHz): δ = 199.3 (s, C=O), 136.9 (s, Ph), 133.3 (d, Ph), 128.6 (d, 2 C, Ph), 128.1 (d, 2 C, Ph), 52.9 (t, C-1'), 46.3

(t, C-6), 44.7 (d, C-2), 31.9 (t, C-3), 25.2 (t, C-5), 24.3 (t, C-4) ppm. MS (ESI): m/z (%) = 204 [M + 1]⁺ (100).

Data for **19b**·HCl:^[37] ¹H NMR (400 MHz, D₂O): δ = 7.98–7.92 (m, 2 H, Ph), 7.70–7.63 (m, 1 H, Ph), 7.55–7.48 (m, 2 H, Ph), 3.73–3.63 (m, 1 H, 2-H), 3.57–3.48 (m, 1 H, 1'-H), 3.44–3.33 (m, 2 H, 6-H, 1'-H'), 3.05 (td, J = 12.4, 2.8 Hz, 1 H, 6-H'), 1.99–1.91 (m, 1 H, 5-H), 1.91–1.80 (m, 2 H, 3-H), 1.70–1.49 (m, 3 H, 4-H, 5-H') ppm.

1-Methyl-5,6,7,8-tetrahydro-oxazolo[3,4-*a*]pyridin-3-one (21): Prepared as described for **18a**, starting from **16d** (100 mg, 0.41 mmol), to give, after purification by flash chromatography (*n*-hexane/EtOAc, 3:1; R_f = 0.07), pure **21** (38 mg, 60%) as a white waxy solid, m.p. 45.6–46.4 °C. ¹H NMR (400 MHz): δ = 3.51 (t, J = 6.0 Hz, 2 H, 5-H), 2.43 (t, J = 6.4 Hz, 2 H, 8-H), 1.98 (s, 3 H, CH₃), 1.83–1.76 (m, 2 H, 6-H), 1.71–1.64 (m, 2 H, 7-H) ppm. ¹³C NMR (100.4 MHz): δ = 155.6 (s, C=O), 130.4 (s, C-1), 117.2 (s, C-9), 40.5 (t, C-5), 22.4 (t, C-8), 20.0 (t, C-6), 19.3 (t, C-7), 9.8 (q, CH₃) ppm. MS (ESI): m/z (%) = 329 [2M + Na]⁺ (100), 176 [M + Na]⁺ (37). C₈H₁₁NO₂ (153.18): calcd. C 62.73, H 7.24, N 9.14; found C 63.05, H 6.98, N 8.91.

Acknowledgments

Financial support from the University of Florence is acknowledged. B. F. thanks the European Commission for a Marie Curie fellowship (FP7-PEOPLE-2012-ITN, Project: ECHONET “Expanding capability in Heterocyclic Organic Synthesis”, No. 316379). Ente Cassa di Risparmio di Firenze is acknowledged for granting a 400 MHz NMR instrument. SGI/IZO-SGIker (UPV-EHU) is acknowledged for allocation of computational resources. The authors would like to thank Dr. Gabriele Prina Cerai for carrying out some experiments, and Dr. Milán Szöri for useful discussions. Dr. Maurizio Passaponti and Dr. Cristina Faggi are acknowledged for technical assistance.

- [1] For recent examples, see: a) R. Li, X. Wang, Z. Wei, C. Wu, F. Shi, *Org. Lett.* **2013**, *15*, 4366–4369; b) G. S. Buchanan, H. Dai, R. P. Hsung, A. I. Gerasuto, C. M. Scheinebeck, *Org. Lett.* **2011**, *13*, 4402–4405; c) A. I. Gerasuto, R. P. Hsung, *J. Org. Chem.* **2007**, *72*, 2476–2484; d) R. P. Hsung, L.-L. Wei, H. M. Sklenicka, C. J. Douglas, M. J. McLaughlin, J. A. Mulder, L. J. Yao, *Org. Lett.* **1999**, *1*, 509–512; e) E. Gayon, M. Szymczyk, H. Gérard, E. Vrancken, J.-M. Campagne, *J. Org. Chem.* **2012**, *77*, 9205–9220; f) A. Noole, M. Borissova, M. Lopp, T. Kanger, *J. Org. Chem.* **2011**, *76*, 1538–1545; g) A. Abdukader, Q. Xue, A. Lin, M. Zhang, Y. Cheng, C. Zhu, *Tetrahedron Lett.* **2013**, *54*, 5898–5900; h) J. Huang, Y. Liang, W. Pan, Y. Yang, D. Dong, *Org. Lett.* **2007**, *9*, 5345–5348.
- [2] a) N. N. Salama, N. D. Eddington, D. Payne, T. L. Wilson, K. R. Scott, *Curr. Med. Chem.* **2004**, *11*, 2093–2103; b) I. O. Edafiogho, S. B. Kombian, K. V. V. Ananthlakshmi, N. N. Salama, N. D. Eddington, T. L. Wilson, M. S. Alexander, P. L. Jackson, C. D. Hanson, K. R. Scott, *J. Pharm. Sci.* **2007**, *96*, 2509–2531.
- [3] I. O. Edafiogho, M. G. Qaddoumi, K. V. V. Ananthlakshmi, O. A. Phillips, S. B. Kombian, *Eur. J. Med. Chem.* **2014**, *76*, 20–30.
- [4] For the most recent syntheses, see: a) N. D. Koduri, Z. Wang, G. Cannell, K. Cooley, T. Mesfin Lemma, K. Miao, M. Nguyen, B. Frohock, M. Castaneda, H. Scott, D. Albinescu, S. R. Hussaini, *J. Org. Chem.* **2014**, *79*, 7405–7414; b) H.-D. Vu, J. Renault, T. Roisnel, N. Gouault, P. Uriae, *Eur. J. Org. Chem.* **2014**, 4506–4514; c) M. C. Martin, D. V. Patil, S. France, *J. Org. Chem.* **2014**, *79*, 3030–3039; d) P.-Q. Huang, W. Ou, K.-J. Xiao, A.-E. Wang, *Chem. Commun.* **2014**, *50*, 8761–8763; e)

- D. L. Priebsenow, C. Bolm, *RSC Adv.* **2013**, *3*, 10318–10322; see also ref.^[11] and references cited therein.
- [5] For recent examples, see: a) S. K. Ghosh, G. S. Buchanan, Q. A. Long, Y. Wei, Z. F. Al-Rashid, *Tetrahedron* **2008**, *64*, 883–893; b) F. Josefík, M. Svobodová, V. Bertolasi, P. Šimůnek, *Beilstein J. Org. Chem.* **2013**, *9*, 1463–1471; c) F. Josefík, M. Svobodová, V. Bertolasi, P. Šimůnek, V. Macháček, N. Almonasy, E. Černošková, H. M. Sklenicka, R. P. Hsung, *J. Organomet. Chem.* **2012**, *699*, 75–81.
- [6] C. Herdeis, J. Telsler, *Eur. J. Org. Chem.* **1999**, 1407–1414.
- [7] C. Herdeis, P. Küpper, S. Plé, *Org. Biomol. Chem.* **2006**, *4*, 524–529.
- [8] S. Fréville, P. Delbecq, V. M. Thuy, H. Petit, J. P. Célérier, G. Lhommet, *Tetrahedron Lett.* **2001**, *42*, 4609–4611.
- [9] J. P. Michael, C. B. de Koning, D. P. Pienaar, *Synlett* **2006**, 383–386.
- [10] B. A. D. Neto, A. A. M. Lapis, A. B. Bernd, D. Russowsky, *Tetrahedron* **2009**, *65*, 2484–2496.
- [11] A. Oppedisano, C. Prandi, P. Venturello, A. Deagostino, G. Goti, D. Scarpi, E. G. Occhiato, *J. Org. Chem.* **2013**, *78*, 11007–11016.
- [12] a) G. Satyalakshmi, K. Suneel, D. B. Shinde, B. Das, *Tetrahedron: Asymmetry* **2011**, *22*, 1000–1005; b) S. Fustero, D. Jiménez, J. Moscardó, S. Catalán, C. del Pozo, *Org. Lett.* **2007**, *9*, 5283–5286.
- [13] R. W. Bates, N. F. M. Aslam, C. H. Tang, O. Simon, *Tetrahedron* **2014**, *70*, 2134–2140.
- [14] a) P. R. Krishna, B. K. Reddy, P. Srinivas, *Tetrahedron* **2012**, *68*, 841–845; b) W. A. Maio, S. Sinishtaj, G. H. Posner, *Org. Lett.* **2007**, *9*, 2673–2676.
- [15] a) W.-H. Chiou, G.-T. Chen, C.-L. Kao, Y.-K. Gao, *Org. Biomol. Chem.* **2012**, *10*, 2518–2520; b) T. K. Beng, R. E. Gawley, *J. Am. Chem. Soc.* **2010**, *132*, 12216–12217.
- [16] The carbodeauration process has been studied with allylic cations generated in situ: a) M. C. Blanco Jaimes, V. Weingand, F. Rominger, A. S. K. Hashmi, *Chem. Eur. J.* **2013**, *19*, 12504–12511; b) A. S. K. Hashmi, C. Lothshütz, R. Döpp, M. Ackermann, J. de Buck Becker, M. Rudolph, C. Scholz, F. Rominger, *Adv. Synth. Catal.* **2012**, *354*, 133–147.
- [17] R. Robles-Machin, J. Adrio, J. C. Carretero, *J. Org. Chem.* **2006**, *71*, 5023–5026.
- [18] E.-S. Lee, H.-S. Yeom, J.-H. Hwang, S. Shin, *Eur. J. Org. Chem.* **2007**, 3503–3507.
- [19] A. Buzas, F. Gagosz, *Synlett* **2006**, 2727–2730.
- [20] In the case of *N*-Boc-2-ethynylpyrrolidine, whereas Gagosz and Buzas reported the formation of the 5-*exo-dig* product only, Shin et al. reported the formation of a 3:1 mixture of 5-*exo-dig* and 6-*endo-dig* compounds. However, the catalysts, solvents, and reaction times were different.
- [21] a) D. Malhotra, L.-P. Liu, M. S. Mashuta, G. B. Hammond, *Chem. Eur. J.* **2013**, *19*, 4043–4050; b) C. H. Oh, J. H. Kim, B. K. Oh, J. R. Park, J. H. Lee, *Chem. Eur. J.* **2013**, *19*, 2592–2596; c) E. Rettenmeier, A. M. Schuster, M. Rudolph, F. Rominger, C. A. Gade, A. S. K. Hashmi, *Angew. Chem. Int. Ed.* **2013**, *52*, 5880–5884; *Angew. Chem.* **2013**, *125*, 5993–5997; d) N. Ghosh, S. Nayak, B. Prabagar, A. K. Sahoo, *J. Org. Chem.* **2014**, *79*, 2453–2462; e) L. Pawar, F. C. Pigge, *Tetrahedron Lett.* **2013**, *54*, 6067–6070; f) W. Rao, P. W. H. Chan, *Chem. Eur. J.* **2014**, *20*, 713–718; g) O. Seppänen, M. Muuronen, J. Helaja, *Eur. J. Org. Chem.* **2014**, 4044–4052.
- [22] a) R. Cai, D. Wang, Y. Chen, W. Yan, N. R. Geise, S. Sharma, H. Li, J. L. Petersen, M. Li, X. Shi, *Chem. Commun.* **2014**, *50*, 7303–7305; b) P. Nun, R. S. Ramón, S. Gaillard, S. P. Nolan, *J. Organomet. Chem.* **2011**, *696*, 7–11; c) M. Kumar, G. B. Hammond, B. Xu, *Org. Lett.* **2014**, *16*, 3452–3455.
- [23] D. Wang, R. Cai, S. Sharma, J. Jirak, S. K. Thummanapelli, N. G. Akhmedov, H. Zhang, X. Liu, J. L. Petersen, X. Shi, *J. Am. Chem. Soc.* **2012**, *134*, 9012–9019.
- [24] A. Guérinot, W. Fang, M. Sircoglou, C. Bour, S. Bezzenine-Lafollée, V. Gandon, *Angew. Chem. Int. Ed.* **2013**, *52*, 5848–5852; *Angew. Chem.* **2013**, *125*, 5960–5964.
- [25] M. Kumar, J. Jasinski, G. B. Hammond, B. Xu, *Chem. Eur. J.* **2014**, *20*, 3113–3119.
- [26] More catalytic systems were reported in a more recent paper: W. Fang, M. Presset, A. Guérinot, C. Bour, S. Bezzenine-Lafollée, V. Gandon, *Chem. Eur. J.* **2014**, *20*, 5439–5446.
- [27] Á. Sinai, Á. Mészáros, T. Gáti, V. Kudar, A. Palló, Z. Novák, *Org. Lett.* **2013**, *15*, 5654–5657.
- [28] S. Hanessian, E. Therrien, J. Zhang, W. van Otterlo, Y. Xue, D. Gustafsson, I. Nilsson, O. Fjellström, *Bioorg. Med. Chem. Lett.* **2009**, *19*, 5429–5432.
- [29] K. Tchabanenko, R. M. Adlington, A. R. Cowley, J. E. Baldwin, *Org. Lett.* **2005**, *7*, 585–588.
- [30] E. G. Occhiato, C. Prandi, A. Ferrali, A. Guarna, P. Venturello, *J. Org. Chem.* **2003**, *68*, 9728–9741.
- [31] M. C. Kozłowski, Z. Xu, A. G. Santos, *Tetrahedron* **2001**, *57*, 4537–4542.
- [32] C. Herdeis, *Synthesis* **1986**, 232–233.
- [33] D. Scarpi, L. Bartali, A. Casini, E. G. Occhiato, *Eur. J. Org. Chem.* **2013**, 1306–1317.
- [34] a) F. Lepifre, S. Clavier, P. Bouysson, G. Coudert, *Tetrahedron* **2001**, *57*, 6969–6975; b) K. C. Nicolaou, G.-Q. Shi, K. Namoto, F. Bernal, *Chem. Commun.* **1998**, 1757–1758.
- [35] Other attempts to open the urethane ring by using reducing agents such as DIBAL-H (diisobutylaluminum hydride) or Super-H (lithium triethylborohydride) at low temperature failed, and only produced complex mixtures of by-products.
- [36] E. G. Occhiato, A. Casini, A. Guarna, D. Scarpi, *Eur. J. Org. Chem.* **2011**, 6544–6552.
- [37] J. F. Stevens, H. Hart, H. Hendriks, T. M. Malingré, *Phytochemistry* **1992**, *31*, 3917–3924.
- [38] J. D. Ha, J. H. Cha, *J. Am. Chem. Soc.* **1999**, *121*, 10012–10020.
- [39] We tried the same approach with a similar, saturated *N*-Boc-protected alkyne, but the reduction of the double bond of the enyne was troublesome, due to the sensitivity of the *N*-Boc group to TFA, and so this approach gave only poor yields. However, when the little amount of the reduced substrate obtained in this way was submitted to the gold-catalysed reaction, only the 6-*endo* compound was formed.
- [40] S. Suga, Y. Tsutsui, A. Nagaki, J. Yoshida, *Bull. Chem. Soc. Jpn.* **2005**, *78*, 1206–1217.
- [41] Degradation of this compound took place to a very small extent in CDCl₃ solution during spectroscopic characterization (see Supporting Information).
- [42] a) A. González Pérez, C. Silva López, J. Marco-Contelles, O. Nieto Faza, E. Soriano, A. R. de Lera, *J. Org. Chem.* **2009**, *74*, 2982–2991; b) E. Soriano, J. Marco-Contelles, *Chem. Eur. J.* **2008**, *14*, 6771–6779; see also: c) A. Correa, N. Marion, L. Fensterbank, M. Malacria, S. P. Nolan, L. Cavallo, *Angew. Chem. Int. Ed.* **2008**, *47*, 718–721; *Angew. Chem.* **2008**, *120*, 730–733.
- [43] This was expected, because Gagosz used CH₂Cl₂ at room temp., whereas we used refluxing toluene.
- [44] T. J. Harrison, G. R. Dake, *J. Org. Chem.* **2005**, *70*, 10872–10874.
- [45] With different substrates, in a study aimed at the preparation of fused carbocycles, the 5-*exo*/6-*endo-dig* selectivity has been reported to depend on the steric and electronic properties of the gold(I) complex. F. Barabé, P. Levesque, I. Korobkov, L. Barriault, *Org. Lett.* **2011**, *13*, 5580–5583.
- [46] BHandHLYP was used as implemented in Gaussian09 (0.5 E_{X}^{HF} + 0.5 $E_{\text{X}}^{\text{LSDA}}$ + 0.5 $\Delta E_{\text{X}}^{\text{Becke88}}$ + $E_{\text{C}}^{\text{LYP}}$).
- [47] M. J. Frisch, G. W. Trucks, H. B. Schlegel, G. E. Scuseria, M. A. Robb, J. R. Cheeseman, G. Scalmani, V. Barone, B. Mennucci, G. A. Petersson, H. Nakatsuji, M. Caricato, X. Li, H. P. Hratchian, A. F. Izmaylov, J. Bloino, G. Zheng, J. L. Sonnenberg, M. Hada, M. Ehara, K. Toyota, R. Fukuda, J. Hasegawa, M. Ishida, T. Nakajima, Y. Honda, O. Kitao, H. Nakai,

- T. Vreven, J. A. Montgomery Jr., J. E. Peralta, F. Ogliaro, M. Bearpark, J. J. Heyd, E. Brothers, K. N. Kudin, V. N. Staroverov, R. Kobayashi, J. Normand, K. Raghavachari, A. Rendell, J. C. Burant, S. S. Iyengar, J. Tomasi, M. Cossi, N. Rega, J. M. Millam, M. Klene, J. E. Knox, J. B. Cross, V. Bakken, C. Adamo, J. Jaramillo, R. Gomperts, R. E. Stratmann, O. Yazyev, A. J. Austin, R. Cammi, C. Pomelli, J. W. Ochterski, R. L. Martin, K. Morokuma, V. G. Zakrzewski, G. A. Voth, P. Salvador, J. J. Dannenberg, S. Dapprich, A. D. Daniels, O. Farkas, J. B. Foresman, J. V. Ortiz, J. Cioslowski, D. J. Fox, *Gaussian 09*, revision D.01, Gaussian, Wallingford CT, **2013**.
- [48] 3D structures were drawn using the CyLview software: C. Y. Legault, *CYLview*, v. 1.0b, Université de Sherbrooke, **2009** (<http://www.cylview.org>).
- [49] Y. Zhao, D. G. Truhlar, *Theor. Chem. Acc.* **2008**, *120*, 215–241.
- [50] C. Gonzalez, H. B. Schlegel, *J. Phys. Chem.* **1990**, *94*, 5523–5527.
- [51] J. P. Foster, F. Weinhold, *J. Am. Chem. Soc.* **1980**, *102*, 7211–7218.

Received: February 11, 2015
Published Online: April 8, 2015